GOLD(I) COMPLEXES AND CO OXIDATION CATALYSTS

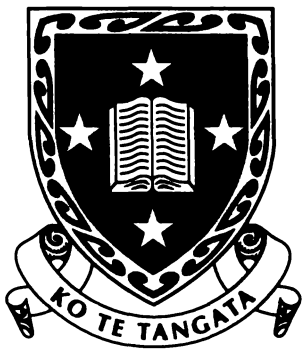

The University of Waikato

Te Whare Wānanga o Waikato

A thesis

submitted in partial fulfilment

of the requirements for the degree

of

Doctor of Philosophy

at the

University of Waikato

by

TREVOR J. MATHIESON

University of Waikato

1998

ABSTRACT

Isonitrile gold(I) nitrates, (RNC)$AuNO_3$ (R = Bu^t, Et or Xy) have been prepared and fully characterised. These join the rare set of gold(I) species exhibiting ligation to oxygen and are the first examples of gold(I) bonded to both carbon and oxygen. Molecular aggregations of the monomeric units were revealed by X-ray crystal structure determinations. The aggregations are the result of secondary Au--Au interactions. These interactions are also apparent in the structures of the analogous complexes (RNC)AuCl (R = Et or Xy), which were characterised for comparative purposes.

(EtNC)AuCl and (Bu^tNC)$AuNO_3$ formed zig-zag chain structures from which the other unprecedented structures can be derived. (EtNC)$AuNO_3$ formed a concertinaed chain, (XyNC)$AuNO_3$ (**1**) a compressed chain and (XyNC)AuCl a tetrameric chain. The formations of these supramolecular motifs are attributed to various steric and electronic ligand influences on the inherent Au--Au attraction. In addition, intermolecular π-π contacts were observed for the (XyNC)AuX (X = Cl or NO_3) structures.

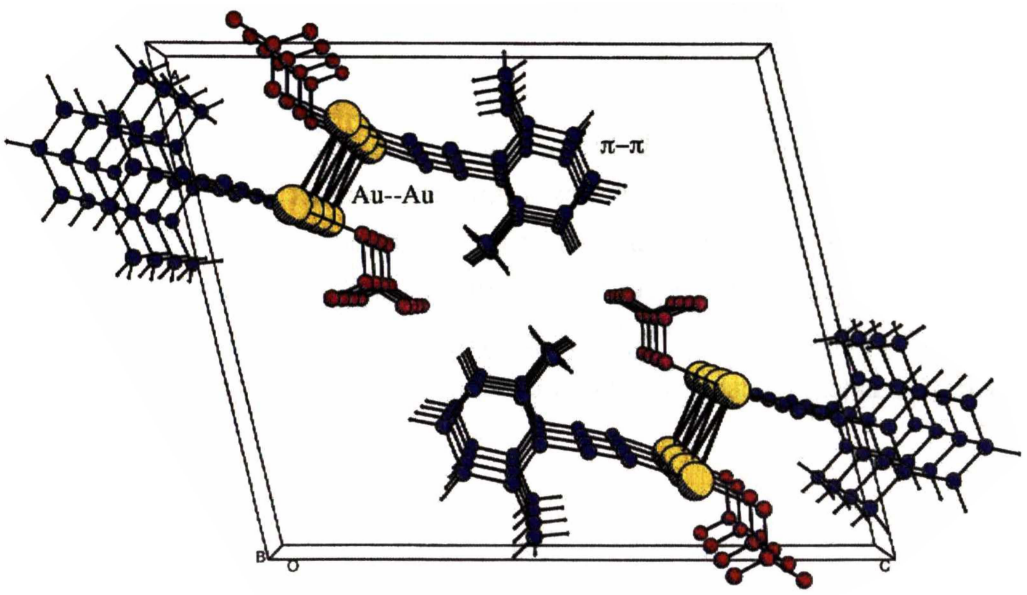

(1)

In each instance, the Au--Au interactions for (RNC)$AuNO_3$ were significantly shorter than those of the analogous (RNC)AuCl structure. The results demonstrated that the non-polarisable nitrate anion enhances the Au--Au attraction. This is contrary to previous theoretical calculations, which predict that soft anions enhance the Au--Au attraction. The structure of the ionic $[(XyNC)_2Au]^+NO_3^-$ complex was also characterised. This did not exhibit Au--Au contacts; the packing structure was instead based on infinite π-π stacking.

The potential of gold(I) complexes as precursors to supported gold catalysts was assessed. The complexes were adsorbed (from a solution phase) onto transition metal oxide supports which were subsequently vacuum dried and calcined. Scanning Electron Microscopy (SEM) revealed a range of gold particle sizes on the calcined materials. The extent of gold dispersion was dependent on the chemical properties of the complex employed.

The use of the stable (Ph_3P)AuCl, (Ph_3P)AuMe and (Bu^tNC)AuCl complexes resulted in relatively large gold particles (20-200 nm). In the case of (Ph_3P)AuMe, metallic gold crystals were observed. Under ambient conditions these materials were inactive for CO oxidation. Under the same testing conditions, efficient catalytic CO oxidation was observed over materials prepared by using the unstable (Bu^tNC)$AuNO_3$ complex as a precursor. The gold particles on the active catalyst were too small to be resolved by SEM.

The observed CO oxidation activity was proposed to be a two-component catalytic reaction involving gold nano-particles in intimate contact with a reducible oxide support. Reactant inhibition, which is commonly observed for catalysts with inert supports, is avoided in this system. This form of catalysis has received considerable recent attention for the CO oxidation reaction and provides guidance for attempts to enhance other heterogeneous catalytic processes.

ACKNOWLEDGEMENTS

It is with great appreciation that I acknowledge Professor Brian Nicholson, so congenial a supervisor was he. It mattered not whether my news was of success, a wildly enthusiastic (but usually patently ridiculous) crystal structure prediction or another attractive (yet ultimately useless) gold mirror; always welcome was I to his office and the veritable fountain of knowledge contained within.

Many thanks also to Associate Professor Alan Langdon and Dr. Neil Milestone for helpful advice and support with the surface catalysis aspects of this research. Neil and the team at IRL were always helpful during my visits to Wellington, which was much appreciated. Dr. Ralph Thomson provided assistance with the NMR spectroscopy and also shared a few pleasant walks around the golf course (which were spoilt only by a little white ball). Alf Harris and Dave Wild at the Waikato Microscope Unit are thanked for giving me a free rein on the SEM.

Much gratitude is extended toward Allen Oliver, for it was he who safely transported my fragile wee crystals to the University of Auckland for X-ray data collection. For the X-ray data sets, Associate Professor Cliff Rickard is also thanked. The Chemistry Department provided financial support for this research which was much appreciated. The technical staff were all helpful at one stage or another and unwisely let me borrow many an item of equipment.

Thank you to Richard, Kate and Mike Chapman, your help and support, especially during the last few weeks, has been invaluable. A big thank you to Mum, Dad, Linda and Grant who have remained very supportive throughout and have maintained a sensible and curious interest as to why I should wish to dissolve gold.

To Sarah, a written word will never justify your importance to me. If the one thing this work achieves is to make you proud, then I will be happy.

TABLE OF CONTENTS

CHAPTER THREE
(RNC)AuX COMPLEXES 37

CHAPTER FIVE
SUPPORTED GOLD CATALYSTS 121

LIST OF FIGURES

LIST OF TABLES

LIST OF ABBREVIATIONS

m.p.	-	melting point
Decomp.	-	decomposition
Me	-	methyl
Bu^t	-	tertiary butyl
Et	-	ethyl
Xy	-	xylyl
Ph	-	phenyl
Mes	-	mesityl
acac	-	acetylacetonate
X	-	mono-anionic ligand
L	-	neutral ligand
YSZ	-	yttria-stabilised zirconia
dppm	-	1,2 bis(diphenylphosphine)methane
SEM	-	Scanning Electron Microscopy
TEM	-	Transmission Electron Microscopy
EDAX	-	Energy Dispersive X-ray Analysis
ESMS	-	Electrospray Mass Spectroscopy
NMR	-	Nuclear Magnetic Resonance
δ	-	chemical shift (ppm)
d	-	doublet (NMR)
t	-	triplet (NMR)
q	-	quartet (NMR)
DSC	-	Differential Scanning Calorimetry
STA	-	Simultaneous Thermal Analysis
IR	-	infra-red
ν	-	stretching frequency
CVD	-	Chemical Vapour Deposition

CHAPTER ONE

INTRODUCTION

"Gold and civilisation wax and wane together."[1]

Will Durant - Historian

Throughout history the possession of elemental gold has provided power and prestige to many nations, societies and individuals. Until recently, from a technological point of view, it can be said that the pursuit of gold has been for nothing more than chemical durability and an aesthetically pleasant yellow gleam.[2] It is used extensively in jewellery and decorative pieces but practical usage has been limited to applications such as dental fillings.

This trend has changed during the latter decades of the 20th century. This is apparent in the electronics industry which makes use of gold for specialised applications.[3] Furthermore, specific gold complexes are used in the therapeutic treatment of rheumatoid arthritis and the potential of gold drugs as anti-tumour agents is receiving some attention.[4]

In the past, the chemistry of gold was not studied in depth. This is attributable to a lack of reactivity, a high cost and the ease with which gold compounds decompose.[5] Influenced by the increasing practical utilisation, studies of the physical and chemical properties of gold have become more frequent and detailed.[6] This recent expansion of gold research has led to the discovery of many interesting properties, some of which have further widened the scope for technological application. Au(I)--Au(I) attractive interactions and the catalytic activity associated with metallic gold nano-particles are topical examples of these properties and form the basis of the research presented in this thesis.

---

[1] J. St. John, *Noble Metals*, Time-Life Books, Amsterdam, 1984, p. 29.
[2] *The Periodic Table of the Elements*, (Poster), Time-Life books, 1987.
[3] See for example: Y. Okinaka and M. Hoshino, *Gold Bull.*, 1998, **31**, 3; R. J. Puddephatt and I. Treurnicht, *J. Organomet. Chem.*, 1987, **319**, 129.
[4] See for example: D. H. Brown and W. E. Smith, *Chem. Soc. Rev.*, 1980, **9**, 217; P. J. Sadler, *Adv. Inorg. Chem.*, 1991, **36**, 1; C. F. Shaw III, in *Metal Compounds in Cancer Therapy*, ed. S. P. Fricker, Chapman & Hall, London, 1994, p. 47-64.
[5] R. J. Puddephatt, *The Chemistry of Gold*, Elsevier, Amsterdam, 1978, p. v.
[6] R. V. Parish, *Gold Bull.*, 1997, **30**, 3.

1·1 GOLD(I) CRYSTALLOGRAPHY

The pleasant appearance of crystals can be attributed to the planeness and general symmetry of their faces. These characteristics are outer manifestations of recurring chemical interactions between the structural units. The nature of these interactions is often well defined, such as the electrostatic attraction between cations and anions in NaCl. Covalent bonding between carbon atoms in diamond and hydrogen bonding within the structure of ice are further examples.[7]

Complications arise when organometallic complexes crystallise because the molecular packing arrangements are the result of various intermolecular interactions. One of the more defined cases involves linear two-coordinate gold(I) complexes. These show potential for molecular aggregation by way of intermolecular attraction between the gold centres. This phenomenon is known as auriophilicity, a term coined by H. Schmidbaur.[8]

It has been established that these energetically favourable Au--Au contacts can result in the formation of dimeric, oligomeric and polymeric aggregations of gold(I) complexes. A detailed discussion is provided in section 2·2, which emphasises that the steric and electronic properties of the ligands are important in determining the extent of the Au--Au interactions. In the present project, novel auriophilic motifs were characterised as a result of unique ligand combinations.

Many supramolecular solid state materials possess unique electronic, optical, magnetic and mechanical properties, some of which have potential for practical application.[9] Auriophilicity is emerging as a feasible technique of crystal engineering, whereby structures may be specifically designed employing the directional properties of Au--Au intermolecular interactions.[10]

---

[7] W. J. Moore, *Physical Chemistry*, Longman Group, London, 5th edn., 1987, p. 865-870.
[8] H. Schmidbaur, *Chem. Soc. Rev.*, 1995, **24**, 391.
[9] P. M. van Calcar, M. M. Olmstead and A. L. Balch, *Inorg. Chem.*, 1997, **36**, 5231.
[10] R. J. Puddephatt, *J. Chem. Soc., Chem. Commun.*, 1998, 1055; S. Pathaneni and G. R. Desiraju, *J. Chem. Soc., Dalton Trans.*, 1993, 319.

1·2 THE EXEMPLAR OF SURFACE CATALYSIS

The boundaries that define phase change have provided some intriguing aspects of chemical research. The interfaces defined by solid surfaces have received considerable attention, including their potential for catalytic reactions.[11]

No other surface adsorbed entity has been studied more thoroughly than CO, particularly the oxidation reaction on metal surfaces, research of which dates back to the classic works of I. Langmuir in the 1920s.[12] The abundant interest in this relatively simple reaction can be linked to it providing a suitable model for research of surface catalysis.[13] The investigation of model catalysts provides insight of fundamental catalytic processes.[14] Indeed, studies of CO chemisorption and subsequent oxidation are of importance to various aspects of surface science research.[15]

There has been a general acceptance that catalytic oxidation of CO on surfaces is unfavourable under ambient conditions. Recently though, it has become apparent that specific two-component catalysts (composed of tiny noble metal particles in intimate contact with oxide supports) are highly active for CO oxidation at low temperatures.[16] These catalysts are a remarkable development, especially when noted that *"For those of us familiar with conventional CO oxidation catalysts, which are active only at temperatures above about 150 °C, observation of rapid CO oxidation at room temperature can be startling."*[17]

The catalytic oxidation of CO under ambient conditions is a process of significant technological interest. The understanding of this reaction on surfaces has been progressively developed. Simple metal surfaces are inactive, although metal defect sites have potential because CO and oxygen contact is enhanced. A two-component catalyst system acts by way of a bi-functional mechanism, in which both the oxidising support and the supported metal contribute active function.

---

[11] See for example: D. Kondarides and X. E. Verykios, *J. Catal.*, 1996, **158**, 363; T. Komaya, A. T. Bell, Z. Weng-Sieh, R. Gronsky, F. Engelke, T. S. King and M. Pruski, *J. Catal.*, 1994, **150**, 400; G. J. Edens, A. Hamelin and M. J. Weaver, *J. Phys. Chem.*, 1996, **100**, 2322.

[12] I. Langmuir, *Trans. Faraday Soc.*, 1922, **17**, 621; cited in Fushs *et. al.*, ref. 167.

[13] T. Sueyoshi, T. Sasaki and Y. Iwasawa, *J. Phys. Chem.*, 1996, **100**, 1048.

[14] S. Hong and H. H. Richardson, *J. Phys. Chem.*, 1993, **97**, 1258.

[15] J. C. Campuzano, in *The Chemical Physics of Solid Surfaces and Heterogeneous Catalysis*, eds. D. A. King and D. P. Woodruff, Elesvier, Oxford, 1990, vol. 3, ch. 4, p. 395.

[16] M. Haruta, *Catal. Today*, 1997, **36**, 153.

[17] R. K. Herz, A. Badlani, D. R. Schryer and B. T. Upchurch, *J. Catal.*, 1993, **141**, 219.

1·3 THESIS OUTLINE

This research investigates two aspects of gold chemistry, both of which are of current international interest. The first incorporates a crystallographic study of novel gold(I) complexes, with a view to better understanding the parameters that control auriophilicity. The second focuses on the recent discovery that metallic gold has potential for catalytic CO oxidation, specifically when highly dispersed on transition metal oxide supports.

The crystallography and catalysis topics are discussed separately. They are linked however, in that gold(I) complexes which exhibited supramolecular structural features were utilised as precursors to supported gold catalysts.

Chapter Two

This Chapter presents a literature review outlining the general features of gold chemistry and auriophilicity.

Chapter Three

This Chapter describes new research on isonitrile gold(I) complexes, (RNC)AuX. Variations in the R group (R = Bu^t, Et or Xy) and the anion (X = Cl or NO_3) led to a diverse set of solid state structures dominated by intermolecular Au--Au contacts. The results provided further basis for the design and prediction of crystal packing arrangements of gold(I) species. The (RNC)AuX complexes were also characterised by elemental analysis, IR and NMR.

Chapter Four

This Chapter presents a literature review of catalytic CO oxidation. The reaction on the surfaces of transition metals is reviewed initially, followed by descriptions of two-component catalytic systems. In addition, the general properties of CO are discussed briefly, including distribution and bio-toxicity.

Chapter Five

This Chapter describes the preparation of supported gold materials and their testing for catalytic CO oxidation. Reproduction of the pioneering coprecipitation and gold-sputtering syntheses were carried out initially. A catalyst preparation method was developed which involved the deposition of gold complexes onto specific transition metal oxide supports. There has been little development of this general preparative technique, particularly in the specific area of low temperature CO oxidation catalysts.‡

The prepared materials were tested for CO oxidation efficiency under ambient conditions by passing gas mixtures over catalyst beds and monitoring the outlet gas stream.§ The observed activities of the materials were rationalised in terms of the structures of the catalysts (based on SEM observations) and the chemistries of the precursors used.

Chapter Six

This Chapter provides an overview of the project in which the literature surveys are linked with the experimental results. Overall conclusions are used to formulate recommendations for the future development of both auriophilicity and two-component surface catalysis.

‡ Parallel work was published during the course of this work; see ref. 242.

§ The catalytic testing was carried out at Industrial Research Limited (IRL), Wellington.

CHAPTER TWO

GOLD AND AURIOPHILICITY

-A LITERATURE REVIEW

"Gold hath these natures - greatness of weight, closeness of parts, fixation, pliantness or softness, immunity from rust, colour or tincture of yellow. If a man can make a metal that hath all of these properties let men dispute whether it be gold or no."[18]

Francis Bacon - 17th century philosopher

2·1 THE CHEMISTRY OF GOLD

The properties described by Francis Bacon explain the attraction metallic gold has held throughout history and the failures of alchemy would only have enhanced this fascination. Modern scientific research has provided some explanation for the unique status of metallic gold and this element will assuredly remain an important influence in the future, due to increased technological application and continued use as a financial standard.[19]

The inorganic and coordination chemistry of gold also forms a remarkable exposé in which oxidation states -I to V have been characterised, with I and III being prevalent.[20] The general chemistry of gold is outlined in the following review of literature, which includes metallic properties, the features of the two common oxidation states and organometallic chemistry. Auriophilicity is discussed in section 2·2 with focus on intermolecular Au--Au interactions between LAuX molecules. Gold cluster chemistry is briefly outlined along with some reported observations of related d^{10} metallophilic interactions.

---

[18] J. Bronowski, *The Ascent of Man*, BBC, London, p. 136.
[19] D. M. P. Mingos, *J. Chem. Soc., Dalton Trans.*, 1996, 561.
[20] R. J. Puddephatt and J. J. Vittal, in *Encyclopedia of Inorganic Chemistry*, ed. R. B. King, John Wiley & Sons, Chichestor, 1994, vol. 3, p. 1320.

2·1·1 Metallic

Gold is the least reactive of all the metals, being the only one not chemically attacked by either oxygen or sulphur at any temperature. If gold is to react in aqueous solution (in the absence of coordinating ligands) it must be oxidised as follows:

$$\mathbf{Au \rightarrow Au^{+}\,(aq) + e^{-}}$$

The inertness of gold is emphasised by the redox potential for the above reaction, which would result in the reduction of H_2O.[21] Gold is not oxidised by dissolved oxygen in the presence of either strong acids or strong alkalis, the only metal for which this is the case. The dissolution of gold in aqueous solutions requires the presence of both an oxidising agent and a strong coordinating species. Thus, gold dissolves in a mixture of concentrated HCl and HNO_3 but neither acid has any appreciable effect by itself. This mixture is called *aqua regia*, or the 'water of royalty'. The dissolving mechanism is dependent on the ligating action of the chloride ion, gold also dissolving in a mixture of HCl and oxidising iron(III) species.[21]

Gold has an electron configuration of $(Xe)4f^{14}5d^{10}6s^{1}$, therefore, like silver and copper, possesses a single *s* electron outside a completed *d*-shell. Despite a similar electronic structure, the chemical traits of gold are dissimilar to those of the remaining two group eleven elements. This can be attributed to the relativistic effect which is outlined as follows:

- As a result of high nuclear charge, electrons which penetrate to the nucleus accelerate to speeds close to that of light which results in an acquisition of mass.[6]

- The *s*-orbitals (and *p* to a lesser extent) therefore contract and are stabilised. Their electrons are able to more effectively shield the *d*- and *f*-electrons, hence these orbitals expand in size.[22]

- As a result of *s*- and *p*-orbital stabilisation and *d*-orbital destabilisation, significant hybridisation is promoted. This allows the *d*-electrons and orbitals to participate more readily in chemical bonding.[23]

---

[21] Ref. 5, pp. 5-20.
[22] N. Bartlett, *Gold Bull.*, 1998, **31**, 22.
[23] A. Grohmann and H. Schmidbaur, in *Comprehensive Organometallic Chemistry II*, eds. G. Wilkinson, F. G. A. Stone and E. W. Abel, Pergamon, Oxford, 1995, p. 3.

The group eleven elements have relatively high first ionisation energies. Removing the $4s^1$ electron from copper, for example, requires more energy than from potassium. The valence electron of copper is exposed to a greater effective nuclear charge due to poor shielding by the relatively dispersed $3d^{10}$ electrons. The relativistic influence enhances the effect for gold in which the $6s^1$ electron is imperfectly protected from the nuclear charge by two diffuse sub-shells, $4f^{14}$ and $5d^{10}$. The difficulty of removing the $6s^1$ from gold provides explanation for the inertness of this metal.[24]

The expanding use of gold in the electronics industry, particularly in micro-circuitry, is favoured by the high electrical conductivity of this metal. The necessity of thin plating and wires for such components is ideally suited to gold, which is very malleable and ductile.[25] Moreover, the corrosion resistance of gold allows components to be used for marine applications where other metals are susceptible to oxidative degradation.[26]

In comparison with the other noble metals, gold is considered to be the least useful as a catalytic material. This is attributed to a lack of propensity for the chemisorption of molecules, due to the filled $5d$ orbital. However, excellent oxidative catalysis has been observed recently on highly dispersed gold nano-particles (refer to Chapter Four).[27] The catalytic activity of the gold particles is reliant on their contact with an active oxidising support.

The use of gold complexes in homogeneous catalysis has found little utility and examples in the literature are rare. Some recent progress has been made in the addition of alcohols to alkynes.[28]

2·1·2 Gold(I)

The removal of the $6s^1$ electron from metallic gold results in the gold(I) oxidation state, which has an electron configuration of $[Xe]4f^{14}5d^{10}6s^0$. This is somewhat misleading in that gold(I) complexes are usually derived from the reduction of gold(III) compounds in the presence of stabilising ligands. Three- and four-coordinate gold(I) complexes are known,[29] but they are not numerous with gold(I) chemistry being characterised by linear two-coordinate species.

---

[24] Ref. 5, pp. 14-15.
[25] M. M. B. Holl, P. F. Seidler, S. P. Kowalczyz and F. R. McFeely, *Inorg. Chem.*, 1994, **33**, 510.
[26] D. D. Parrish, J. S. Holloway and F. C. Fehsenfeld, *Environ. Sci. Technol.*, 1994, **28**, 1615.
[27] G. J. Hutchings, *Gold Bull.*, 1996, **29**, 123; and ref. cited therein.
[28] J. H. Teles, S. Brode and M. Chabanas, *Angew. Chem. Int. Ed. Engl.*, 1998, **37**, 1415.
[29] M. C. Gimeno and A. Laguna, *Chem. Rev.*, 1997, **97**, 511.

The aqueous gold(I) ion is very unstable with respect to disproportionation:

$$3Au^{+}\ (aq) \rightarrow Au^{3+}\ (aq) + 2Au\ (s)$$

The $[Au(OH_2)_2]^+$ ion has not been characterised and the aqueous chemistry of gold(I) persists only when strongly ligated, for example $[Au(CN)_2)]^-$ (aq). A small number of gold(I) binary compounds AuX (X = CN, Br or Cl) are stable and these generally exhibit polymeric crystal structures with linear coordination (Figure 2·1).[30] Very unstable binary complexes like $Au(CO)_2$ have been characterised spectroscopically using matrix isolation techniques.[31]

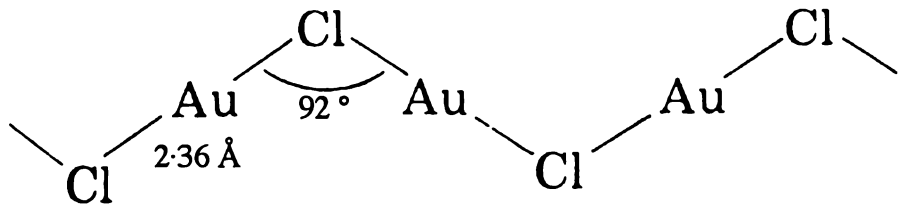

Figure 2·1 Crystalline AuCl

The promotion of hybridisation by relativistic effects has been invoked to explain the predominance of gold(I) linear two-coordinate species. Hybridisation of $5d_Z^2$ and $6s$ allows the electron pair from $5d_Z^2$ to be placed in Ψ_1 (see A in Figure 2·2). Mixing of Ψ_2 and $6p_Z$ form the bonding Ψ_3 and Ψ_4 hybrid orbitals (B).[32] Donor ligands will interact with these orbitals along the molecular z-axis.[33]

---

[30] Ref. 5, p. 34.
[31] D. McIntosh and G. A. Ozin, *Inorg. Chem.*, 1977, **16**, 51.
[32] Ref. 5, p. 17.
[33] F. A. Cotton and G. Wilkinson, *Advanced Inorganic Chemistry*, J. Wiley & Sons, London, 1988, p. 941.

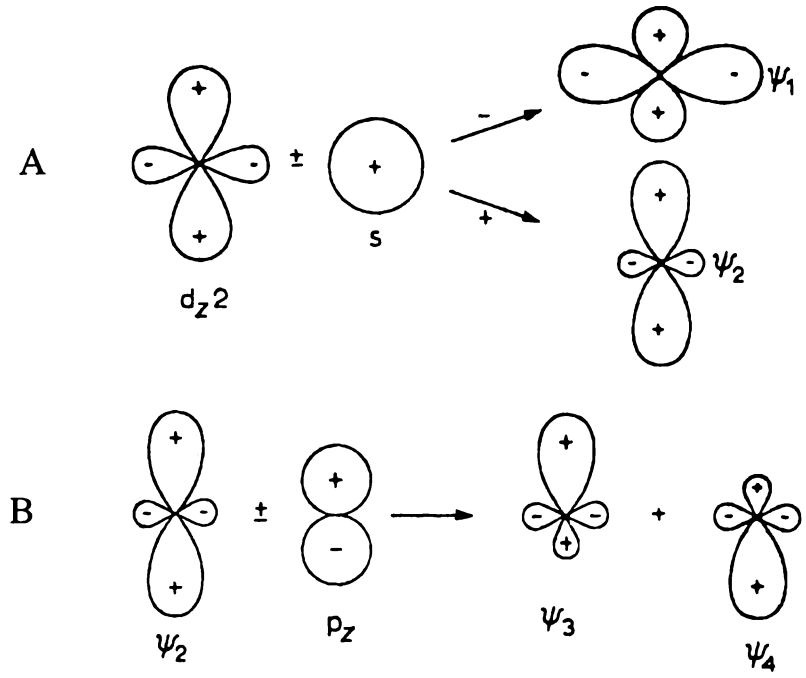

Figure 2·2 Formation of gold(I) linear complexes

Gold(I) complexes generally take the form of LAuX (L = neutral ligand; X = anionic ligand). The ionic species $[L_2Au]^+$ and $[AuX_2]^-$ have also been observed. These linear complexes are characterised by a strong preference for large polarisable donor atoms. This is consistent with the perception that the gold(I) ion is a particularly soft Lewis acid and forms strong associations with soft Lewis bases.[8]

It is evident that gold(I) is a soft (class b) metal ion by comparing the stability of various gold(I) complexes. An obvious trait is the behaviour of gold(I) in the presence of ligands with dual coordination modes, for example NCO acts as a nitrogen donor ligand and SCN is bound by the sulphur atom.[34] A striking case is the acac anion,[35] which coordinates to nearly all the transition metal ions as a bi-dentate oxygen donor ligand. Acac coordinates to gold(I) by way of the central carbon atom.[36]

---

[34] Ref. 5, pp. 22-24.
[35] A. N. Nesmeyanov, E. G. Perevalova, Y. T. Struchkov, M. Y. Antipin, K. I. Grandberg and V. P. Dyadchenko, *J. Organomet. Chem.*, 1980, **201**, 343.
[36] D. Gibson, *Coord. Chem. Rev.*, 1969, **4**, 225.

Gold(I) phosphine complexes of the type $(R_3P)AuX$ have been characterised extensively. Thiol (R_2S) and isonitrile (RNC) complexes are reasonably well documented but examples of amine and nitrile gold(I) species are relatively uncommon.[37] This trend is a general reflection on the stability afforded to the gold(I) centre by the neutral ligand. Gold(I) complexes are usually prepared (in the first instance) by treating the tetrachloroaurate ion $[AuCl_4]^-$ with oxidisable ligands, for example, R_3P, R_2S or RNC. The reaction generally proceeds by way of reductive elimination of a neutral $LAuCl_3$ intermediate. Expeditious ligand exchange reactions are often utilised which improve overall yields, for example:

$$\mathbf{(Me_2S)AuCl + Ph_3P \rightarrow Me_2S + (Ph_3P)AuCl}$$

A range of anions have been characterised for LAuX and $[AuX_2]^-$ complexes, with the halides (excluding fluoride) and CN being prevalent. Oxygen donor anions are particularly uncommon and the few examples structurally characterised have invariably been isolated with stabilising phosphine ligands.[38] Complexes containing gold(I)-oxygen bonds are of low thermal stability and decompose readily to metallic gold. They are useful synthetic intermediates with their reactions based on the displacement of the oxygen-donor ligand by ligands with greater affinity for gold.[39]

2·1·3 Gold(III)

The majority of gold(III) complexes are square planar species that are consistent with $5d_{X2-y2}$, $6s$, $6p_X$ and $6p_Y$ hybridisation. A common example is $[AuCl_4]^-$. This complex is a convenient starting point for the preparation of both gold(III) and, by way of reduction in the presence of coordinating ligands, gold(I) complexes. The reduction of $[AuCl_4]^-$ under appropriate conditions may provide highly coloured solutions of colloidal metallic gold. $[AuCl_4]^-$ is commonly procured in the form of hydrated crystals of tetrachloroauric acid, $HAuCl_4 \cdot nH_2O$, which are obtained by evaporation of an *aqua regia* solution of gold.

---

[37] See for example: P. G. Jones and B. Ahrens, *Chem. Ber.*, 1997, **130**, 1813; J. Yau and D. M. Mingos, *J. Chem. Soc., Dalton Trans.*, 1997, 1103.
[38] Ref. 5, p. 58.
[39] R.V. Parish, *Gold Bull.*, 1997, **30**, 55.

Gold(III) is also a soft (class b) metal ion. Based on a higher charge, it is more likely to associate with non-polarisable ligands than gold(I), hence forming complexes with a wider range of ligands. However, substitution reactions of both gold(I) and gold(III) complexes are characterised by the replacement of a ligand with one of greater polarisability. To achieve the opposite a driving force is required, for example the precipitation of an insoluble salt:

$$(Me_2AuI)_2 + 2Tl(acac) \rightarrow 2TlI\ (s) + 2Me_2Au(acac)$$

In this case the acac ligand is coordinated by way of the conventional oxygen bonding mode.[40] Addition of R_3P to solutions of $Me_2Au(acac)$ results in the formation $(R_3P)Me_2Au(acac)$, which exhibits carbon-bonded acac similar to that found in (Ph_3P)Au-acac.[41]

Characterised gold(III)-oxygen bonds are prevalent compared with the gold(I) oxidation state, although they are not particularly numerous. $[Au(OH)_4]^-$ is formed by the treatment of $[AuCl_4]^-$ (aq) with OH^- (aq) and this can be dehydrated to give Au_2O_3. The hydroxide is sparingly soluble in strong acid but there is no evidence for the formation of the $[Au(OH_2)_4]^{3+}$ ion.[42] The air- and moisture-sensitive $[Au(NO_3)_4]^-$ anion has been characterised as a potassium salt and exhibits mono-dentate nitrate ligands.[43] Few organo-gold(III) complexes containing oxo-anionic ligands are known; those that have been characterised are usually unstable, for example dry $[Me_2Au(OH)]_4$ detonates by touching.[44]

2·1·4 Organo-gold chemistry

"*...gold has no affinity for carbon. Complex organic compounds of gold in which gold is directly attached to carbon are incapable of existence, or at least cannot be isolated.*"[45]

Considering this early appraisal, organo-gold chemistry has made significant progress. In fact, the gold-carbon bond is of relatively high stability and alkyl derivatives of gold were among the first organometallic compounds to be prepared.[46]

---

[40] S. Shibata, K. Lijima and T. H. Baum, *J. Chem. Soc., Dalton Trans.*, 1990, 1519.
[41] S. Komiya and J. K. Kochi, *J. Am. Chem. Soc.*, 1977, **99**, 3695.
[42] Ref. 5, p. 38.
[43] Ref. 5, p. 85.
[44] J. Vicente, M. D. Bermudez, F. J. Carrion and P. G. Jones, *J. Organomet. Chem.*, 1996, **508**, 53.
[45] A. Feldt, *Klin. Wochenschr.*, 1926, **5**, 299; cited in ref. 46.
[46] G. K. Anderson, *Advan. Organomet. Chem.*, 1983, **20**, 39.

A mono-anionic alkyl group (R) is relatively polarisable, thus is expected to have affinity for gold.[6] Two-electron donor, σ-bonded alkyl ligands are difficult to replace once attached to gold ions but they exert a strong *trans*-influence. Gold(III) compounds with two R groups opposite each other are therefore reactive, with $[AuR_4]^-$ and $[AuR_2]^-$ complexes being particularly unstable.[39]

Transmetallation reactions are often used in the production of organo-gold complexes. Gold-halide bonds are easily broken by the action of Grignard or organo-lithium alkyl transfer reagents, for example the reaction of LiPh with $(Ph_3P)AuCl$ provides $(Ph_3P)AuPh$. With auric halides the favoured product is $Au_2X_2R_4$ with excess alkylating agent often resulting in $[AuR_4]^-$ or $[AuR_3X]^-$ species.[39]

Carbon-bonded ligands other than alkyls are important in the coordination chemistry of gold. CO is weakly ligated in the unstable (OC)AuCl complex in which the carbonyl stretching frequency is similar to that of free CO. This indicates that the back-bonding from gold(I) is insignificant.[47] The typical reaction of (OC)AuCl is the displacement of the CO ligand. In contrast, RNC and CN form relatively strong associations with gold ions. This is a result of their stronger Lewis acid properties with less reliance on π-acceptance. The coordination of RNC ligands invariably results in an increase in the C≡N stretching frequency, a consequence of σ-donation to the gold centre of a lone pair which is anti-bonding with respect to the C≡N bond.[48]

Alkene and alkyne complexes of gold are known,[49] both σ-bonding (see Figures 2·10 and 3·42 for examples of gold(I) alkynyl complexes of the type LAuC≡CR) and η^2 coordination (see Figure 2·27) having been characterised.

The recent expansion of organo-gold chemistry has been rapid, particularly in the development of practical applications. Many organo-gold complexes are quite volatile and are used as precursors for chemical vapour deposition (CVD) of metallic gold films. Organo-gold compounds are also used as medicinal agents and have exhibited interesting physical properties such as luminescence, liquid crystalline phases and the ability to form one-dimensional rod polymers.[50]

---

[47] Ch. Elschenbroich and A. Salzer, *Organometallics*, VCH, Weinheim, 2nd edn., 1992, pp. 180-181.
[48] P. M. Treichel, *Adv. Organomet. Chem.*, 1973, **11**, 21.
[49] Ref. 5, pp. 148-151.
[50] R. V. Parish, *Gold Bull.*, 1998, **31**, 14.

2·2 AURIOPHILICITY

An intriguing aspect of gold(I) chemistry is the observation of close Au--Au contacts in the solid state, which are indicative of attractive interactions. This phenomenon has been termed auriophilicity. A wealth of structural evidence for auriophilicity has been published in recent literature, which includes the often remarkable consequences for crystal packing.[23]

This section outlines the topic of auriophilicity, with emphasis on intermolecular aggregation of mono-nuclear complexes. Initially, the theoretical treatment of Au--Au interactions is discussed. Examples are then described which provide insight to the factors which influence auriophilicity.

2·2·1 General

Classical theories of chemical bonding cannot provide a sound explanation for auriophilic Au--Au interactions.[51] It would normally be expected that two gold(I) centres would repel each other on close contact.[52] Schmidbaur has described the phenomenon as the *"..the unprecedented affinity between gold(I) atoms even with 'closed shell' electron configurations and equivalent electrical charges."*[53] The existence of Au--Au contacts has been established by crystallographic analysis of gold(I) complexes. Attempting to rationalise a sound theoretical basis for this complicated phenomenon has proven to be a formidable, yet fascinating, task.

Some comparisons have been drawn between the pseudo-halogen character of gold and the ability of halogens to form short attractive halogen--halogen contacts in the solid state.[10] The pseudo-halogen nature of gold is evidenced by relatively high electronegativity, the formation of Au_2 (g) dimers and the metallic atoms being one electron short of the closed shell $5d^{10}6s^2$ configuration.§ However, this analogy does not provide a satisfactory explanation for the attraction between d^{10} gold(I) centres.

Theoretical models of inorganic chemistry recognised that gold(I) has the formal electron configuration of [Xe]$4f^{14}5d^{10}6s^06p^0$. Attractive Au--Au contacts have been interpreted as donation of electron density from filled *d*-orbitals on one metal centre to empty *p*-orbitals on another.[19]

---

[51] P. Pyykkö and F. Mendizabel, *Chem. Eur. J.*, 1997, **3**, 1458.
[52] P. Pyykkö, J. Li and N. Runeberg, *Chem. Phys. Lett.*, 1994, **218**, 133.
[53] H. Schmidbaur, *Gold Bull.*, 1990, **23**, 11.
§ The halogens are also one electron short of a closed-shell configuration.

More advanced calculations have accounted for the influence of relativity on the orbitals of the large gold(I) nucleus. Hence, the energy gap between the 6*s*, 6*p* and 5*d* orbitals is diminished, allowing significant hybridisation.[54] Resulting hybrid orbitals have been proposed to give electron cloud overlap in the xy plane, resulting in auriophilic interactions orthogonal to the linear molecules.[55]

Pyykkö has proposed that electron correlation effects (rather than hybridisation) are the basis for the auriophilic attraction, such that relativistic effects act only to enhance.[56] This form of interaction involves the instantaneous positioning of electrons on one gold atom which induce polarisation of electrons on an adjacent atom.[57] Thus, instantaneous interactions occur which, when time averaged, result in auriophilic contacts.

2·2·2 Au--Au distances

The gaseous Au_2 dimer has a bond length of 2·47 Å with a bond dissociation energy of 288 kJ mol^{-1}. This is likely to represent the shortest distance possible between two gold atoms. The inter-atom distance in bulk metallic gold is 2·88 Å with a bond energy in the order of 100 kJ mol^{-1}. Intermolecular Au--Au interaction distances of greater than 3·0 Å are associated with energy of ~30 kJ mol^{-1}, which is comparable to that of hydrogen bonding.[19]

Gold contacts are thought to be energetically insignificant only when the distance exceeds 3·6 Å,[19] this distance being twice that of the estimated van der Waals radii of gold(I). However, the Cambridge Crystallographic Files exhibit Au--Au contact distances up to 4·0 Å[10] and some crystal structures indicate that contacts of ~3·8 Å may influence molecular packing.[58]

Given the inherent Au--Au attraction, the actual strength of the intermolecular interactions is influenced by the steric bulk of the ligands. The electronic influence of coordinated ligands is not as simple to define.

---

[54] Y. Jiang, S. Alvarez and R. Hoffmann, *Inorg. Chem.*, 1985, **24**, 749.
[55] L. F. Veiros and M. J. Calhorda, *J. Organomet. Chem.*, 1996, **510**, 71.
[56] P. Pyykkö and Y. Zhao, *Angew. Chem. Int. Ed. Engl.*, 1991, **30**, 604.
[57] Ref. 7, p. 914.
[58] M. J. Irwin, L. Manojlovic-Muir, K. W. Muir, R. J. Puddephatt and D. S. Yufit, *J. Chem. Soc., Chem. Commun.*, 1997, 219.

Pyykkö has carried out extensive theoretical calculations on Au--Au interactions in a series of hypothetical $(H_3P)AuX$ dimers and concluded that polarisable anions result in a stronger Au--Au attraction.[59] The theoretical conclusions of Pyykkö are supported by the general supposition that polarisable ligands reduce the residual positive charge on the gold centres and will hence diminish electrostatic repulsion.[19] However, experimental observation (which is described in the following sub-section) remains inconclusive.

2·2·3 LAuX crystallography

The structural data available for LAuX complexes show that Au--Au interactions are ubiquitous in the solid phase of these compounds and may promote the formation of a supramolecular crystal structure.[60] The following four aspects of intermolecular auriophilicity have been used whilst describing LAuX crystal structures:

(i) The interaction mode

The aggregation of LAuX complexes generally involves one of three principal modes (Figure 2·3).[61] On rare occasions, combinations of these modes are observed in a single structure. A is described as an anti-parallel interaction with a head-to-tail ligand arrangement. B is an interaction with crossed ligands which are not necessarily perpendicular. C is an anti-parallel interaction (with a head-to-head ligand arrangement).

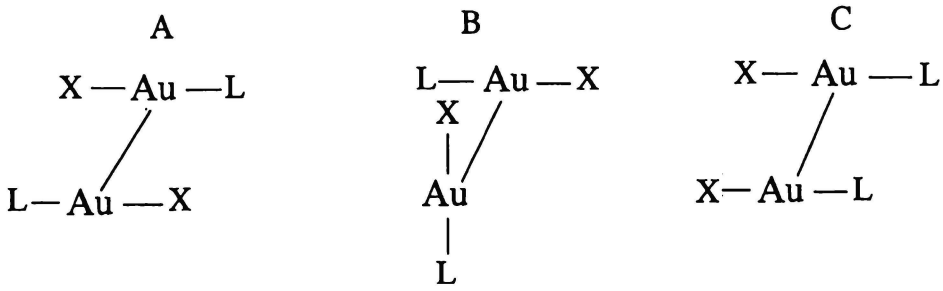

Figure 2·3 Interaction modes of LAuX aggregation

[59] P. Pyykkö, N. Runeberg and F. Mendizabal, *Chem. Eur. J.*, 1997, **3**, 1451.
[60] P. Pyykkö and F. Mendizabel, *Inorg. Chem.*, 1998, **37**, 3018; and refs. therein.
[61] W. Schneider, K. Angermaier, A. Sladek and H. Schmidbaur, *Z. Naturforsch.*, 1996, **51b**, 790.

(ii) The degree of polymerisation

LAuX molecules can form dimers, oligomers, chain polymers and sheets. The degree of polymerisation is determined by a number of factors, although the steric size of the ligands is the prevalent influence.[61] Large ligands, for example Ph_3P, tend to preclude the formation of Au--Au contacts completely.[62]

(iii) The auriophilic coordination number

This is closely linked to the degree of polymerisation and can be defined as the number of Au--Au interactions that any particular gold(I) centre makes.[63] Small ligands generally allow greater connectivity between gold(I) centres.

(iv) The Au--Au intermolecular distance

This provides a general guide to the attraction two gold(I) centres have for each other, shorter distances indicating a stronger interaction. Crossed ligand dimers of LAuX molecules often have relatively short Au--Au contacts, as steric repulsion between the ligands is minimised and each gold(I) centre forms only one interaction. More extensive aggregates exhibit higher auriophilic coordination numbers but the Au--Au contacts tend to be longer.

All four of these concepts are discussed with the following reported cases of intermolecular LAuX aggregation. Further examples from the literature are provided in Chapter Three, where they provide direct comparison with the novel structures presented therein.

(1,3,5-triaza-7-phosphaadamantane)AuX (X = Cl or Br) have been characterised as isostructural dimeric 'crossed lollipops' (Figure 2·4).[64] The relatively short intermolecular Au--Au distances are 3·092 Å and 3.107 Å respectively, which does not support the theory of soft anions enhancing the Au--Au attraction.

---

[62] S. Ahrland, K. Dreisch, B. Noren and Å. Oskarsson, *Acta Chem. Scand.*, 1987, **41a**, 173.
[63] J. Vicente, M.-T. Chicote, M.-D. Abrisqueta, R. Guerrero and P. G. Jones, *Angew. Chem. Int. Ed. Engl.*, 1997, **36**, 1203.
[64] Z. Assefa, B. G. McBurnett, R. J. Staples, J. P. Fackler Jr., B. Assmann, K. Angermaier and H. Schmidbaur, *Inorg. Chem.*, 1995, **34**, 75.

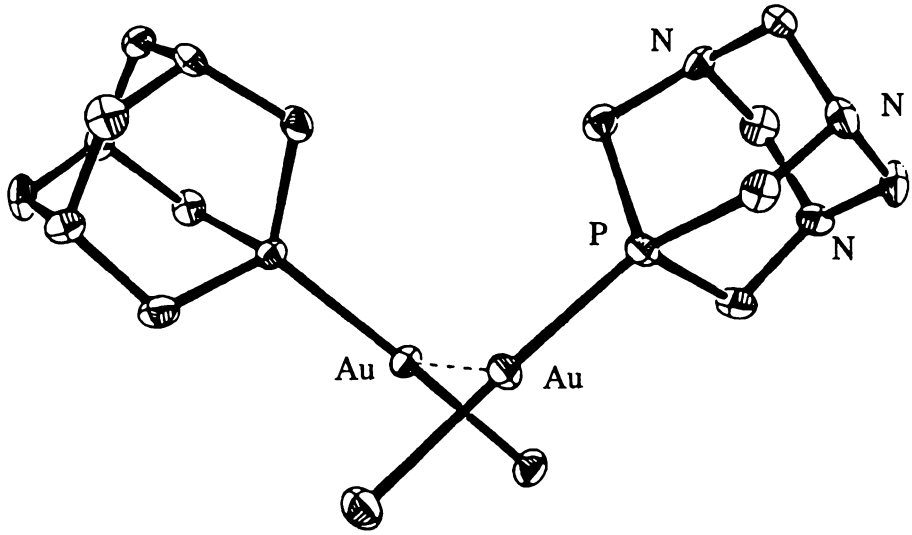

Figure 2·4 (1,3,5-triaza-7-phosphaadamantane)AuCl dimer

The series of (Me_2PhP)AuX (X = Cl, Br or I) crystal structures have been characterised, each forming a crossed dimer (Figure 2·5).[65] The Au--Au contact distances are 3·23 Å, 3·12 Å and 3·10 Å respectively, supporting the results of Pyykkö's theoretical calculations.

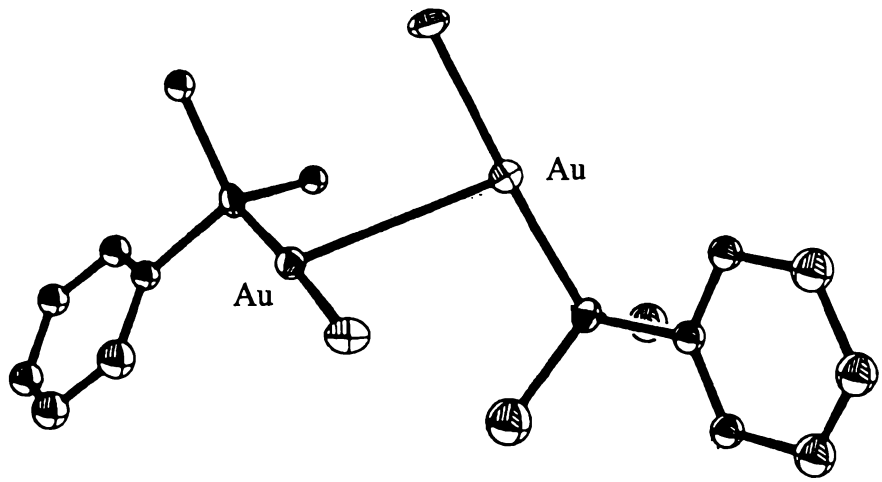

Figure 2·5 (Me_2PhP)AuCl dimer

[65] D. V. Toronto, B. Weissbart, D. S. Tinti and A. L. Balch, *Inorg. Chem.*, 1996, **35**, 2484.

In addition, trimeric (Me_2PhP)AuCl was obtained as a rare auriophilic polymorph.

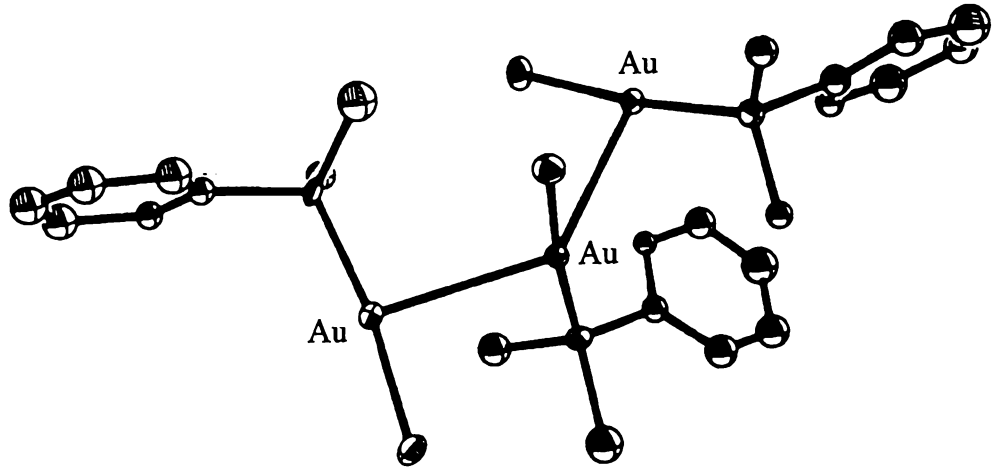

Figure 2·6 (Me_2PhP)AuCl trimer

The (Me_3P)AuX (X = Cl, Br or CN) complexes have been found to crystallise as isostructural polymeric chains with the crossed ligands forming approximate helices. The structures are depicted in Figures 2·7, 3·17 and 2·8 respectively and the Au--Au contact distances of each is listed in Table 2·1.

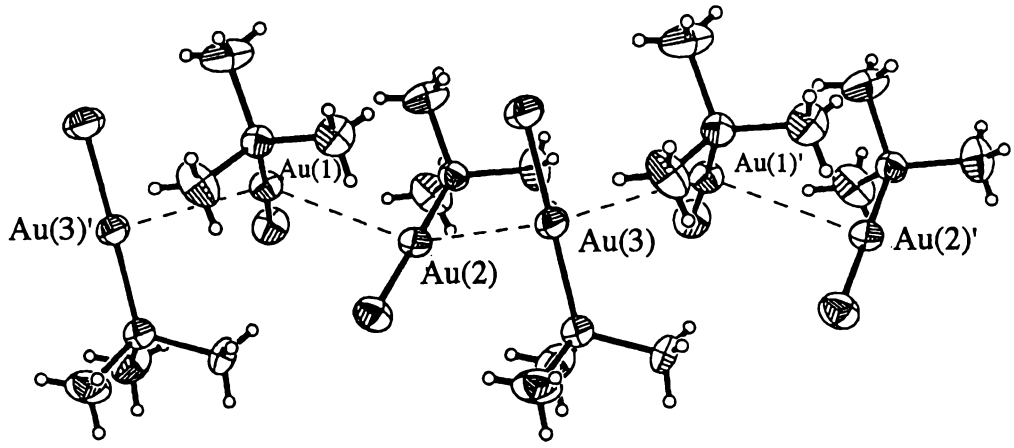

Figure 2·7 Chain of (Me_3P)AuCl molecules

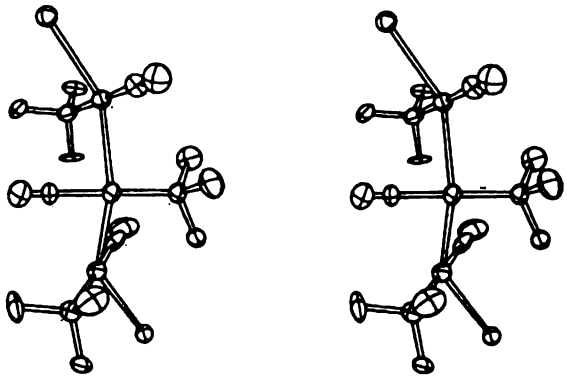

Figure 2·8 Stereoview of $(Me_3P)AuCN$ crystal packing

Table 2·1 Au--Au distances in $(Me_3P)AuX$ complexes

	Au(1)-Au(2)	Au(2)-Au(3)	Au(3)-Au(1)'	Mean Au--Au
$(Me_3P)AuCl$[66]	3·356(1)	3·271(1)	3·386(1)	3·34
$(Me_3P)AuBr$[67]	3·648(1)	3·548(2)	3·980(2)	3.73
$(Me_3P)AuCN$[68]	3·320(2)	3·236(2)	3·312(1)	3.29

The data in Table 2·1 does not support the theory of soft ligands promoting the auriophilic attraction,[67] which would have predicted a decrease in the Au--Au distance in the order Cl>Br>CN. The size of the anion appears to correlate more logically with the observed Au--Au contact distances. It was noted that $(Me_3P)AuBr$ appeared to be broken into a series of trimers with a long Au(1)'--Au(3) distance.[67] $(Me_3P)AuI$ relinquishes the polymeric structure completely and exhibits a dimer with a single crossed Au--Au interaction of 3·168 Å (Figure 2·9).[62] The short distance of this dimer does not indicate that the iodide has enhanced the Au--Au interaction, as the dimeric structure cannot be compared with the helical chain polymer.

[66] K. Angermaier, E. Zeller and H. Schmidbaur, *J. Organomet. Chem.*, 1994, **472**, 371.
[67] K. Angermair, G. A. Bowmaker, E. N. de Silva, P. C. Healy, B. E. Jones and H. Schmidbaur, *J. Chem. Soc., Dalton Trans.*, 1996, 3121.
[68] S. Ahrland, B. Aurivillius, K. Dreisch, B. Noren and Å. Oskarsson, *Acta Chem. Scand.*, 1992, **46a**, 262.

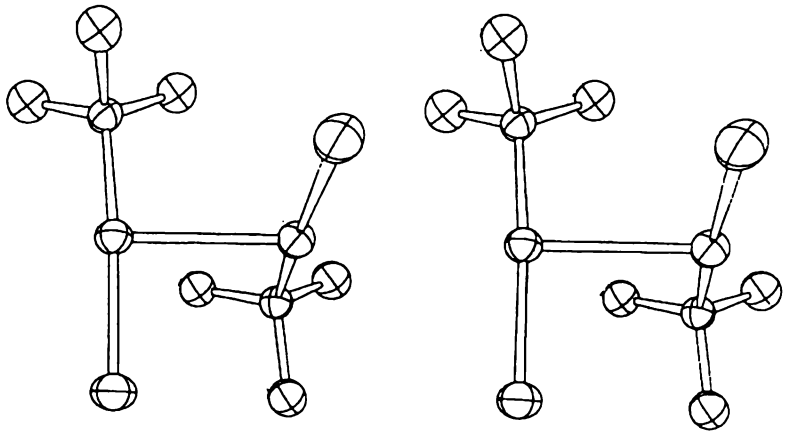

Figure 2·9 Stereoview of the $(Me_3P)AuI$ dimer

$(R_3P)AuX$ complexes are a commonly studied LAuX species but the auriophilic structures of (RNC)AuX have received some attention. $(HC{\equiv}CC_6H_3(3\text{-}Me)\text{-}4\text{-}NC)AuC{\equiv}CBu^t$ has been structurally characterised (Figure 2·10).[69] The apparent distortion of the molecules from true linearity was proposed to be due to counterbalancing of the auriophilic attraction (Au--Au 3·479(2) Å) with steric congestion of the adjacent Bu^t and aryl groups.

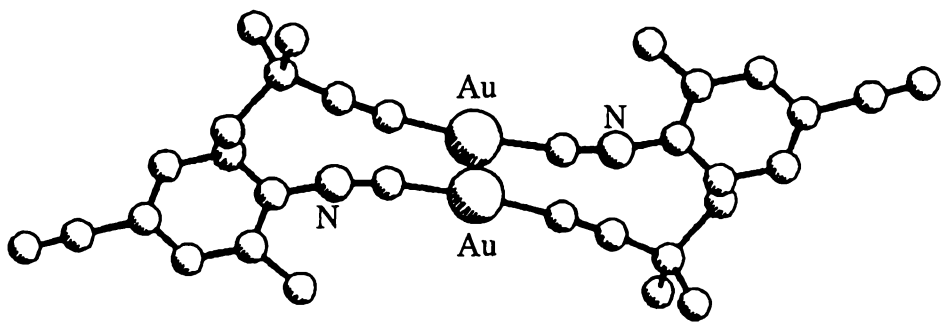

Figure 2·10 Crystal packing of $(H\text{-}C{\equiv}CC_6H_3(3\text{-}Me)\text{-}4\text{-}NC)AuC{\equiv}CBu^t$

The supramolecular structure of several (RNC)AuX complexes was recently reported.[61] For the (PhNC)AuX series (X = Cl, Br or I), polymeric zig-zag chains were formed.

---

[69] G. Jia, N. C. Payne, J. J. Vittal, R. J. Puddephatt, *Organometallics*, 1993, **12**, 4771.

The Au--Au distances increase in the order Cl<Br<I, which is contrary to the general theory of Pyykkö. The structure of (PhNC)AuCl is depicted in Figure 2·11 (Au--Au' 3·463 Å). The molecular packing of the bromide (Figure 2·12) and iodide homologues is isostructural. This structure may contain face-to-edge aromatic ring interactions, in addition to the long Au--Au contacts (mean Au--Au distances: X = Br, 3·59 Å; X = I, 3·77 Å).

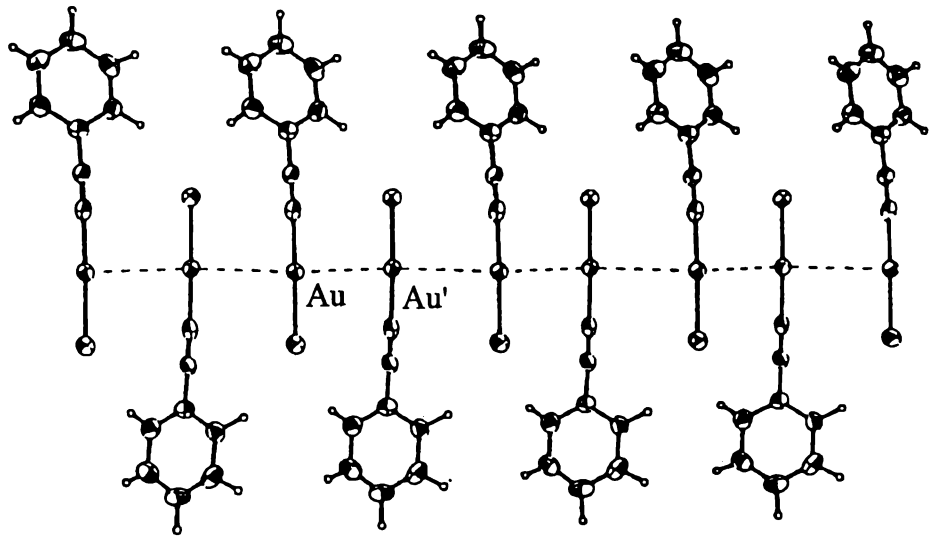

Figure 2·11 Anti-parallel zig-zag chain of (PhNC)AuCl

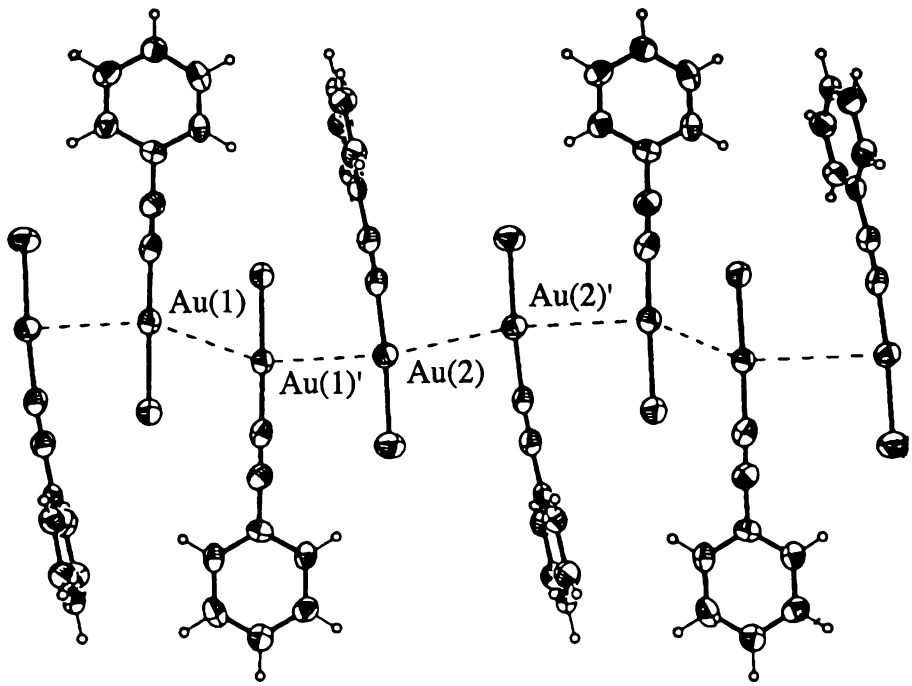

Figure 2·12 Anti-parallel zig-zag chain of (PhNC)AuX (X = Br or I)

$(MeOC(O)CH_2NC)AuX$ (X = Cl or Br) form sheet structures with both anti-parallel and crossed ligand interactions (Figure 2·13) and Au--Au contact distances all of ~3·5 Å. $(MeOC(O)CH_2NC)AuI$ exhibits a crossed ligand structure (Figure 2·14),[61] which avoids possible repulsion between the large iodide ion and the adjacent isonitrile ligand. The Au--Au contact of this dimer is 3·191(1) Å.

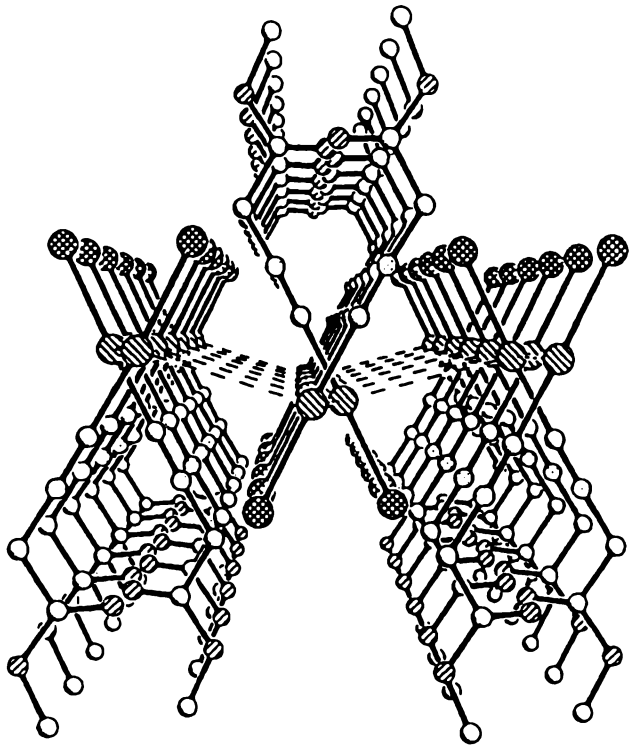

Figure 2·13 Sheet structure of $(MeOC(O)CH_2NC)AuX$ (X = Cl or Br)

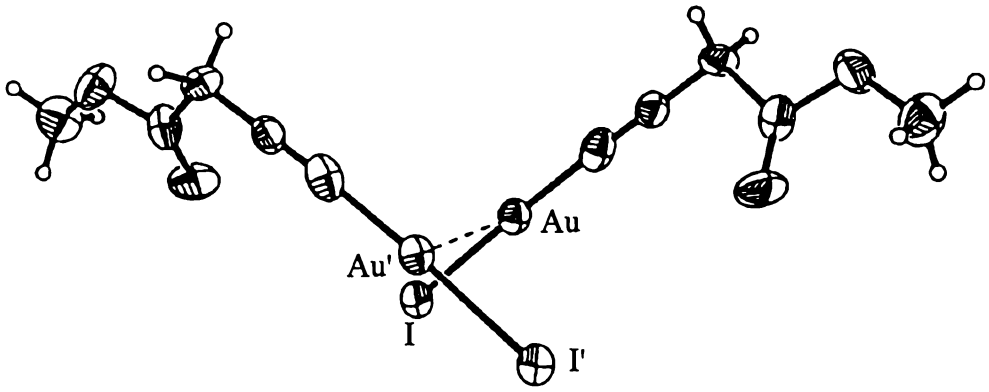

Figure 2·14 Dimer of $(MeOC(O)CH_2NC)AuI$

Au--Au interactions appear to govern the crystal packing of many small mono-nuclear LAuX complexes. However, interactions between ligands have been recognised. Molecules of $(Ph_2C{=}NH)AuCl$ have been found to crystallise as a zig-zag chain (Figure 2·15). The polymer is based on anti-parallel Au--Au interactions (Au--Au 3·363(1) Å) which are supported by hydrogen bonding between the chloride ligand and the N-H centre (Cl--H 2·57(1) Å) of the coordinated imine.[70] The isomeric $[(Ph_2C{=}NH)_2Au]^+[AuCl_2]^-$ species was also obtained, the crystal structure of which is described in sub-section 2·2·4.

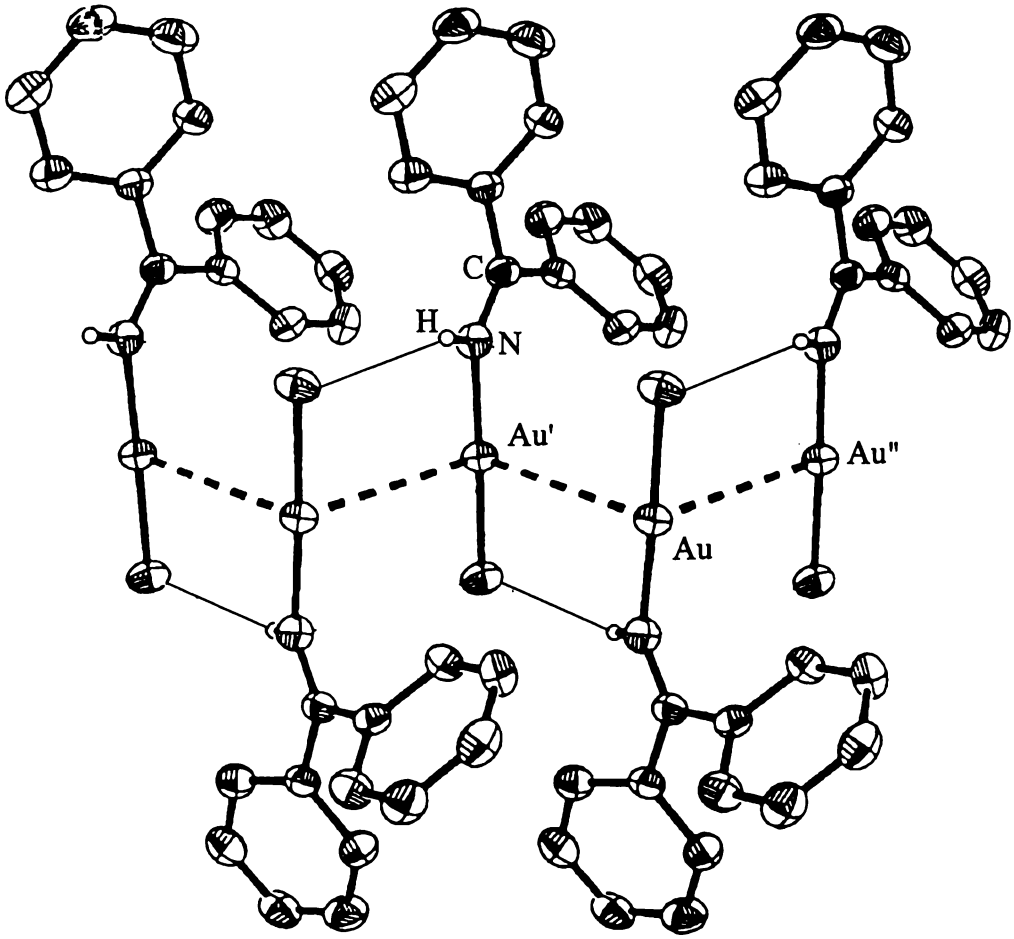

Figure 2·15 Chain of $(Ph_2C{=}NH)AuCl$

Another supramolecular structure based on auriophilicity and hydrogen bonding was observed in the crystal packing of $2\text{-}[(Bu^tNC)AuS]C_6H_4CO_2H$. In this case, the two secondary bonding interactions are completely separate (Figure 2·16), with the tetranuclear units exhibiting alternating Au--Au (3·157(2) Å) and OH--O (1·78(1) Å) contacts.[71]

[70] W. Schneider, A. Bauer and H. Schmidbaur, *J. Chem. Soc., Dalton Trans.*, 1997, 415.
[71] W. Schneider, A. Bauer and H. Schmidbaur, *Organometallics*, 1996, **15**, 5445.

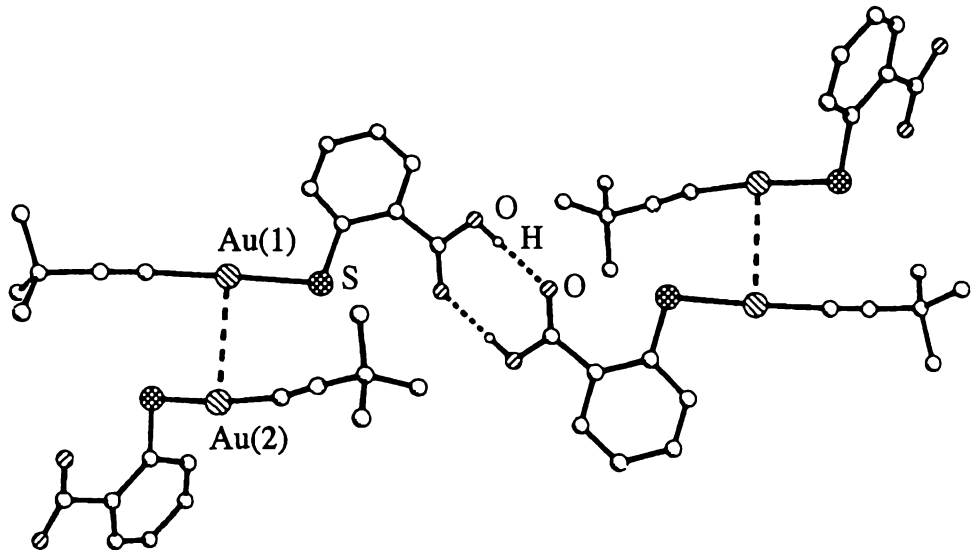

Figure 2·16 Tetranuclear units of 2-[(Bu^{t}NC)AuS]$C_6H_4CO_2H$

The crystal structure of $(Ph_3P)AuSCH_2CO_2H$ does not exhibit Au--Au contacts (Figure 2·17), which can be explained by the presence of the large Ph_3P ligand. The supramolecular array is based instead on hydrogen bonding (OH--O 1.41(3) Å) and Au--S contacts of 3·131 Å.[72]

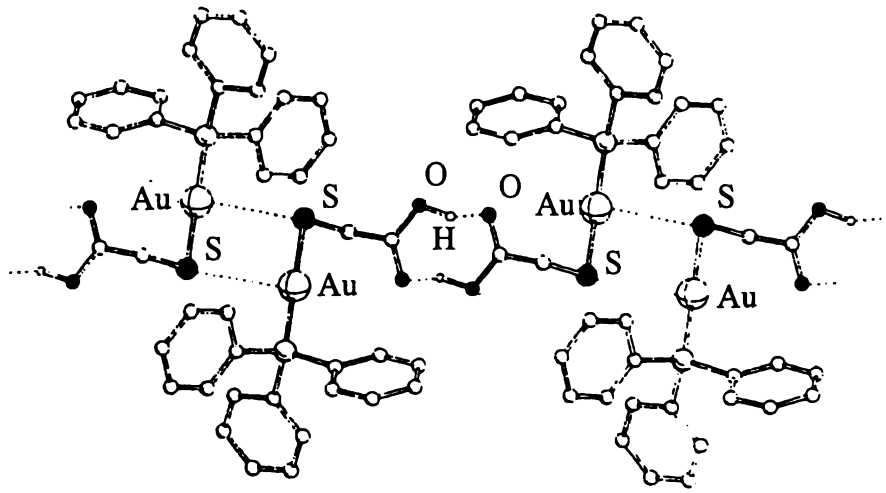

Figure 2·17 Molecular packing of $(Ph_3P)AuSCH_2CO_2H$

[72] P. Bishop, P. Marsh, A. K. Brisdon, B. J. Brisdon and M. F. Mahan, *J. Chem. Soc., Dalton Trans.*, 1998, 675.

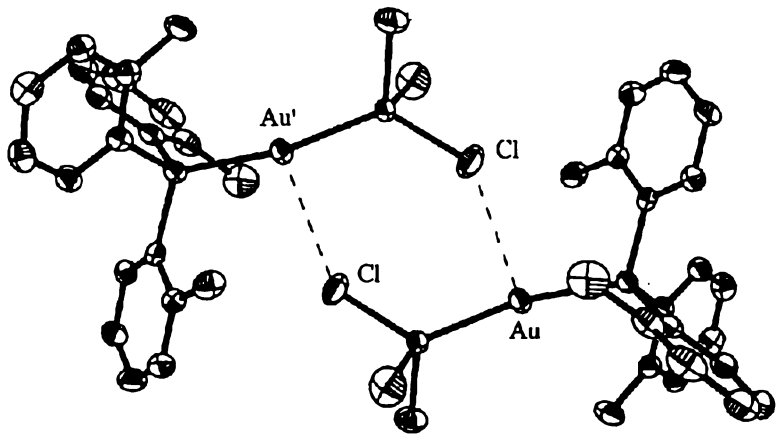

Figure 2·18 Molecular packing (*o*-tolyl$_3$P)AuGeCl$_3$

(*o*-tolyl$_3$P)AuGeCl$_3$ crystallises as a centrosymmetric dimer, based on Au--Cl contacts of 3·299(3) Å (Figure 2·18). It was noted that Au--Cl interactions may gain favour if steric effects make Au--Au contacts unachievable.[73] However, the GeCl$_3$ anion appears to favour the inherent auriophilic interaction as (Ph$_3$P)AuGeCl$_3$ forms a dimeric structure (Figure 2·19) with a very short Au--Au contact of 2·960(1) Å.[74] This appears to be the only (Ph$_3$P)AuX complex that exhibits Au--Au contacts in the solid state.

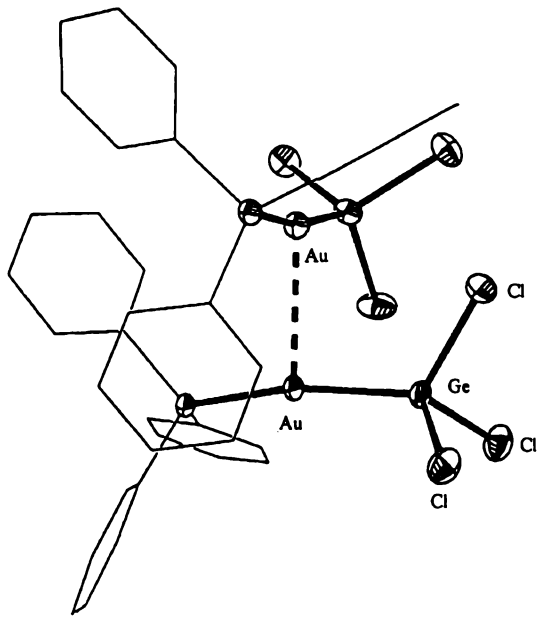

Figure 2·19 Dimer of (Ph$_3$P)AuGeCl$_3$

[73] A. Bauer and H. Schmidbaur, *J. Am. Chem. Soc.*, 1996, **118**, 5324.
[74] A. Bauer, A. Schier and H. Schmidbaur, *J. Chem. Soc., Dalton Trans.*, 1995, 2919.

2·2·4 $[L_2Au]^+[AuX_2]^-$ structures

The equilibrium $2LAuX \leftrightarrow [L_2Au]^+ + [AuX_2]^-$ is present in the majority of LAuX solutions. In some cases, presumably when a favourable crystal packing structure is available, bis-ligated species will be removed from solution and structures of the type $[L_2Au]^+[AuX_2]^-$ are characterised.[75] $[(Ph_2C{=}NH)_2Au]^+[AuCl_2]^-$ for example, was obtained from a recrystallisation that also afforded $(Ph_2C{=}NH)AuCl$.[70] It exhibits a tetrameric aggregation as illustrated in Figure 2·20.

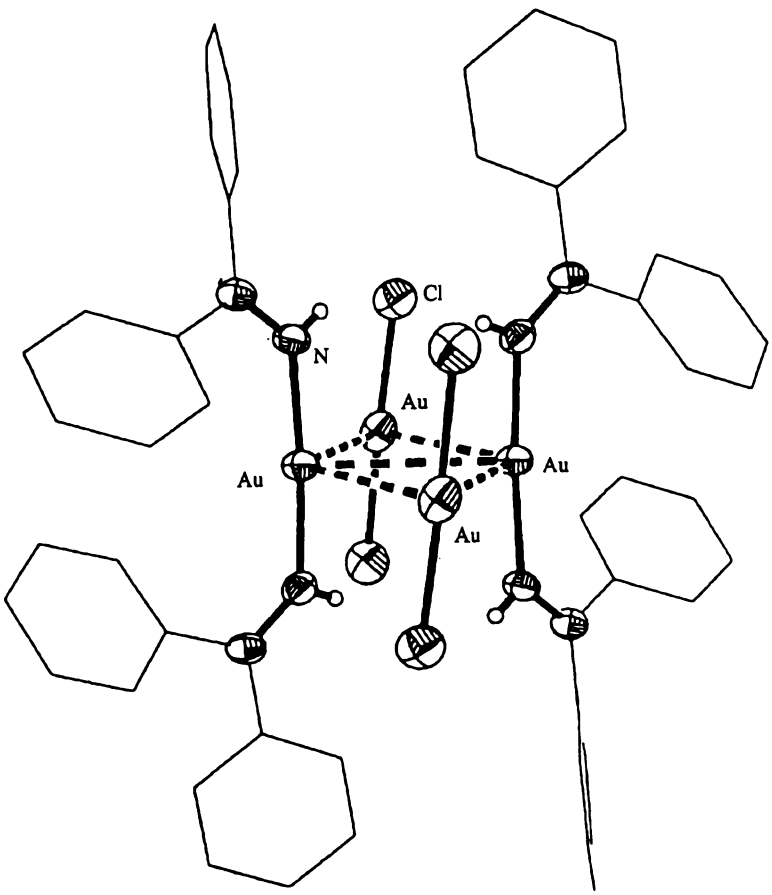

Figure 2·20 Molecular packing of $[(Ph_2C{=}NH)_2Au]^+[AuCl_2]^-$

As depicted in Figure 2·21, a linear chain of gold(I) centres with equidistant spacings was characterised in the ionic crystal structure of $\{[(MesNC)_2Au]^+[Au(GeCl_3)_2]^-\}$.[76] A similar cation-anion sequence, which is influenced by electrostatic forces, was found in the chain structure of $\{[(tetrahydrothiophene)_2Au]^+[AuCl_2]^-\}$.[77]

[75] M. S. Hussain, A. R. Al-Arfaj, M. N. Akhtar and A. A. Isab, *Polyhedron,* 1996, **15**, 2781.
[76] A. Bauer, W. Schneider and H. Schmidbaur, *Inorg. Chem.*, 1997, **36**, 2225.
[77] S. Arhland S. B. Noren and A. Oskarsson, *Inorg. Chem.*, 1985, **24**, 1330.

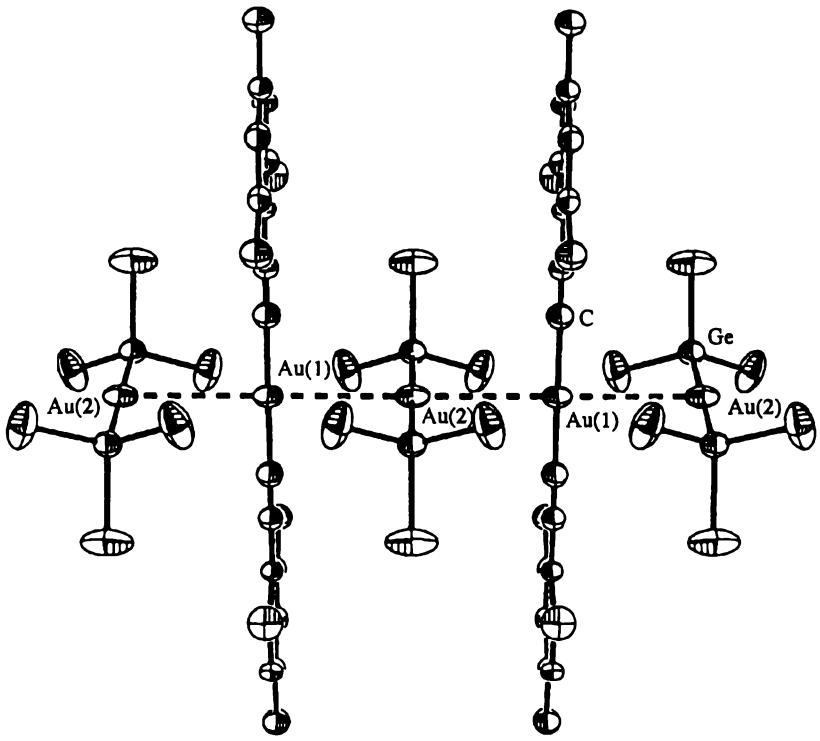

Figure 2·21 Molecular packing of $\{[(MesNC)_2Au]^+[Au(GeCl_3)_2]^-\}$

The $\{[(Me_2PhP)_2Au]^+[Au(GeCl_3)_2]^-\}_2$ tetramer has been characterised which exhibits an ion sequence (+---+) contrary to the rules of coulombic attraction.[73] This structure demonstrated that auriophilicity is able to overcome electrostatic repulsion, indeed a very short Au--Au contact of 2·881(1) Å was characterised between the two central $[Au(GeCl_3)_2]^-$ anions (Figure 2·22).

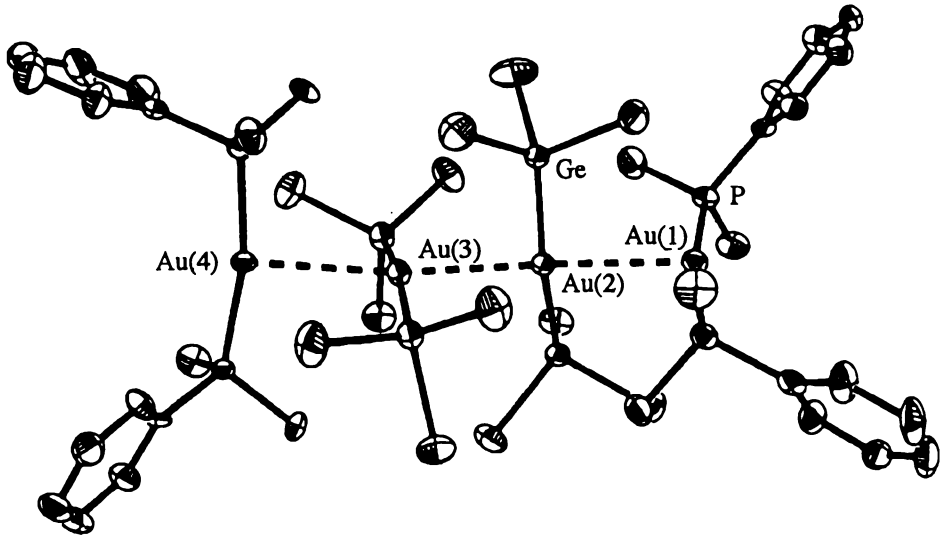

Figure 2·22 Tetramer of $\{[(Me_2PhP)_2Au]^+[Au(GeCl_3)_2]^-\}$

Furthermore, as depicted in Figure 2·23, an ion sequence of (-++-) was observed in the crystal structure of $\{[(pyridine)_2Au]^+[AuI_2]^-\}_2$.[78]

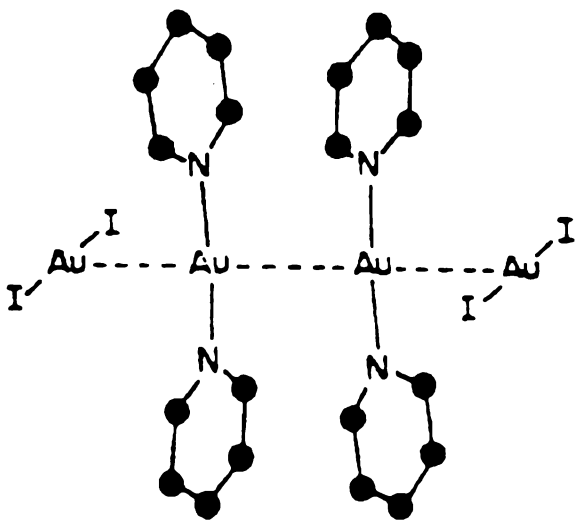

Figure 2·23 Tetramer of $\{[(pyridine)_2Au]^+[AuI_2]^-\}$

2·2·5 Intramolecular auriophilicity

This form of auriophilicity is not directly related to the practical work presented in this thesis but a few illustrative examples will outline some of the remarkable chemistry that has been associated with intramolecular Au--Au contacts.

Homo-nuclear gold clusters are generally stabilised by phosphine ligands,[79] whereas intramolecular Au--Au contacts stabilise a series of hyper-coordinated main group species.[80] These arise from the aggregation of $[(R_3P)Au]$ fragments around a interstitial atom. Their structures are often at variance with classical valence rules.[81] Interested readers are directed to a general review by Schmidbaur from which an example is depicted in Figure 2·24.[8]

---

[78] R. J. Puddephatt, in *Comprehensive Coordination Chemistry*, ed. G. Wilkinson, Pergamon, Oxford, 1987, vol. 5, p. 880; and ref. cited therein.
[79] R. Boca, *J. Chem. Soc., Dalton Tran.*, 1994, 2061.
[80] F. Canales, M. C. Gimeno, A. Laguna and P. G. Jones, *Organometallics*, 1996, **15**, 3412.
[81] F. Canales, M. C. Gimeno, A. Laguna and P. G. Jones, *J. Am. Chem. Soc.*, 1996, **118**, 4839.

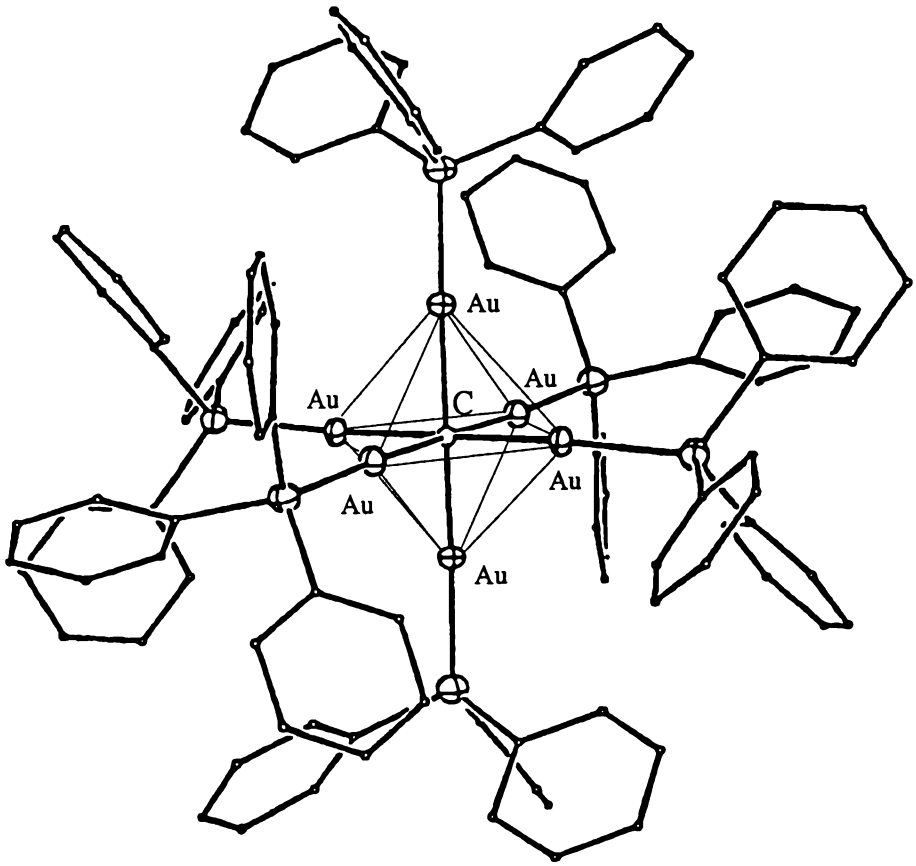

Figure 2·24 Octahedral $\{[(Ph_3P)Au]_6C\}^{2+}$ cluster

Short intramolecular Au--Au contacts are often associated with bridging ligands, for example the structure of $\{Au_2[S_2CN(C_2H_4OMe)_2]_2\}$ has intramolecular Au--Au contacts of 2·790 (1) Å (Figure 2·25).[72] This structure also exhibits intermolecular Au--Au contacts of 3·157 (1) Å.

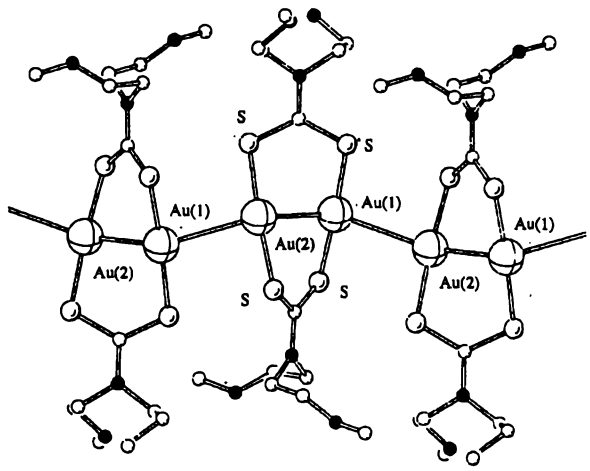

Figure 2·25 Crystal packing of $\{Au_2[S_2CN(C_2H_4OMe)_2]_2\}$

Mixed intra- and intermolecular auriophilicity was also observed in the crystal structure of $[Au_3(MeN{=}COMe)_3]$, in which each gold centre is auriophilic four-coordinate (Figure 2·26). Much of the interest in this complex has focused on the observed solvent-stimulated luminescence.[82]

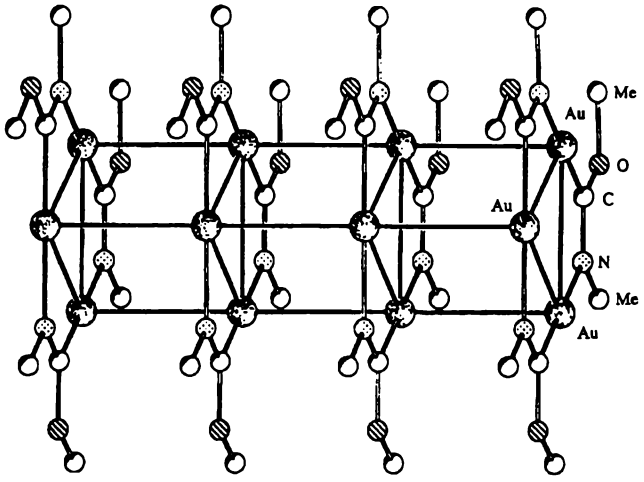

Figure 2·26 Crystal packing of $[Au_3(MeN{=}COMe)_3]$

The crystal structure of $[(AuC{\equiv}CBu^t)_6]_2$ exhibits gold atoms coordinated to $C{\equiv}CBu^t$ ligands in three modes (η^1-η^1, η^1-η^2 and η^2-η^2).[83] This remarkable auriophilic motif features two interlocking hexagonal rings of gold atoms (Figure 2·27), which are stabilised by inter- and intramolecular Au--Au contacts of ~3·3 Å.

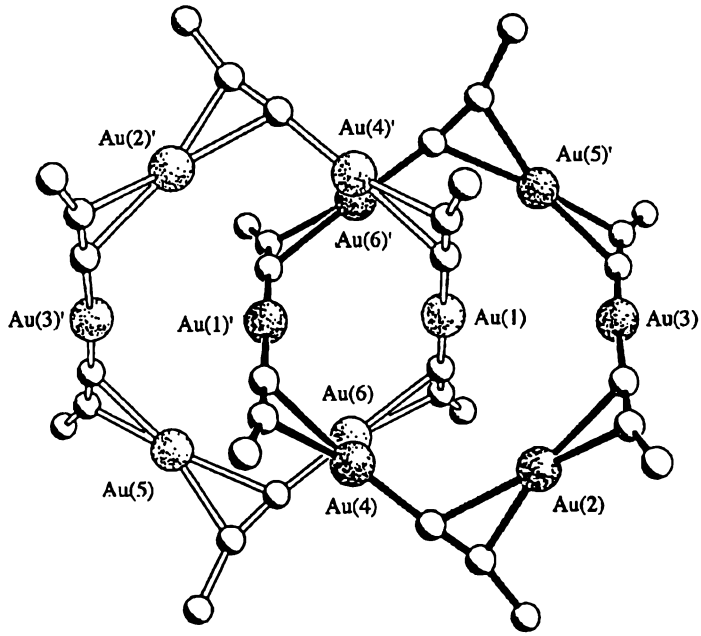

Figure 2·27 Crystal structure of $[Au(C{\equiv}CBu^t)_6]_2$

[82] J. C. Vickery, M. M. Olmstead, E. Y. Fung and A. L. Balch, *Angew. Chem. Int. Ed. Engl.*, 1997, **36**, 1179.

2·2·6 Metallophilicity of d^{10} complexes

Closed shell d^{10}--d^{10} interactions could also occur between copper(I), silver(I) and mercury(II) complexes.[84] Some experimental evidence is emerging, a recent example for copper being the crystal structure of [Cu(1,1'-bis(2-pyridyl)octamethylferrocene)]$^{+}$[$CuCl_2$]$^{-}$ (Figure 2·28).[85] This exhibits a Cu--Cu distance of 2·81 Å, which is approximately twice that of the van der Waal radii of copper(I).[86] Evidence for argentiophilic interactions was discovered in the crystal structure of Tl[$Ag(CN)_2$], which exhibits Ag--Ag contacts of 3·11 Å between the [$Au(CN)_2$]$^{-}$ anions.[87]

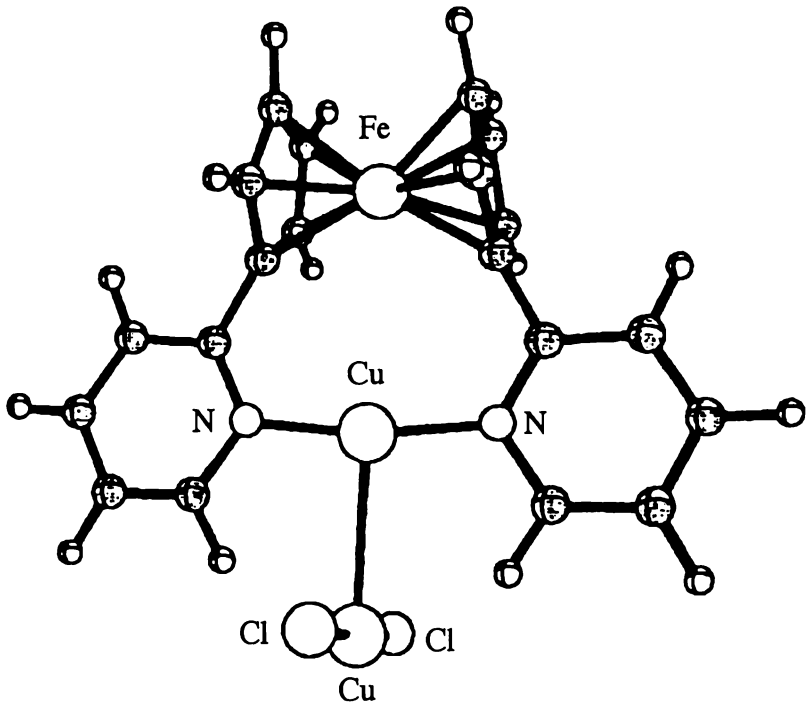

Figure 2·28 Proposed cupriophilic interaction

[83] D. M. Mingos, J. Yau, S. Menzer and D. J. Williams, *Angew. Chem., Int. Ed. Engl.*, 1995, **34**, 1894.
[84] P. Pyykkö, *Chem. Rev.*, 1997, **97**, 597.
[85] J.-M. Poblet and M. Benard, *J. Chem. Soc., Chem. Commun.*, 1998, 1179.
[86] U. Siemeling, U. Vorfeld, B. Neumann and H.-G. Stammler, *J. Chem. Soc., Chem. Commun.*, 1997, 1723.
[87] M. A. Omary, T. R. Webb, Z. Assefa, G. E. Shankle and H. H. Patterson, *Inorg. Chem.*, 1998, **37**, 1380.

The crystal structures of $Hg(C{\equiv}CR)_2$ (R = Ph or $SiMe_3$) have been characterised recently (Figure 2·29).[88] The molecular packing of each appears to be influenced by both Hg--Hg and Hg(II)--η^2 C≡C intermolecular contacts.

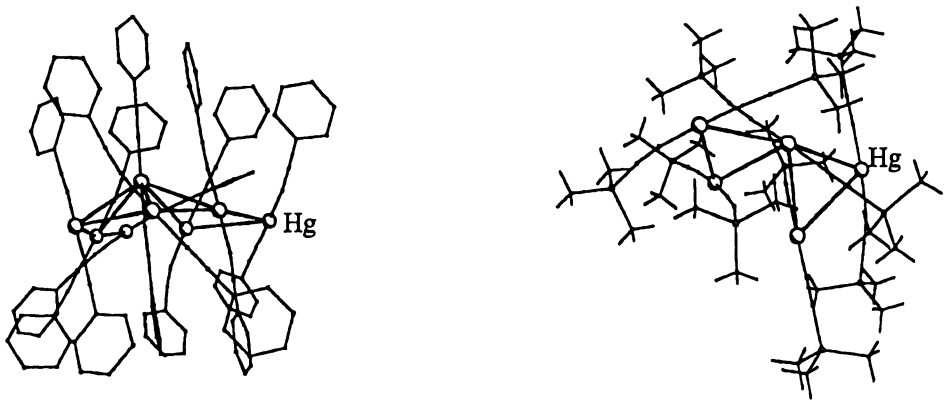

Figure 2·29 Molecular packing of $Hg(C{\equiv}CR)_2$ complexes

Intramolecular hetero-nuclear d^{10} metallophilicity is apparent in the structure of $[Au_4Ag(CH_2SiMe_3)_4(\mu\text{-dppm})_2]^+[SO_3CF_3]^-$, which exhibits four Au-Ag bonds (Figure 2·30), with additional Au--Au contacts.[89]

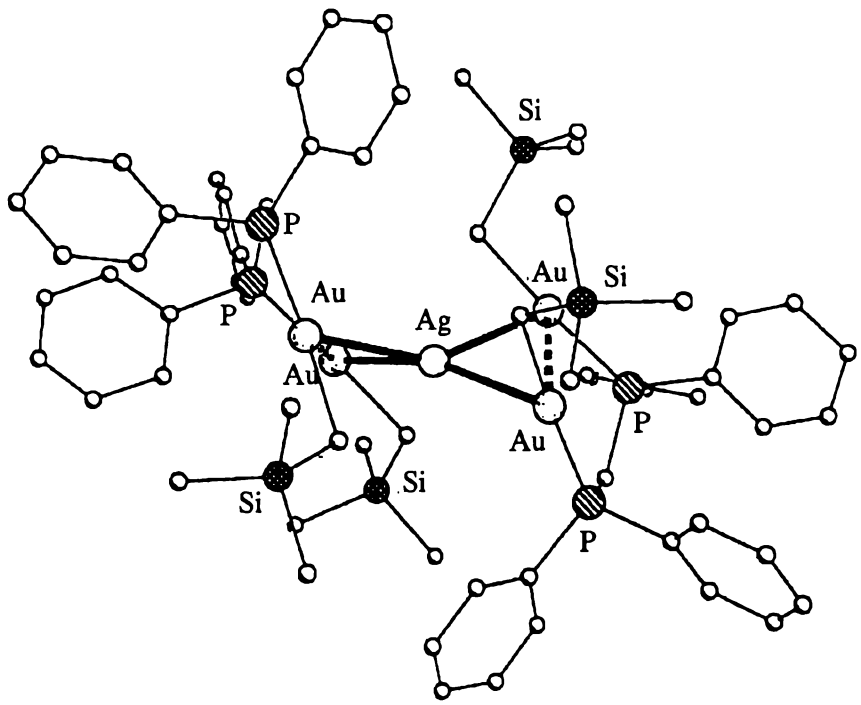

Figure 2·30 $[Au_4Ag(CH_2SiMe_3)_4(\mu\text{-dppm})_2]^+$ cation

[88] S. J. Faville, W. Henderson, T. J. Mathieson and B. K. Nicholson *J. Organomet. Chem.*, submitted for publication.
[89] M. Contel, J. Garrido, M. C. Gimeno and M. Laguna, *J. Chem. Soc., Dalton Trans.*, 1998, 1083.

2·3 SUMMARY

The fascination for (and desire to possess!) metallic gold has influenced the course of history. The widespread use of gold as an economic standard can be attributed to the characteristics of this metal, which include extreme inertness, high cohesive energy and a distinctive appearance. Scientific research has provided some explanation for these properties, in which the relativistic effect is assuming increasing importance.

Linear gold(I) and square planar gold(III) species are ubiquitous in the coordination chemistry of gold, as is the preference for polarisable ligands. Complexes which contain non-polarisable ligands are generally unstable and prone to substitution reactions. This is consistent with gold(I) and gold(III) being classified as soft metal cations. Gold complexes which exhibit gold-oxygen bonds are relatively rare.

In the past, gold has not been regarded to be a useful material for heterogeneous catalysis. Recent advances have been made, particularly when gold is highly dispersed over oxide supports. The development of this form of gold catalyst (which has been shown to be highly active for CO oxidation) is discussed in Chapter Four.

An interesting aspect of the coordination chemistry of gold is the observation of energetically favourable Au(I)--Au(I) contacts, which has been termed auriophilicity. Classical theories of chemical bonding do not account for this form of interaction which has resulted in some extraordinary solid state structures.

Intermolecular Au--Au interactions between mono-nuclear gold complexes (LAuX) are influenced by the properties of the ligands. As the number of characterised crystal structures exhibiting Au--Au contacts increase, a greater understanding of ligand influences will result. This will ultimately lead to predictable structural patterns from which auriophilic crystal structures can be engineered. As a result of specific ligand influences, unprecedented auriophilic structural motifs were characterised in this project. These are discussed in Chapter Three.

CHAPTER THREE

(RNC)AuX COMPLEXES

This Chapter presents a systematic study of (RNC)AuX (R = Bu^t, Et or Xy; X = Cl or NO_3) complexes with emphasis being placed on crystallography.§ Various ligand influences on the inherent Au--Au attraction produced a remarkable set of solid state supramolecular structures. The ligands were selected specifically to allow comparisons to be made with one another and with ligands from previously characterised structures in the literature.

As an archetypical soft cation,[90] gold(I) forms very few complexes with oxygen-donor ligands and those that have been structurally characterised contain a ligated tertiary phosphine.[91] The (RNC)AuNO_3 complexes, which incorporate a standard isonitrile ligand and an η^1 nitrate anion, exhibit the first characterised carbon-gold(I)-oxygen linkage. The syntheses and characterisation of new compounds containing gold(I)-oxygen bonds is of significance, the effect the non-polarisable nitrate anion has on the supramolecular chemistry of (RNC)AuX complexes being of particular interest. It provides appropriate comparison with complexes containing soft anions, which have been thought to enhance auriophilicity.[84]

Discussion in this Chapter gives the impression that the molecular crystal packing is controlled by obvious intermolecular forces, such as Au--Au interactions or π-π aromatic ring stacking. However, it is accepted that multiple factors are involved in the formation of any particular crystal structure, therefore none of the proposed ligand influences are unequivocal. Descriptions, such as 'compressed' chain, do not represent physical processes occurring during crystallisation, rather they assist visualisation and understanding of the characterised structures.

---

§ Including the previously characterised (Bu^{t}NC)AuCl complex.

[90] J. Yau, D. M. P. Mingos, S. Menzer and D. J. Williams, *J. Chem. Soc., Dalton Trans.*, 1995, 2575.

[91] *Cambridge Structural Database*, April 1998 release.

3·1 SYNTHESIS OF RNC AND (RNC)AuX

3·1·1 Preparation of RNC ligands

Caution: Care should be taken to avoid contact with the non-ligated RNC ligands, as they have a particularly repugnant odour and are potentially toxic. The isolation of XyNC (s) in a fumehood is not as imperative as for the liquid Bu^t and Et homologues, but is still recommended.

RNC (R = Bu^t, Et or Xy) were prepared from the corresponding amine (RNH_2) by way of two-phase Hoffman carbene addition.[92]

$$\mathbf{RNH_2 + CHCl_3 + NaOH\ (aq) \rightarrow RNC}$$

Bu^tNC and EtNC were isolated by distillation from the organic phase at 93 °C and 78 °C respectively. Crystalline XyNC was also obtained from the Hoffman reaction by simply allowing the organic phase to evaporate in a fumehood. This was purified by vacuum sublimation providing colourless crystals. Previously, solid isonitriles have been prepared by the dehydration of RNHCHO,[93] but the method utilised in this project appears to be more convenient. The RNC ligands were stored at -25 °C.

3·1·2 Preparation of (RNC)AuCl

$$\mathbf{Au \rightarrow HAuCl_4 \rightarrow [(CH_2)_4S]AuCl \rightarrow (RNC)AuCl}$$

Synthesis of $HAuCl_4 \cdot 3H_2O$

$HAuCl_4 \cdot 3H_2O$ was prepared by dissolving metallic gold in *aqua regia* and removing the excess HNO_3 by evaporation with three portions of additional HCl.[94] The

Synthesis of $[(CH_2)_4S]AuCl$

$$2(CH_2)_4S + HAuCl_4 + H_2O \rightarrow [(CH_2)_4S]AuCl\ (s) + R_2SO + 3HCl$$

$HAuCl_4 \cdot 3H_2O$ (2·221 g, 5·67 mmol) was dissolved in MeOH (20 cm^3). Added dropwise to this stirred solution was $(CH_2)_4S$ (1 cm^3, 11·34 mmol) in MeOH (5 cm^3).[95] This gave rise to a red precipitate which converted quickly to a white precipitate. Stirring was continued for 15 minutes. The precipitate was collected on a fritted glass filter, washed with two 5 cm^3 portions of EtOH and dried under vacuum to provide microcrystalline $[(CH_2)_4S]AuCl$ (1·744 g, 96%). M.p. 120 °C (decomp.). The solid was stored at -25 °C.

Synthesis of $(Bu^tNC)AuCl$

$$[(CH_2)_4S]AuCl + Bu^tNC \rightarrow (Bu^tNC)AuCl + (CH_2)_4S$$

$[(CH_2)_4S]AuCl$ (1·744 g, 5·45 mmol) was dissolved in CH_2Cl_2 (30 cm^3). Added dropwise to this stirred solution was Bu^tNC (1 cm^3) in CH_2Cl_2 (5 cm^3).[96] The clear solution was filtered after 20 minutes and evaporated under vacuum affording microcrystalline $(Bu^tNC)AuCl$ (1·591 g, 93%). M.p. 164 °C (decomp.).

Synthesis of (EtNC)AuCl[§]

As for $(Bu^tNC)AuCl$; from $[(CH_2)_4S]AuCl$ (0·411 g, 1·28 mmol) and EtNC (0·25 cm^3) providing microcrystalline (EtNC)AuCl (0·311 g, 90%). M.p. 115 °C. (Found: C, 12·59; H, 1·92; N, 4·68%. C_3H_5AuClN requires C, 12·53; H, 1·75; N, 4·87%.)

Synthesis of (XyNC)AuCl[†]

As for $(Bu^tNC)AuCl$; from $[(CH_2)_4S]AuCl$ (0·240 g, 7·50 mmol) and XyNC (0·099 g, 7·56 mmol) providing (after recrystallisation from CH_2Cl_2/petroleum spirits) microcrystalline (XyNC)AuCl (0·239 g, 88%). M.p. 142 °C. (Found: C, 30·12; H, 2·15; N, 3·80%. C_9H_9AuClN requires C, 29·73; H, 2·49; N, 3·85%.)

---

[95] R. Uson, A. Laguna and M. Laguna, *Inorg. Synth.*, 1989, **26**, 85.

[96] F. Bonati and G. Minghetti, *Gazz. Chim. Ital.*, 1973, **103**, 373; cited in ref. 5, p. 44.

§ (EtNC)AuCl has been referred to in a patent for producing metallic gold films: *CA.*, 77, 10/904.

† (XyNC)AuCl has been used for synthesising Au-Pt clusters: C. E. Briant, D. I. Gilmour and D. M. P. Mingos, *J. Chem. Soc., Dalton Trans.*, 1986, 835.

3·1·3 Preparation of (RNC)AuNO$_3$

This was adapted (in that more precaution was required to avoid decomposition) from the preparation of (Ph$_3$P)AuNO$_3$.[97]

Synthesis of (Bu^{t}NC)AuNO$_3$

$$(Bu^tNC)AuCl + AgNO_3 \rightarrow (Bu^tNC)AuNO_3 + AgCl\ (s)$$

An argon-flushed Schlenk flask containing AgNO$_3$ (0·301 g, 1·78 mmol) in MeOH (30 cm^3) was fitted with a self-pressurising dropping funnel and a magnetic stirring bar. The flask was covered with tin foil to exclude light and chilled to -45 °C; these conditions were maintained throughout the reaction. Added dropwise to the stirred solution was (Bu^{t}NC)AuCl (0·450 g, 1·43 mmol) in CH$_2$Cl$_2$ (10 cm^3). After addition was complete, the mixture was stirred for a further 30 minutes. The solvent was removed under vacuum and without delay the solid residue was extracted with 5 cm^3 of cold CH$_2$Cl$_2$. The filtered extract was treated with petroleum spirits (60-80 °C) to precipitate microcrystalline (Bu^{t}NC)AuNO$_3$ (0·324 g, 66%). M.p. 118 °C (violent decomp.). (Found: C, 17·76; H, 2·47; N, 8·30%. Calc. for C$_5$H$_9$AuN$_2$O$_3$: C, 17·55; H, 2·65; N, 8·19%).

Synthesis of (EtNC)AuNO$_3$

As for (Bu^{t}NC)AuNO$_3$; from (EtNC)AuCl (0·103 g, 3·58 mmol) and AgNO$_3$ (0·075 g, 4·44 mmol) affording microcrystalline (EtNC)AuNO$_3$ (0·076 g, 68%). M.p. 107 °C (decomp.). (Found: C, 11·79; H, 1·59; N, 8·82%. Calc. for C$_3$H$_5$AuN$_2$O$_3$: C, 11·47; H, 1·60; N, 8·92%).

Synthesis of (XyNC)AuNO$_3$

As for (Bu^{t}NC)AuNO$_3$; from (XyNC)AuCl (0·137 g, 3·77 mmol) and AgNO$_3$ (0·075 g, 4·44 mmol) affording microcrystalline (XyNC)AuNO$_3$ (0·114 g, 77%). M.p. 122 °C (decomp.). (Found: C, 27·69; H, 2·04; N, 7·30%. Calc. for C$_9$H$_9$AuN$_2$O$_3$: C, 27·71; H, 2·33; N, 7·18%).

---

[97] A. M. Mueting, B. D. Alexander, P. D. Boyle, A. L. Casalnuovo, L. N. Ito, B. J. Johnson and L. H. Pignolet, *Inorg. Synth.*, 1992, **29**, 279.

3·2 NMR OF RNC AND (RNC)AuX

As a result of small coupling constants and quadrupolar relaxation,[98] spin-spin coupling to the ^{14}N (I = 1) nucleus is generally not observed in NMR spectroscopy. Small isonitrile species provide an exception,[61] which is attributable to rapid rotation in solution and the symmetrical environment of the nitrogen atom.[99] This characteristic ^{14}N coupling was generally observed in the ^{1}H and ^{13}C spectra of $(RNC)AuNO_3$, (RNC)AuCl and RNC [R = Bu^t (Table 3·1), Et (Table 3·2) or Xy (Table 3·3)].

Table 3·1 ^{1}H and ^{13}C chemical shifts (δ) for Bu^tNC species

	$(Bu^tNC)AuNO_3$	$(Bu^tNC)AuCl$	Bu^tNC
^{1}H $(C\underline{H}_3)_3CN{\equiv}C$	1·60	1·57 (t) [$^{3}J_{H\text{-}N}$ (2·1)]	1·38 (t) [$^{3}J_{H\text{-}N}$ (2·0)]
^{13}C $(\underline{C}H_3)_3CN{\equiv}C$	29·7	29·8	30·7
^{13}C $(CH_3)_3\underline{C}N{\equiv}C$	60·1	59·2	54·1 (t) [$^{1}J_{C\text{-}N}$ (5·1)]
^{13}C $(CH_3)_3CN{\equiv}\underline{C}$	122·2 (t) [$^{1}J_{C{\equiv}N}$ (24)]	132·3 (t) [$^{1}J_{C{\equiv}N}$ (25)]	152·8 (t) [$^{1}J_{C{\equiv}N}$ (4·4)]

t = 1:1:1; [Coupling (Hz)]

The ^{1}H spectra of the free Bu^tNC ligand and $(Bu^tNC)AuCl$ exhibited a characteristic 1:1:1 triplet for the nine equivalent $C\underline{H}_3$ protons.[92] This was not observed in the spectrum of $(Bu^tNC)AuNO_3$ (Table 3·1), which is attributable to a loss of molecular symmetry. $^{1}J_{C\text{-}N}$ coupling was only observed for the free ligand. $^{1}J_{C{\equiv}N}$ coupling was resolved for all three Bu^tNC species, indicating that the localised C≡N environment has high symmetry irrespective of the overall molecular structure. The $^{1}J_{C{\equiv}N}$ coupling constant increased on ligation as a result of diminished lone pair *s* character on the carbon atom,[100] the observed values being similar to those previously quoted for gold(I) isonitrile complexes.[61]

[98] M. J. Taylor, D. J. Calvert and C. M. Hobbis, *Magn. Reson. Chem.*, 1990, **28**, 16.
[99] J. Mason, ed., *Multinuclear NMR*, Plenum Press, New York, 1987, pp. 345-349.
[100] Ref. 99, p. 361.

All of the EtNC species exhibited ^{1}H-^{14}N coupling for both the $C\underline{H}_2$ and $C\underline{H}_3$ protons (Table 3·2). Figure 3·1 depicts the ^{1}H multiplets for $(CH_3C\underline{H}_2NC)AuCl$ (which is split into a quartet of triplets by coupling to both $C\underline{H}_3$ and ^{14}N) and for $(C\underline{H}_3CH_2NC)AuCl$ (which is split into a triplet of triplets by coupling to both $C\underline{H}_2$ and ^{14}N).

Table 3·2 ^{1}H and ^{13}C NMR chemical shifts (δ) for EtNC species

	$(EtNC)AuNO_3$	(EtNC)AuCl	EtNC
^{1}H $C\underline{H}_3CH_2N{\equiv}C$	1·53 (t of t)	1·51 (t of t)	1·31 (t of t)
	$[^{3}J_{H\text{-}H}$ (7·3)]	$[^{3}J_{H\text{-}H}$ (7·3)]	$[^{3}J_{H\text{-}H}$ (7·3)]
	$[^{3}J_{H\text{-}N}$ (2·9)]	$[^{3}J_{H\text{-}N}$ (2·9)]	$[^{3}J_{H\text{-}N}$ (2·5)]
^{1}H $CH_3C\underline{H}_2N{\equiv}C$	3·75 (q of t)	3·72 (q of t)	3·37 (q of t)
	$[^{3}J_{H\text{-}H}$ (7·3)]	$[^{3}J_{H\text{-}H}$ (7·3)]	$[^{3}J_{H\text{-}H}$ (7·3)]
	$[^{2}J_{H\text{-}N}$ (2·3)]	$[^{2}J_{H\text{-}N}$ (2·3)]	$[^{2}J_{H\text{-}N}$ (2·0)]
^{13}C $\underline{C}H_3CH_2N{\equiv}C$	13·9	13·9	15·0
^{13}C $CH_3\underline{C}H_2N{\equiv}C$	39·8 (t)	39·6 (t)	36·3 (t)
	$[^{1}J_{C\text{-}N}$ (6·6)]	$[^{1}J_{C\text{-}N}$ (6·8)]	$[^{1}J_{C\text{-}N}$ (6·5)]
^{13}C $CH_3CH_2N{\equiv}\underline{C}$	128·4	134·0 (t)	155·0 (t)
		$[^{1}J_{C{\equiv}N}$ (26)]	$[^{1}J_{C{\equiv}N}$ (5·7)]

t = 1:1:1; t of t = 1:2:1 of 1:1:1; q of t = 1:2:2:1 of 1:1:1; [Coupling (Hz)]

^{1}H NMR of pure EtOH exhibits a quartet of doublets for the $C\underline{H}_2$ protons, due to coupling to both $C\underline{H}_3$ and $O\underline{H}$.[101] It has been noted that it is unlikely to resolve a quartet of triplets in the $CH_3C\underline{H}_2CH_2$- fragment, due to similar coupling constants.[102] For the EtNC species, the highly resolved multiplets (Figure 3·1) are a result of the ^{1}H-^{14}N coupling constants being significantly less than those of ^{1}H-^{1}H (Table 3·2). The extensive resolution of ^{1}H-^{14}N and ^{13}C-^{14}N coupling for the relatively asymmetric EtNC, (EtNC)AuCl and $(EtNC)AuNO_3$ molecules could be the result of their thin linear structures and free rotation of the Et-N bond.

[101] Ref. 7, p. 816.
[102] T. W. G. Solomons, *Organic Chemistry*, John Wiley & Sons, Toronto, 1988, p. 594.

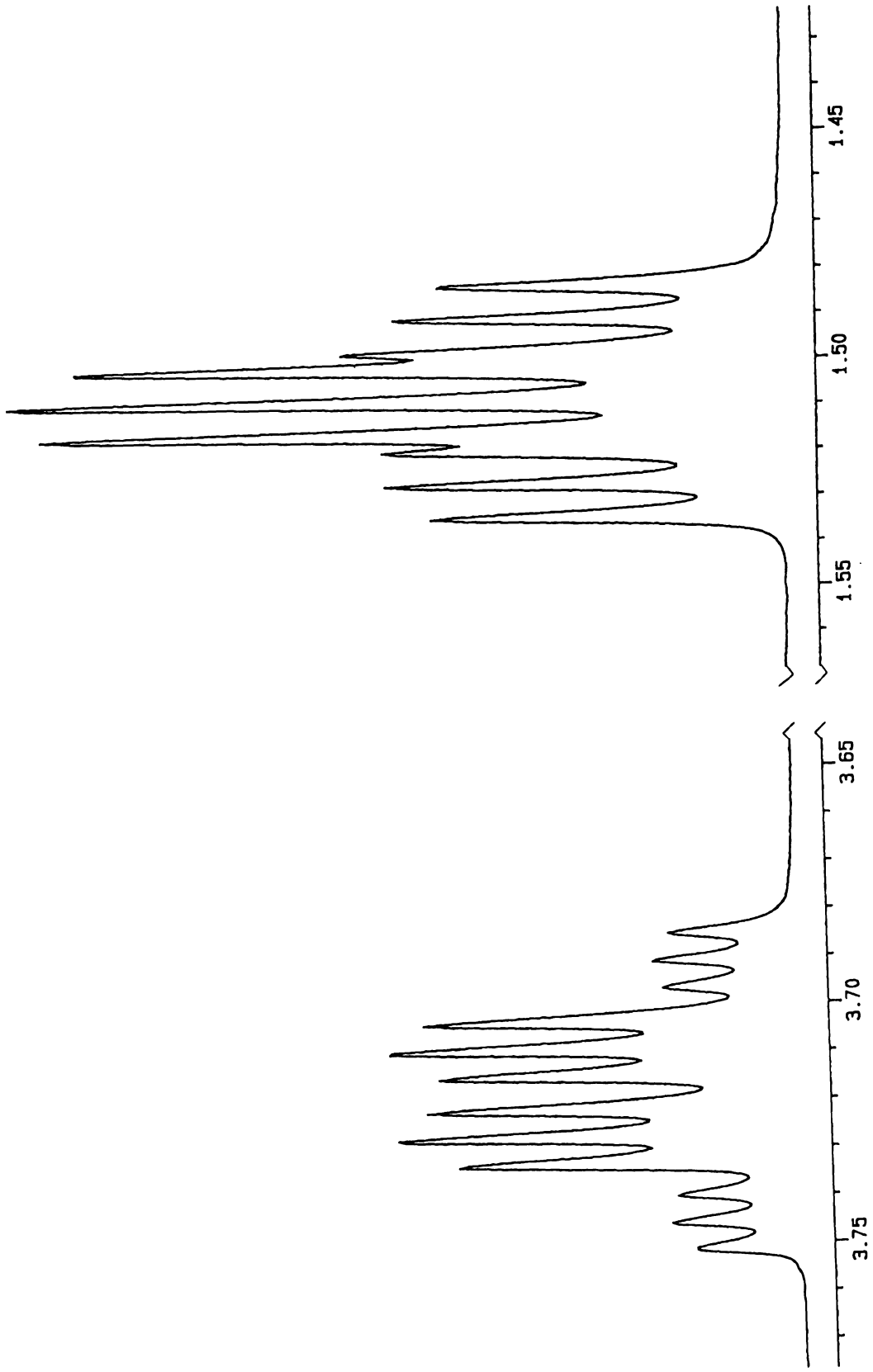

Figure 3·1 ^{1}H spectrum of (EtNC)AuCl

For the larger XyNC species, $^{1}J_{C\equiv N}$ coupling was resolved only for (XyNC)AuCl, the N≡C peaks for XyNC and (XyNC)$AuNO_3$ appearing as broad singlets.

Table 3·3 ^{1}H and ^{13}C chemical shifts (δ) for XyNC species

	(XyNC)$AuNO_3$	(XyNC)AuCl	XyNC
^{1}H CH_3	2·47	2·44	2·42
^{1}H *meta*-CH	7·19 (d)	7·16 (d)	7·09 (d)
	[$^{3}J_{H-H}$ (7·8)]	[$^{3}J_{H-H}$ (7·7)]	[$^{3}J_{H-H}$ (7·3)]
^{1}H *para*-CH	7·37 (t)	7·33 (t)	7·17 (t)
	[$^{3}J_{H-H}$ (7·7)]	[$^{3}J_{H-H}$ (7·7)]	[$^{3}J_{H-H}$ (7·5)]
^{13}C CH_3	18·7	18·7	18·9
^{13}C *ipso*-C	124·1 (t*)	124·3 (t*)	126·7 (t*)
	[$^{1}J_{C-N}$ (14)]	[$^{1}J_{C-N}$ (14)]	[$^{1}J_{C-N}$ (12)]
^{13}C *meta*-C	128·5	128·6	127·8
^{13}C *para*-C	131·0	131·5	128·7
^{13}C *ortho*-C	136·5	136·2	134·8
^{13}C N≡C	134·9	144·9 (t*)	167·9
		[$^{1}J_{C\equiv N}$ (27)]	

d = 1:1; t = 1:2:1; t* = 1:1:1; [Coupling (Hz)]

The ^{1}H and ^{13}C chemical shifts (δ) for RNC [R = Bu^t, Et or Xy] were all within the ranges expected for the proposed structural formulae.[103] The ^{13}C chemical shift (δ) of the ligating carbon atom (RNC) is sensitive to changes in molecular structure.[104] The results listed in Tables 3·1-3·3 show a consistent trend with an upfield shift, attributable to an increase in the C≡N bond force constant,[105] occurring on coordination of the RNC ligand. This is consistent with the coordinating lone pair on the carbon atom being anti-bonding with respect to the C≡N bond.[48] The extent of the upfield shift is correlated to the electronegativity of the *trans* ligand X, which is exemplified by the trend in (δ) of [Bu^tNC (~153)] > [(Bu^tNC)AuBr (~136)][61] > [(Bu^tNC)AuCl (~132)] > [(Bu^tNC)$AuNO_3$ (~122)].

[103] Ref. 102, p. 582 & 604.
[104] E. Singleton and H. E. Oosthuizen, *Adv. Organomet. Chem.*, 1983, 209.
[105] Ref. 99, p. 295.

3·3 IR OF RNC AND (RNC)AuX

IR spectra (Table 3·4) of the RNC ligands and (RNC)AuX complexes exhibited bands characteristic of ν(C≡N). The $(RNC)AuNO_3$ complexes produced peaks consistent with mono-dentate nitrate vibrations.[106]

Table 3·4 IR bands for RNC and (RNC)AuX

	ν(C≡N)	ν(N-O)
Bu^tNC	2135	-
$(Bu^tNC)AuCl$	2251	-
$(Bu^tNC)AuNO_3$	2258	1512, 1272, 977
EtNC	2151	-
(EtNC)AuCl	2266	-
$(EtNC)AuNO_3$	2267	1522, 1274, 978
XyNC	2122	-
(XyNC)AuCl	2215	-
$(XyNC)AuNO_3$	2215	1529, 1274, 958

IR spectra (cm^{-1}) were recorded from KBr disks

Coordination of the RNC ligands to the AuX fragment characteristically resulted in an increase in the ν(C≡N) value, which is consistent with the NMR results from the previous section. RNC ligands do not accept appreciable electron density from the metal centres to which they are coordinated.[48] For comparison, CO coordination is generally reliant on back donation from the metal centre into orbitals which are anti-bonding with respect to the C≡O bond, hence the general observation of a reduction of ν(C≡O) on coordination.

In terms of the ν(C≡N) value, the results show no significant difference between the chloride and nitrate complexes. Differences were anticipated because of the dissimilar *trans*-influences of the chloride and nitrate ligands. Moreover, the trend observed for the ^{13}C chemical shift of the ligating carbon atom suggested that the gold-carbon and C≡N bonds were strongest in the $(RNC)AuNO_3$ complexes.

[106] K. Nakamoto, *Infrared and Raman Spectra of Inorganic and Coordination Compounds*, John Wiley and Sons, New York, 3rd edn., 1977, pp. 244-246.

3·4 CRYSTAL STRUCTURE REFINEMENT

3·4·1 (Bu^tNC)$AuNO_3$

X-ray quality crystals were grown from a CH_2Cl_2 solution by vapour diffusion with petroleum spirits (30-40 °C) at 4 °C. The crystals formed rectangular blocks and maintained a clear, colourless appearance when kept in the dark at -25 °C. They were prone to decomposition under ambient conditions as evidenced by the formation of purple colloidal gold. They were particularly sensitive to light exposure.

Table 3·5 Crystal data and structure refinement for (Bu^tNC)$AuNO_3$

Formula	$C_5H_9AuN_2O_3$	**$T_{max, min}$**	0·102, 0·023
M_r	342·11	**F(000)**	624
Crystal system	monoclinic	**Crystal size/mm**	0·43/0·34/0·23
Space group	$P2_1/n$	**θ-range/°**	3 to 28
a/Å	8·1005(1)	**Total data**	4105
b/Å	13·5595(3)	**Unique data**	1921
c/Å	10·6118(1)	**R_{int}**	0·055
β/°	102·18	**R_1 (2σ(I)-data)**	0·0536
V/Å^3	881·07(3)	**R_1 (all data)**	0·0631
Z	4	**wR_2**	0·1443
D_c/g cm^{-3}	2·579	**GoF**	1·012
μ(Mo-Kα)/mm^{-1}	16·7	**Final Δe/ e Å^{-3}**	2·32/-3·12

Opposite page → Figure 3·2 (Bu^tNC)$AuNO_3$ molecule
Selected bond distances (Å) and angles (°): Au(1)-C(1) 1·92(1); Au(1)-O(1) 2·05(1); C(1)-N(1) 1·14(2); N(2)-O(1)-Au(1) 113·6(7); C(1)-Au(1)-O(1) 176·6(4)

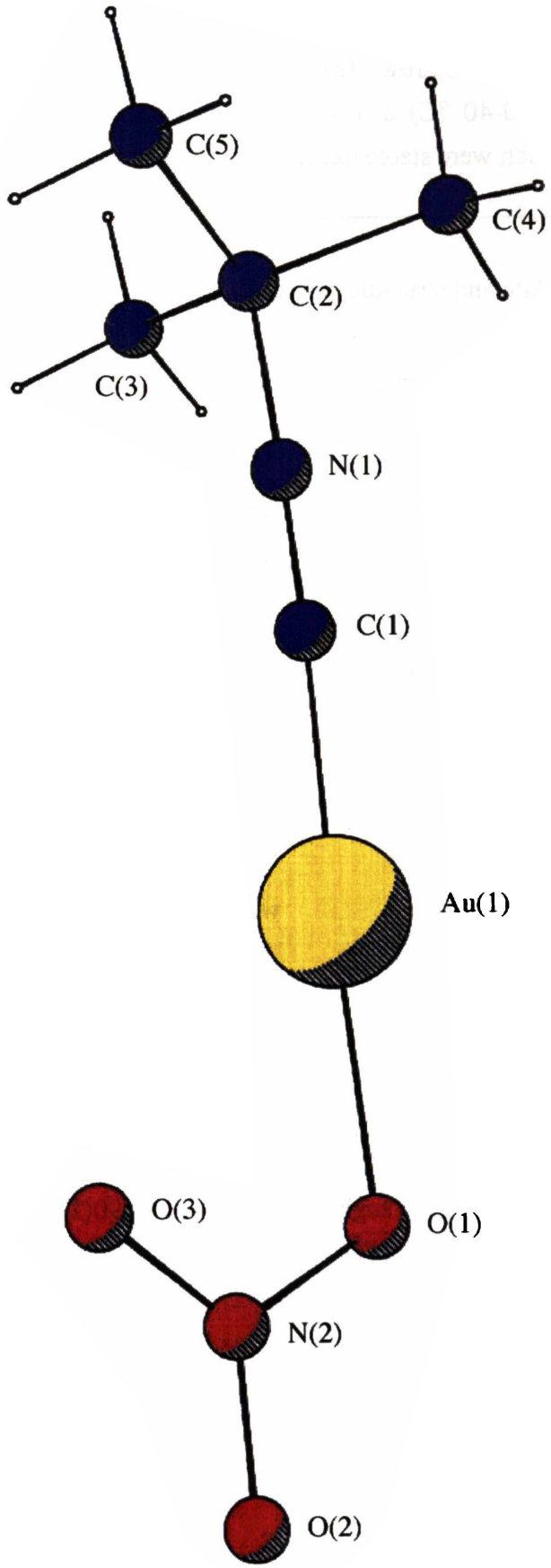
C(5)
C(4)
C(2)
C(3)
N(1)
C(1)
Au(1)
O(3)
O(1)
N(2)
O(2)

3·4·2 (EtNC)AuCl

X-ray quality crystals were grown from a CH_2Cl_2 solution by vapour diffusion with petroleum spirits (30-40 °C) at room temperature. The crystals formed clear, colourless plates which were stable under ambient conditions.

Table 3·6 Crystal data and structure refinement for (EtNC)AuCl

Formula	C_3H_5AuClN	**$T_{max, min}$**	0·912, 0·058
M_r	287·50	**F(000)**	252
Crystal system	monoclinic	**Crystal size/mm**	0·18/0·15/0·05
Space group	$P2_1/m$	**θ-range/°**	2 to 28
a/Å	20·7234(7)	**Total data**	1742
b/Å	6·3014(7)	**Unique data**	680
c/Å	10·0629(11)	**R_{int}**	0·051
β/°	96·100(2)	**R_1 (2σ(I)-data)**	0·0549
V/Å^3	281·37(5)	**R_1 (all data)**	0·0562
Z	2	**wR_2**	0·1385
D_c/g cm^{-3}	3·393	**GoF**	1·055
μ(Mo-Kα)/mm^{-1}	26·5	**Final Δe/ e Å^{-3}**	4·26, -4·26

Opposite page → Figure 3·3 (EtNC)AuCl molecule
Selected bond distances (Å) and angle (°): Au(1)-C(1) 1·90(2); Au(1)-Cl(1) 2·277(5); C(1)-N(1) 1·20(2); C(1)-Au(1)-Cl(1) 177·9(6)

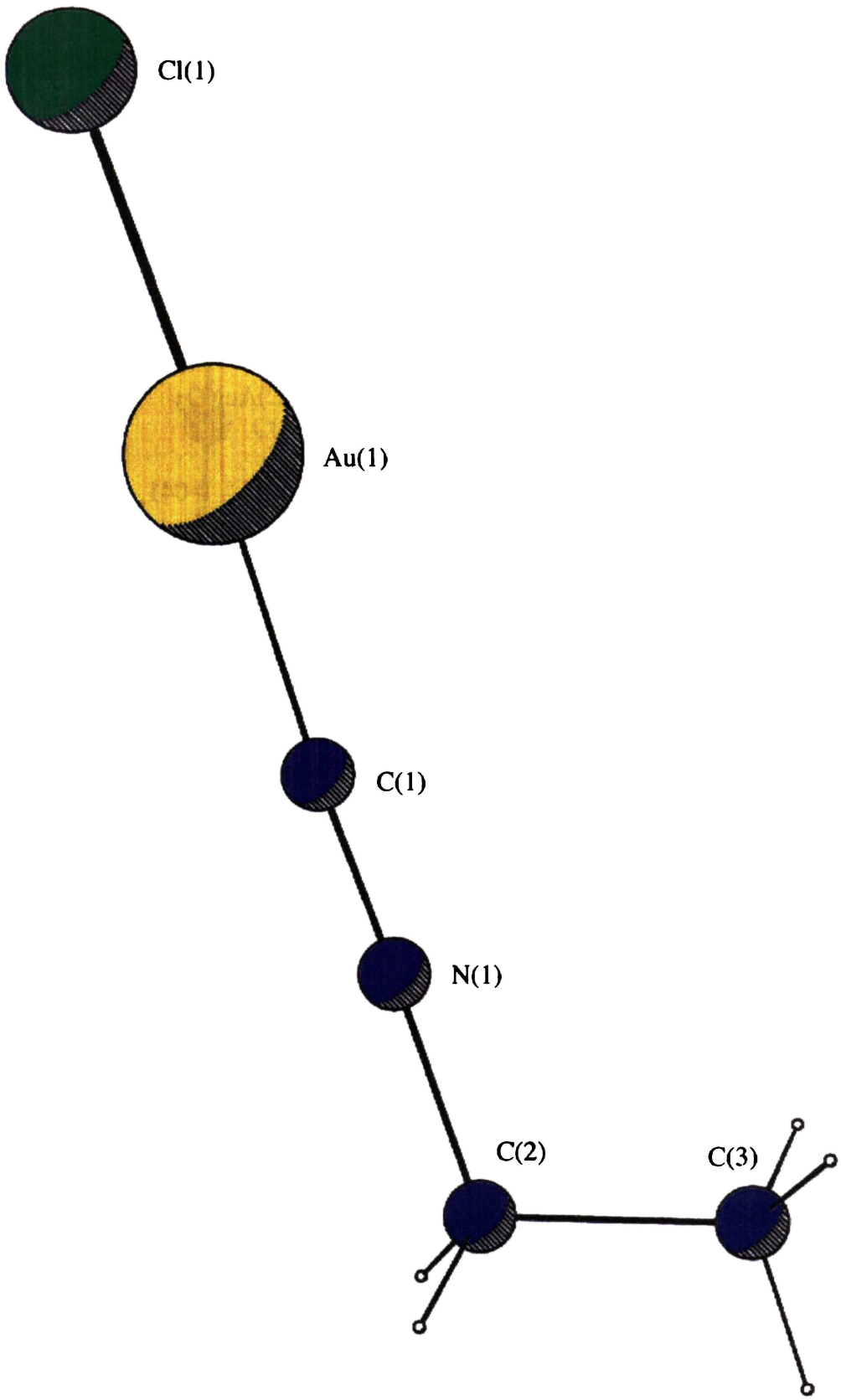
Cl(1)
Au(1)
C(1)
N(1)
C(2)
C(3)

3·4·3 (EtNC)$AuNO_3$

X-ray quality crystals were grown from a CH_2Cl_2 solution by vapour diffusion with petroleum spirits (30-40 °C) at 4 °C. The first crystals to appear were long thin needles but as the solution became enriched in hydrocarbon the crystals grew as rectangular blocks. Based on unit cell dimensions, the structures of both crystal forms were identical. The stability of crystalline (EtNC)$AuNO_3$ was similar to that of (Bu^tNC)$AuNO_3$.

Table 3·7 Crystal data and structure refinement for (EtNC)$AuNO_3$

Formula	$C_3H_5AuN_2O_3$	**$T_{max,\ min}$**	0·041, 0·003
M_r	314·06	**F(000)**	1120
Crystal system	monoclinic	**Crystal size/mm**	0·45/0·39/0·29
Space group	$P2_1/n$	**θ-range/°**	2 to 25
a/Å	10·6513(3)	**Total data**	7434
b/Å	7·8684(1)	**Unique data**	2267
c/Å	20·3639(1)	**R_{int}**	0·048
β/°	96·987(1)	**R_1 (2σ(I)-data)**	0·0470
V/Å^3	1288·31(3)	**R_1 (all data)**	0·0544
Z	8	**wR_2**	0·1370
D_c/g cm^{-3}	3·238	**GoF**	1·036
μ(Mo-Kα)/mm^{-1}	22·7	**Final Δe/ e Å^{-3}**	2·29/-3·56

Opposite page → **Figure 3·4** Two crystallographically independent (EtNC)$AuNO_3$ molecules

Selected bond distances (Å) and angles (°): Au(1)-C(11) 1·92(1); Au(1)-O(11) 2·03(1); Au(2)-C(21) 1·94(2); Au(2)-O(21) 2·04(1); N(11)-C(11) 1·13(2); N(21)-C(21) 1·11(2); Au(1)-Au(2) 3·193(1); N(11)-C(12) 1·46(2); N(21)-C(22) 1·78(4); C(12)-C(13) 1·49(2); C(22)-C(23) 1·27(3); C(11)-Au(1)-O(11) 177·0(5); C(21)-Au(2)-O(21) 177·8(5); C(11)-N(11)-C(12) 178·9(14); N(11)-C(12)-C(13) 112·7(12); C(21)-N(21)-C(22) 159(3); C(23)-C(22)-N(21) 82(3)

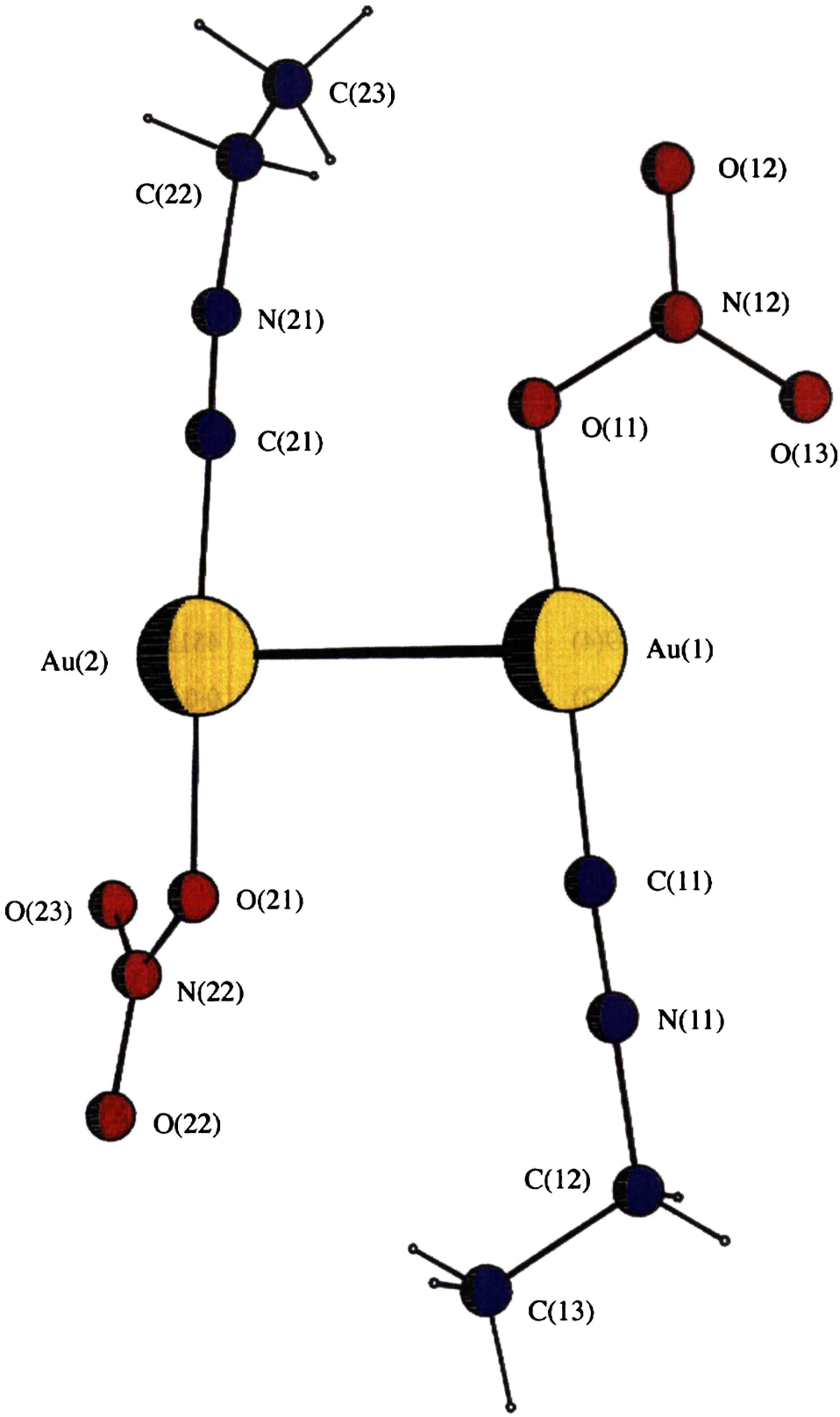
C(23)
C(22)
N(21)
C(21)
O(12)
N(12)
O(11)
O(13)
Au(2)
Au(1)
O(23)
O(21)
N(22)
O(22)
C(11)
N(11)
C(12)
C(13)

3·4·4 (XyNC)AuCl

X-ray quality crystals were grown from a CH_2Cl_2 solution by vapour diffusion with petroleum spirits (30-40 °C) at room temperature. The faceted,§ colourless crystals were stable under ambient conditions.

Table 3·8 Crystal data and structure refinement for (XyNC)AuCl

Formula	C_9H_9AuClN	**$T_{max, min}$**	0·367, 0·174
M_r	363·59	**F(000)**	1328
Crystal system	monoclinic	**Crystal size/mm**	0·60/0·11/0·10
Space group	$P2_1/n$	**θ-range/°**	2 to 28
a/Å	4·4626(5)	**Total data**	11807
b/Å	17·3099(4)	**Unique data**	4511
c/Å	11·0902(2)	**R_{int}**	0·040
β/°	97·846(1)	**R_1 (2σ(I)-data)**	0·0402
V/Å^3	2025·59(8)	**R_1 (all data)**	0·0610
Z	8	**wR_2**	0·0970
D_c/g cm^{-3}	2·385	**GoF**	1·013
μ(Mo-Kα)/mm^{-1}	14·7	**Final Δe/ e Å^{-3}**	3·37, -1·48

Opposite page → Figure 3·5 Two crystallographically independent (XyNC)AuCl molecules

Selected bond distances (Å) and angles (°): Au(1)-C(11) 1·93(1); Au(1)-Cl(1) 2·251(2); Au(2)-C(21) 1·94(1); Au(2)-Cl(2) 2·263(2); Au(1)-Au(2) 3·356(1); N(11)-C(11) 1·15(1); N(21)-C(21) 1·12(1); C(11)-Au(1)-Cl(1) 177·1(2); C(21)-Au(2)-Cl(2) 178·6(3)

§ The largest procured was a 460 mg square bipyramid.

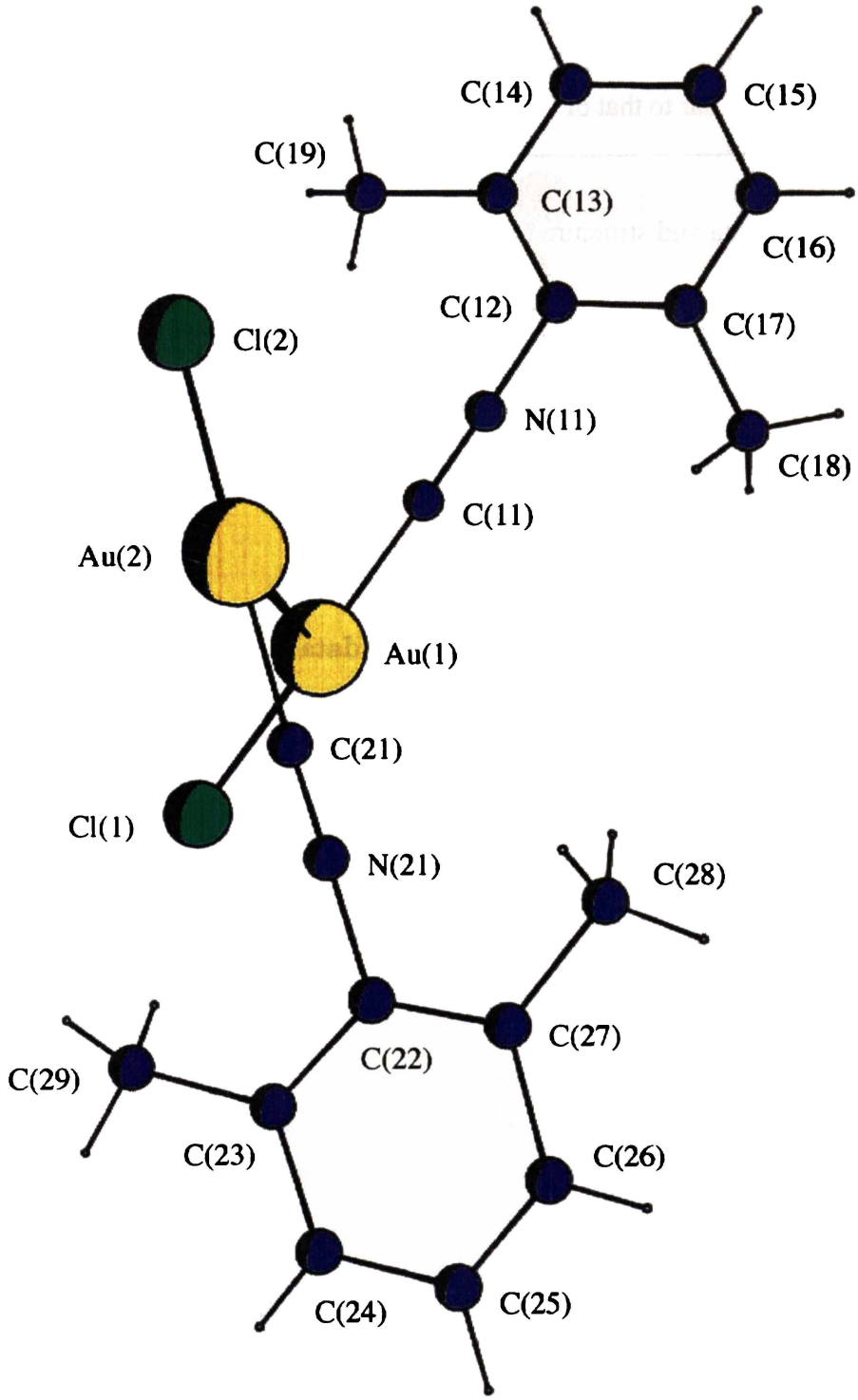
C(14)
C(15)
C(19)
C(13)
C(16)
C(12)
C(17)
Cl(2)
N(11)
C(18)
C(11)
Au(2)
Au(1)
C(21)
Cl(1)
N(21)
C(28)
C(27)
C(22)
C(29)
C(23)
C(26)
C(24)
C(25)

3·4·5 (XyNC)$AuNO_3$

X-ray quality crystals were grown from a CH_2Cl_2 solution by vapour diffusion with petroleum spirits (30-40 °C) at -25 °C. The crystals formed thin needles which exhibited stability similar to that of (Bu^tNC)$AuNO_3$.

Table 3·9 Crystal data and structure refinement for (XyNC)$AuNO_3$

Formula	$C_9H_9AuN_2O_3$	**$T_{max, min}$**	0·527, 0·047
M_r	390·15	**F(000)**	720
Crystal system	monoclinic	**Crystal size/mm**	0·54/0·11/0·05
Space group	$P2_1/n$	**θ-range/°**	2 to 25
a/Å	6·2642(1)	**Total data**	5881
b/Å	3·7802(2)	**Unique data**	1774
c/Å	8·0762(6)	**R_{int}**	0·058
β/°	103·76(1)	**R_1 (2σ(I)-data)**	0·0649
V/$Å^3$	1002·69(7)	**R_1 (all data)**	0·0762
Z	4	**wR_2**	0·1652
D_c/g cm^{-3}	2·584	**GoF**	1·005
μ(Mo-Kα)/mm^{-1}	14·7	**Final Δe/ e $Å^{-3}$**	7·12/-4·28

Opposite page → Figure 3·6 (XyNC)$AuNO_3$ molecule
Selected bond distances (Å) and angle (°): Au(1)-C(1) 1·91(2); Au(1)-O(1) 2·03(1); N(1)-C(1) 1·15(2); C(1)-Au(1)-O(1) 174·8(5)

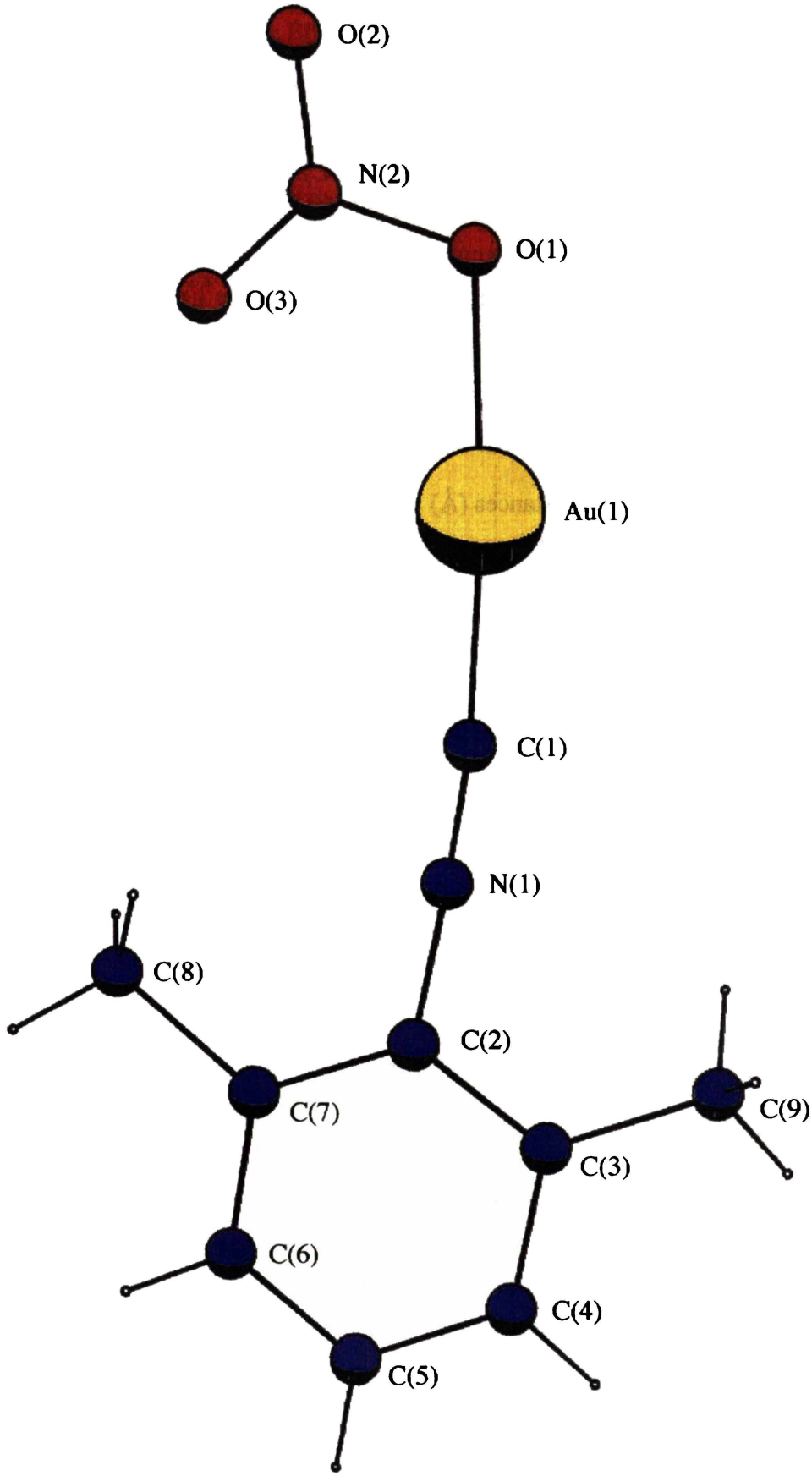
O(2)
N(2)
O(1)
O(3)
Au(1)
C(1)
N(1)
C(8)
C(2)
C(7)
C(9)
C(3)
C(6)
C(4)
C(5)

3·5 BOND PARAMETERS OF (RNC)AuX

The (RNC)AuX molecules were found to be characteristic linear two-coordinate gold(I) species, all exhibiting a C(1)-Au(1)-X angle close to 180° (Table 3·10). The average Au(1)-O(1) bond distance for the (RNC)$AuNO_3$ complexes is 2·04(1) Å, which is the first characterised for a carbon-gold(I)-oxygen linkage. The Au(1)-O(1) distances and Au(1)-O(1)-N(2) angles are not significantly different to those of (Ph_3P)$AuNO_3$.[107] As expected for a mono-dentate nitrate ligand, the oxygen-N(2) distance of the ligated O(1) atom is significantly longer than those of the non-coordinating O(2/3) atoms.

Table 3·10 Selected bond distances (Å) and angles (°) of (RNC)AuX

	(EtNC)AuCl	(XyNC)AuCl†	(EtNC)$AuNO_3$†	(Bu^tNC)$AuNO_3$	(XyNC)$AuNO_3$
Au-Cl	2·277(5)	2·257(2)			
Au-C(1)	1·90(2)	1·94(1)	1·93(2)	1·92(1)	1·91(2)
C(1)-N(1)	1·20(2)	1·14(1)	1·12(2)	1·14(2)	1·15(2)
Au-O(1)			2·03(1)	2·05(1)	2·03(1)
O(1)-N(2)			1·32(2)	1·31(1)	1·33(2)
O(2/3)-N(2)			1·21(2)	1·22(2)	1·20(2)
Cl-Au-C(1)	177·9(6)	177·8(3)			
O(1)-Au-C(1)			177·4(5)	176·6(4)	174·8(5)
Au-O(1)-N(2)			115·0(8)	113·6(7)	110·7(8)

†Averaged for the two independent molecules

Full lists of bond parameters are displayed in the Appendices

The C(1)-N(1) bond of (EtNC)AuCl is relatively long. This may be attributed to the interchain packing structure of (EtNC)AuCl (see Figure 3·25) which is not inconsistent with each gold centre forming secondary η^2 interactions with adjacent isonitrile C≡N bonds. The [(RNC)Au] fragments otherwise exhibit Au(1)-C(1) and C(1)-N(1) bond distances similar to those from the literature.[61] Changing the anion from chloride to nitrate appears to have little influence on the Au(1)-C(1) and C(1)-N(1) bond distances, which is consistent with the observed IR data.

[107] J.-C. Wang, M. N. I. Khan and J. P. Fackler Jr., *Acta Cryst.*, 1989, **C45**, 1008.

There are significant differences between the crystallographically independent EtNC ligands of (EtNC)$AuNO_3$. The EtNC(2) ligand has unusual bond parameters (refer to Figure 3·4). Specifically, the C(21)-N(21)-C(22) and N(21)-C(22)-C(23) angles are acute, the N(21)-C(22) bond is long and the C(22)-C(23) bond is short. This was attributed to dubious positioning of the C(22) atom as a result of difficulties in accurately locating small atoms in the close proximity of gold atoms.

3·6 SOLID-STATE AGGREGATION OF (RNC)AuX

The following has been written on the assumption that readers have familiarity with certain descriptions of Au--Au interactions between linear two-coordinate gold(I) molecules. If necessary, reference can be made to sub-section 2·2·3 for explanation of terms.

3·6·1 (Bu^tNC)$AuNO_3$

(Bu^tNC)$AuNO_3$ crystallised as a zig-zag chain with anti-parallel Au--Au interactions (Figure 3·7). This form of polymeric aggregation is relatively common for LAuX complexes. There is only one crystallographically unique gold centre and only one chain angle but there are two alternating Au--Au distances of 3·296(1) Å and 3·323(1) Å. The two distances can be represented respectively as [Au(1) x, y, z]--[Au(1)" 1-x, 1-y, 1-z], which is within the unit cell and [Au(1) x, y, z]--[Au'(1) -x, 1-y, 1-z], which crosses between two adjacent unit cells. This structure exhibits two unique inversion centres as illustrated in Figure 3·8.

Overleaf → Figure 3·7 Zig-zag chain of (Bu^tNC)$AuNO_3$
Gold contact distances (Å) and angle (°): Au(1)-Au(1)' 3·296(1); Au(1)-Au(1)" 3·323(1); Au(1)'-Au(1)-Au(1)" 142·29(3)

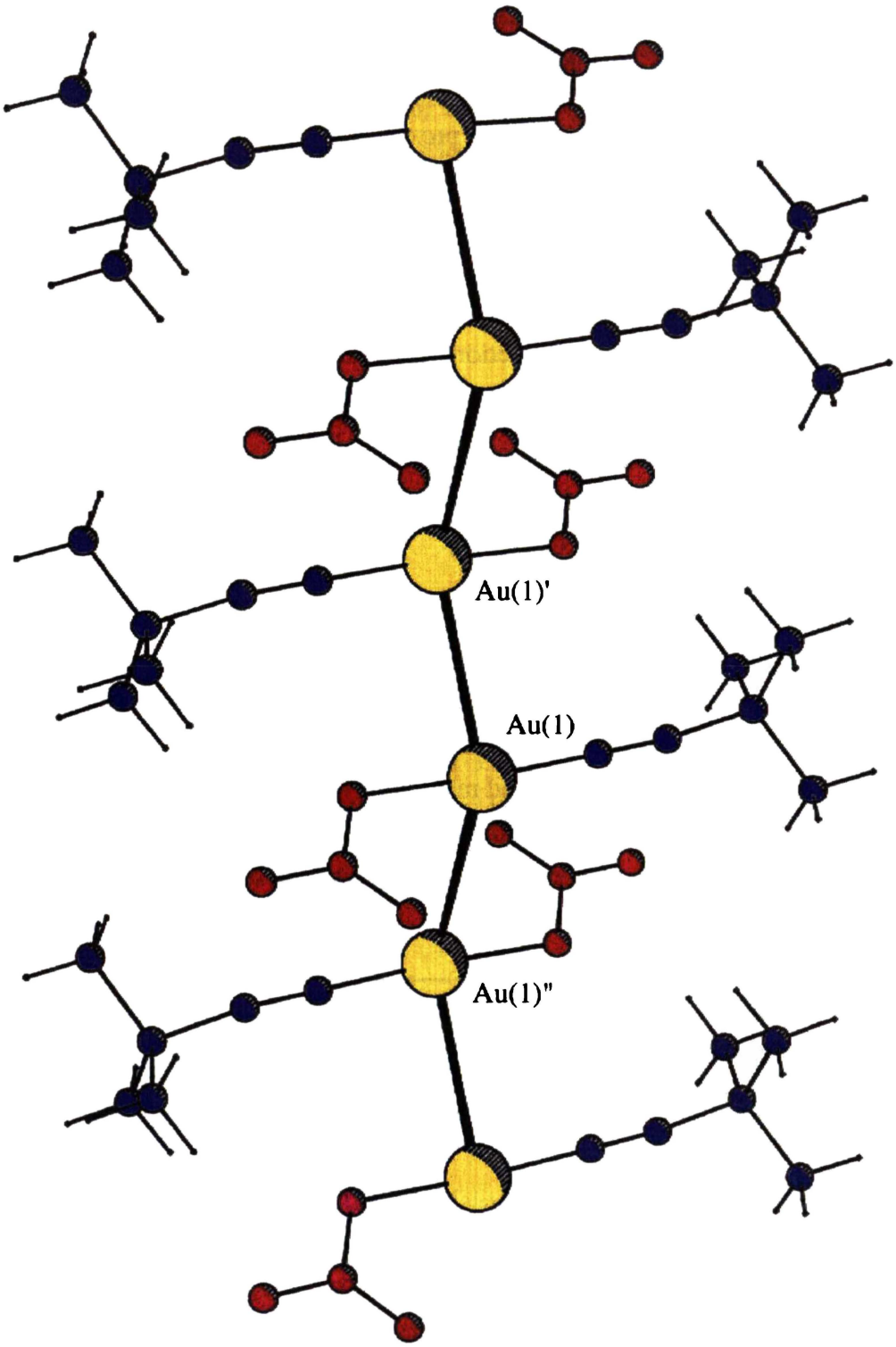
Au(1)'
Au(1)
Au(1)"

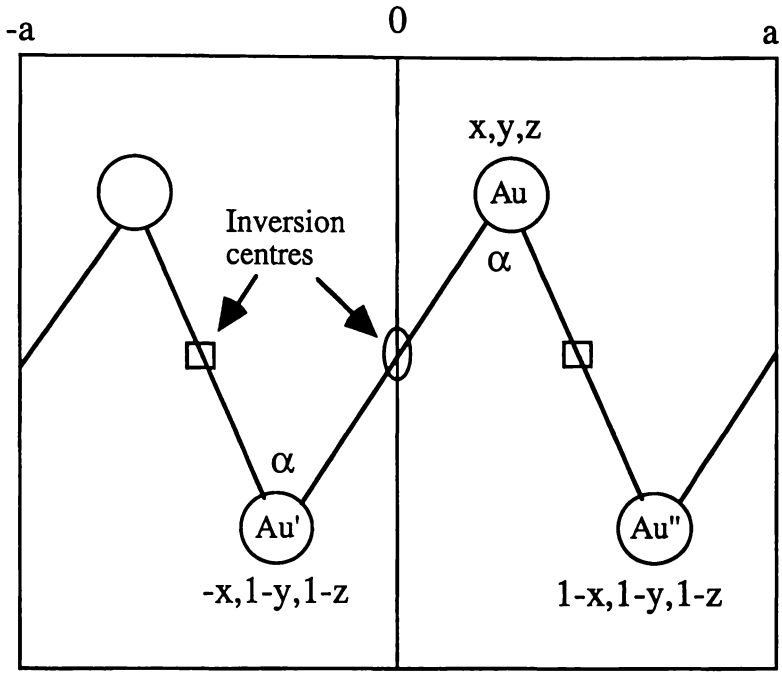

Figure 3·8 Two unique inversion centres of the (Bu^{t}NC)AuNO$_3$ chain
$\alpha = 142°$

The Au--Au distances found in the chain of (Bu^{t}NC)AuNO$_3$ form an interesting comparison with those of (Bu^{t}NC)AuX homologues from the literature. It appears that the nitrate anion has a significant effect on the Au--Au interaction. Isostructural chains have been characterised for (Bu^{t}NC)AuCl,[108] (Bu^{t}NC)AuCN,[109] and (Bu^{t}NC)AuBr[61] but with longer Au--Au interactions (Table 3·11).

Table 3·11 Gold contact parameters of (Bu^{t}NC)AuX zig-zag chains

	NO_3	CN	Br	Cl
Au--Au (Å)	3·31	3·57	3·69	3·70
Au--Au--Au (°)	142	130	128	127

A comparison of the Au--Au distances can be made as all four chains are isostructural (Figure 3·9 depicts the bromide example). The significance of the relatively wide (Bu^{t}NC)AuNO$_3$ chain angle is difficult to determine.

[108] D. S. Eggleston, D. F. Chodosh, R. L. Webb and L. L. Davis, *Acta Cryst.*, 1986, **C42**, 36.
[109] C.-M. Che, H.-K. Yip, W.-T. Wong and T.-F. Lai, *Inorg. Chim. Acta*, 1992, **197**, 177.

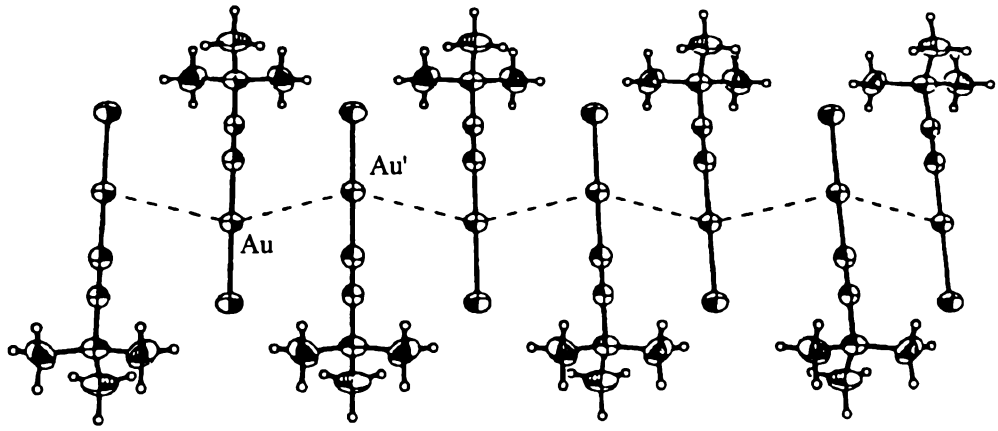

Figure 3·9 Zig-zag chain of (Bu^{t}NC)AuBr

It is apparent that the weakly coordinated nitrate anion enhances the inherent Au--Au attraction, compared with the more strongly coordinated halide and CN anions. This could be a result of changes in electron density on the gold centres.

It was noted that the coordinated nitrate anion is positioned (see Figures 3·22 and 3·24) with the two non-ligating oxygen atoms at a maximum distance from the adjacent isonitrile ligands. The linear CN ligand and the longer gold-halide bonds place the comparative anions in positions where they are more susceptible to repulsion with adjacent electron-rich isonitrile C≡N bonds. Such contact could counterbalance the Au--Au interactions. However, it appears unlikely the Au--Au contacts in the chain of (Bu^{t}NC)AuCl are restricted in such a way, as shorter anti-parallel Au--Au contacts have been observed in other (RNC)AuCl crystal structures (see Figure 2·11 for example).

The molecular crystal packing of (Bu^{t}NC)AuC≡CSi(Me)$_3$ was recently reported and exhibits the shortest Au--Au interaction (3·12 Å) of any (RNC)AuX aggregation (Figure 3·10).[110] (Bu^{t}NC)AuC≡CSi(Me)$_3$ is a (Bu^{t}NC)AuX complex, but it is not appropriate to directly compare this Au--Au contact distance with those observed in the chain structure of (Bu^{t}NC)AuNO$_3$. The shorter interaction is predictable in that the crossed ligands minimise steric repulsion. Furthermore, the connectivity of this novel tetramer is such that the average auriophilic coordination number is one and a half, compared with two in the zig-zag chain.

[110] J. Vicente, M.-T. Chicote, M.-D. Abrisqueta and P. G. Jones, *Organometallics*, 1997, **16**, 5628.

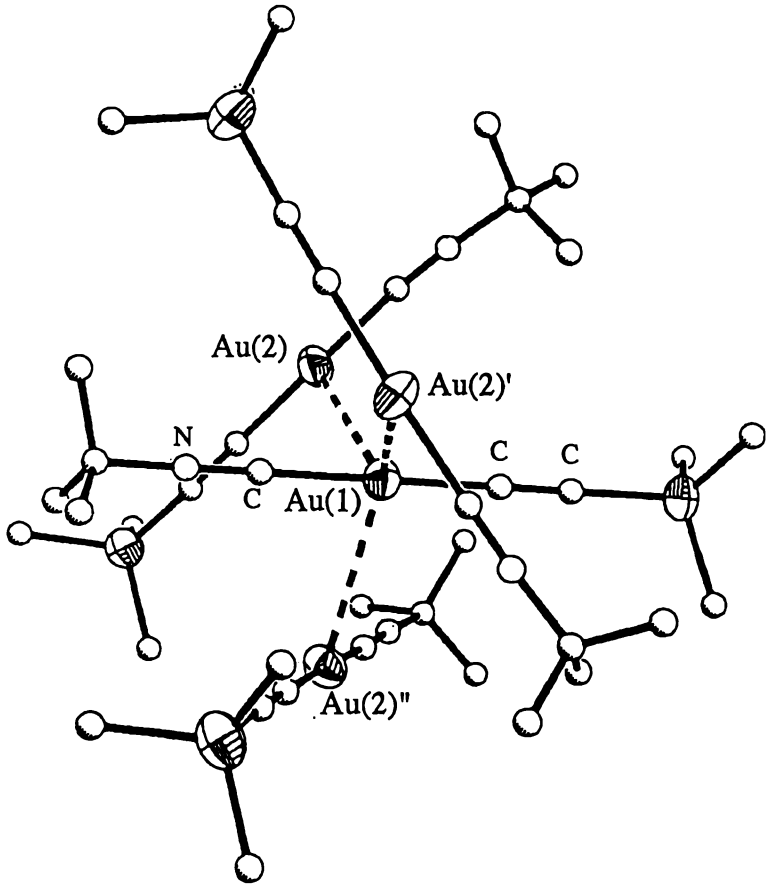

Figure 3·10 (Bu^tNC)AuC≡CSi(Me)$_3$ tetramer

3·6·2 (EtNC)AuCl

Molecules of (EtNC)AuCl crystallise as a zig-zag chain (Figure 3·12), which is based on anti-parallel Au--Au interactions of 3·553(1) Å. This distance is shorter than that found in the chain of (Bu^tNC)AuCl (3·70 Å), which is predictable on steric grounds. However, the chain structure of (MeNC)AuCl was reported recently and was found to exhibit a "surprisingly long" Au--Au distance of 3·64 Å (Figure 3·11).[61]

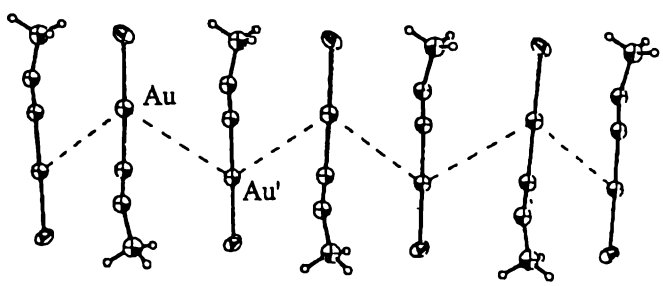

Figure 3·11 Zig-zag chain of (MeNC)AuCl

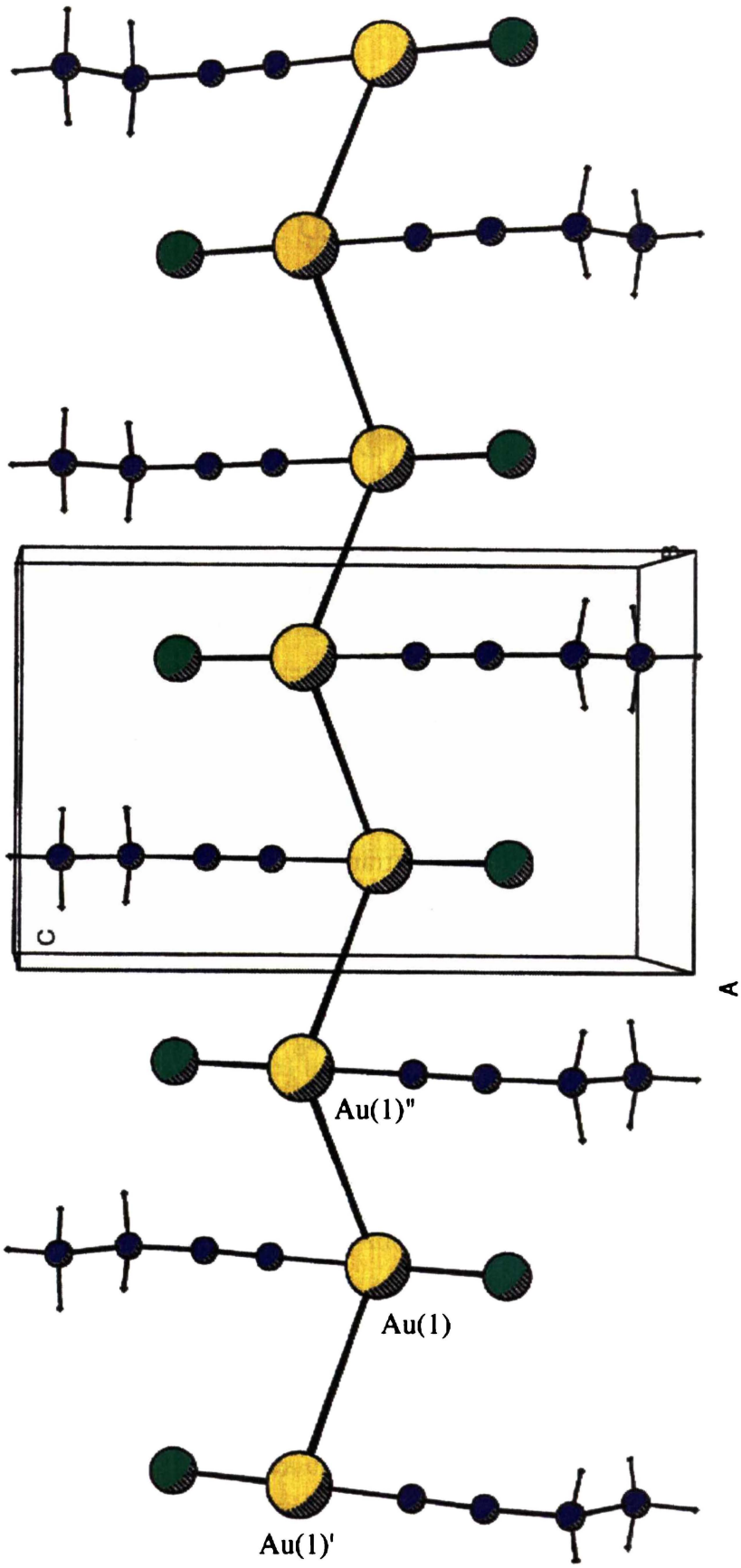
C
A
Au(1)"
Au(1)
Au(1)'

3·6·3 (EtNC)AuNO$_3$

The two crystallographically unique molecules of (EtNC)AuNO$_3$ form a dimer (see Figure 3·4) based on an anti-parallel Au--Au interaction of 3·193(1) Å. The overall crystal architecture is polymeric and exhibits a novel auriophilic motif (Figure 3·13). Two dimers link with opposite orientation by way of two parallel Au--Au interactions of 3·358(1) Å [Au(1)--Au(2)' and Au(1)'--Au(2)] leading to a pseudo-tetrameric structure. The diamond shaped tetramer exhibits an internal anti-parallel contact of 3·194(1) Å (Au(1)--Au(1)'). The middle of this internal interaction is the inversion centre of the tetrameric unit. This structure is comparable to that of [(Ph$_2$C=NH)$_2$Au]$^+$[AuCl$_2$]$^-$ (see Figure 2·20).

The tetramers of (EtNC)AuNO$_3$ are linked together by an anti-parallel interaction of 3·287(1) Å (Au(2)--Au(2)''). The overall structure is therefore comprised of a series of linked centrosymmetrical tetramers. This molecular packing can be described as a 'collapsed' or 'concertinaed' zig-zag chain (Figure 3·14). Each gold centre is auriophilic three-coordinate through a combination of parallel and anti-parallel interactions.

In comparison with the structure of (EtNC)AuCl, the auriophilic coordination number increases from two to three when the chloride is replaced with nitrate. Considering the increased number of intermolecular contacts, relatively long interactions could be expected for the (EtNC)AuNO$_3$ structure. However, the observed Au--Au distances of 3·19 Å, 3·28 Å and 3·35 Å are all significantly shorter than those characterised in the auriophilic two-coordinate chain of (EtNC)AuCl, which has a single repeating Au--Au distance of 3·55 Å.

← **Opposite page Figure 3·12** Unit cell and zig-zag chain of (EtNC)AuCl
Gold contact distance (Å) and angle (°): Au(1)-Au'(1) 3·553(1); Au'(1)-Au(1)-Au''(1) 124·90(1)

Overleaf → Figure 3·13 Concertinaed chain of (EtNC)AuNO$_3$
Gold contact distances (Å): Au(1)-Au(2) 3·193(1); Au(1)-Au(1)' 3·194(1); Au(2)-Au(2)'' 3·287(1); Au(1)'-Au(2) 3·358(1)

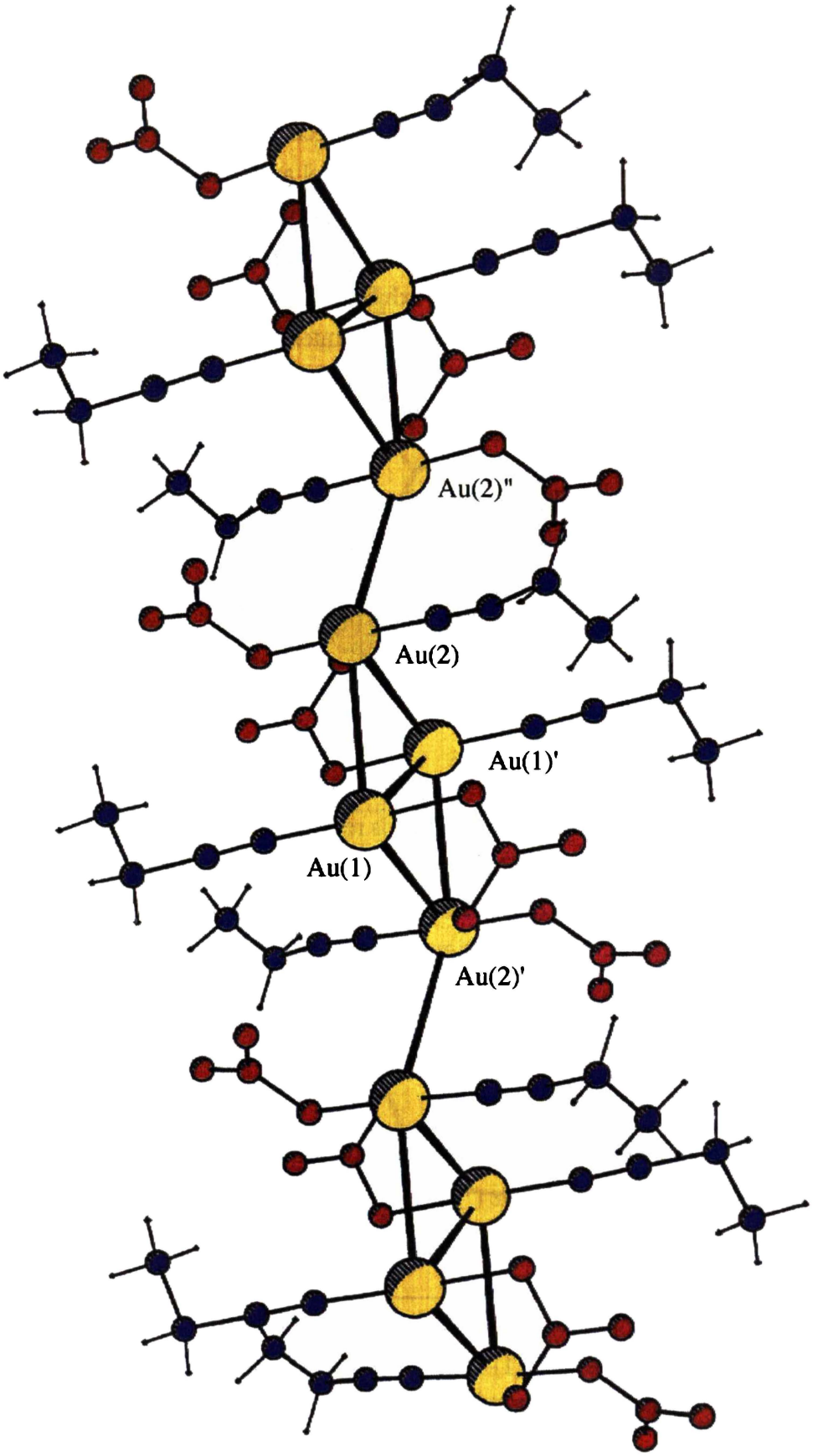
Au(2)"
Au(2)
Au(1)'
Au(1)
Au(2)'

It is apparent that the nitrate ligand bestows an increased auriophilic capacity, such that the crystal structure of (EtNC)$AuNO_3$ represents an attempt to increase the number of Au--Au contacts. This could be an electronic effect but the steric differences between the nitrate and chloride anions are not discounted as having some influence on the Au--Au interactions.

The nitrate anions of (EtNC)$AuNO_3$ direct their non-ligating oxygen atoms away from the adjacent isonitrile ligands, a feature also of (Bu^tNC)$AuNO_3$ crystal packing. If chloride was hypothetically incorporated in the packing structure of (EtNC)$AuNO_3$, the closest distance between the chloride ligands and adjacent isonitrile C≡N bonds would be ~3·2 Å. There is uncertainty as to whether this would represent an energetically significant repulsion. This discussion is further complicated by the proposal that the crystal structure of (OC)AuCl contains Cl--C *attractive* interactions (see Figure 3·28 and accompanying text).

The comparison between (EtNC)$AuNO_3$ and (EtNC)AuCl is based on the electronic influence of the anion and possible (X--(C≡N) interactions. Appropriate comparison of the steric influence of the isonitrile ligand can be made between the supramolecular structures of (EtNC)$AuNO_3$ and (Bu^tNC)$AuNO_3$ (see Figure 3·7). Replacing the relatively bulky Bu^t group (from the structure of (Bu^tNC)$AuNO_3$) with Et also promotes a collapse of the zig-zag chain. In this case, the more extensive molecular aggregation is not due to an increase in the inherent Au--Au attraction or a lack of Cl--(C≡N) repulsions. Simply, more space is created by replacing two Me groups with two hydrogen atoms.

The concertinaed chain description is conceptualised by deriving the structure from that of a hypothetical zig-zag chain, similar to those observed for (Bu^tNC)$AuNO_3$ and (EtNC)AuCl (Figure 3·14). The apparent enhancing effect of nitrate on the Au--Au attraction and the relatively small Et group promotes the collapse of the chain. This seemingly folds it into the observed linked tetramers which exhibit a variety of Au-Au-Au angles, ranging from 58° to 154°.

There appears to be little previous speculation for the concept of multi-centred intermolecular Au--Au interactions. This may have basis within the tetramers of (EtNC)$AuNO_3$, which contain two triangles of gold centres. Two of the sides of these triangles have essentially the same distance (3·19 Å), which is not the result of crystallographic symmetry constraints.

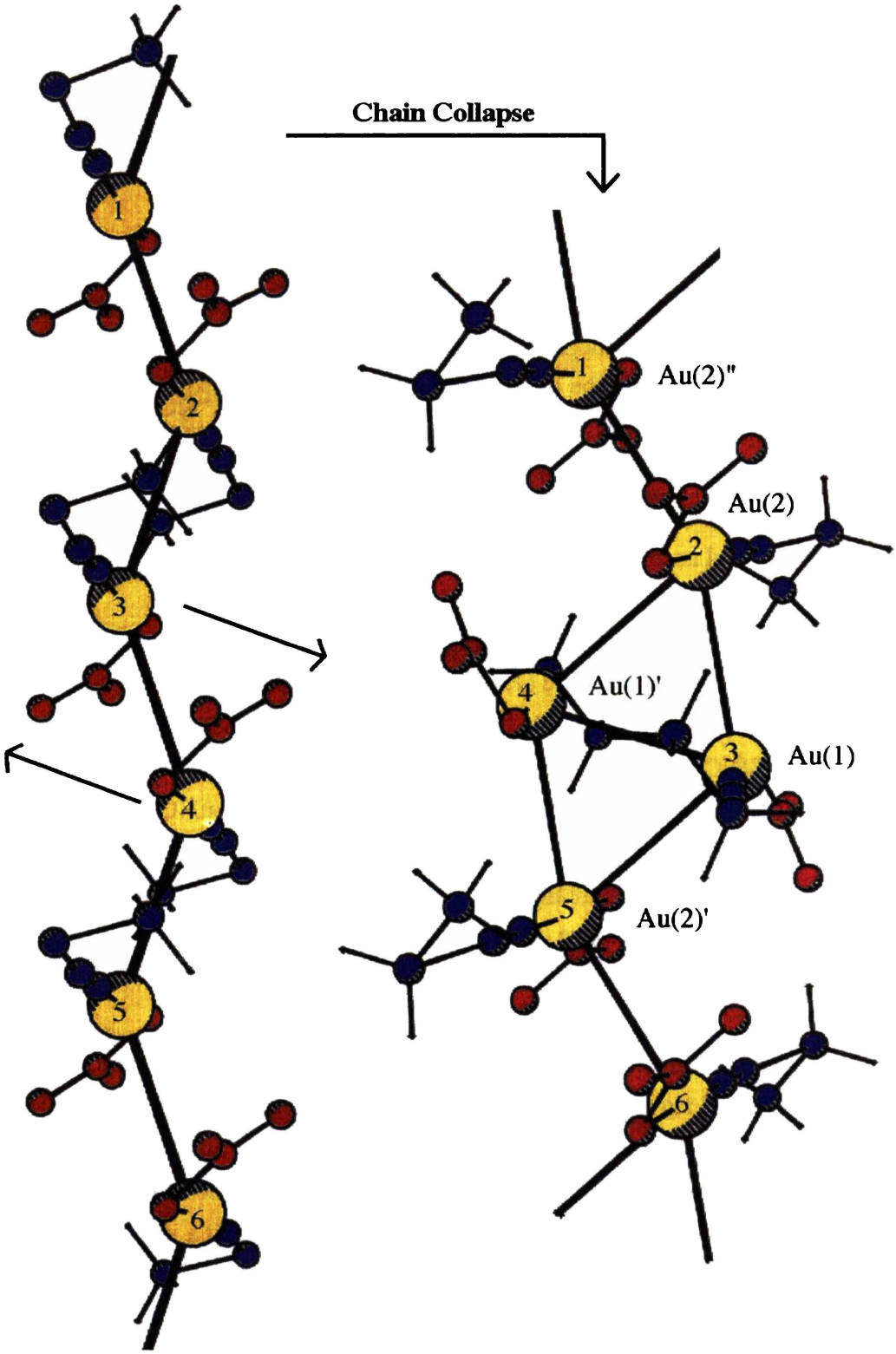
Chain Collapse
1
2
3
4
5
6
Au(2)"
Au(2)
Au(1)'
Au(1)
Au(2)'

3·6·4 (XyNC)AuCl

The two crystallographically unique molecules of (XyNC)AuCl form a dimer (see Figure 3·5) based on a crossed ligand Au--Au interaction of 3·355(1) Å [Au(1)--Au(2)]. The dimers are linked by way of a single anti-parallel Au--Au interaction of 3·654(1) Å (Au(1)--Au(1)'), resulting in a tetrameric structure (Figure 3·15). This tetramer is unlike the one observed for (EtNC)$AuNO_3$, which is formed by the unification of two dimers with three Au--Au contacts. Moreover, the tetramers of (EtNC)$AuNO_3$ are linked whereas those of (XyNC)AuCl appear to be isolated from further Au--Au interactions and take the form of a short chain.

The (XyNC)$AuNO_3$ tetramers appear to be fragments in a broken polymeric chain (Figure 3·16). A possible zig-zag chain structure with exclusive anti-parallel interactions is prevented by the terminal molecules of the short chain forming crossed ligand interactions. This does not preclude the possibility of an auriophilic polymer, indeed it is apparent that there is *potential* for the linking of the tetramers by an anti-parallel Au--Au interaction. However, the distance between the terminal gold centres (Au(2)--Au(2")) of adjacent tetramers is 4·071(1) Å, which is too long to invoke an attractive Au--Au interaction.[111]

← **Opposite page Figure 3·14** Collapse of a zig-zag chain
Hypothetical zig-zag chain of (EtNC)$AuNO_3$ (left); Observed concertinaed chain (right)
Gold contact angles (°) of the linked tetramers: Au(2)-Au(1)-Au(1)' 63·42(2); Au(2)-Au(1)-Au(2)' 121·70(2); Au(1)'-Au(1)-Au(2)' 58·28(2); Au(1)-Au(2)-Au(1)' 58·30(2); Au(2)"-Au(2)-Au(1)' 98·13(2); Au(1)-Au(2)-Au(2)" 154·61(3)

Overleaf (left)→ Figure 3·15 Tetramer of (XyNC)AuCl
Gold contact distances (Å) and angle (°): Au(1)--Au(2) 3·355(1); Au(1)--Au(1)' 3·655(1); Au(1)-Au(1)'-Au(2)' 97·60(1)

Overleaf (right)→ Figure 3·16 Broken chain of (XyNC)AuCl
Gold spacing distance (Å) and angle (°): Au(2)--Au(2)" 4·071(1); Au(2)"-Au(2)-Au(1) 124·32(1)
The dashed red line represents the chain fragmentations

[111] A. Kolb, P. Bissinger and H. Schmidbaur, *Inorg. Chem.*, 1993, 32, 5132.

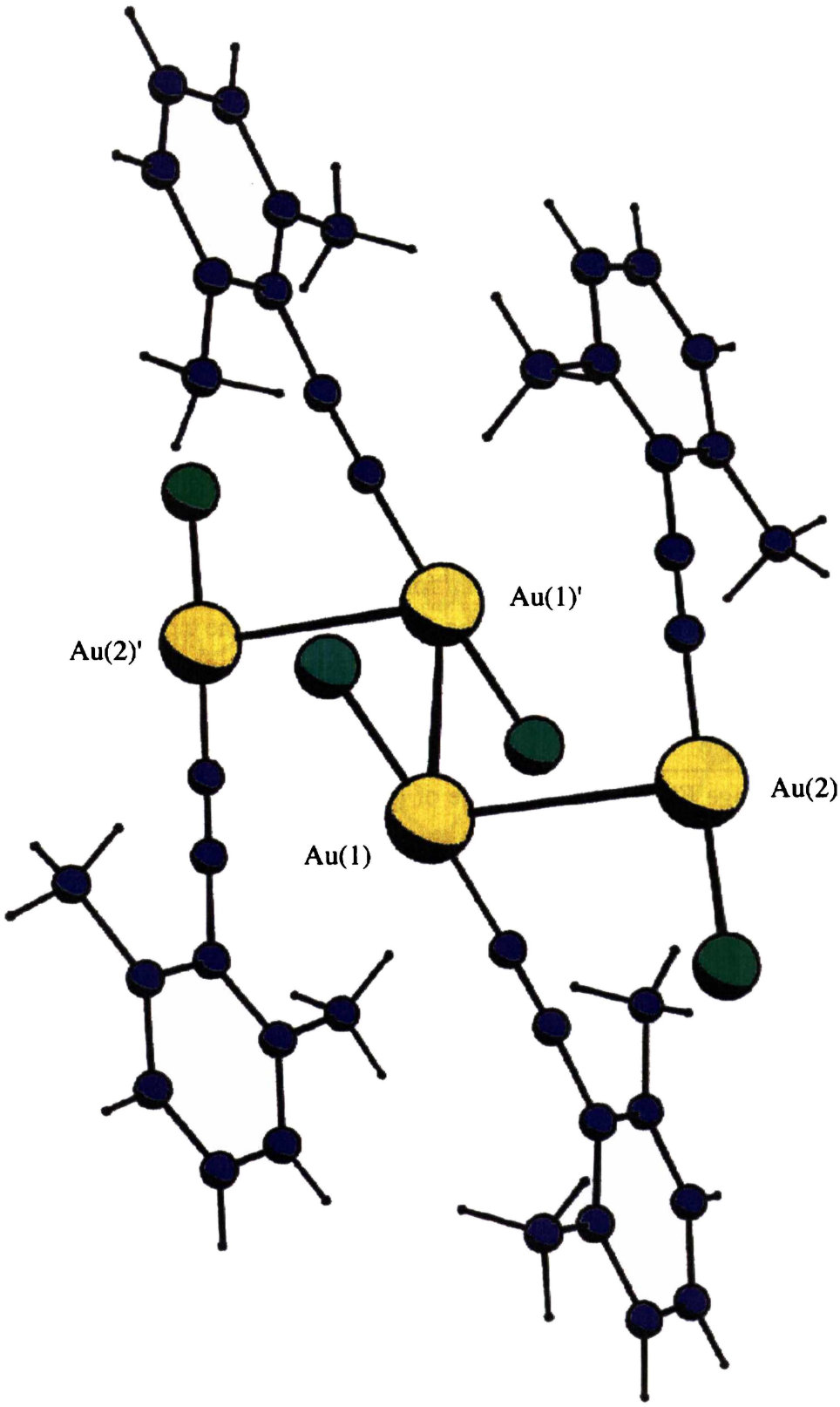
Au(1)'
Au(2)'
Au(2)
Au(1)

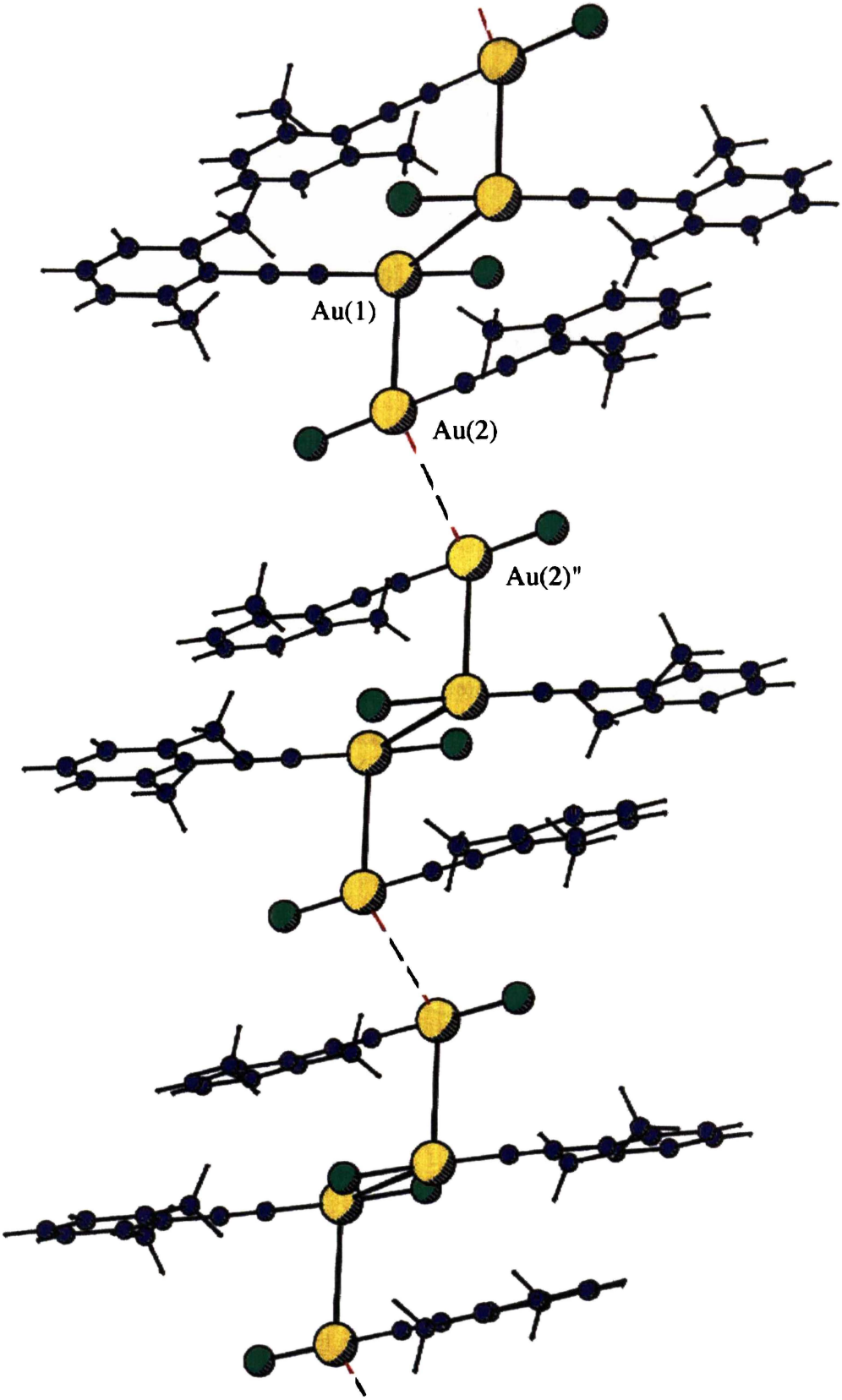
Au(1)
Au(2)
Au(2)"

The fragmented chain structure of (XyNC)AuCl has similarities to the crystal structure of (Me_3P)AuBr, which exhibits ligand helices and appears to be broken into short chain trimers (Figure 3·17). In this case, the terminal gold centres (Au(1) and Au(3)') are separated by a distance of 3·98 Å.[67]

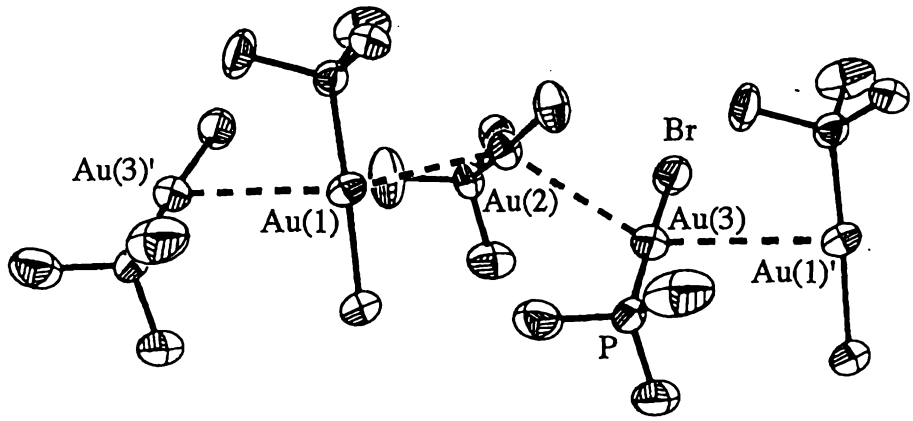

Figure 3·17 Trimers of (Me_3P)AuBr

The self-assembly of gold(I) molecules into tetramers is not without precedent. (Bu^tNC)AuC≡CSi(Me_3) (see Figure 3·10), the square aggregates of (Piperidine)AuCl (Figure 3·18)[112] and chain tetramers of [(L_2Au)$^+$--(AuX_2)$^-$] (see Figure 2·22) are further examples. However, the chain tetramer of (XyNC)AuCl appears to be unique for neutral LAuX molecules.

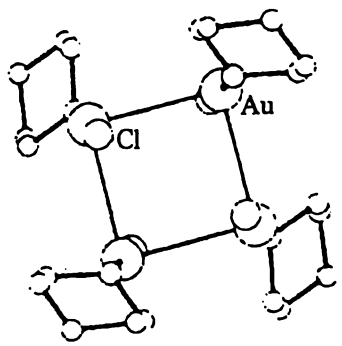

Figure 3·18 Square tetramer of (piperidine)AuCl

In terms of size, the aromatic Xy group is in between that of Ph and Mes, therefore the (XyNC)AuCl structure provided an interesting comparison with the reported structures of (PhNC)AuCl and (MesNC)AuCl.[61] They were found to form a consistent series of auriophilic structural motifs, based on the steric influence of their isonitrile ligands.

---

[112] J. J. Guy, P. J. Jones, M. J. Mays and G. M. Sheldrick, *J. Chem. Soc., Dalton Trans.*, 1977, 8.

(PhNC)AuCl forms a chain structure with anti-parallel Au--Au interactions of 3·46 Å (see Figure 2·11). (MesNC)AuCl forms an independent dimer (Figure 3·19), with a single anti-parallel Au--Au contact of 3·34 Å. The tetrameric (XyNC)AuCl structure is a bridging intermediate between these two motifs, with the central molecules of the tetramer being arranged in a similar fashion to that of the (MesNC)AuCl dimer.

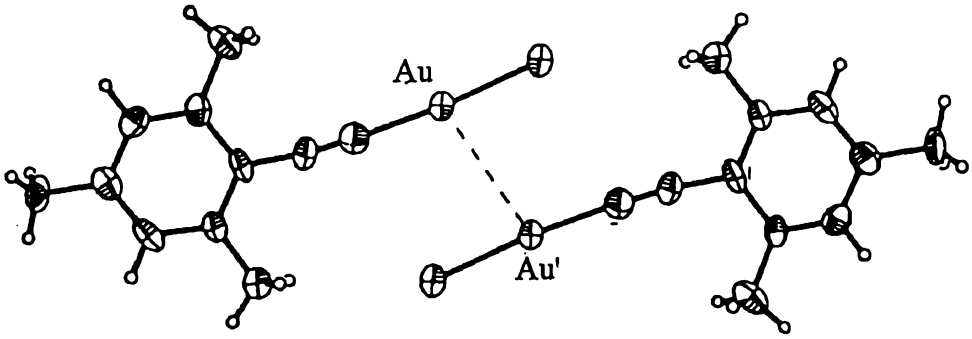

Figure 3·19 Dimer of (MesNC)AuCl

The comparison of the (PhNC)AuCl, (XyNC)AuCl, and (MesNC)AuCl crystal structures illustrates that Au--Au interactions do not entirely control molecular packing in LAuX crystal structures. Since the energy associated with Au--Au interactions is not overwhelming, minor differences in the steric influence of ligands can contribute significantly to the energy balance of each structural formation.

3·6·5 (XyNC)AuNO$_3$

The crystal packing of (XyNC)AuNO$_3$ molecules resulted in a unique 'compressed' chain structure (Figure 3·20). The Au-Au-Au angle of 71° within the chain is acute compared with previously characterised zig-zag chains, which generally exhibit Au-Au-Au angles of ~120-140°.

Initially, it appears that each gold centre is auriophilic four-coordinate (Figure 3·21) and the chain compression is a result of parallel Au--Au interactions between every second gold centre of the zig-zag chain [(Au(1)'--Au(1)"]. The flat Xy groups are able to stack, permitting these extensive Au--Au contacts. The compressed chain structure is not inconsistent with the presence of three-centred auriophilic interactions.

Overleaf → Figure 3·20 Compressed chain of (XyNC)AuNO$_3$
Gold contact distances (Å) and angle (°): Au(1)-Au(1)' 3·245(1); Au(1)'-Au(1)" 3·780(1); Au(1)'-Au(1)-Au(1)" 71·23(2)

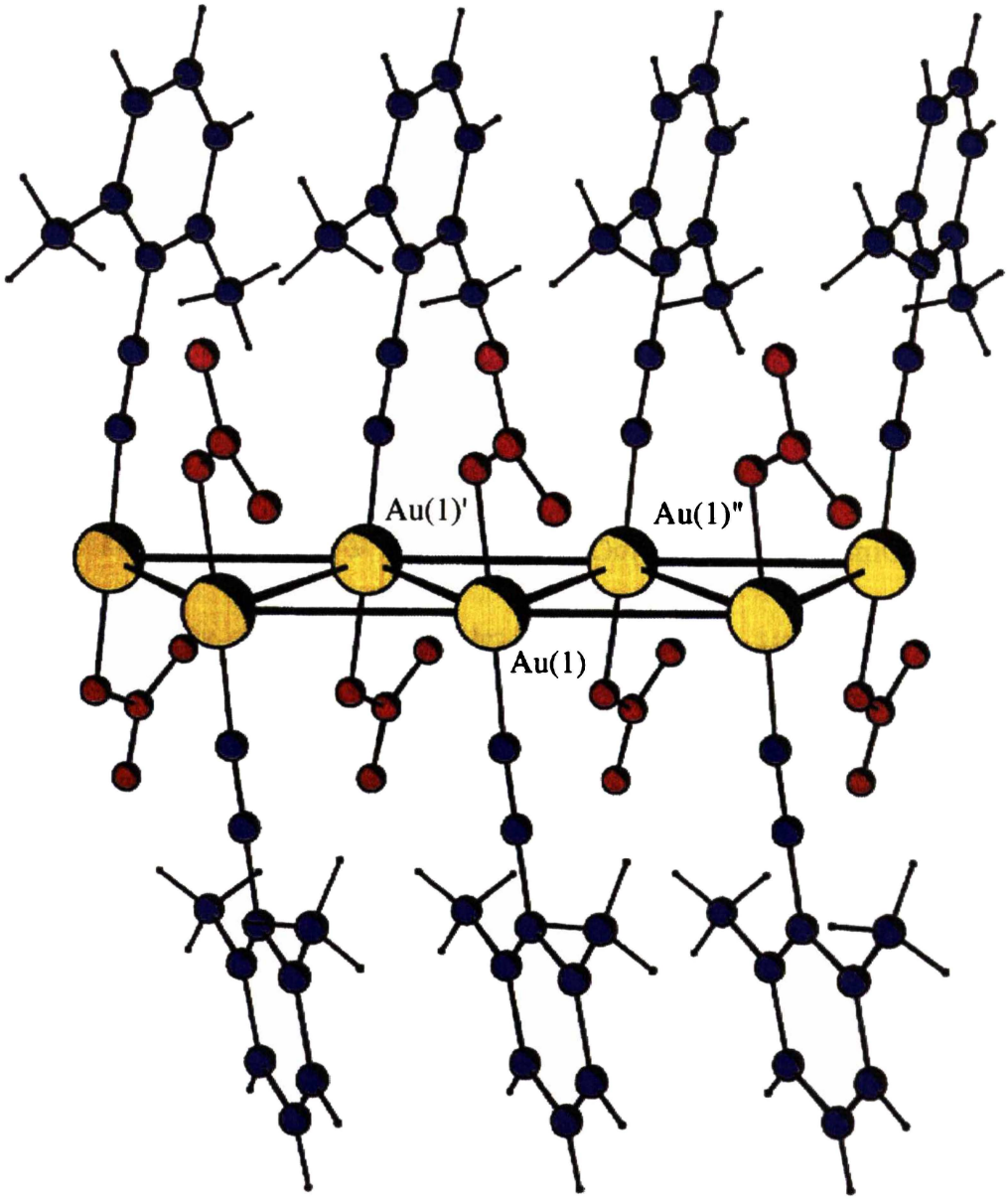
Au(1)'
Au(1)"
Au(1)

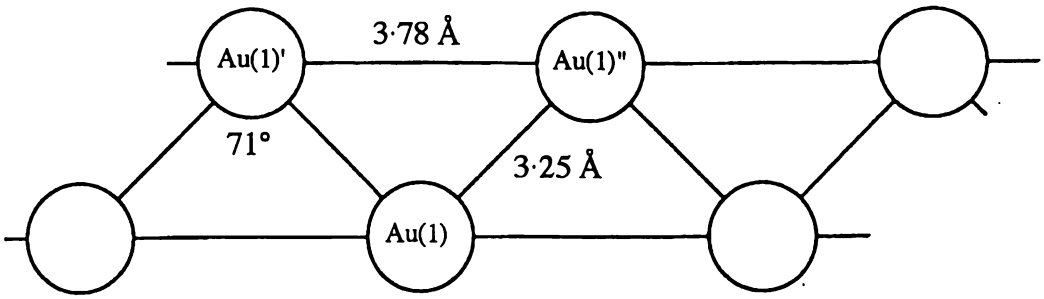

Figure 3·21 Linked gold triangles of (XyNC)$AuNO_3$

There is some uncertainty that a distance of 3·780(1) Å represents an energetically significant interaction. It was noted that the zig-zag chain of (PhNC)AuI (Figure 2·12)[61] exhibits Au--Au interactions of >3·8 Å. It could be presumed that a distance of ~3·8 Å represents an interaction; otherwise this chain would not have formed.

A number of aromatic hydrocarbons are known to crystallise with either stacked or herring-bone structures.[113] The Xy--Xy separation of 3·780(1) Å in the structure of (XyNC)$AuNO_3$ may be indicative of significant π-π interaction. The comparative distance between the stacked carbon sheets of graphite is 3·35 Å.[114] Edge-to-face phenyl 'embraces' have been identified in the molecular packing of metal complexes.[115] Graphitic, or face-to-face, interactions have also been observed in crystal packing of aromatic organometallic species.[116] However, infinite π-π stacking appears to have little precedent for metal complexes.

Assuming that Au(1)'--Au(1)" represents an attractive contact (Figure 3·20), the structure can be described as two parallel straight chains of gold centres, with parallel Au--Au interactions of 3·78 Å along the chains and anti-parallel Au--Au interactions of 3·25 Å between. It is apparent that when chloride from the broken chain of (XyNC)AuCl (see Figure 3·16) is replaced by nitrate, the fragments link. Moreover, the primary Au--Au distances are reduced and the chain compresses. This provides further evidence for the coordination of nitrate (compared with chloride) enhancing auriophilicity in (RNC)AuX complexes.

---

[113] G. R. Desiraju, *Crystal Engineering: The Design of Organic Solids*, Elsevier, Amsterdam, 1989, p. 87.
[114] K. M. Mackay and R. A. Mackay, *Introduction to Modern Inorganic Chemistry*, International Textbook Company, 3rd edn., 1986, p. 82.
[115] C. Hasselgren, P. A. W. Dean, M. L. Scudder, D. C. Craig and I. Dance, *J. Chem. Soc., Dalton Trans.*, 1997, 2019.
[116] D. Braga, F. Grepioni and G. R. Desiraju, *Chem. Rev.*, 1998, **98**, 1375.

3·7 INTERCHAIN PACKING OF (RNC)AuX

The previous section described the auriophilic aggregation of (RNC)AuX molecules. This section describes how the aggregations are positioned in the solid-state, relative to one another. Some reference is made to the previous section, providing further insight into the possible factors determining the extent of the Au--Au contacts.

3·7·1 (Bu^tNC)$AuNO_3$

Depicted in Figure 3·24 is the unit cell of (Bu^tNC)$AuNO_3$, the view of which looks down the zig-zag chains. The stereoview of (Bu^tNC)$AuNO_3$ unit cell packing illustrates how the nitrate anions are positioned to minimise possible contact with the adjacent isonitrile ligands (Figure 3·22). There are two separate orientations of the chains, even though each is crystallographically identical. The interchain packing is very similar to that of (Bu^tNC)AuCl (Figure 3·23).

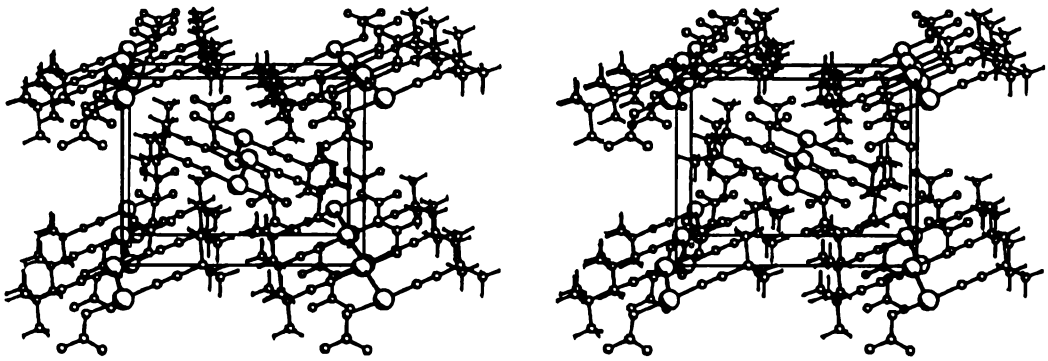

Figure 3·22 Stereoview of (Bu^tNC)$AuNO_3$ cell packing

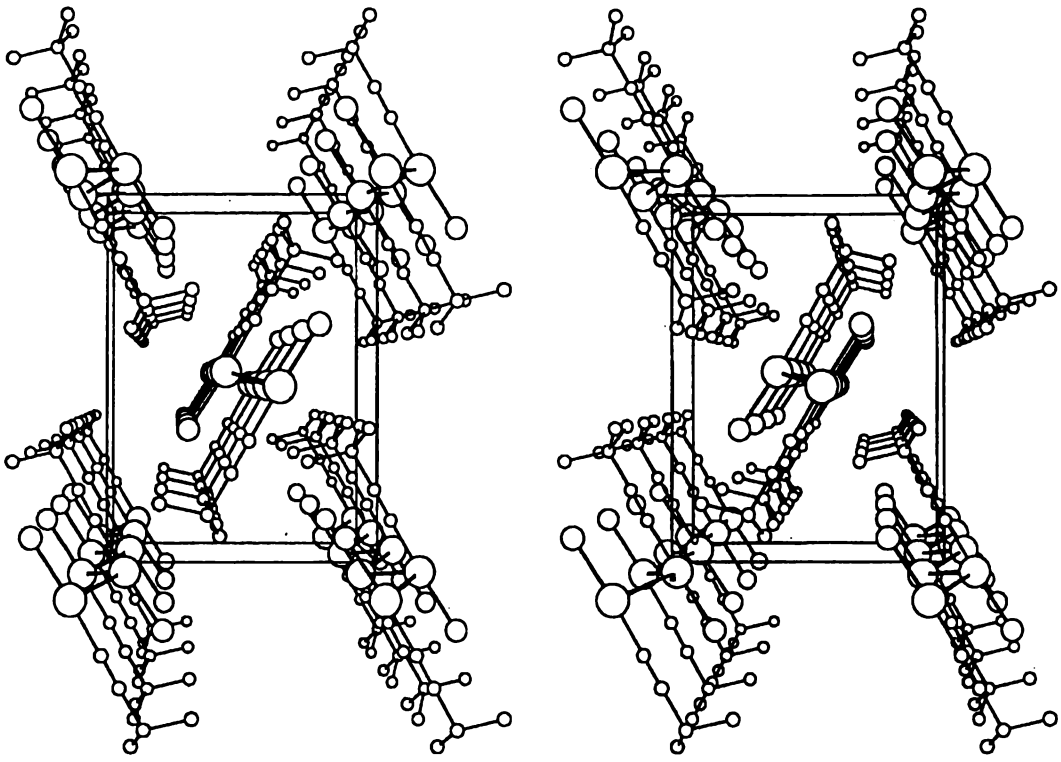

Figure 3·23 Stereoview of (Bu^{t}NC)AuCl cell packing

3·7·2 (EtNC)AuCl

The intrachain packing of (EtNC)AuCl is predictable, in that the Me groups of the EtNC ligands are positioned between the chloride ligands of the two adjacent molecules. The resulting thin chain structures stack and the interchain gold centres appear to form a series of steps (Figure 3·25). The shortest distance between the gold centres of separate (EtNC)AuCl chains is 4·462(1) Å. A stereoview of adjacent (EtNC)AuCl chains is depicted in Figure 3·26, in which the separate chains appear similar to those of (Bu^{t}NC)AuCl. However, there is only one chain orientation observed in the interchain packing of (EtNC)AuCl.

Overleaf (left) → Figure 3·24 Cell packing of (Bu^{t}NC)AuNO$_3$

Overleaf (right) → Figure 3·25 Layers of (EtNC)AuCl chains

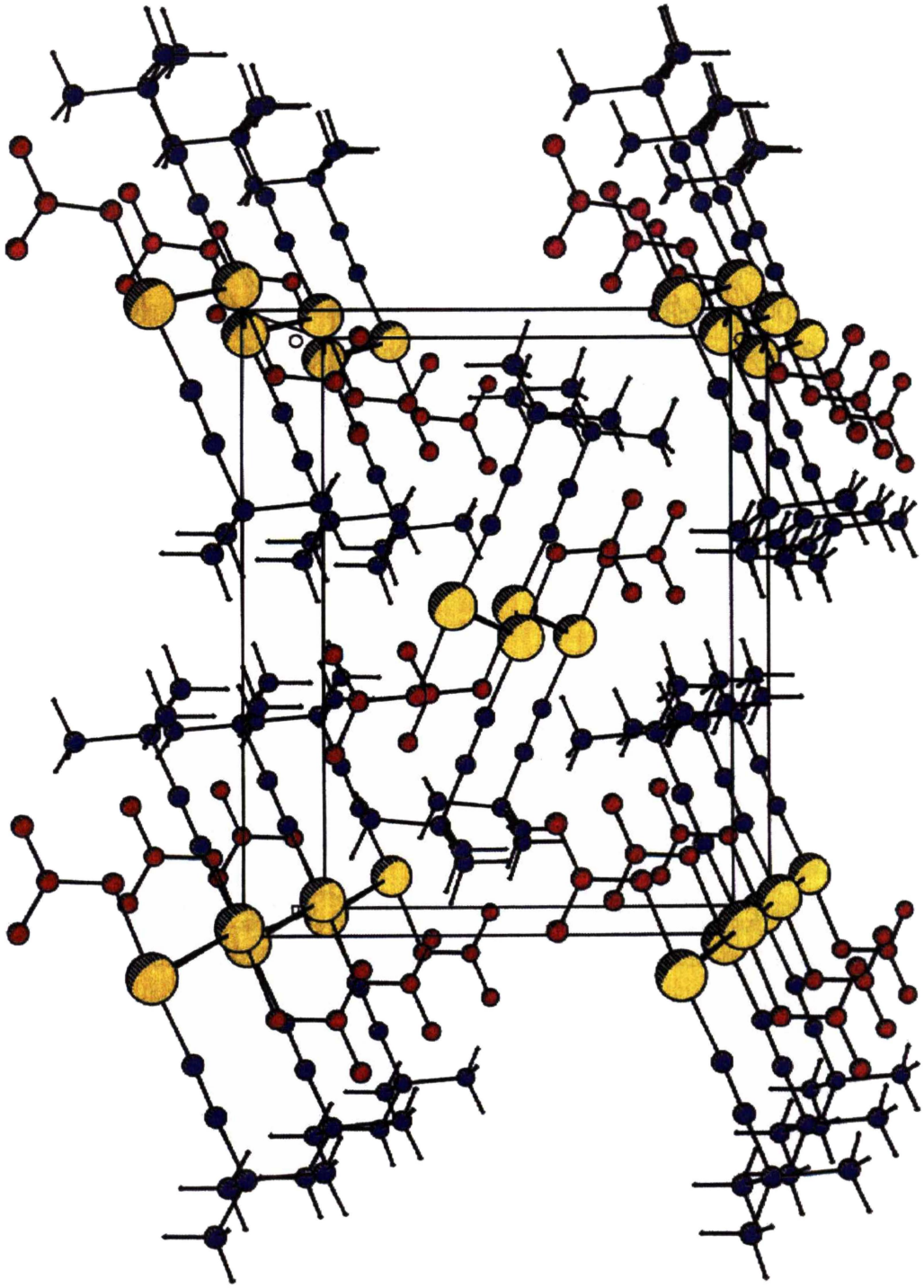

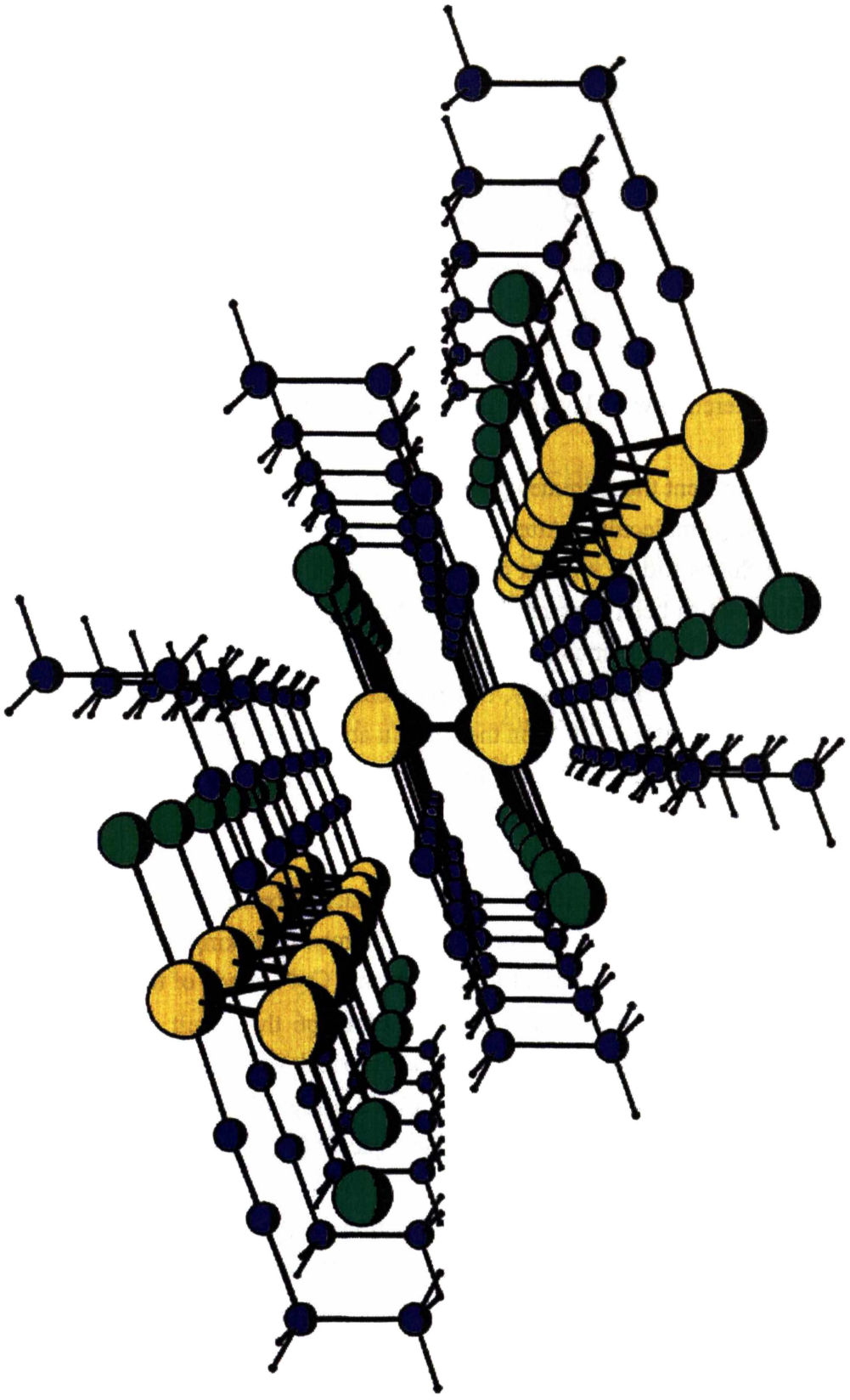

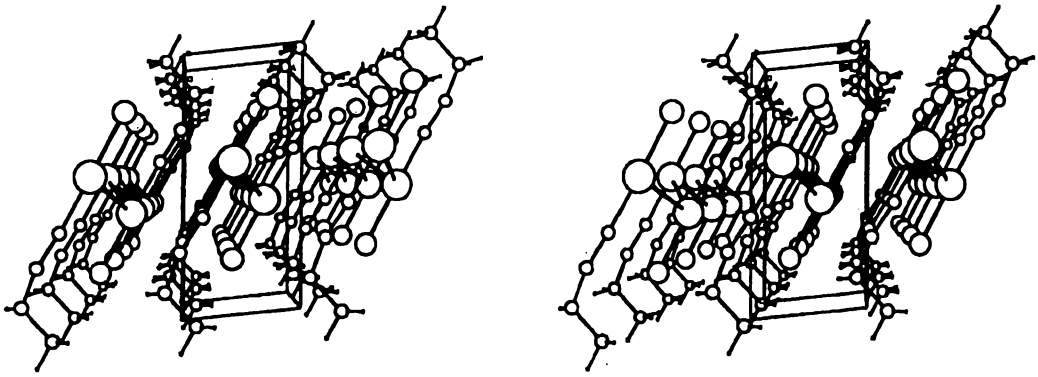

Figure 3·26 Stereoview of layered (EtNC)AuCl chains

Gold sheets represent the extreme upper-limit of auriophilic attraction for linear two-coordinate gold(I) molecules. After due consideration of Figure 3·25, it is possible to visualise the chains sliding without obvious inhibition, allowing a gold sheet to form. Such a structure has been characterised for (MeNC)AuCN (Figure 3·27), where the extensive Au--Au interactions (~3·5-3·7 Å) explain the observed insolubility in all common solvents.[117] Incidentally, this provides further evidence for the chloride anion having a suppressive effect on the Au--Au attraction. Replacement of chloride, from the chain structure of (MeNC)AuCl (Figure 3·11), with CN results in the formation of a sheet.

A possible explanation for the lack of Au--Au interaction between the observed chains of (EtNC)AuCl was provided by studying the interchain packing. The rows of gold centres from one chain are adjacent to the isonitrile C≡N bonds of the neighbouring chain. The interchain positioning may therefore be the result of energetically significant η^2 [Au--(C≡N)] interactions, a proposal which is supported by the observed C(1)-N(1) bond length for (EtNC)AuCl being relatively long (Table 3·4). The distance between the gold centres and the adjacent C≡N bonds is ~3·5 Å.

The suggestion of Au--(C≡N) attractive interactions in the structure of (EtNC)AuCl can be compared to the proposed concept of anion--(C≡N) interactions influencing the Au--Au contact distance. The C≡N bonds in the packing structure of (EtNC)AuCl could be susceptible to two forms of interaction. In one direction, intrachain contact with chloride anions which result in a relatively long Au--Au interactions of 3·55 Å. In the opposite direction, an interchain attraction with gold centres which is responsible for the positioning of the adjacent polymers.

---

[117] S. Esperas, *Acta Chem. Scand.*, **A30**, 1976, 527.

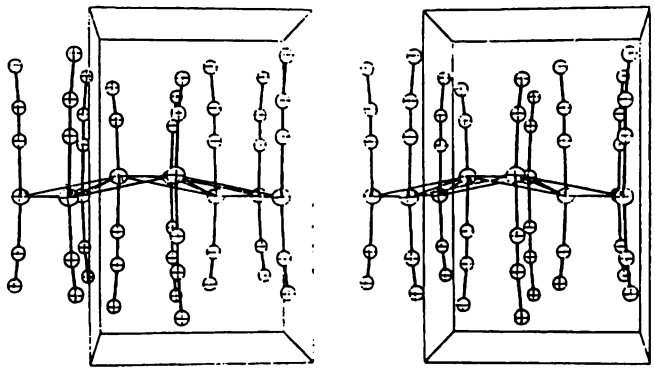

Figure 3·27 Stereoview of (MeNC)AuCN crystal packing

(MeOC(O)CH_2NC)AuCl (see Figure 2·13)[61] and (OC)AuCl also crystallise as gold sheets, the gold centres being auriophilic three- and four-coordinate respectively. The possibility of contact between chloride ligands and neighbouring electron-rich triple bonds is quite apparent in the sheet structure of (OC)AuCl (Figure 3·28). The structure was proposed to contain both Au--Au (3·38 Å) and Cl--C attractive interactions,[118] but the crinkling of the sheet could be a result of Cl--(C≡O) repulsions.

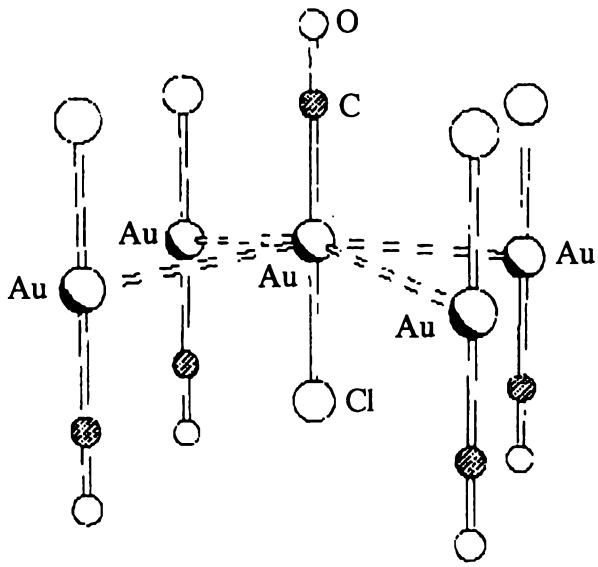

Figure 3·28 Gold sheet of (OC)AuCl

[118] D. B. D. Amico and F. Calderazzo, *Gold Bull.*, 1997, **30**, 21.

3·7·3 (EtNC)$AuNO_3$

The cell diagram and interchain packing (Figure 3·31) of (EtNC)$AuNO_3$ is similar to that of (Bu^{t}NC)$AuNO_3$, in that there are two chain orientations. As for (EtNC)AuCl, (EtNC)$AuNO_3$ appears capable of forming a sheet, for example, rotating the two chains at the top of the cell diagram would result in an layer of (EtNC)$AuNO_3$ molecules. Due to the asymmetric form of both EtNC and ligated nitrate, a sheet structure of (EtNC)$AuNO_3$ would probably require long Au--Au interactions. The concertinaed chain structure with fewer (but stronger) Au--Au contacts is the preferred packing arrangement (Figures 3·29 and 3·30).

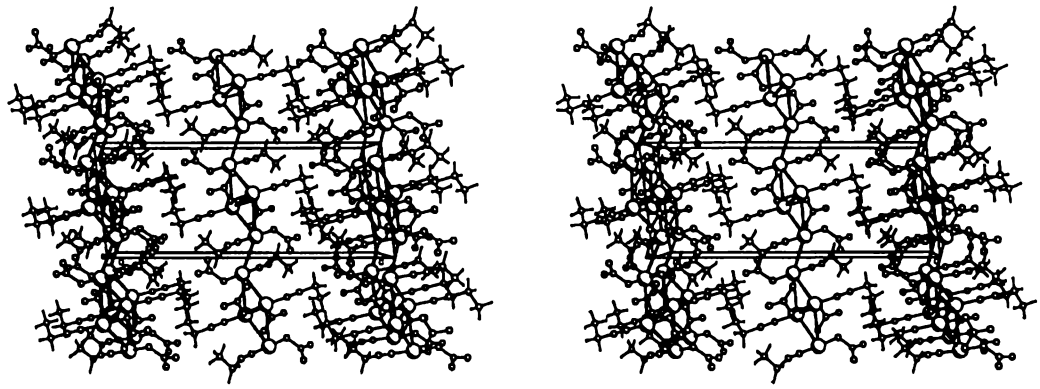

Figure 3·29 Stereoview of (EtNC)$AuNO_3$ cell packing: b axis view

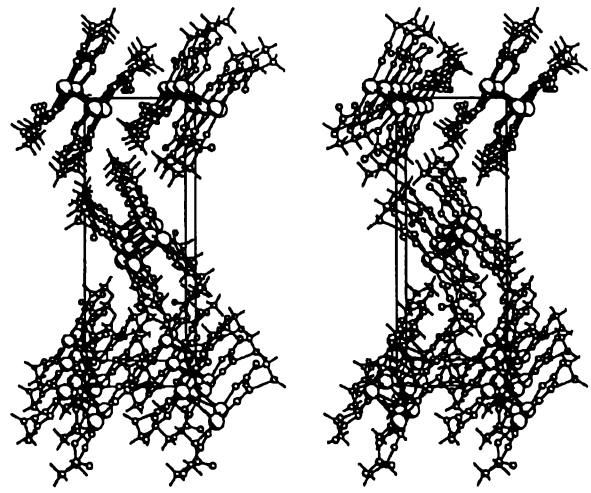

Figure 3·30 Stereoview of (EtNC)$AuNO_3$ cell packing: a axis view

Opposite page → Figure 3·31 Cell packing of (EtNC)$AuNO_3$

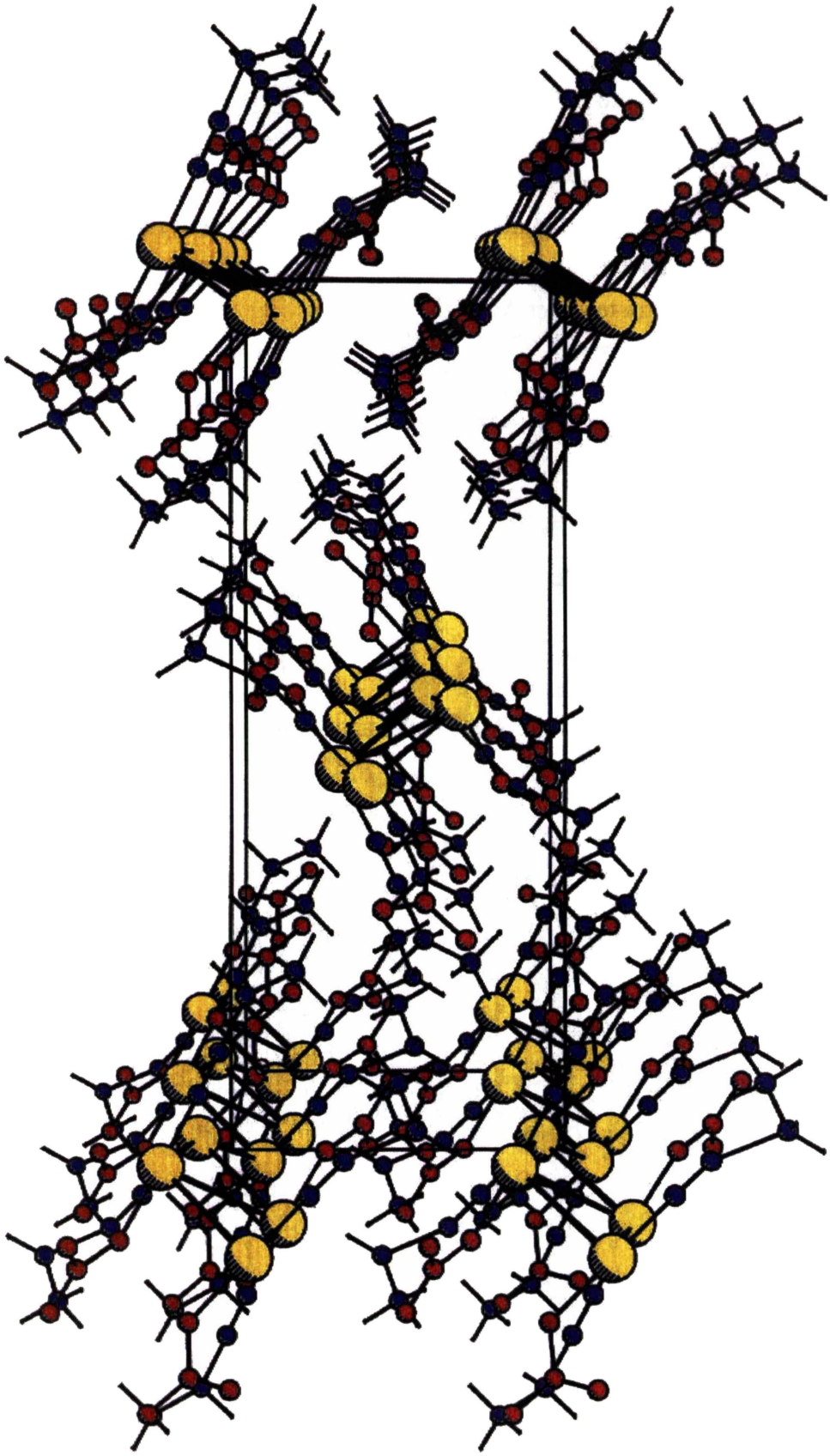

3·7·4 (XyNC)AuCl

The cell packing of (XyNC)AuCl is depicted in Figure 3·34, in which all of the Xy rings are co-planar (Figure 3·32). The positioning of the (XyNC)AuCl tetramers is proposed to be the result of graphitic interactions between Xy rings from adjacent tetramers with Au--Xy interactions also being apparent (Figure 3·33). This provides explanation for the lack of auriophilic polymerisation. The overall molecular packing structure appears to be composed of an intricate network of inter-tetramer π-π and Au--Xy interactions and intra-tetramer Au--Au contacts.

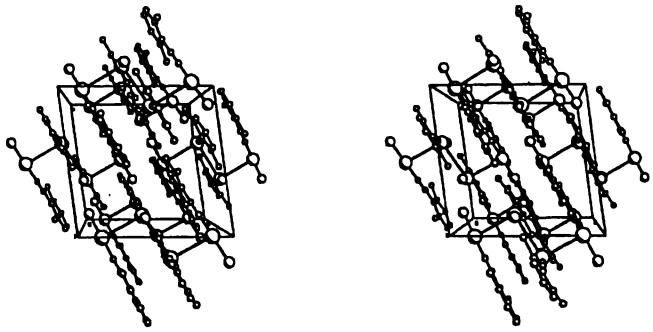

Figure 3·32 Stereoview of (XyNC)AuCl cell packing: b axis view

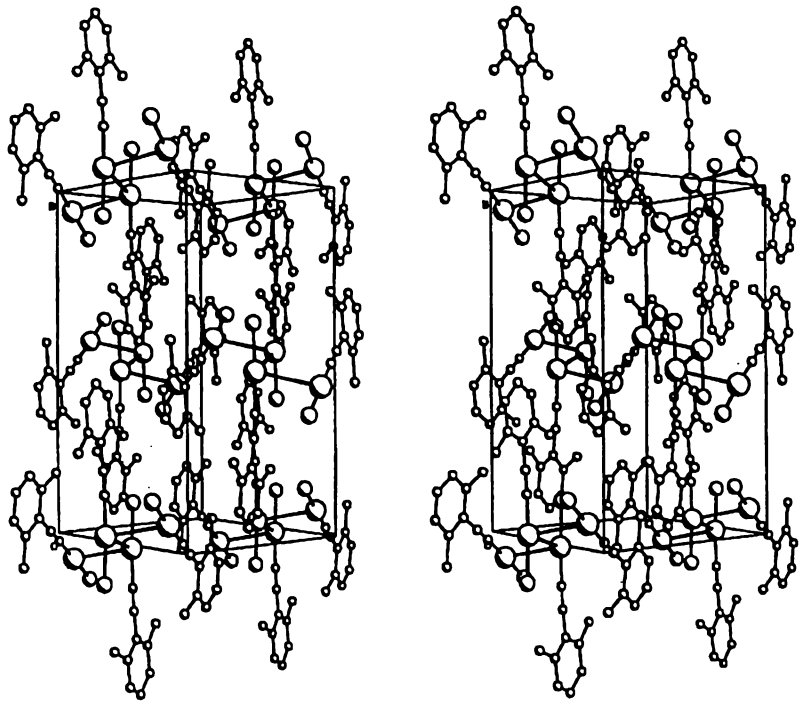

Figure 3·33 Stereoview of (XyNC)AuCl packing: cell diagonal view

Opposite page → Figure 3·34 Unit cell packing of (XyNC)AuCl
The Xy groups of the 'central' fragmented chain are coloured a lighter shade of blue for clarity

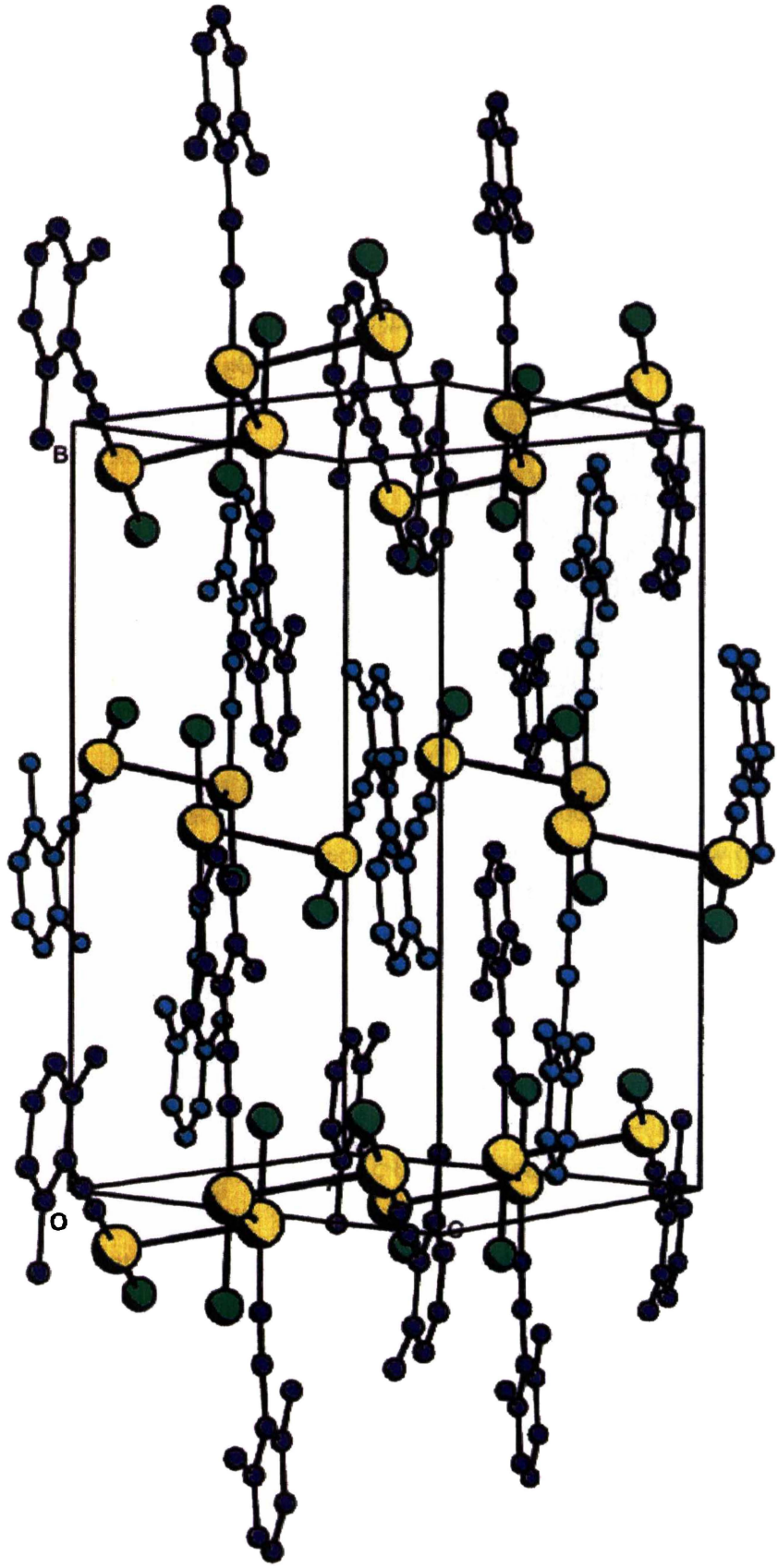
B
O
C

3·7·5 (XyNC)$AuNO_3$

The crystal structure of (XyNC)$AuNO_3$ is illustrated in Figures 3·35 and 3·36, in which rows of Au--Au interactions and graphitic π-π stacking are apparent. These secondary interactions are more extensive than those observed for (XyNC)AuCl. Figure 3·35 shows unequivocally that the asymmetric nitrate ligand positions the $-NO_2$ fragment away from the electron rich C≡N bond of the adjacent isonitrile ligand. Although not as easily discerned, this is also apparent in the polymeric structures of (Bu^tNC)$AuNO_3$ (see Figure 3·22) and (EtNC)$AuNO_3$ (see Figure 3·13). For the (XyNC)$AuNO_3$ structure it appears that there is no significant repulsion, at a separation of 3·25 Å, between the lone pairs of the coordinated oxygen atom and the adjacent isonitrile ligands.

If chloride hypothetically replaced nitrate in the observed structure of (XyNC)$AuNO_3$ the chloride ligands would be 3·78 Å apart. This would not result in a repulsive Cl--Cl interaction, indeed Cl--Cl interactions are known to be attractive and have been utilised in crystal engineering.[119]

The slightly longer Au-Cl bond would mean that rows of coordinated chloride ligands would line up with the C≡N bonds of the adjacent isonitrile ligands, with Cl--(C≡N) distances of 3·25 Å. These Cl--(C≡N) spacings may represent a repulsion, which would explain the observed preference of (XyNC)AuCl for an open tetrameric structure (see Figure 3·15). Also explained would be the general observation that (RNC)AuCl complexes have relatively long anti-parallel Au--Au interactions, which are generally >3·4 Å. However, it was noted that the crossed ligand interaction of (XyNC)AuCl [Au(1)--Au(2)] was not particularly short and is not influenced by possible Cl--(C≡N) repulsion (see Figure 3·5).

A chain of gold centres with exclusive parallel-ligand Au--Au interactions has never been characterised but can be visualised in the straight chain of molecules which form one side of the compressed chain of (XyNC)$AuNO_3$ (Figure 3·35). (XyNC)AuCl or (PhNC)AuCl[61] would have had some potential to form such a structure, with π-π stacking on one side of the Au--Au contacts and Cl--Cl interactions on the other.

Opposite page → Figure 3·35 Cell packing of (XyNC)$AuNO_3$

[119] Ref. 113, p. 175.

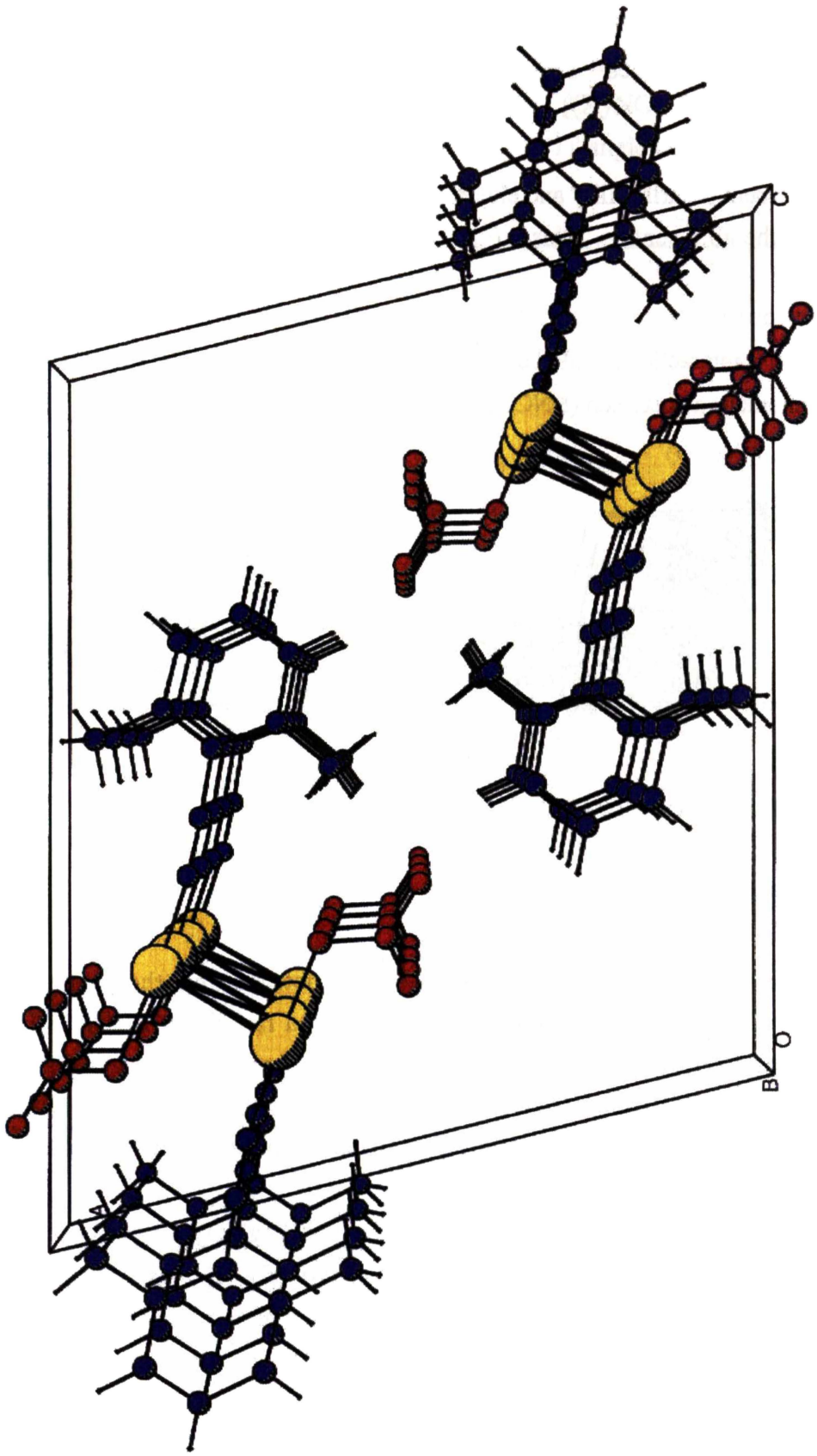
c
b
a

In conjunction with the Bu^{t}NC and EtNC analogues, it is proposed that the replacement of the chloride anion with nitrate enhances the prevalent Au--Au attraction in (RNC)AuX complexes. This could be due to one of (or a combination of) two factors:

(i) The different polarisability and electronegativity of the anions changes the electron density on the gold centres. This influences the inherent attraction that they have for each other.

(ii) Cl--(C≡N) interactions could be significant, in that they counterbalance anti-parallel Au--Au interactions between (RNC)AuX complexes.

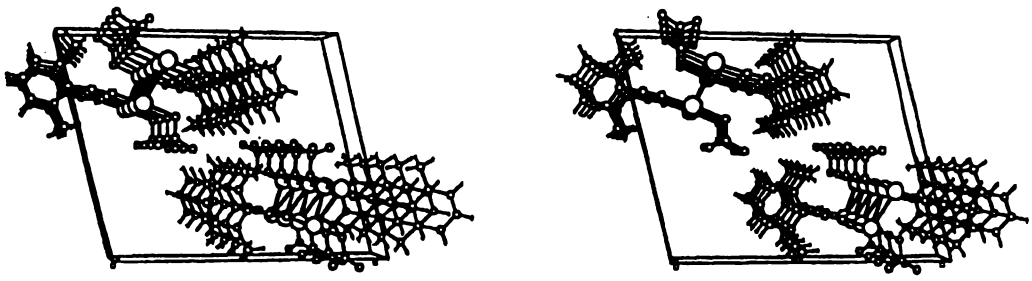

Figure 3·36 Stereoview of (XyNC)$AuNO_3$ chain packing

3·8 $[(XyNC)_2Au]^+NO_3^-$

The polarity of the solvent was important in determining the longevity of (RNC)$AuNO_3$ solutions. (RNC)$AuNO_3$ decomposed rapidly in MeOH, whereas fragile CH_2Cl_2 solutions could be stabilised by adding a small quantity of petroleum spirits. The (XyNC)$AuNO_3$ complex was particularly unstable which could be related to aromatic isonitriles having more π-acceptor character than aliphatic examples.[120]

In an initial attempt to determine the structure of (XyNC)$AuNO_3$, a crystal of solvated $[(XyNC)_2Au]^+NO_3^-$ was isolated and characterised. It was presumed that decomposition during synthesis and crystallisation had released XyNC ligands into solution. These were able to displace the weakly coordinated nitrate ligands providing $[(XyNC)_2Au]^+$ cations and non-coordinating nitrate anions.§ A fragment of the $[(XyNC)_2Au]^+NO_3^-$ crystal for which X-ray data was collected decomposed at 111 °C.

---

[120] P. Fantucci, L. Naldini, F. Cariati and V. Valenti, *J. Organomet. Chem.*, 1974, **64**, 109.

§ $(RNC)_2Au^+$ ions always formed the major peak in ESMS of the (RNC)AuX complexes.

The data was consistent with the space groups C2, Cm or C2/m, with the latter being chosen for refinement. The gold atom was located by direct methods, lying on a site of 2/m symmetry. A subsequent difference map located the other atoms of the cation. Hydrogen atoms were not included in the refinement. $[(XyNC)_2Au]^+$ is a linear two-coordinate species (Figure 3·37). The C(1)-Au(1)-C(1)' angle of 180° and the planar rings are required by crystallographic symmetry.

Table 3·12 Crystal data and structure refinement for $[(XyNC)_2Au]NO_3/MeOH/0{\cdot}5CH_2Cl_2$

Formula	$C_{19{\cdot}5}H_{22{\cdot}5}AuClN_3O_4$	**$T_{max,\ min}$**	0·618, 0·407
M_r	595·32	**F(000)**	577
Crystal system	monoclinic	**Crystal size/mm**	0·22/0·11/0/05
Space group	C2/m	**θ-range/°**	2 to 26
a/Å	15·1075(6)	**Total data**	6203
b/Å	6·7276(1)	**Unique data**	1237
c/Å	8·3385(3)	**R_{int}**	0·023
β/°	107·925(2)	**R_1 (2σ(I)-data)**	0·0420
V/Å^3	1106·11(5)	**R_1 (all data)**	0·0499
Z	2	**wR_2**	0·1165
D_c/g cm^{-3}	1·781	**GoF**	1·035
μ(Mo-Kα)/mm^{-1}	6·8	**Final Δe/ e Å^{-3}**	0·892/-1·737

Overleaf (left) → Figure 3·37 The $[(XyNC)_2Au]^+$ cation
Selected bond distances (Å) and angles (°): Au(1)-C(1) 1·97(1); N(1)-C(1) 1·14(1); N(1)-C(2) 1·40(1); C(1)-Au(1)-C(1)' 180·0; N(1)-C(1)-Au(1) 179·7(9); C(1)-N(1)-C(2) 179·6(9)

Overleaf (right) → Figure 3·38 Cell packing of the $[(XyNC)_2Au]^+$ cations
The XyNC ligands of the 'interlocking' cation are coloured a lighter shade of blue for clarity; (2) is (1) rotated clockwise around the a axis

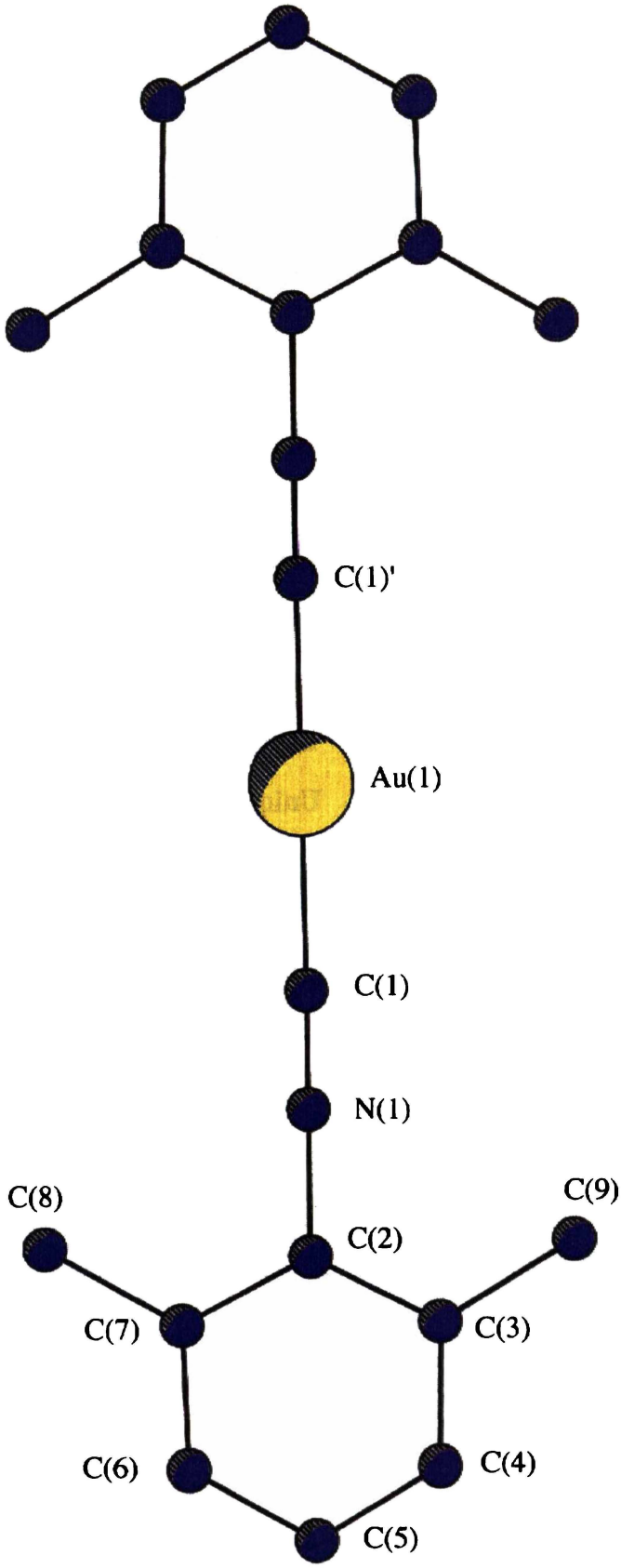
C(1)'
Au(1)
C(1)
N(1)
C(8)
C(9)
C(2)
C(7)
C(3)
C(6)
C(4)
C(5)

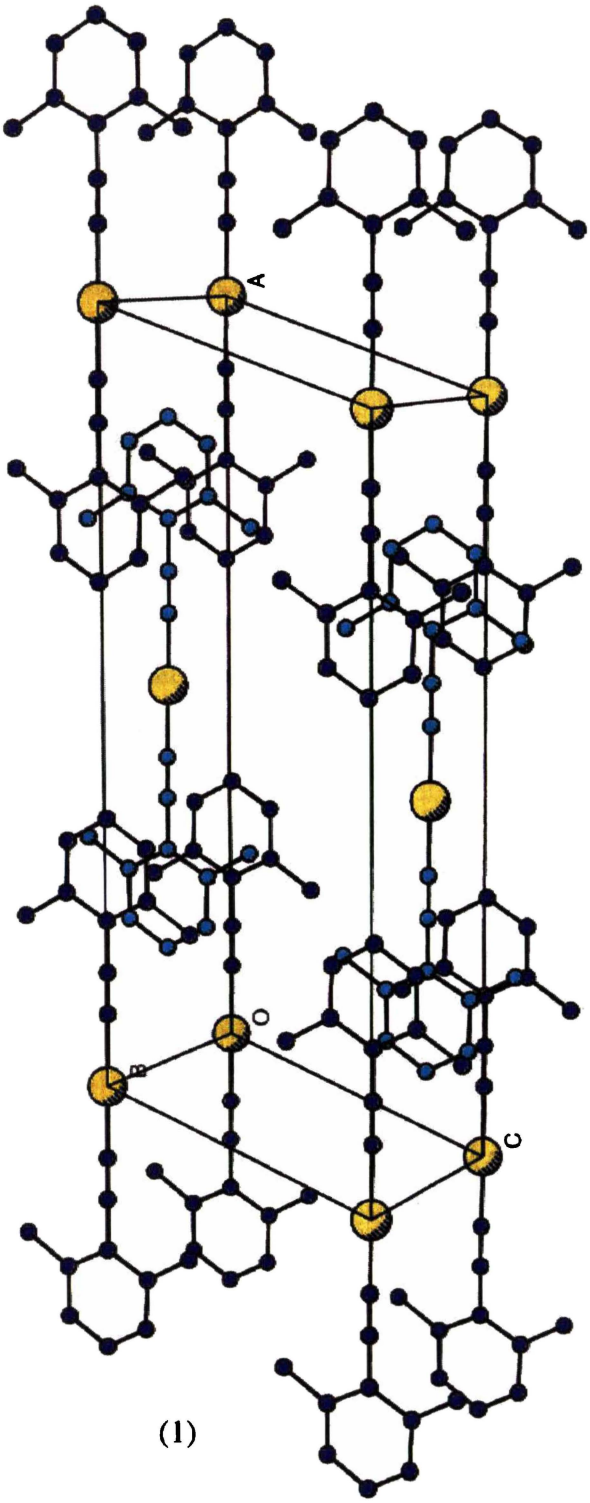

(1)

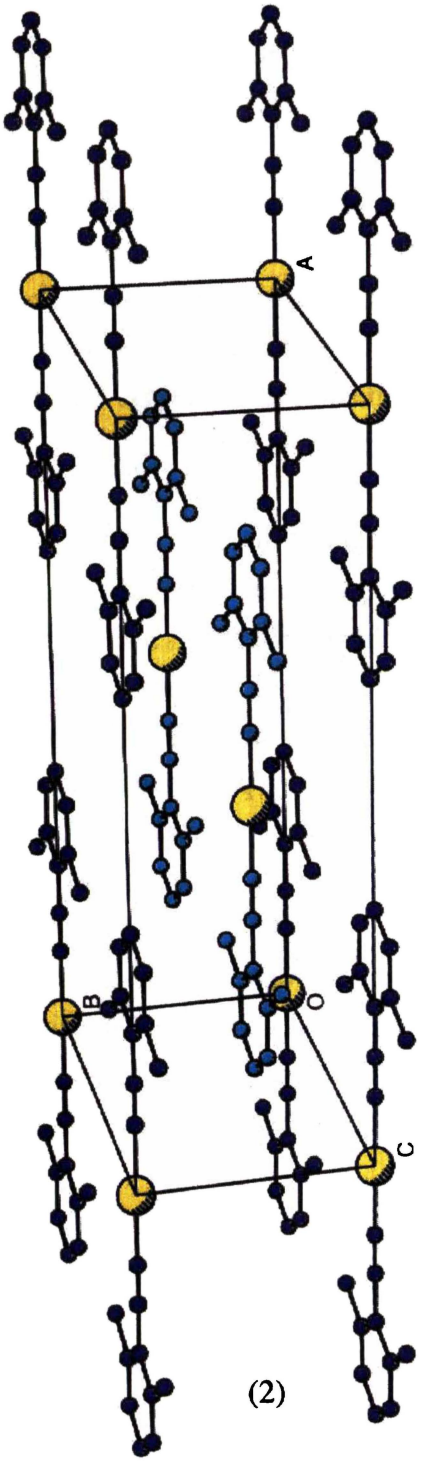

(2)

The structure, which features $[(XyNC)_2Au]^+$ cations and nitrate anions occupying sites of 2/m and m symmetry respectively, does not exhibit auriophilic Au--Au interactions. The shortest Au--Au distance is defined by the b axis (6·728(1) Å). The structure appears to be based on the infinite π-π stacking of interlocking cations (Figure 3·38), resulting in zig-zag chains of Xy rings (Figure 3·44). The a axis of the unit cell would conceivably be shorter if no π-π interaction was present.

Single graphitic (face-to-face) interactions have been observed between metal complexes.[116] As noted in the discussion of the $(XyNC)AuNO_3$ structure, infinite graphitic stacking appears to be unprecedented in the field of organometallic chemistry. The distance between the π-π stacked Xy groups is 3·36 Å, which is half the unit cell b axis. This is very similar to the distance (3·35 Å) separating the sheets in the structure of graphite.

The length of the a and b axes appears to be controlled by π-π stacking. The c axis distance is influenced by the presence of CH_2Cl_2 molecules of crystallisation, which were characterised with a site occupancy of approximately one half. The two chloride atoms were well defined but the carbon (based on the tetrahedral arrangement of CH_2Cl_2) was disordered between two symmetry equivalent sites. The CH_2Cl_2 molecules were positioned between two cationic gold centres which occupied the c axis, a result of two attractive Au--Cl interactions of 2·99 Å (Figure 3·39). Chains are formed along the c axis represented by -Cl--Au--Cl-(CH_2)-Cl--Au--Cl-.

The non-coordinating nitrate anion was disordered over two equivalent sites and was superimposed on an entity consistent with a molecule of MeOH. It appears that this site of the crystal lattice was occupied equally by nitrate and MeOH, the occupancy probably of random order.§ The red atoms in Figures 3·39 and 3·41 represent this site.

Opposite page → Figure 3·39 Solvated $[(XyNC)_2Au]^+$ cations and nitrate anions
Selected bond distances (Å) and angles (°): Au(1)-Cl(1) 2·99(1); Cl(1)-C(91) 1·76(3); Cl(1)-C(91)-Cl(1)' 97(2)

§ Note that electrical neutrality means that each of the sites can only contain half a nitrate ion.

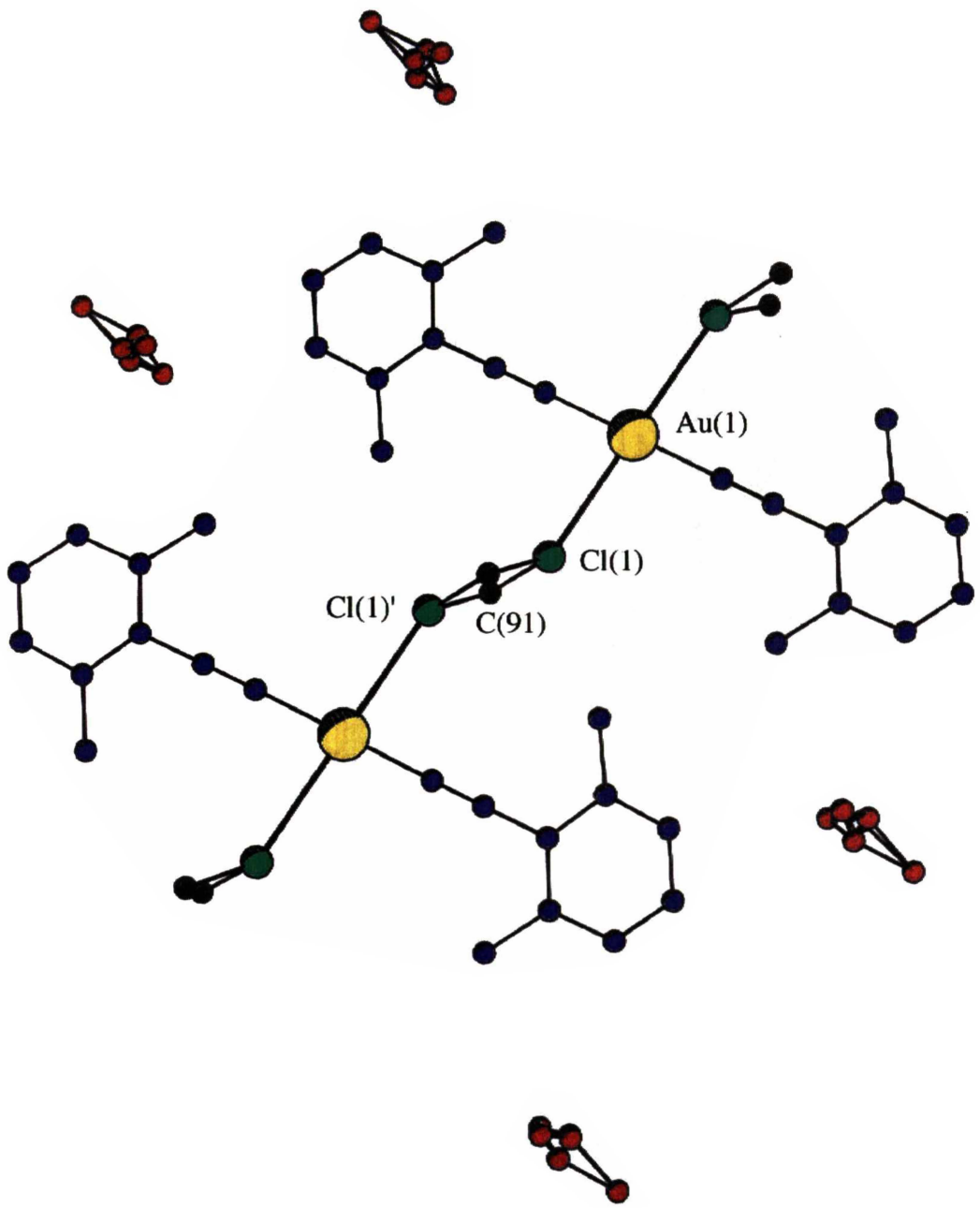
Au(1)
Cl(1)
Cl(1)'
C(91)

It was possible to refine the structure with a non-disordered nitrate in the lower space groups but there were pseudo-symmetry problems and the refinement did not give significantly better agreement factors. The disordered nitrate structure in the higher symmetry space group was the preferred refinement.

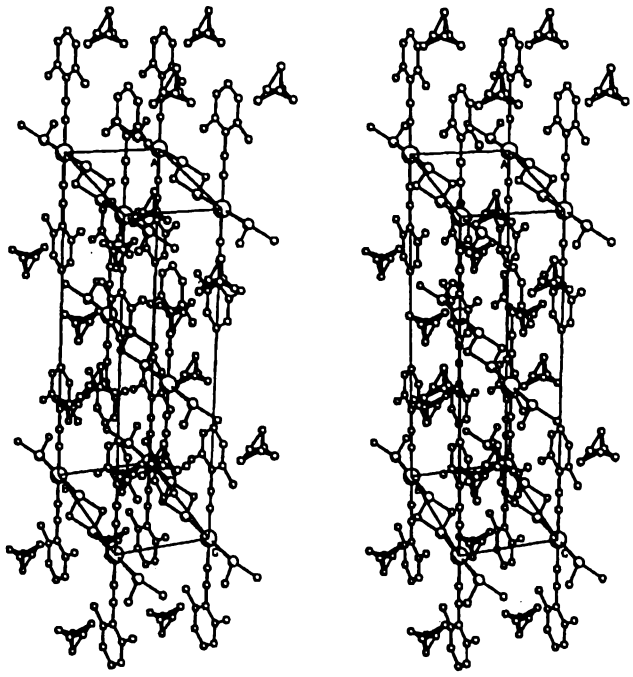

Figure 3·40 Stereoview of $[(XyNC)_2Au]NO_3/MeOH/0{\cdot}5CH_2Cl_2$ cell packing

The overall structure exhibits interwoven chains of stacked Xy groups (along the b axis) and -Cl--Au--Cl-(CH_2)-Cl--Au--Cl- (along the c axis), the resulting internal space being occupied by nitrate and MeOH (Figure 3·40).

Opposite page → Figure 3·41 $[(XyNC)_2Au]NO_3/MeOH/0{\cdot}5CH_2Cl_2$ cell packing

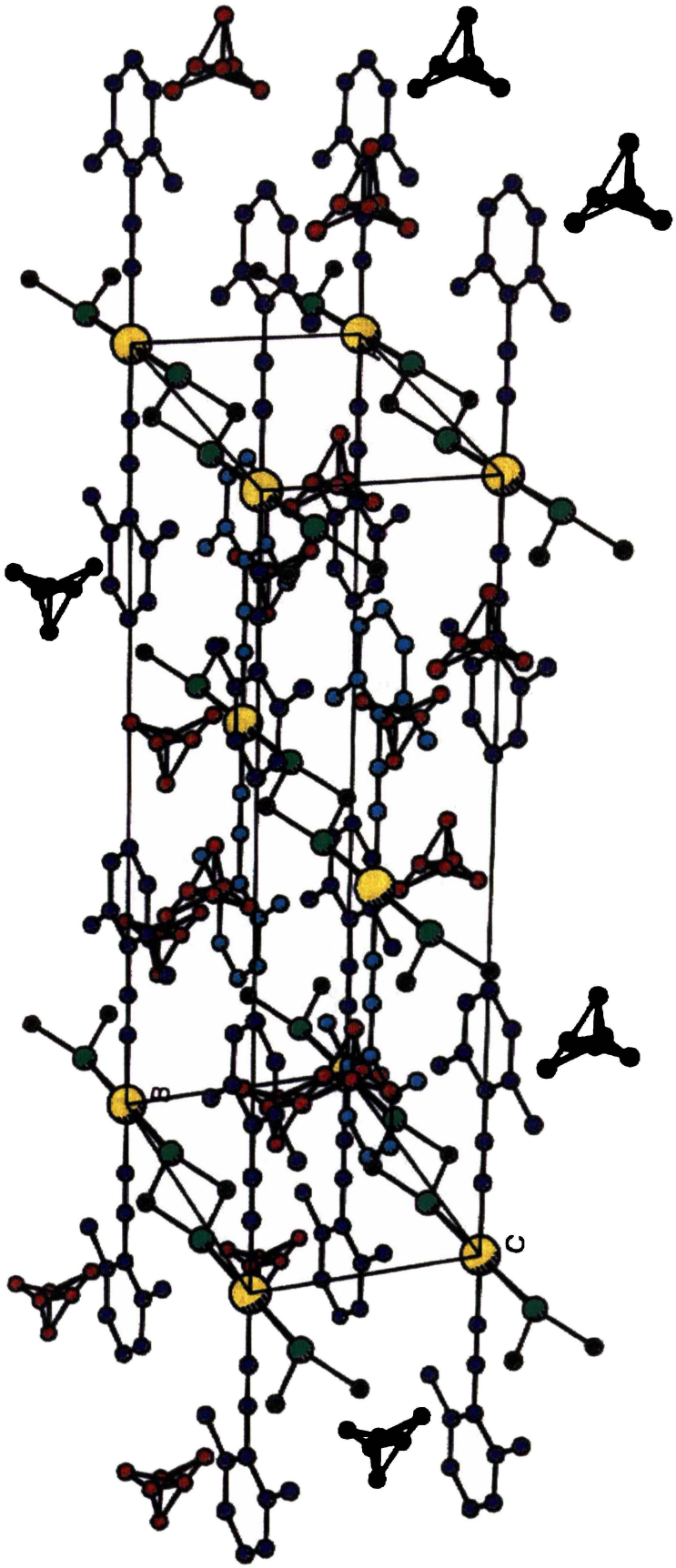
b
c

An appropriate comparison can be made with the neutral complex (XyNC)AuC≡CPh,[121] which is of similar molecular shape but does not have a non-coordinating anion. This complex crystallises as an isolated dimer (Figure 3·42) with an anti-parallel Au--Au interaction of 3·33 Å and two Ph--Xy π-π interactions. It may have been expected that this complex would form an infinite chain based on the observed arrangement of the dimer.

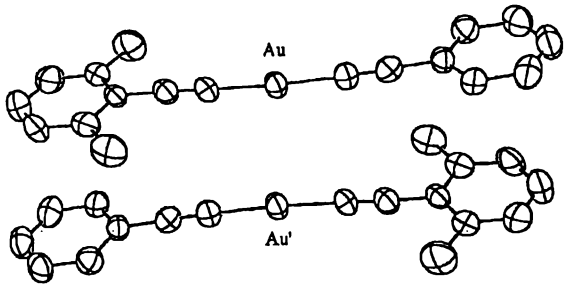

Figure 3·42 Dimer of (XyNC)AuC≡CPh

The symmetrical $[(XyNC)_2Au]^+$ cations in contrast do not form Au--Au interactions, the crystal structure being based on infinite graphitic stacking (Figure 3·44). The lack of Au--Au contact is attributed to the presence of the non-coordinating nitrate anion and effective solvation of the cation by CH_2Cl_2.

In addition to Au--Au intramolecular interactions, an intramolecular graphitic interaction was observed in the structure of the macrocyclic $\{\mu$-[bis(dicyclohexylphosphinomethane)]$Au_2(CNC_6H_4NC)\}_2$ cation (Figure 3·43).[122] As was the case for (XyNC)AuC≡CPh, the π-π stacking is not extended to form a supramolecular structure.

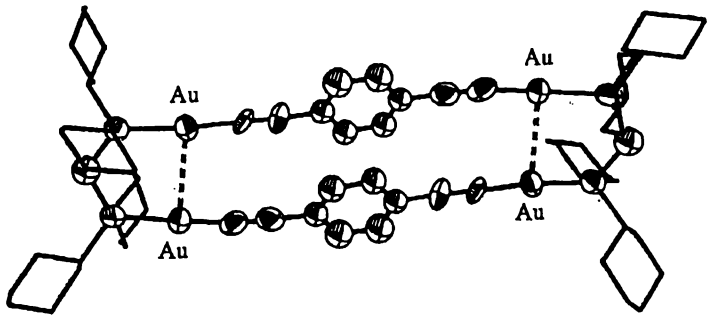

Figure 3·43 Di-isonitrile gold(I) macrocycle

Opposite page → **Figure 3·44** Infinite π-π stacking of $[(XyNC)_2Au]^+$ cations

[121] H. Xiao, K.-K. Cheung and C.-M. Che, *J. Chem. Soc., Dalton Trans.*, 1996, 3699.
[122] M. J. Irwin, L. M. Rendina, J. J. Vittal and R. J. Puddephatt, *J. Chem. Soc., Chem. Commun.*, 1996, 1281.

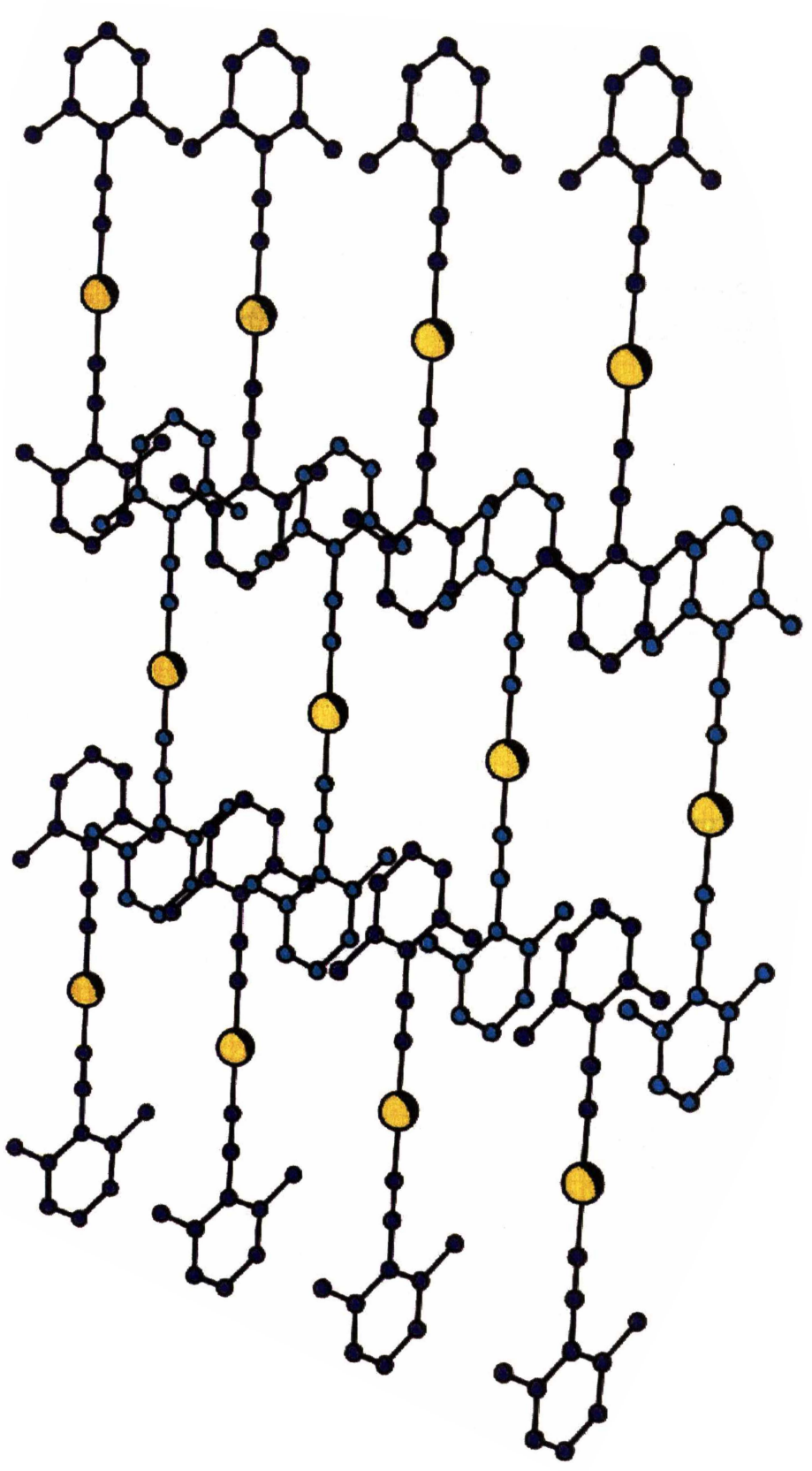

The crystal structures of the ionic complexes $[(MesNC)_2Au]^+BF_4^-$, $[(PhNC)_2Au]^+BF_4^-$ and $[(MeNC)_2Au]^+CF_3SO_3^-$ were recently characterised.[123] In direct contrast to the planar $[(XyNC)_2Au]^+$ cation, the aromatic rings of $[(PhNC)_2Au]^+$ (1) and $[(MesNC)_2Au]^+$ (2) are twisted out of plane and there is no π-π stacking (Figure 3·45).

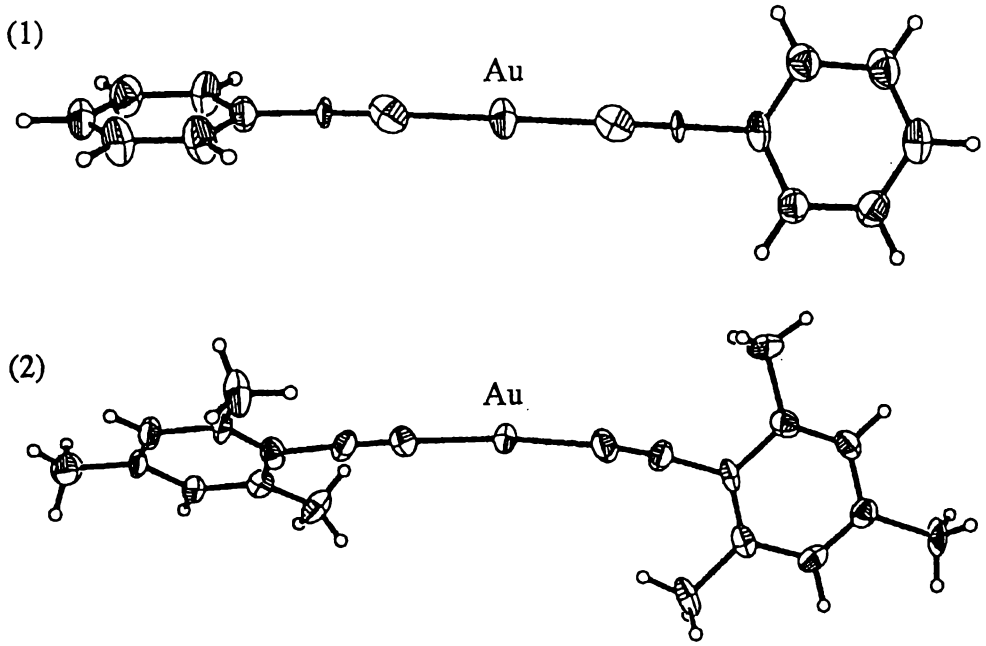

Figure 3·45 Aromatic bis-isonitrile cations

$[(MeNC)_2Au]^+$ formed a chain based on parallel Au--Au interactions of 3·62 Å (Figure 3·46). The chain is crinkled to accommodate the non-coordinating $CF_3SO_3^-$ anions.

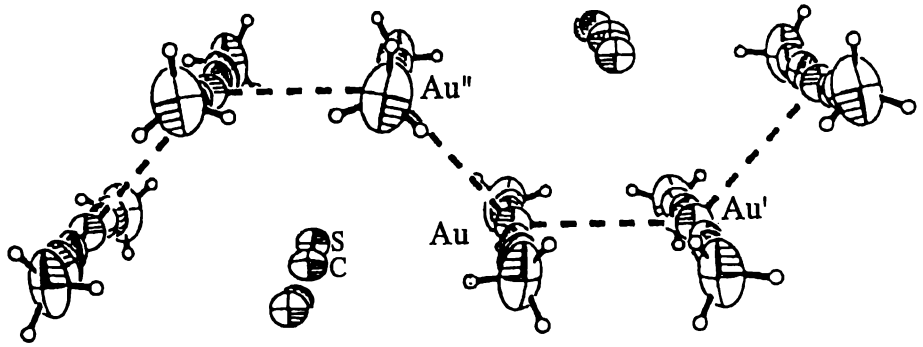

Figure 3·46 Chain of $[(MeNC)_2Au]^+$ cations

123 W. Schneider, A. Sladek, A. Bauer, K. Angermaier and H. Schmidbaur, *Z. Naturforsch.*, 1997, **52b**, 53.

CHAPTER FOUR

CATALYSIS AND CO

-a literature review

" *Many bodies...have the property of exerting on other bodies an action which is very different from chemical affinity. By means of this action they produce decomposition in bodies, and form new compounds into the composition of which they do not enter. This new power, hitherto unknown, is common both in organic and inorganic nature...I shall...call it catalytic power. I shall also call catalysis the decomposition of bodies by this force.*"

"Catalysts are substances which by their mere presence evoke chemical reactions that would not otherwise take place."

- J. J. Berzelius[124]

4·1 CATALYSIS FUNDAMENTALS

The term catalysis was used in ancient Greece to describe a decline in society and is derived from *cata* (down) and *lysein* (break). Berzelius probably considered that catalytic action defied the principles of chemical reactivity and his insight initiated the scientific concept of catalysis.[125] This was further developed by W. Ostwald, who noted that catalysts only have kinetic influence. They change the rates of reaction but have no effect on the thermodynamic equilibrium.[126]

The lowering of the reaction activation energy is the fundamental principle of catalysis. However, catalytic action is not only that of producing a significant reaction rate. As noted by Berzelius, it may lead to alternative reaction mechanisms and products.[127]

---

[124] J. J. Berzelius, *Edinburgh New Philosophical Journal,* 1836, **XXI**, 223; cited in ref. 127, p. vii.
[125] G. C. Bond, *Heterogeneous Catalysis: Principles and Applications*, Claredon, Oxford, 1974, p. 6.
[126] Ref. 7, p. 408.
[127] I. M. Campbell, *Catalysis at Surfaces*, Chapman and Hall, New York, 1988, p. viii.

A catalyst is a substance that increases the rate of approach to equilibrium of a chemical reaction without being consumed itself. Reaction kinetics are the quantitative key to this definition, whereas catalytic reaction mechanisms provide qualitative explanation.[128] Typically, reactants combine with a catalyst and the consequential change of their electronic properties and geometric positioning lead to reaction rate enhancement.[129]

The strength of the reactant-catalyst interaction is vital to the activity of the catalyst. Weak contact results in small quantities of reactant being associated with the catalyst and minimal electronic perturbation of the reactant molecules. If the contact is too strong, an unreactive 'compound' will be formed. A compromise of binding strength is therefore required, in that the association must be strong enough to produce a significant concentration of reactant in contact with the catalyst, but not too strong so as to produce stable intermediates that inhibit the catalytic process.[130]

As a subject, catalysis unifies many aspects of chemistry. Inorganic chemistry is usually required for catalyst preparation. In contrast, catalytic processes frequently involve the reaction of organic molecules. Physical chemistry is used in the study of catalytic reactivity and chemical engineering is required for industrial applications.[131] Furthermore, the catalytic action of enzymes is central to the study of biochemistry.[132]

A large number of industrialised chemical reactions rely on catalysis. There are three main requirements of catalysts that are used in practical applications:[133]

(i) a significant rate of catalytic conversion,

(ii) a high selectivity for specific product(s) and

(iii) a physical stability which minimises the need for regeneration.

---

[128] B. C. Gates, *Catalytic Chemistry*, John Wiley & Sons, Toronto, 1992, p. 2.
[129] J. R. Anderson, *Structure of Metallic Catalysts*, Academic Press, London, 1975, p. 21.
[130] Ref. 127, pp. 162-163.
[131] Ref. 128, p. vii.
[132] L. Stryer, *Biochemistry*, W. H. Freeman & Company, New York, 3rd edn., 1988, p. 177.
[133] Ref. 127, p. 4.

4·1·1 Heterogeneous catalysis

The theory of heterogeneous catalysis indicates that many reactions (which are unfavoured in a homogeneous phase) will proceed on the surface of a solid. The immobilisation of reactants on surfaces leads to physical contact and subsequent chemical reaction. However, the success of a heterogeneous catalyst is not always based on spatial effects. The reactant can be chemically modified and hence rendered more reactive.[134]

The following elementary steps can typically be identified for catalytic surface reactions:[134]

(i) reactant diffusion to the surface,
(ii) reactant adsorption on the surface,
(iii) reaction on the surface,
(iv) product desorption from the surface and
(v) product diffusion away from the surface.

The overall rate of a surface reaction is seldom influenced by steps (i) and (v). However, some exceptions have been provided by porous solid catalysts (particularly when large molecules are involved) and by catalysts that are extremely active. Provided that significant surface coverage is achieved, the catalytic activity of a uni-molecular surface reaction is inversely proportional to the strength of the reactant adsorption. For a Langmuir-Hinshelwood mechanism (see sub-section 4·3·1) the rate of a bi-molecular surface reaction between A and B is generally proportional to the product of the surface coverage (θ) of each reactant:[135]

$$\textbf{Rate} = \textit{rate constant}.\theta_A.\theta_B$$

Heterogeneous catalysts are prone to catalytic poisoning. The surface inhibitor may be one of the following:

(i) an impurity mixed with the reactants,
(ii) a by-product from the reaction or
(iii) one reactant of a bi-molecular reaction.

---

[134] Ref. 7, pp. 500-502.
[135] Ref. 125, p. 23

Studying the structures of catalytic surfaces presents many difficulties and models of reaction intermediates on surface sites are often speculative in nature.[136] However, describing reactant species on surfaces is vital to understanding surface catalysis.[137] Insight has been gained from the study of heterogeneous CO oxidation, which is described in section 4·3.

4·1·2 Homogeneous catalysis

The majority of industrial catalysts are heterogeneous but the use of homogeneous catalysis is becoming increasingly popular. Homogeneous catalysis has specific advantages and disadvantages, outlined as follows:[138]

Advantages

(i) it can be characterised in solution by techniques such as NMR,
(ii) it can be systematically modified to change the reactivity,
(iii) the catalyst preparation is reproducible,
(iv) the activity is highly selective and
(v) it makes efficient use of expensive catalytic metals;

Disadvantages

(i) mild temperatures must be used (to preserve the solvated catalyst) which often result in relatively low activities and turnover rates,
(ii) the concentration of active sites is restricted by the solubility of a homogeneous catalyst and
(iii) the products are difficult to separate from the catalysts. However, homogeneous catalysts can be attached to supports which facilitate the separation.[139]

---

136 Ref. 128, p. 312.
137 Yuan Kou, Hong-li Wang, Jian-zhong Niu and Wei-jie Ji, *J. Phys. Chem.*, 1996, **100**, 2330.
138 Ref. 128, p. 15.
139 Ref. 127, p. 59.

4·1·3 Transition metals and catalysis

A metallic surface atom does not have a full complement of nearest neighbours and chemisorption occurs as a result of molecules interacting with these free valencies. This is a form of chemical reaction, for there is a rearrangement of electron density.[140] The majority of catalytically active materials are transition metals or transition metal complexes. This implies that the *d*-orbitals and valence electrons are important for catalysis. Generally, the adsorption strength on transition metals for the following gases is in the sequence:

$$O_2 > C_2H_2 > C_2H_4 > CO > H_2 > CO_2 > N_2$$

The surfaces of some metals are very reactive and will chemisorb all of these gases. The only metal with an inability to chemisorb oxygen is gold.[141] The surfaces of metals from the left hand side of the transition series chemisorb CO dissociatively. In contrast, metals to the right (for example, platinum) tend to chemisorb CO molecularly.[142]

Transition metals are characterised by their ability to form a variety of oxidation states, which favours homogeneous catalysis by transition metal complexes. The catalytic mechanisms often involve sequential steps of reductive elimination and oxidative addition reactions.[143]

4·2 CO

4·2·1 Metal carbonyls

CO is a prolific and extensively studied ligand in the field of transition metal coordination chemistry. The established Dewer-Chatt-Duncanson theory of CO coordination has been described in detail.[144] To briefly explain this model, CO is a strong π-acceptor and a weak σ-donor. Metal-to-CO back-donation of electron density thus performs an important role in the majority of transition metal carbonyl derivatives, which are termed *classical* metal carbonyls.

---

[140] Ref. 128, p. 326.
[141] Ref. 125, p. 21.
[142] Ref. 15, p. 393.
[143] Ref. 128, pp. 76-77.
[144] See for example: ref. 15, p. 392; ref. 127, p. 138; ref. 145.

The back-donation is from filled *d*-orbitals on the transition metal to anti-bonding molecular orbitals on CO. The C≡O triple bond is therefore weakened on coordination (which is easily detected by a decrease of ν(C≡O) in the IR spectra), but this is compensated for by a strengthening of the metal-CO bond.

Less common are the *non-classical* metal carbonyls, which form when CO coordinates to species that have little propensity for back-donation. Examples include (OC)AuCl (of which the ν(C≡O) frequency is similar to that of the free CO ligand)[47] and $[Hg(CO)_2]^{2+}$.[145]

4·2·2 Distribution, sources and detection of CO

The concentration of CO in the atmosphere is ~100 ppb.[147] However, CO is a common pollutant and continental air masses may have concentrations in the order of 1-3 ppm. Apart from CO_2, more CO is discharged into the atmosphere than any other gaseous pollutant. The main anthropogenic sources are fossil fuel burning,[146] industrial processes (in particular foundry and petroleum refining), biomass burning, heating, cooking and waste incineration. CO is also emitted from oceans, soils, plants, forest fires, volcanic gases and atmospheric oxidation of methane and other hydrocarbons.[147]

Uptake by soils and the oceans is significant, but the removal of atmospheric CO is due mainly to reaction with hydroxide radicals. As the atmospheric concentration of hydroxide varies with the seasons, CO concentration also exhibits an annual cycle with higher levels in winter.[148]

Methods for the detection of CO include gas chromatography, electrochemical sensors[149] and Fourier transform IR (FTIR).[150] FTIR of coordinated CO is frequently used to study the binding sites of catalytic surfaces.[151]

---

145 F. Aubke and C. Wang, *Coord. Chem. Rev.*, 1994, **137**, 483.
146 N. M. Zoumakis, A. G. Kelessis, M. Petrakakis, K. Nikolaou and T. I. Kozyraki, *Sci. Total Environ.*, 1994, **146/147**, 401.
147 O. Badr and S. D. Probert, *Appl. Energy*, 1994, **49**, 99.
148 P. C. Novelli, K. A. Masarie, P. P. Tans and P. M. Lang, *Science*, 1994, **263**, 1587.
149 H. Yan and C.-C. Liu, *Sensors and Actutors B*, 1994, **17**, 165.
150 P. J. Medvecz and K. M. Nichols, *Appl. Spectrosc.*, 1992, **46**, 1887.
151 See for example: J. A. Anderson, *J. Chem. Soc., Faraday Trans.*, 1992, **88**, 1197; P. B. Rasband and W. C. Hecker, *J. Catal.*, 1993, **139**, 551; S. Trautmann and M. Baerns, *J. Catal.*, 1994, **150**, 335.

4·2·3 CO toxicity

CO is toxic with the potential hazard being compounded by the colourless, odourless and non-irritant properties of this gas.[152] There has been suggestion that low levels of CO may have some beneficial biological function.[153] However, potentially fatal CO poisoning is possible if an individual is exposed to a CO source without adequate ventilation. Purifying air by removal of CO from domestic, industrial, and automotive emissions is therefore desirable.[147]

CO is a dangerous asphyxiant because it combines strongly with haemoglobin, thus reducing the ability of blood to carry oxygen to cellular tissues.[154] Lethargy, disorientation, nausea, vomiting and coma are the acute neurological symptoms of CO poisoning.[152] Psychiatric abnormalities are also observed in seemingly recovered patients.[155]

CO poisoning in the workplace has been reported in various situations, usually from enclosed buildings. Those recognised to be at risk include the operators of hydrocarbon-fuelled forklifts,[156] foundry employees[157] and grain storage workers.[158]

Treatment for CO poisoning is initiated by providing adequate ventilation and maintaining the airway, followed by hyperbaric oxygen treatment (HBO). No other therapeutic action has been shown to alleviate the toxic effects of CO.[155] To prevent a toxic exposure to CO, the maximum safe CO concentrations in breathing air has been set at 35 ppm for one hour or 9 ppm for 8 hours.[156]

It is accepted that the best method for CO removal is oxidation to carbon dioxide.[159] The catalytic converters utilised in the exhaust systems of automobiles are capable of efficient CO oxidation, but only when operating at elevated temperatures.[160]

---

[152] D. Risser and B. Schneider, *J. Forensic Sci.*, 1995, **40**, 368.
[153] P. A. Rodgers, H. J. Vreman, P. A. Dennery and D. K. Stevenson, *Seminars in Perinatology*, 1994, **18**, 2.
[154] S. Selvakumar, M. Sharan, M. P. Singh, *J. Theor. Biol.*, 1993, **162**, 321.
[155] K. R. Hardy and S. R. Thom, *J. Toxicol., Clin. Toxicol.*, 1994, **32**, 613.
[156] T. A. Fawcett, R. E. Moon, P. J. Fracica, G. Y. Mebane, D. R. Thiel and C. A. Piantadosi, *J. Occupational Medicine*, 1992, **34**, 12.
[157] R.-S. Koskela, *Scand. J. Work. Environ. Health*, 1994, **20**, 286.
[158] C. P. Whittle, C. J. Waterford, P. C. Annis and H. J. Banks, *J. Stored Prod. Res.*, 1994, **30**, 23.
[159] A. Baiker, D. Gasser, J. Lenzner, A. Reller and R. Schlogl, *J. Catal.*, 1990, **126**, 555.
[160] See for example: D. N. Benton and S. J. Schmieg, *J. Catal.*, 1993, **144**, 9; G. W. Graham, A. D. Logan and M. Shelef, *J. Phys. Chem.*, 1993, **97**, 5445; B. K. Cho, *J. Catal.*, 1994, **148**, 697.

There are several desirable applications for the catalytic oxidation of CO at ambient temperature,[161] for example:

(i) removing CO from air in enclosed spaces such as submarines, warehouses, mines, and the enclosed cabins of cars, trucks, and tractors,[162]

(ii) the regeneration of carbon dioxide in sealed laser units,[163]

(iii) a CO filter cartridge which can be incorporated into gas masks,[164]

(iv) the removal of CO from pressurised breathing mixtures for both recreational and commercial diving applications.

Recently, catalysts have been developed that are effective for CO oxidation under ambient conditions (refer to section 4·4). The use of these materials for practical applications has been investigated.[165]

4·3 CO OXIDATION ON SURFACES

No other adsorbed entity has been more thoroughly studied than CO. This is explained by:[166]

(i) the simplicity of the CO molecule,

(ii) the industrial importance of CO chemistry and

(iii) that techniques such as IR, photoelectron spectroscopy and temperature programmed desorption are applicable to CO study.

---

161 G. B. Hoflund, S. D. Gardner, D. R. Schryer, B. T. Upchurch and E. J. Kielin, *Appl. Catal. B*, 1995, **6**, 117.
162 N. W. Cant and N. J. Ossipoff, *Cat. Today*, 1997, **36**, 125.
163 J. Araña, P. Ramirez de la Piscina, J. Llorca, J. Sales and N. Homs, *Chem. Mater.*, 1998, **10**, 1333.
164 V. Kiernan, *New Scientist*, 1996, 20.
165 See for example: M. Haruta, T, Takase, T. Kobayashi and S. Tsubota, *Cat. Sci. Tech.*, 1991, **1**, 331; Y.-M. Kang and B.-Z. Wan, *Appl. Catal. A*, 1995, **128**, 53.
166 Ref. 15, p. 389.

In addition, the oxidation of CO on metal surfaces has been repeatedly described as the exemplar reaction of heterogeneous catalysis.[167] Insight has been provided by studying CO oxidation under well defined conditions. It has been noted that catalytic processes occurring under ambient pressure may not be detected in model single-crystal studies under vacuum (which has been referred to as the pressure gap) and 'real' poly-crystalline catalyst surfaces are unlike those of model catalysts (the material gap).[168]

4·3·1 CO oxidation on platinum

"There are two possibilities. A CO molecule can condense on a surface of platinum and an O atom can condense beside it, and then the two can interact. Or you can have an O atom adsorbed on the surface and the CO molecule can combine with it during collision."[169]

-I. Langmuir

There is now universal agreement that the former proposal by Langmuir was correct, that is, both molecules adsorb on platinum metal surfaces before they react.[170] This is referred to as the Langmuir-Hinshelwood mechanism and involves the reaction of adsorbed CO molecules and dissociatively adsorbed oxygen.[171]

Where V is a vacant site on the surface, three elemental steps have been proposed:[172]

$$O_2\,(g) + 2V \rightarrow 2O\,(ads)$$

$$CO\,(g) + V \rightarrow CO\,(ads)$$

$$CO\,(ads) + O\,(ads) \rightarrow CO_2\,(g) + 2V$$

---

167 See for example: K.-H. Allers, H. Pfnür, P. Feulner and D. Menzel, *J. Chem. Phys.*, 1994, **100**, 3985; S. Fuchs, T. Hahn and H.-G. Lintz, *Chem. Eng. Process.*, 1994, **33**, 363; J. Szanyi, D. W. Goodman, *J. Phys. Chem.*, 1994, **98**, 2972.

168 X. Xu and D. W. Goodman, *J. Phys. Chem.*, 1993, **97**, 7711.

169 T. Engel and G. Ertl, in *The Chemical Physics of Solid Surfaces and Heterogeneous Catalysis*, eds. D. A. King and D. P. Woodruff, Elsevier, New York, 1982, vol. 4, ch. 3, p. 73.

170 B. J. Brosilow, E. Gulari and R. M. Ziff, *J. Chem. Phys.*, 1993, **98**, 674.

171 M. Falcke and H. Engel, *J. Chem. Phys.*, 1994, **101**, 6255.

172 M. C. Lemos and A. Cordoba, *Phys. Rev. B*, 1994, **49**, 648.

The dissociative oxygen adsorption occurs only on adjacent sites. The reaction between O (ads) and CO (ads) situated on adjacent metal sites is fast and the carbon dioxide desorbs as it is formed.[173] This reaction exemplifies the catalytic action of a metallic surface. The surface participates through the formation of chemical bonds, but the association is transient and the metallic surface is recovered unchanged after the reaction.[174]

The rate of surface CO oxidation is controlled by the adsorption characteristics of the reactants.[175] One of the reactants is usually on the surface in significant quantities and the availability of the other reactant limits the rate of the reaction. The adsorption of CO on platinum is stronger than that of oxygen, thus the rate of CO *desorption* (a process that produces sites for oxygen adsorption) usually controls the overall reaction rate. The activation energy for the oxidation of CO on platinum is therefore related to the activation energy of CO desorption.[176] The ease of CO desorption increases as the coverage increases due to CO--CO lateral repulsions.[177]

The rate of CO oxidation on platinum is influenced by the reaction temperature and concentration of the reactants. At low temperatures, in the presence of significant quantities of CO and oxygen, CO is adsorbed on the surface and the rate is inversely proportional to the partial pressure of CO (P_{CO}) and proportional to P_{O_2}. Under these circumstances the surface may become covered with CO, precluding catalysis. At high temperatures the rate is proportional to P_{CO} because CO desorption rates from the surface are significant.[178]

When the P_{CO}:P_{O_2} ratio is high (given that the temperature is moderate), platinum will be covered with CO and the rate will be inversely proportional to P_{CO}. At low P_{CO}:P_{O_2} ratios, a platinum surface may become enriched with oxygen and the carbon dioxide production rate will then be proportional to P_{CO}. The reaction rate will increase with increasing oxygen coverage up to a certain point, at which stage the reaction rate switches to a negative dependency on P_{O_2}.[179] Under such conditions the surface is essentially oxidised and the reaction rate will decrease dramatically. The role of surface oxygen in reactions on metal surfaces has been reviewed.[180]

---

[173] J. Szanyi, W. K. Kuhn and D. W. Goodman, *J. Phys. Chem.*, 1994, **98**, 2978.
[174] Ref. 127, p. 3.
[175] A. Szabo, M. A. Henderson, J. T. Yates Jr, *J. Chem. Phys.*, 1992, **96**, 6191.
[176] J. Xu and J. T. Yates Jr., *J. Chem. Phys.*, 1993, **98**, 725.
[177] P. Araya and J. Cortes, *J. Chem. Phys.*, 1994, **101**, 1668.
[178] G. G. Jernigan and G. A. Somorjai, *J. Catal.*, 1994, **147**, 567.
[179] B. N. Racine and R. K. Herz, *J. Catal.*, 1992, **137**, 158.
[180] M. W. Roberts, *Chem. Soc. Rev.*, 1989, **18**, 451.

The influence of surface repulsions, attractions (both of which may result in islands of either CO or O) and reactions are accounted for in stochastic Monte Carlo simulations of CO oxidation on metal surfaces.[181] During these simulations the surface appears to exhibit fixed islands of oxygen atoms with a mobile CO phase.[182] Carbon dioxide formation occurs at the edge of the oxygen islands.[175]

4·3·2 Oscillations and patterns in CO surface catalysis

Rate oscillations and the formation of chemical patterns are phenomena often observed in reactions catalysed on a surface.[183] Various reactions have exhibited oscillatory behaviour. The oxidation of CO on platinum represents a frequently investigated system.[184] It is of particular interest to determine which elementary steps are involved in causing oscillations and dissipative adsorption structures.[185] Many processes are involved, such as surface diffusion,[186] formation of sub-surface species,[187] surface reconstructions,[188] as well as adsorption, desorption, surface reactions, surface phase transitions and lateral molecular interactions.[189] Direct study of the effects of these processes has been achieved using photo-emission electron microscopy (PEEM).[190]

4·3·3 Structural sensitivity

An important concept of heterogeneous catalysis was proposed in 1925 by H. S. Taylor, who surmised that a metal surface was made up of various unique surface sites, only a few of which may participate in a surface reaction.[191]

---

181 M. Mukesh, *J. Catal.*, 1992, **133**, 153.
182 Ref. 169, p. 80.
183 Y.-S. Lim, M. Berdau, M. Naschitzki, M. Ehsasi and J. H. Block, *J. Catal.*, 1994, **149**, 292.
184 M. Ehsasi, M. Berdau, T. Rebitzki, K.-P. Charle, K. Christmann and J. H. Block, *J. Chem. Phys.*, 1993, **98**, 9177.
185 N. Hartmann, K. Krischer and R. Imbihi, *J. Chem. Phys.*, 1994, **101**, 6717.
186 W. Swiech, C. S. Rastomjee, R. Imbihl, J. W. Evans, B. Rausenberger, W. Engel, A. K. Schmid, A. M. Bradshaw and E. Zeitler, *Surf. Sci.*, 1994, **307**, 138.
187 J. Ree, Y. H. Kim and H. K. Shin, *J. Chem. Phys.*, 1996, **104**, 742.
188 R. F. S. Andrade, D. Lima, G. Dewel and P. Borckmans, *J. Chem. Phys.*, 1994, **100**, 9192.
189 V. Gorodetskii, W. Drachsel and J. H. Block, *J. Chem. Phys.*, 1994, **100**, 6907; V. Gorodetskii, W. Drachsel, M. Ehsasi and J. H. Block, *J. Chem. Phys.*, 1994, **100**, 6915.
190 M. D. Graham, I. G. Kevrekidis, K. Asakura, J. Lauterbach, K. Krischer, H.-H. Rotermund and G. Ertl, *Science*, 1994, **264**, 80.
191 H. S. Taylor, *Proc. R. Soc.* (London) *A*, 1925, **108**, 105; cited in ref. 128, p. 352.

The surface environment of a metal is not necessarily uniform (Figure 4·1).[192] It is generally accepted that CO oxidation on platinum is a structurally-insensitive reaction, in that the overall reaction rate does not depend on the surface arrangement of metal atoms.[193] However, the binding energy of gas adsorbates at defect sites is usually higher than on the terraces of platinum surfaces. Oxygen and CO adsorption both occur preferentially on step sites.[175]

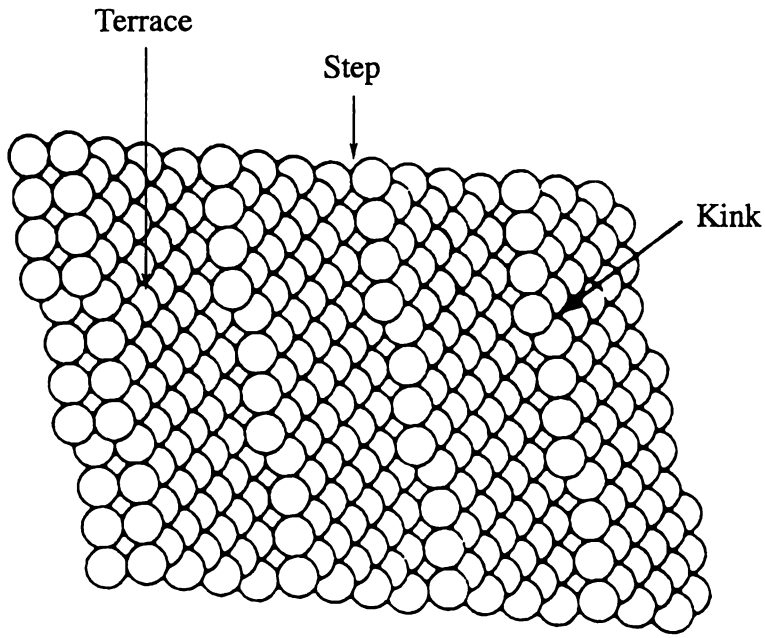

Figure 4·1 Metallic surface characteristics

Geometric models have been developed for CO oxidation on platinum.[176] These predicted different reactivity for the surface species depending on the site to which they are adsorbed. The ideal reaction geometry was CO and oxygen both adsorbed on terrace sites (where the reactants were separated by ~2·0 Å). However, the reaction of CO (terrace) and oxygen (step) was faster even though the reactants are separated by ~2·5 Å (Figure 4·2).

It was concluded that a combination of both geometric and energetic factors determine what reaction conditions are favourable and one isolated factor cannot accurately predict reactivity trends.[176] Similar concepts have been developed for the adsorption of ethylene on platinum.[194]

---

[192] Ref. 128, p. 314.
[193] Ref. 169, p. 75.
[194] J.-F. Paul and P. Sautet, *J. Phys. Chem.*, 1994, **98**, 10906.

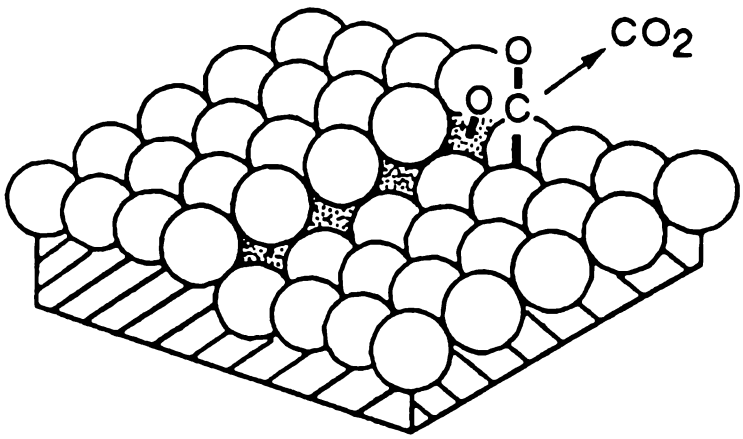

Figure 4·2 Favoured reaction site on platinum

The binding strength and desorption kinetics of CO have been shown to vary with the size of metallic platinum particles, with slower rates of CO oxidation observed on smaller particles.[195] The curvature of small particles may effectively separate the surface adsorption sites. This would reduce repulsive CO--CO interactions and therefore CO desorption rates.

4·3·4 CO oxidation on copper

Metallic copper has a relatively strong affinity for oxygen and generally forms a stable surface oxide. This oxide layer tends to preclude efficient CO oxidation catalysis under standard conditions.[196] Investigation of copper CO oxidation catalysts has been carried out at temperatures of 250-300 °C to determine how the rate of the reaction varies between different oxidation states of copper.[178] Oxidised copper exhibited a low rate of activity but the surface was gradually reduced by reaction with CO. As the metallic characteristics of the surface increased, the rate of reaction increased.

Insight is gained by comparing CO oxidation over model copper catalysts with what is known of the reaction over platinum catalysts. The role of the reactants is reversed, in that oxygen is strongly bound to copper, whereas CO has a weak affinity for this metal. The reaction rate of CO oxidation on copper is usually proportional to P_{CO}.[178]

---

[195] G. S. Zafiris and R. J. Gorte, *J. Catal.*, 1993, **140**, 418.
[196] T. Sueyoshi, T. Sasaki and Y. Iwasawa, *Chem. Phys. Lett.*, 1995, **241**, 189.

4·3·5 Oxide catalysts

CO oxidation can occur when CO is chemisorbed to the surface cations of transition metal oxides.[197] The catalytic process involves redox cycles in which lattice oxygen is released within the carbon dioxide product.[198] The thermally stable $La_{0.9}Ce_{0.1}CoO_3$ perovskite-type oxide has been used commercially for the oxidation of CO and hydrocarbons from gas oven emissions.[199] The commercial CO oxidation catalyst "Hopcalite" is a mixture of MnO_2 and CuO. This mixed oxide is active over a range of temperatures but is deactivated by traces of water.[200]

4·3·6 Bimetallic catalysis

The surfaces of bimetallic materials have unique properties.[201] The catalytic potential of a transition metal can be altered by the addition of a dissimilar metal.[202] This is of technological significance as well as forming further basis for studies of surface phenomena.[203]

The coordination of CO to several bimetallic systems has been investigated,[204] as has catalytic CO oxidation.[205] Bimetallic particles may promote CO and oxygen mixing at lower temperatures.[206] An example is the coating of rhodium with copper,[207] where a charge donation from rhodium to copper occurs, which was proposed to strengthen the copper--CO interaction. Given the inherent weak copper--CO interaction (relative to copper--oxygen), this may enhance the rate of CO oxidation on the copper surface. Alternatively, the bimetallic surface may expose both rhodium and copper atoms whereby the role of the copper atoms is to increase the intrinsically low oxygen coverage on the rhodium surface.

---

197 K. S. R. C. Murthy and J. Ghose, *J. Catal.*, 1994, **147**, 171.
198 Ref. 127, p. 168.
199 H. Yasuda, Y. Fujiwara, M. Mizuno and M. Misono, *J. Chem. Soc., Faraday Trans.*, 1994, **90**, 1183.
200 S. A. Solovev, G. M. Belokleitseva and V. M. Vlasenko, *Z. Prikl. Khim.*, 1992, **65**, 1555.
201 M. J. Lopez, P. A. Marcos and J. A. Alonso, *J. Chem. Phys.*, 1996, **104**, 1056.
202 G. Deganello, D. Duca, L. F. Liotta, A. Martorana, A. M. Venezia, A. Benedetti and G. Fagherazzi, *J. Catal.*, 1995, **151**, 125.
203 W. Juszczyk, Z. Karpinski, D. Lomot, J. Pielaszek and J. W. Sobczak, *J. Catal.*, 1995, **151**, 67.
204 A. K. Santra and C. N. R. Rao, *J. Phys. Chem.*, 1994, **98**, 5962.
205 See for example: P. Praserthdam and T. Majitnapakul, *Appl. Cat. A*, 1994, **108**, 21; A. D. Logan and M. T. Paffett, *J. Catal.*, 1992, **133**, 179; Y. Cai, H. G. Stenger Jr. and C. E. Lyman, *J. Catal.*, 1996, **161**, 123.
206 J. A. Anderson, *J. Catal.*, 1993, **142**, 153.
207 J. Szanyi and D. W. Goodman, *J. Catal.*, 1994, **145**, 508.

4·4 TWO-COMPONENT SURFACE CATALYSIS

4·4·1 Supported metal catalysts

It is known that metal particles of sub-micron dimension have novel chemical and physical properties.[208] These include molecular binding properties different from those of the bulk metal, which may or may not be advantageous to catalysis. One obvious advantage is that efficient use is made of the metal.[209]

Supports are not necessarily inert because they may participate in a catalytic reaction at the metal particle/support interface. Furthermore, the catalytic properties of supported metal particles can be modified by electrical interaction between the particles and the support.[210]

The preparation of a supported metal catalyst usually involves a metal complex dissolved in a fluid phase. This complex is deposited by some means, so that after various treatments active catalytic sites are generated. The degree of dispersion of the metal is limited by the tendency to aggregate during calcination.[211]

CO oxidation catalysts composed of noble metals supported on active reducible metal oxides have been prepared recently.[16] The supports are thought to adsorb oxygen from the gas phase and transfer it to CO that is coordinated on the supported metal.[170] The reaction of CO and oxygen over two-component catalysts has been simulated using Monte Carlo modelling techniques, from which the following conclusions were made:[17]

(i) The Langmuir-Hinshelwood reaction between CO and oxygen proceeds at a negligible rate over metal catalysts near ambient temperature. This is in spite of the reaction being thermodynamically favoured and the fact that several metals (for example, platinum and palladium) can chemisorb both reactants.

---

[208] K. C. Grabar, P. C. Smith, M. D. Musick, J. A. Davis, D. G. Walter, M. A. Jackson, A. P. Guthrie and M. J. Natan, *J. Am. Chem. Soc.*, 1996, **118**, 1148; M. Kubo, A. Stirling, R. Miura, R. Yamauchi and A. Miyamoto, *Catal. Today*, 1997, **36**, 143.
[209] Ref. 129, p. 163.
[210] W.-P. Dow and T.-J. Huang, *J. Catal.*, 1994, **147**, 322.
[211] Ref. 127, p. 73.

(ii) When a clean platinum or palladium surface is in contact with both CO and oxygen under ambient conditions, CO covers the surface, preventing oxygen adsorption. However, at high temperatures (>150 °C) CO desorption rates become significant and produce chemisorption sites for oxygen.

(iii) A composite material made up of a highly interspersed mixture of one type of site (that adsorbs CO) and another type of site (that adsorbs oxygen) would have potential for low temperature CO oxidation. In such a catalyst, CO and oxygen would not compete for the same adsorption sites and therefore CO inhibition of low temperature CO oxidation would be eliminated.

(iv) The separate constituents of the two-component catalyst have no appreciable activity for the oxidation of CO at low temperature. A synergistic interaction is therefore present in the two-component system.

CeO_2 has been studied extensively as a support for noble metal CO oxidation catalysts and is used in automotive exhausts.[212] The CeO_2 support stabilises the highly dispersed metal particles, acts as an oxygen storage component and may substantially change the catalytic properties of the supported metal.[213]

The oxidation of CO on platinum/Al_2O_3 and platinum/CeO_2/Al_2O_3 catalysts has been studied.[214] The catalytic activity on platinum/Al_2O_3 was attributed to the Langmuir-Hinshelwood mechanism over metallic platinum sites. On pre-reduced platinum/CeO_2/Al_2O_3, the catalytic sites were localised at the platinum/CeO_2 interface. CO adsorbed on the platinum near the interface reacted with oxygen from the CeO_2. On pre-oxidised platinum/CeO_2/Al_2O_3, the platinum/CeO_2 active sites were deactivated into PtO_2/CeO_2 sites, while the bulk platinum maintained a metallic state. In this situation, the reaction only occurred on the platinum sites.

CO oxidation under ambient conditions has been observed over supported palladium and platinum catalysts.[215] The enhanced activity of these two-component CO oxidation catalysts appears to result from a combination of suitable materials and specialised preparation techniques.

---

[212] See for example: G. S. Zafiris and R. J. Gorte, *J. Catal.*, 1993, **143**, 86; A. Trovarelli, C. de Leitenburg, G. Dolcetti and Jordi LLorca, *J. Catal.*, 1995, **151**, 111; T. Bunluesin, H. Cordatos and R. J. Gorte, *J. Catal.*, 1995, **157**, 222.

[213] C. Hardarce, R. M. Ormerod and R. M. Lambert, *J. Phys. Chem.*, 1994, **98**, 10901.

[214] C. Serre, F. Garin, G. Belot and G. Maire *J. Catal.*, 1993, **141**, 1; *J. Catal.*, 1993, **141**, 9.

[215] See for example: U. Junges, W. Jacobs, I. Voigt-Martin, B. Krutzsch and F. Schuth, *J. Chem. Soc., Chem. Commun.*, 1995, 2283; D. I. Kochubey, S. N. Pavlova, B. N. Novgorodov, G. N. Kryukova and V. A. Sadykov, *J. Catal.*, 1996, **161**, 500; K. Grass and H.-G. Lintz, *J. Catal.*, 1997, **172**, 446.

Typically, the noble metal is highly dispersed and in intimate contact with a transition metal oxide. The interface of the metal and the metal oxide is considered to be the active site where CO reacts with oxygen from the support.[216] Supported gold catalysts have received considerable attention for CO oxidation and examples are outlined in the following section.

4·5 RECENT PREPARATIONS OF SUPPORTED GOLD CATALYSTS FOR CO OXIDATION

The preparation of gold nano-particles is established[217] and the catalytic chemistry of ultra-fine gold particles is known to be dissimilar to that of the bulk metal.[16] Various research groups (initially M. Haruta and co-workers) have shown that transition metal oxides, when coated with tiny particles of metallic gold, are highly active CO oxidation catalysts.[218] The development of these materials has created an upsurge of interest in the catalytic potential of gold.[219]

It is apparent that dispersed nano-particles of gold have potential for various surface reactions. These include hydrogen oxidation, hydrogenation of CO and carbon dioxide[220] and photo-induced hydrogen production from ethylene glycol.[221]

4·5·1 Coprecipitation

Coprecipitation is an established method for the preparation of active supported gold catalysts with many examples to be found in recent literature.[222]

---

216 S. Imamura, Y. Tsuji, Y. Miyake and T. Ito, *J. Catal.*, 1995, **151**, 279.

217 See for example: M. Brust, J. Fink, D. Bethell, D. J. Schiffrin and C. Kiely, *J. Chem. Soc., Chem. Commun.*, 1995, 1655; K. C. Grabar, R. G. Freeman, M. B. Hommer and M. J. Natan, *Anal. Chem.*, 1995, **67**, 735.

218 Y. Iizuka, H. Fujiki, N. Yamauchi, T. Chijiiwa, S. Arai, S. Tsubota and M. Haruta, *Catal. Today*, 1997, **36**, 115.

219 A. Knell, P. Barnickel, A. Baiker and A. Wokaun, *J. Catal.*, 1992, **137**, 306.

220 H. Sakurai and M. Haruta, *Appl. Catal. A*, 1995, **127**, 93.

221 G. R. Bamwenda, S. Tsubota, T. Kobayashi and M. Haruta, *J. Photochem. Photobiol. A: Chem.*, 1994, **77**, 59.

222 See for example: G. J. Hutchings, M. R. H. Siddiqui, A. Burrows, C. J. Kiely and R. Whyman, *J. Chem. Soc., Faraday Trans.*, 1997, **93**, 187; R. M. T. Sanchez, A. Ueda, K. Tanaka and M. Haruta, *J. Catal.*, 1997, **168**, 125; A. Andreeva, V. Idakiev, T. Tabakova and A. Andreev, *J. Catal.*, 1996, **158**, 354; H. Sakurai, S. Tsubota and M. Haruta, *Appl. Catal. A*, 1993, **102**, 125.

This method involves the addition of a mixed aqueous solution of $HAuCl_4$ and a transition metal species to a weak base under constant stirring. The hydroxide coprecipitate is then washed, vacuum dried and calcined in air. This produces ultra-fine gold particles which can be resolved by Transmission Electron Microscopy (TEM). Figure 4·3 depicts a micrograph of a calcined gold/iron coprecipitate.[223]

Coprecipitation is valid for a select group of transition metals (examples being iron, cobalt and nickel) where the precipitation rates of gold hydroxide and the transition metal hydroxide are comparable at a specific pH.[224] With non-compatible transition metals a related technique has been used successfully, which is called deposition-precipitation. This uses a pre-formed metal oxide and involves a pH controlled interaction between the support and gold hydroxide. Highly active gold/TiO_2 catalysts have been produced by this method.[225] The structure and activity of the coprecipitate materials are dependent on the pH during preparation[226] and the calcination procedure.[227]

A mechanism has been proposed in which CO migrates across the gold particles to the support oxide where it reacts with adsorbed oxygen to form carbon dioxide (Figure 4·4).[228] Surface hydroxide groups may play an important role in the catalytic mechanism.[229] Insight of the reaction mechanism has been provided by FTIR study of CO species absorbed on the gold particles.[230]

It is apparent that gold/metal oxide catalysts are resistant to the presence of water during CO oxidation, whereas oxide catalysts are deactivated.[231] CO is able to interact with the metal oxide (in the presence of moisture) by using the gold particle as a pathway to the oxide surface.[232]

---

223 M. Haruta, N. Yamada, T. Kobayashi and S. Iijima, *J. Catal.*, 1989, **115**, 301.
224 S. Tsubota, M. Haruta, T. Kobayashi, A. Ueda, Y. Nakahara, in *Preparation of Catalysts V*, eds. G. Poncelet, P. A. Jacobs, P. Grange and B. Delmon, Elsevier, Amsterdam, 1991, p. 695-704.
225 F. Boccuzzi, A. Chiorino, S. Tsubota and M. Haruta, *J. Phys. Chem.*, 1996, **100**, 3625.
226 F. Boccuzzi, A. Chiorino, S. Tsubota and M. Haruta, *Catal. Lett.*, 1994, **29**, 225.
227 See for example: S. K. Tanielyan and R. L. Augustine, *Appl. Catal. A*, 1992, **85**, 73; F. E. Wagner, S. Galvango, C. Milone, A. M. Visco, L. Stievano and S. Calogero, *J. Chem. Soc., Faraday Trans.*, 1997, **93**, 3403.
228 M. Haruta, S. Tsubota, T. Kobayashi, H. Kageyama, M. J. Genet and B. Delmon, *J. Catal.*, 1993, **144**, 175.
229 W. S. Epling, G. B. Hofland, J. F. Weaver, S. Tsubota and M. Haruta, *J. Phys. Chem.*, 1996, **100**, 9929; S. D. Jackson, B. M. Glanville, J. Willis, G. D McLellan, G. Webb, R. B. Moyes, S. Simpson, P. B. Wells and R. Whyman, *J. Catal.*, 1993, **139**, 207.
230 See for example: M. A. Bollinger and M. A. Vannice, *Appl. Catal. B*, 1996, **8**, 417; F. Boccuzzi, S. Tsubota and M. Haruta, *J. Elect. Spectro.*, 1993, **64/65**, 241.
231 W. Liu and M. Flytzani-Stephanopoulos, *J. Catal.*, 1995, **153**, 304.
232 D. A. H. Cunningham, T. Kobayashi, N. Kamijo and M. Haruta, *Catal. Lett.*, 1994, **25**, 257.

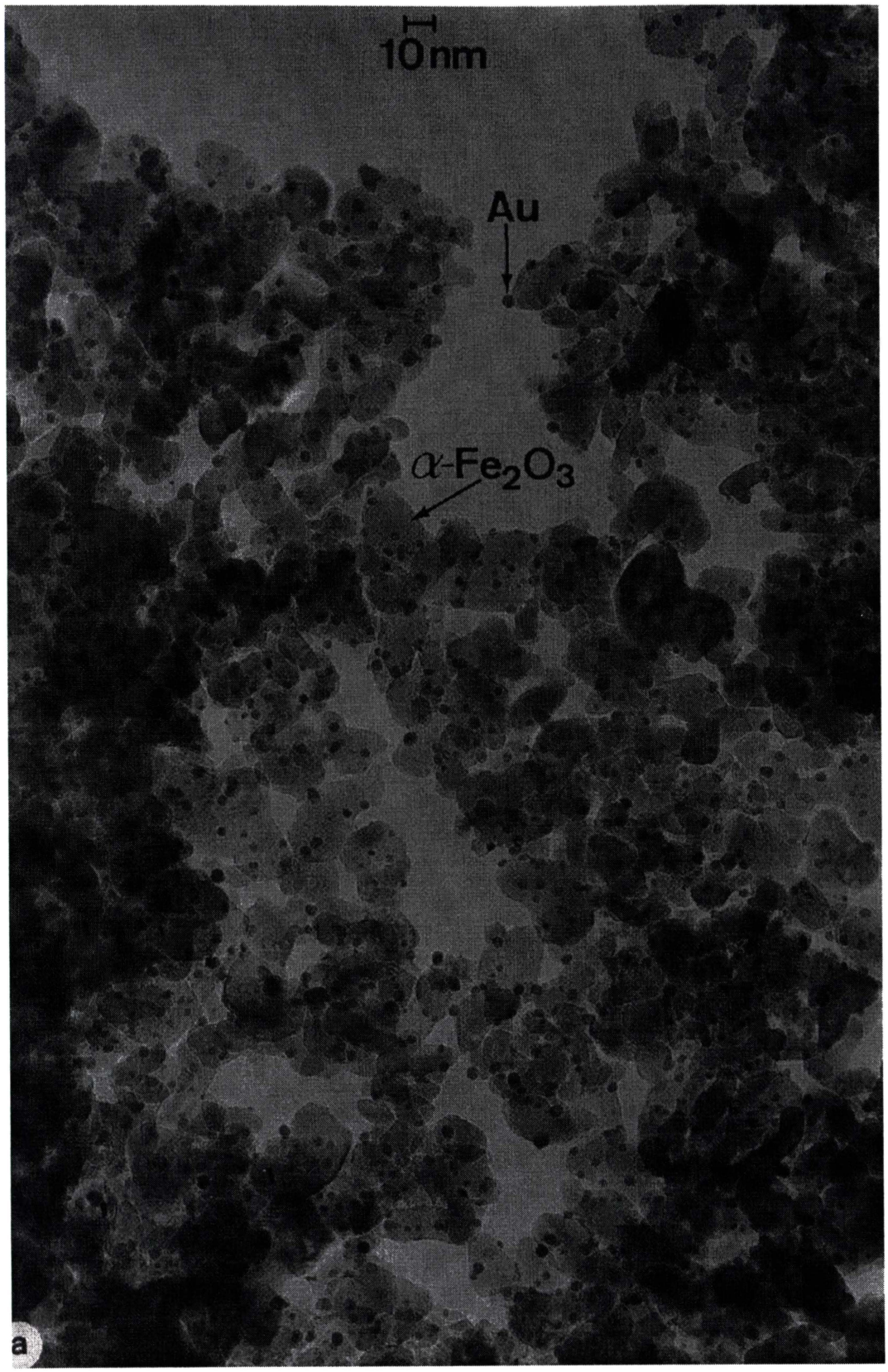

Figure 4·3 TEM of gold nano-particles on Fe_2O_3 [223]

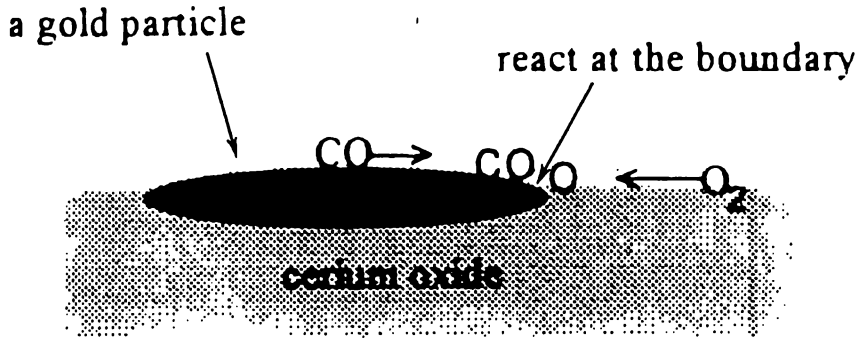

Figure 4·4 Synergic CO oxidation over supported gold [233]

The size of gold particles is important in determining the activity of supported gold catalysts.[234] However, it is difficult to determine the relative influence on activity of metal dispersion as opposed to metal-support interactions.[235]

The rate of CO oxidation on heated coprecipitates has a low dependency on P_{CO} and P_{O_2}.[228] This is consistent with each reactant coordinating to the catalyst surface at different sites (CO on the gold particles and oxygen on the support). In comparison, the rate of CO oxidation on single-component catalysts is generally influenced by the partial pressures of the reactants (refer to sub-section 4·3·1).

4·5·2 Gold alloy precursors

A. Baiker and co-workers have prepared highly active CO oxidation catalysts by heating gold/zirconium/iron alloys. Activation of this material is concurrent with the heating step and the subsequent enrichment of metallic gold on the surface of a zirconium/iron mixed oxide (Figure 4·5). The average diameter of the gold particles is ~20 nm. Once again, the active site was proposed to be the interface of the gold particles and the metal oxide support.[236]

---

233 W. Liu and M. Flytzani-Stephanopoulos, *J. Catal.*, 1995, **153**, 317.
234 D. Cunningham, S. Tsubota, N. Kamijo and M. Haruta, *Res. Chem. Inter.*, 1993, **19**, 1.
235 Ref. 11, T. Komaya *et. al.*
236 A. Baiker, M. Maciejewski, S. Tagliaferri and P. Hug, *J. Catal.*, 1995, **151**, 407.

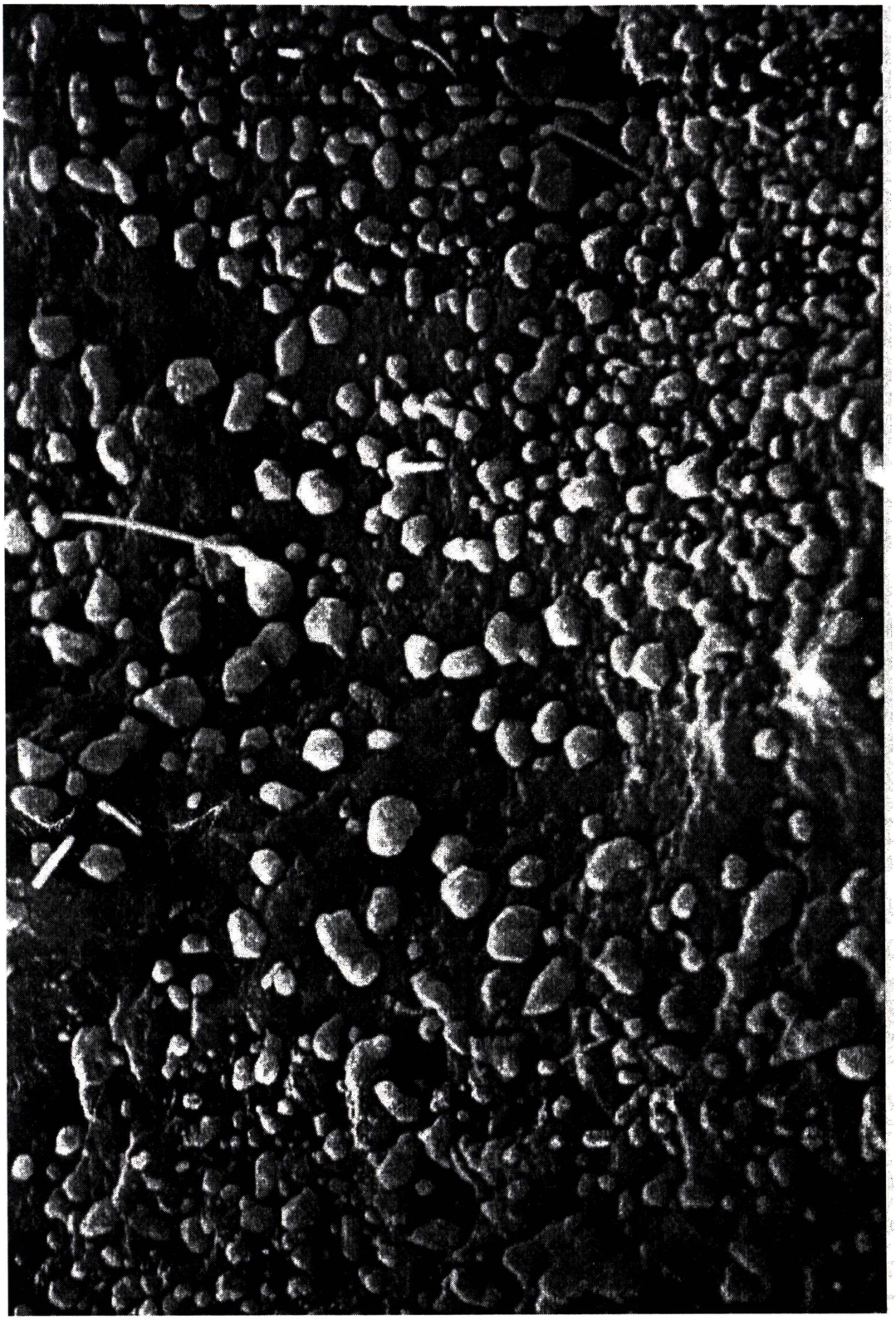

Figure 4·5 Gold particles on calcined alloy [236]

Platinum/CeO_2 catalysts have also been prepared by this method, in this case from a platinum/cerium alloy. It was noted that the activity for CO oxidation of this material was comparable to supported platinum catalysts, prepared by wet chemical techniques.[237]

4·5·3 Chemical vapour deposition

Chemical vapour deposition (CVD) is a method for depositing a metal species onto a dissimilar solid material. Applications of CVD include the deposition of gold in microelectronic circuitry.[238] CVD of $Me_2Au(acac)$ onto TiO_2 results in a highly active CO oxidation catalyst.[239] Active catalysts have also been produced by the sputtering of gold onto oxide supports.[240]

4·5·4 Gold complexes as catalyst precursors

Supported catalysts can be prepared by way of solvent deposition of metal complexes. Phosphine ligated platinum-gold clusters have been investigated, for example, as precursors to highly dispersed bimetallic catalysts.[241] Y. Iwasawa and co-workers have shown that mixing $Fe(OH)_3$ with solutions of $(Ph_3P)AuNO_3$ or $(Ph_3P)_8Au_9(NO_3)_3$, followed by calcination, results in catalysts active for low temperature CO oxidation.[242]

The research presented in Chapter Five of this thesis describes the use of four mono-nuclear gold(I) complexes as catalyst precursors. The results were consistent with those of Iwasawa, in that the use of $(Bu^tNC)AuNO_3$ resulted in active catalysts.[243]

---

237 C. Hardacre, T. Rayment and R. Lambert, *J. Catal.*, 1996, **158**, 102.
238 R. J. Puddephatt, *Polyhedron*, 1994, **13**, 1233.
239 M. Okumura, K. Tanaka, A. Ueda and M. Haruta, *Solid State Ionics*, 1997, **95**, 143.
240 T. Kobayashi, M. Haruta, S. Tsubota and H. Sano, *Sensors and Actuators*, 1990, **B1**, 222; cited in ref. 239.
241 I. V. G. Graf, J. W. Bacon, M. B. Consugar, M. E. Curley, L. N. Ito and L. H. Pignolet, *Inorg. Chem.*, 1996, **35**, 689.
242 Y. Yuan, A. P. Kozlova, K. Asakura, H. Wan, K. Tsai and Y. Iwasawa, *J. Catal.*, 1997, **170**, 191; Y. Yuan, K. Asakura, H. Wan, K. Tsai and Y. Iwasawa, *Chem. Lett.*, 1996, 755.
243 T. J. Mathieson, A. G. Langdon, N. B. Milestone and B. K. Nicholson, *J. Chem. Soc., Chem. Commun.*, 1998, 371.

4·6 SUMMARY

The general chemical properties of CO have been the subject of considerable scientific interest.[244] CO is a useful reagent in organic and inorganic synthetic chemistry. Many reaction processes involving CO are catalytic in nature with CO coordination resulting in reactive intermediates. The transition metals are prone to forming surface oxides therefore only a few can be used as CO oxidation catalysts. The noble metals can be regarded as potentially active for this reaction.[245]

Platinum exhibits excellent activity for CO oxidation but only at elevated temperatures. In the presence of a significant quantities of CO, reactant inhibition occurs under ambient conditions. This is because only one type of chemisorption site is present on the platinum surface.

CO oxidation catalysis has been observed recently under ambient conditions on supported noble metal catalysts. The proposed mechanism for such activity is that CO (associated with the surface of the metal particles) reacts with the reducible support forming carbon dioxide. The catalyst support stores significant quantities of oxygen. The oxygen can diffuse to the active metal/support interface sites and after reaction can be replenished from the gas phase.[246]

When gold is dispersed over oxidising supports (by using specific preparative techniques), the catalytic potential of this metal is enhanced. Various reactions have been shown to take place over supported gold catalysts, but special attention has been drawn to the observation of low temperature CO oxidation. Numerous practical applications for such activity have been identified, including the removal of CO from breathing air.

---

[244] M. C. Zonnevylle, J. J. C. Geerlinds and R. A. van Santen, *J. Catal.*, 1994, **148**, 417.
[245] Ref. 127, p. 167.
[246] R. Schlögl, G. Loose, M. Wesemann and A. Baiker, *J. Catal.*, 1992, **137**, 139.

CHAPTER FIVE

SUPPORTED GOLD CATALYSTS

After observing the general morphology of active CO oxidation materials (see Figures 4·3 and 4·5), it was decided that certain LAuX complexes would be suitable as precursors to highly dispersed supported gold catalysts. The purpose of this Chapter is to describe the preliminary development and investigation of this supposition.

The prepared materials were tested for catalytic CO oxidation under ambient conditions. The discussion of this work emphasises that the potential for producing highly dispersed metallic particles (which is an essential feature of active CO oxidation catalysts) is linked to the chemical properties of the gold complexes.

5·1 COPRECIPITATION AND GOLD-SPUTTERING

Initially, coprecipitation and gold-sputtering catalyst syntheses from the literature were reproduced. These preparations provided a basis for comparison with the preparations that involved gold complexes.

5·1·1 Coprecipitate precursors

Coprecipitation is established in the literature as a suitable method for preparing active CO oxidation catalysts (refer to sub-section 4·5·1). This technique produces a hydroxide material, which incorporates cations of a specific transition metal and a lesser quantity of gold(III) ions. Heating this material results in the formation of a transition metal oxide, supported on which are highly dispersed metallic gold particles. Coprecipitation was reproduced using Fe_2O_3, which appears to be a particularly active support for this form of catalyst. Hydroxide coprecipitates were prepared at ambient temperature by mixing an aqueous solution of iron(III)/gold(III) with one of the carbonate anion.[228]

Preparation of coprecipitate (A)

A solution of Na_2CO_3 (15 g) in H_2O (300 cm^3) was placed in a 600 cm^3 beaker. The beaker was equipped with a large stirring bar and a pH meter and was positioned below two 50 cm^3 burettes. One burette was filled with an aqueous solution of $Fe(NO_3)_3.9H_2O$ (10 g) and $HAuCl_4.3H_2O$ (0·8 g) and the second was filled with 10% w/w Na_2CO_3 (aq). The iron(III)/gold(III) solution was added dropwise with vigorous stirring to the Na_2CO_3 solution, which had an initial pH of 11·7. Each drop resulted in the formation of a light brown precipitate. The pH reduced steadily until it reached 8·5 where it was maintained by dropwise addition of Na_2CO_3 (aq) from the second burette. After addition was complete, the hydroxide was stirred for one hour and then 150 cm^3 of H_2O was added.

The precipitate was allowed to settle overnight and then the colourless supernatant was carefully decanted. The beaker was filled with H_2O, and after a short period of vigorous stirring the precipitate was allowed to settle overnight. This procedure was repeated three times over a period of three days. The precipitate was then thoroughly washed on a Buchner funnel with H_2O. The solid was dried under vacuum for eight hours and then calcined at 400 °C for four hours. This resulted in a dark brown powder of ~10% w/w gold.

Preparation of coprecipitate (B)

A solution of $Fe(NO_3)_3.9H_2O$ (10 g) and $HAuCl_4.3H_2O$ (0·8 g) in H_2O (200 cm^3) was placed in a 600 cm^3 beaker. The beaker was equipped with a large stirring bar and a pH meter. Placed above the beaker was a 50 cm^3 burette, which was filled with a 10% w/w Na_2CO_3 (aq) solution. This solution was added dropwise with vigorous stirring to the iron(III)/gold(III) solution. As the pH increased slowly, the solution turned dark and then a dark brown precipitate formed *en masse*. H_2O was added to reduce the viscosity of the slurry and then stirring was continued for an additional hour.

The precipitate was then treated as for coprecipitate (A). The calcined material was a black powder of ~10% w/w gold.

5·1·2 Gold-sputtering preparations

Supported gold catalysts have been produced previously by gold-sputtering.[140] A reproduction of this general technique was made using a Magnetron Sputter Coater (MSC). The MSC is used for coating SEM samples where, depending on the type of specimen, a thin metallic layer enhances resolution.

Preparation of gold-sputtered Fe_2O_3

A thin layer of Fe_2O_3 was placed in a glass dish. This was positioned on the specimen stage in the vacuum chamber of the MSC (Figure 5·1). Under an atmosphere of low pressure argon, an inert plasma was created consisting of electrons and positive ions. This resulted in the removal of gold from a gold target which was held above the specimen stage. Three samples of Fe_2O_3 were treated for five minutes each, in which time the sides of the glass dishes were coated with visible metallic gold.

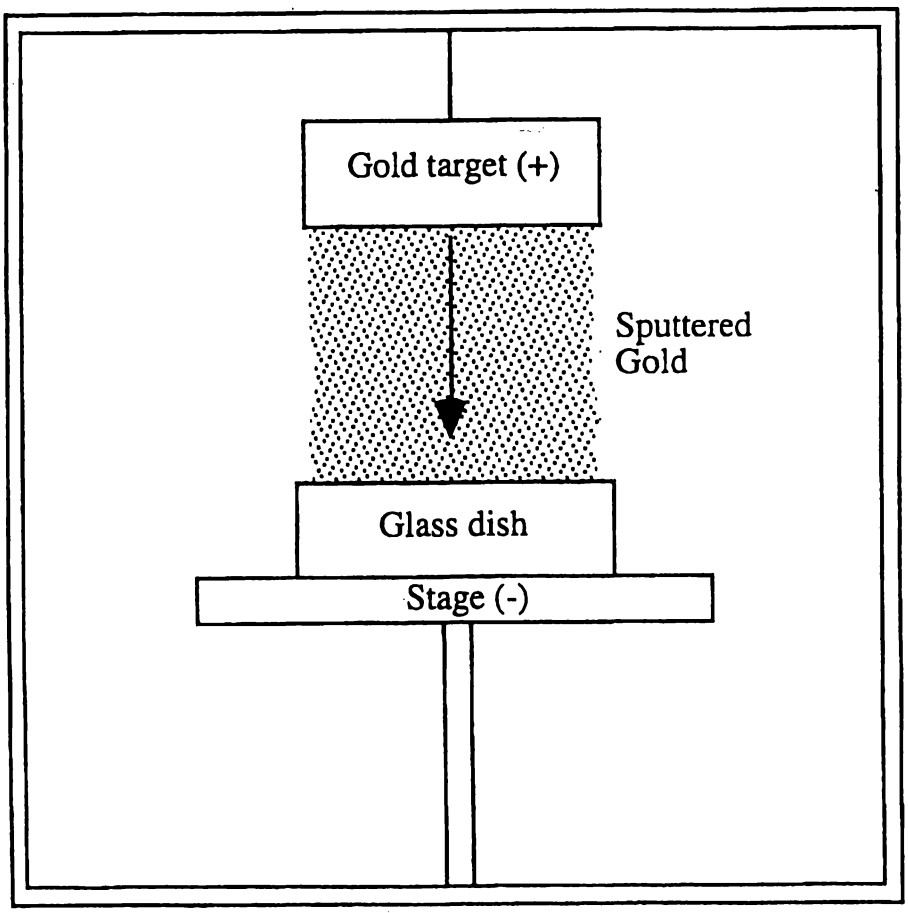

Figure 5.1 Sputtering of gold within the MSC vacuum chamber

5·2 GOLD COMPLEXES AS CATALYST PRECURSORS

With the intention of producing a supported gold material efficient in catalysing the oxidation of CO under ambient conditions, the following preparative procedure was developed:

(i) A transition metal oxide (or hydroxide) support was mixed as a slurry with a volatile organic solvent, in which was dissolved a gold complex. The mixture was stirred for ten hours.

- The expected chemical process was the adsorption of molecules or (if the complex decomposed) fragments of the complex. Ideally, these would be highly dispersed over the support surface.

(ii) The material was dried under vacuum and then calcined in air. Moderate temperatures (300 or 400 °C) were used for the calcination to minimise agglomeration of support particles and coalescence of metallic gold particles.

- It was intended that this would result in the thermolysis of the gold complex (if it had not already decomposed) leaving highly dispersed metallic gold on the support surface. If a metal hydroxide was used, it would be simultaneously converted to a metal oxide.

Iwasawa and co-workers reported success with a similar method during the course of the present research project.[242]

5·2·1 Gold complexes

Suitable gold complexes for this method would have the following characteristics:

(i) A lack of *poisoning* elements.

Specific elements may act as gold surface poisons, preventing the coordination of CO. The halogens and sulphur are typical examples. The independent report of Iwasawa and co-workers described the use of $(Ph_3P)AuNO_3$,[242] which suggested that phosphorus can be tolerated for this preparative technique. However, gold complexes with ligands containing only carbon, oxygen and nitrogen would minimise the potential for catalyst poisoning.

(ii) An *affinity* for the support surface.

The gold complex should be able to attach to the oxide support surface. If decomposition of the gold complex occurs, the resulting gold entity should be capable of adhering to the surface.

(iii) A propensity to form *small* crystals.

If the complex maintains molecular integrity on physical contact with the oxide surface (and during evaporation of the solvent) it will be desirable for it to form small crystals, as these are more likely to result in gold nano-particles during calcination.

(iv) A *clean* thermolysis process under moderate heat.

It is important that the ligands of the gold complex are lost into the vapour phase during decomposition, leaving only metallic gold on the support surface.

(v) A *high* yielding synthesis that affords a *pure* product.

Some potential substrates, such as $[Me_2AuOH]_4$ and $(Bu^tNC)Au(acac)$, were precluded since they were not readily synthesised in good yield.

Based on these criteria four complexes [$(Ph_3P)AuCl$, $(Ph_3P)AuMe$, $(Bu^tNC)AuCl$ and $(Bu^tNC)AuNO_3$] were chosen for comparative analysis of the procedure. The preparation of these complexes and the attempted synthesis of $[Me_2AuOH]_4$ and $(Bu^tNC)Au(acac)$ is described in section 5·7.

5·2·2 Thermolysis of gold complexes

An assessment of the thermal decomposition behaviour of crystalline $(Ph_3P)AuCl$, $(Ph_3P)AuMe$, $(Bu^tNC)AuCl$ and $(Bu^tNC)AuNO_3$ was made. A combination of Simultaneous Thermal Analysis (STA),‡ Differential Scanning Calorimetry (DSC) and observed melting points provided a suitable basis for this purpose. The thermolysis of (RNC)AuX (R = Et or Xy; X = Cl or NO_3) complexes was also investigated.

STA of the gold complexes detected changes in heat (mW) and weight loss (mg) when the gold complexes were heated. STA traces (mW and mg vs temperature) are displayed in this sub-section for each of the gold complexes. These are accompanied by rationalisation of the observed % weight losses in terms of the ligands. Endotherms are represented by negative peaks during STA.

DSC of the gold complexes detected heat changes (mW). The melting points as observed under the microscope (*) are noted with the displayed DSC traces (mW vs temperature). All of the STA and DSC were run in air unless specifically noted. Endotherms are represented by positive peaks during DSC.

Endothermic peaks associated with observed decomposition were attributed to either:

(i) evaporation during decomposition, or

(ii) an initial melting process before decomposition.

DSC of $(Ph_3P)AuCl$ exhibited an endotherm at ~245 °C (Figure 5·3). The endotherm in STA of $(Ph_3P)AuCl$ (Figure 5·2) was associated with a weight loss between 250-330 °C. STA of $(Ph_3P)AuMe$ exhibited an exothermic decomposition which was associated with a loss of weight consistent with ethane formation (Figure 5·4). The loss of ethane has previously been documented during thermolysis of $(Ph_3P)AuMe$[247] and reductive elimination of $(Ph_3P)AuMe_3$.[248]

‡ STA was carried out at Industrial Research Limited, Wellington.

247 A. Tamaki and J. K. Kochi, *J. Organomet. Chem.*, 1973, **61**, 441.

248 P. L. Kuch and R. S. Tobias, *J. Organomet. Chem.*, 1976, **122**, 429.

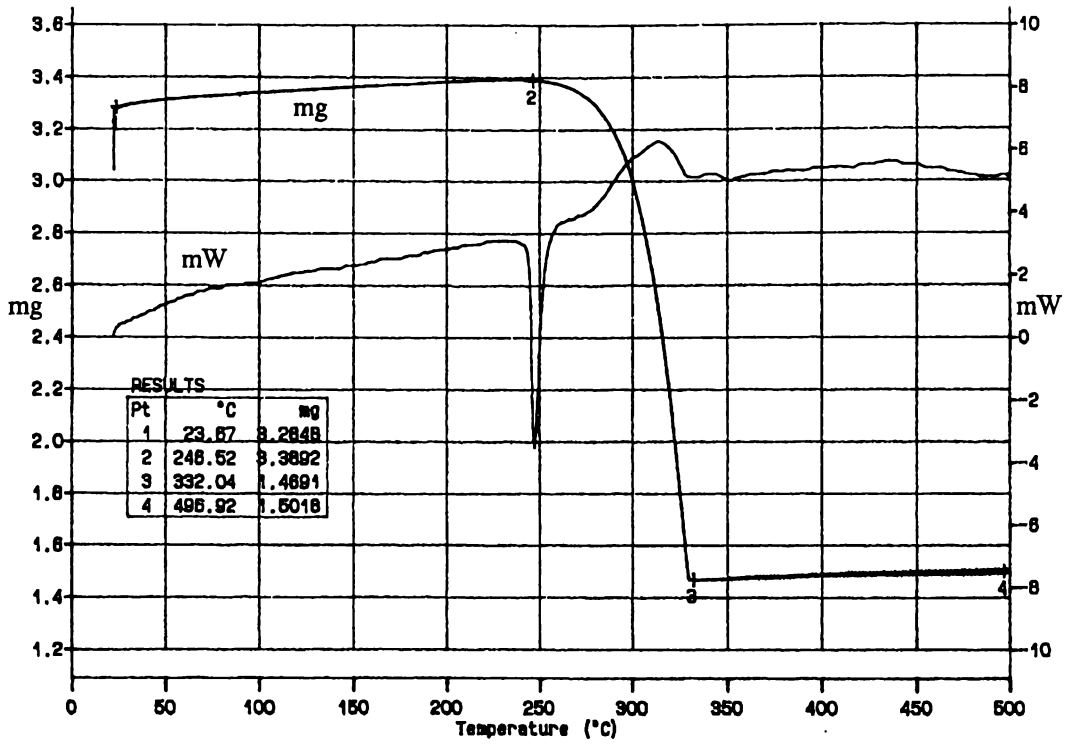

Figure 5·2 STA of $(Ph_3P)AuCl$

Sample weight = 3·230 mg

Weight loss between points two and three ~59% of the total weight‡

- Calculated weight loss of Ph_3P and chloride from $(Ph_3P)AuCl$ ~60%

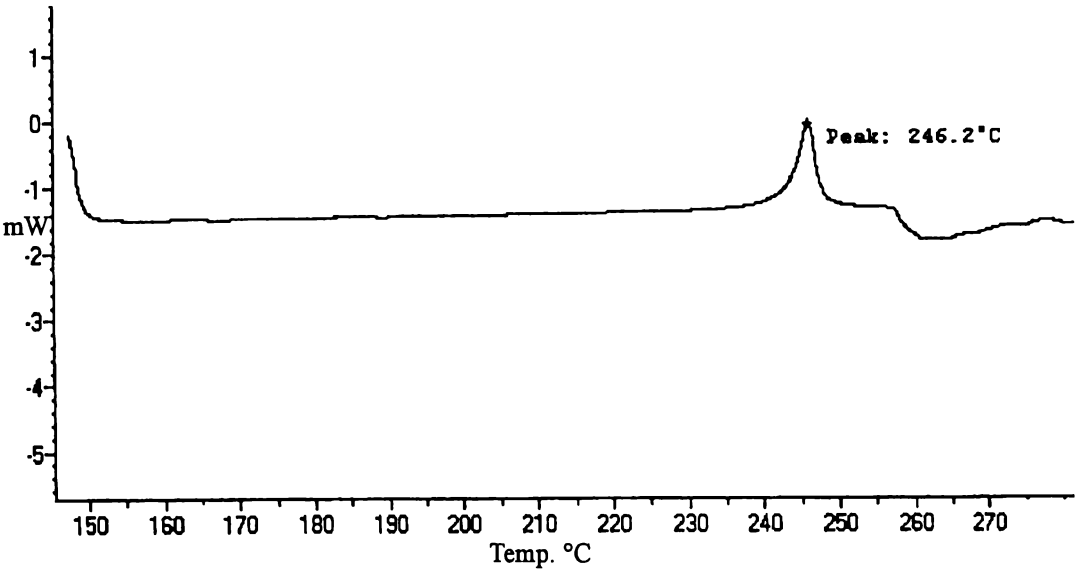

Figure 5·3 DSC of $(Ph_3P)AuCl$§

‡ The calculated weight loss is based on the initial sample weight *not* on the weight at point one.

§ The melting point was too high for observation under the microscope.

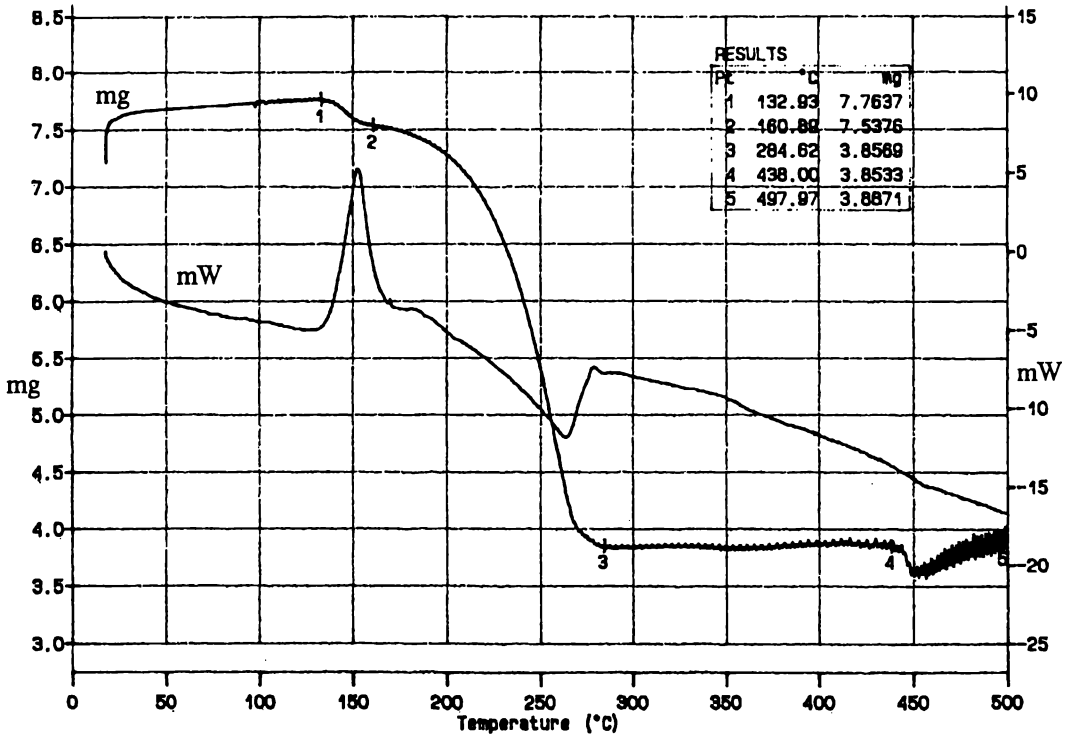

Figure 5·4 STA of $(Ph_3P)AuMe$

Sample weight = 7·243 mg

Weight loss between points one and two ~3% of the total weight

- Calculated weight loss of Me from $(Ph_3P)AuMe$ ~3%

Weight loss between points two and three ~54% of the total weight

- Calculated weight loss of Ph_3P from $(Ph_3P)AuMe$ ~58%

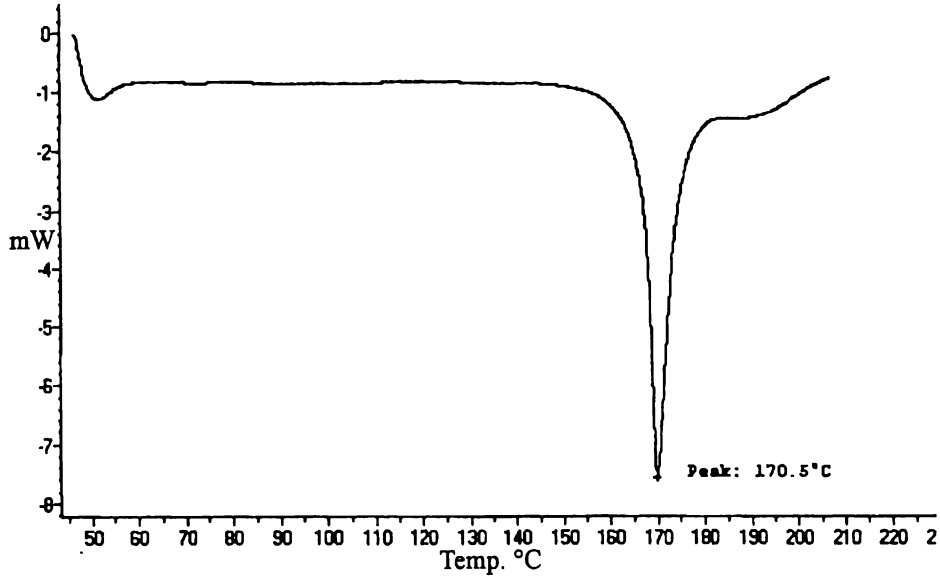

Figure 5·5 DSC of $(Ph_3P)AuMe$ *M.p. 169 °C (Decomp.)

STA of (Bu^{t}NC)AuCl was carried out in air (Figure 5·6) and in a reducing 5% H_2/95% N_2 atmosphere (Figure 5·7). Both exhibited an endotherm associated with a weight loss consistent with evaporation of the Bu^{t}NC ligand. The weight loss above 250 °C is attributed to loss of chloride. When (Bu^{t}NC)AuCl decomposed in air, the loss of chloride occurred over a wide range of temperature up to 500 °C. In the reducing atmosphere the loss occurred rapidly, presumably due to the formation of HCl. In both cases, the loss of chloride appears incomplete.

(EtNC)AuCl and (XyNC)AuCl , in contrast to (Bu^{t}NC)AuCl, were able to form stable melts. DSC of (EtNC)AuCl exhibits a melting endotherm at 116 °C and a decomposition exotherm starting at ~200 °C (Figure 5·10). The melt of (XyNC)AuCl exists between ~140-250 °C (Figure 5·12). At their respective melting points, single crystal growth of (EtNC)AuCl and (XyNC)AuCl was observed from the liquid phase.¶ The fact that (Bu^{t}NC)AuCl did not form a stable melt was tentatively attributed to production of $Me_2C{=}CH_2$ and HCN from the Bu^{t}NC ligand.

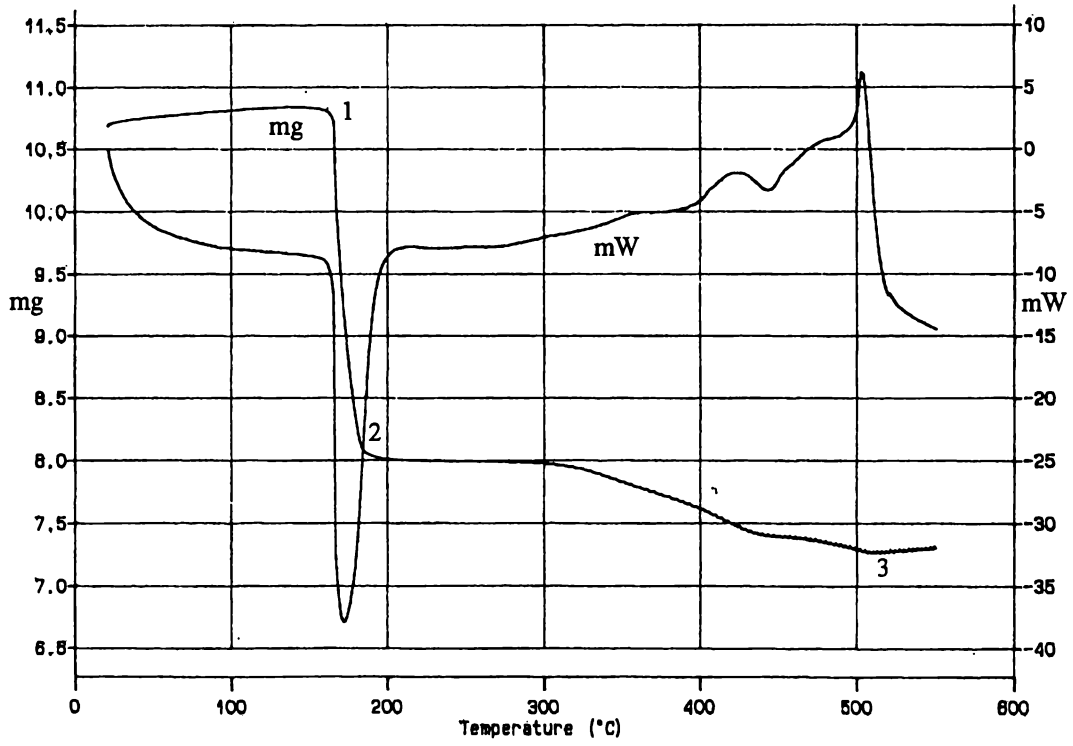

Figure 5·6 STA of (Bu^{t}NC)AuCl

Sample weight = 10·696 mg

Weight loss between points one and two ~**26%** of the total weight

- Calculated weight loss of Bu^{t}NC from (Bu^{t}NC)AuCl ~**26%**

Weight loss between points two and three ~**7%** of the total weight

- Calculated weight loss of chloride from (Bu^{t}NC)AuCl ~**11%**

¶ Under the microscope.

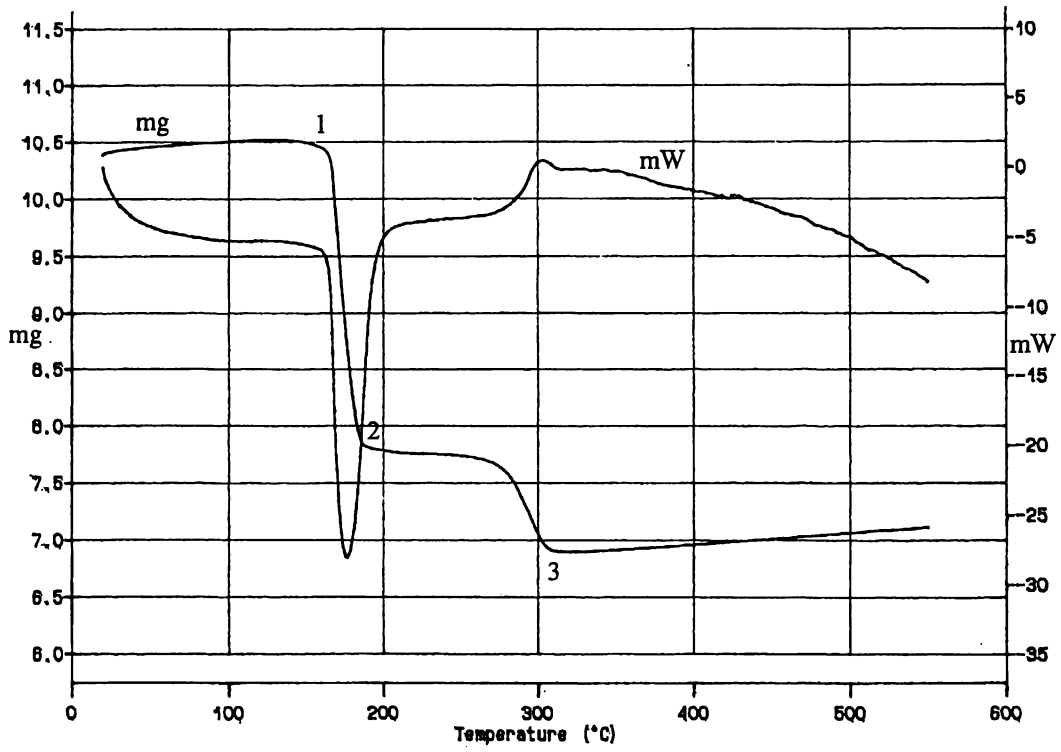

Figure 5·7 STA of (Bu^{t}NC)AuCl run in 5% H_2/95% N_2

Sample weight = 10·388 mg

Weight loss between points one and two ~**26%** of the total weight

- Calculated weight loss of Bu^{t}NC from (Bu^{t}NC)AuCl ~**26%**

Weight loss between points two and three ~**8%** of the total weight

- Calculated weight loss of chloride from (Bu^{t}NC)AuCl ~**11%**

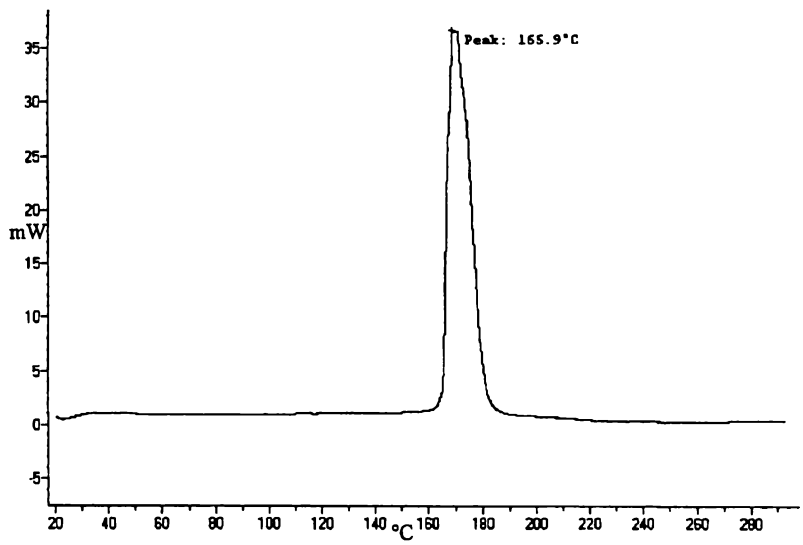

Figure 5·8 DSC of (Bu^{t}NC)AuCl *M.p. 164 °C (Decomp.)

STA of (EtNC)AuCl (Figure 5·9) and (XyNC)AuCl (Figure 5·11) both exhibited endothermic melting with no associated weight loss. The weight loss above 200 °C for both was attributed to decomposition and vaporisation of the melts.

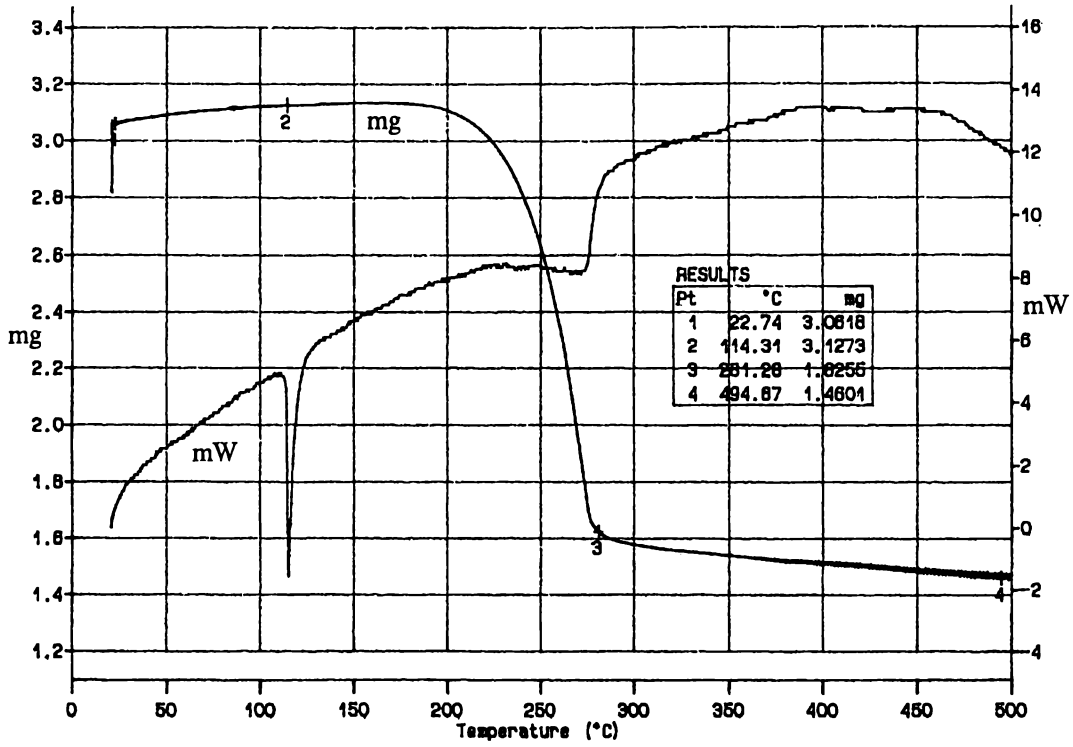

Figure 5·9 STA of (EtNC)AuCl

Sample weight = 3·045 mg

Weight loss between points two and three ~**50%** of the total weight

- (EtNC)AuCl is **69%** w/w gold

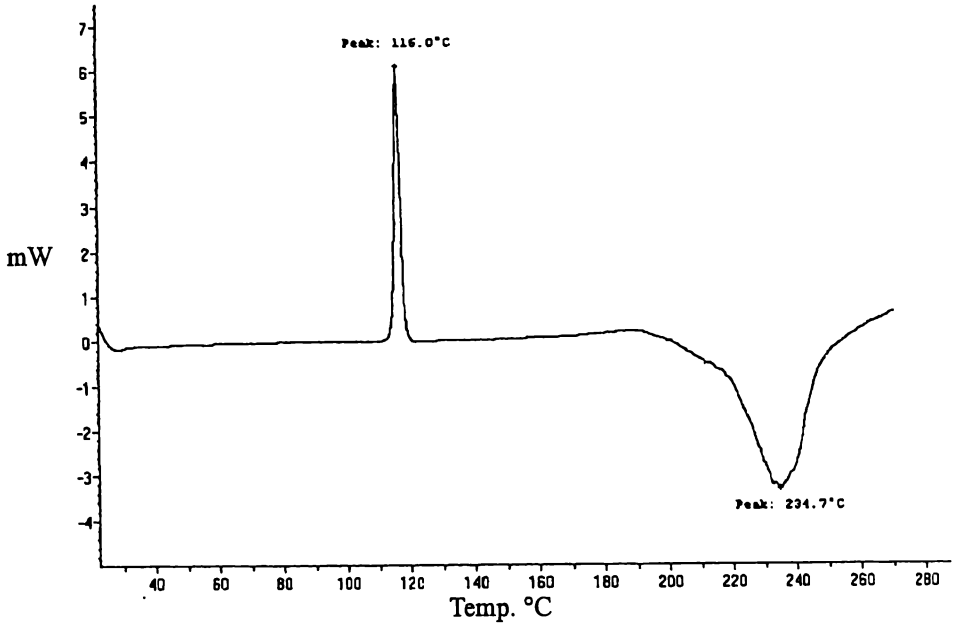

Figure 5·10 DSC of (EtNC)AuCl *M.p. 115 °C

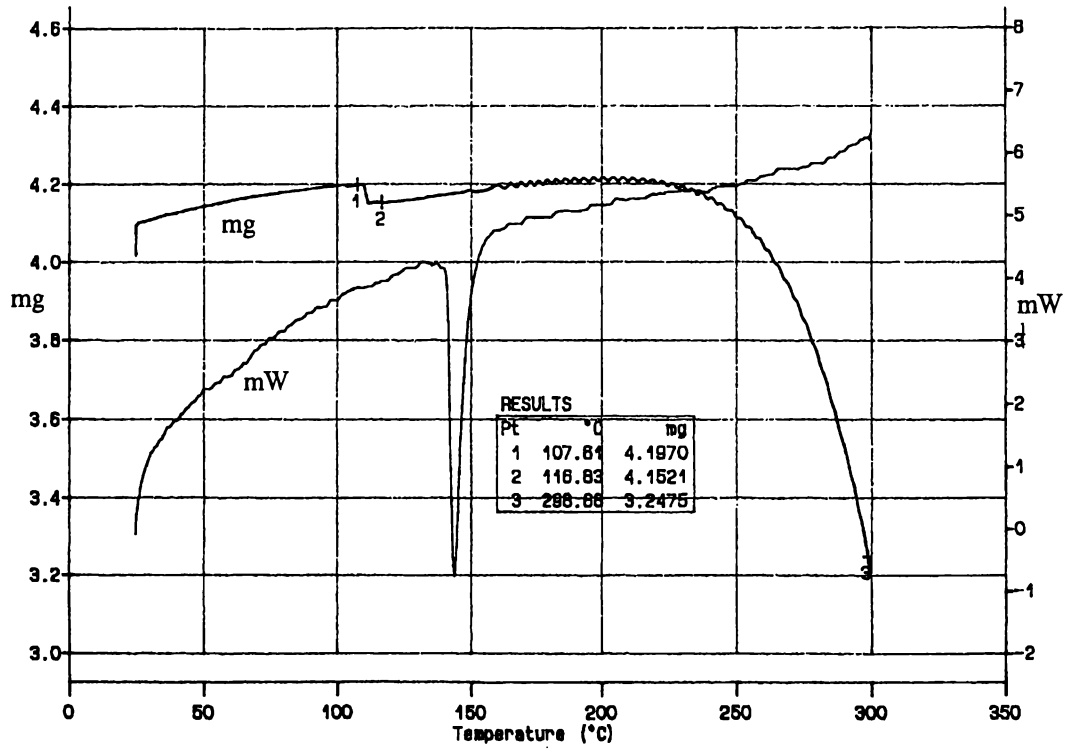

Figure 5·11 STA of (XyNC)AuCl

Sample weight = 4·076 mg

No calculation was possible as the weight is decreasing at point three

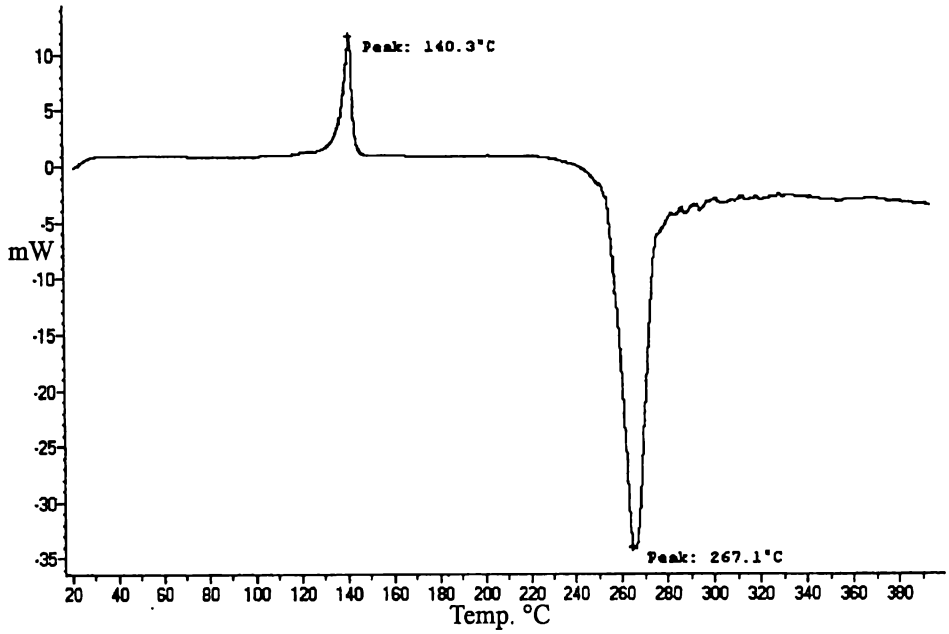

Figure 5·12 DSC of (XyNC)AuCl *M.p. 142 °C

Under the microscope, (Bu^{t}NC)AuNO$_3$ decomposed violently at ~118 °C. STA of (Bu^{t}NC)AuNO$_3$ (Figure 5·13) exhibits a weight loss consistent with that of Bu^t and nitrate. However, the accuracy of this STA trace is dubious, as the overall weight loss indicates that some gold material was lost. This is conceivable based on the explosive nature of (Bu^{t}NC)AuNO$_3$ decomposition.

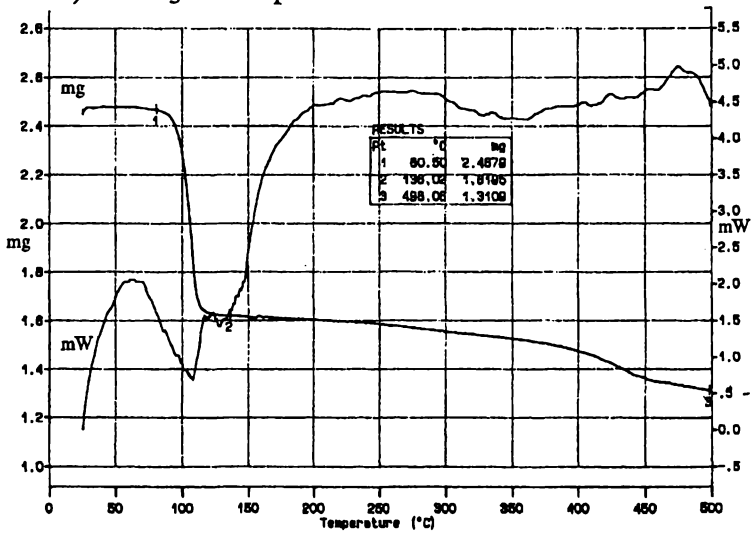

Figure 5·13 STA of (Bu^{t}NC)AuNO$_3$

Sample weight = 2·444 mg

Weight loss between points one and two ~**34%** of the total weight

- Calculated weight loss of Bu^t and nitrate from (Bu^{t}NC)AuNO$_3$ ~**35%**
- Calculated weight loss of Bu^{t}NC from (Bu^{t}NC)AuNO$_3$ ~**24%**

Weight loss between points one and three ~**47%** of the total weight

- (Bu^{t}NC)AuNO$_3$ is ~**57%** w/w gold

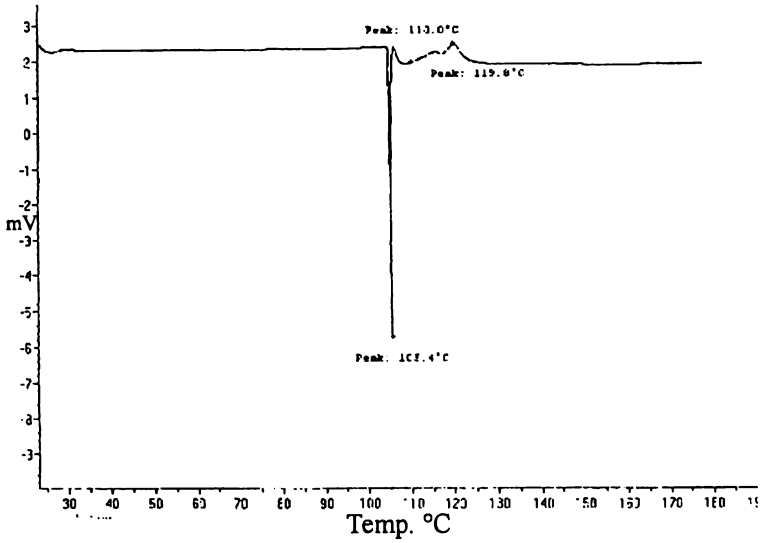

Figure 5·14 DSC of (Bu^{t}NC)AuNO$_3$ *M.p. 118 °C (Decomp.)

The exotherms observed in DSC of (EtNC)$AuNO_3$ (Figure 5·16) and (XyNC)$AuNO_3$ (Figure 5·17) are consistent with their observed decomposition. The (EtNC)$AuNO_3$ sample used for STA was partially decomposed, which explains why the observed weight loss was less than expected (Figure 5·15).

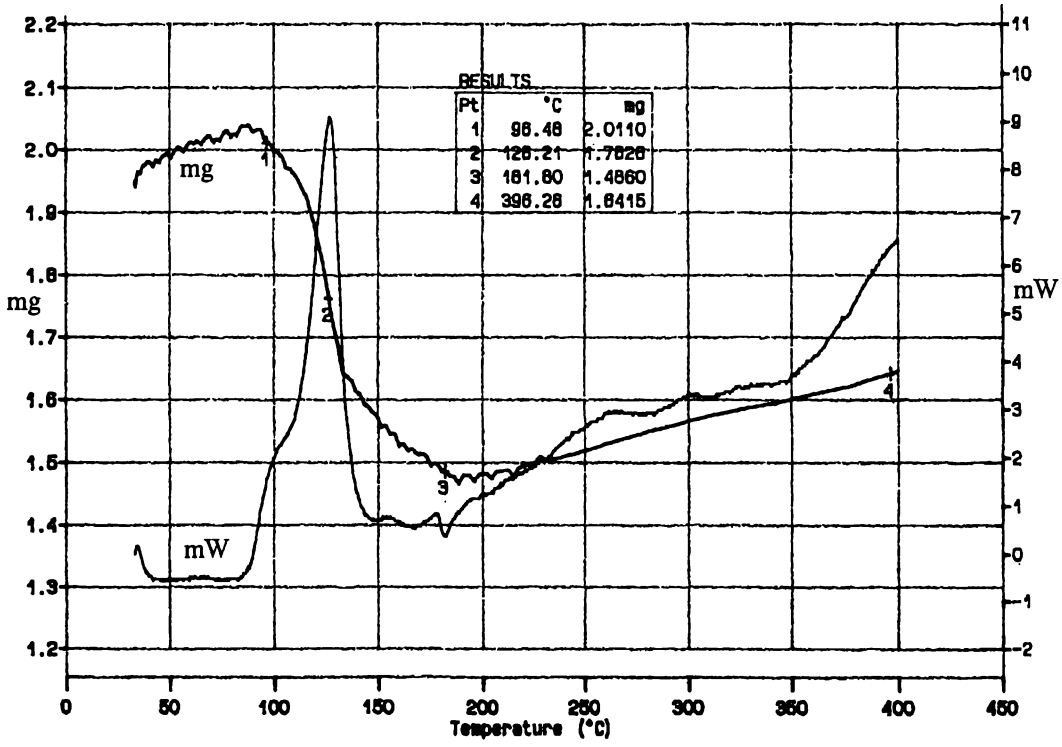

Figure 5·15 STA of (EtNC)$AuNO_3$

Sample weight = 1·945 mg

Weight loss between points one and three ~27% of the total weight

- Calculated weight loss of EtNC and nitrate from (EtNC)$AuNO_3$ ~37%

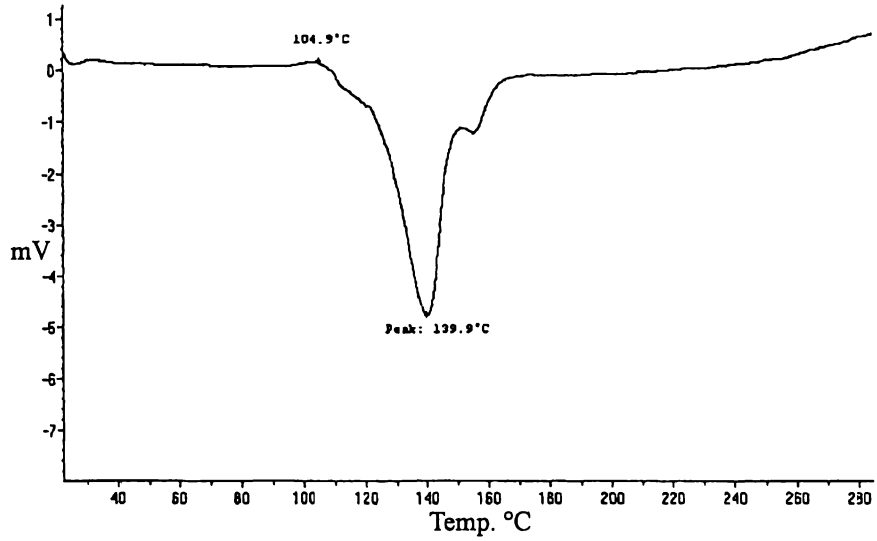

Figure 5·16 DSC of (EtNC)$AuNO_3$ *M.p. 107 °C (Decomp.)

STA of (XyNC)$AuNO_3$ exhibited an exothermic decomposition which was associated with a weight loss consistent with the complete removal of XyNC and nitrate (Figure 5·17).

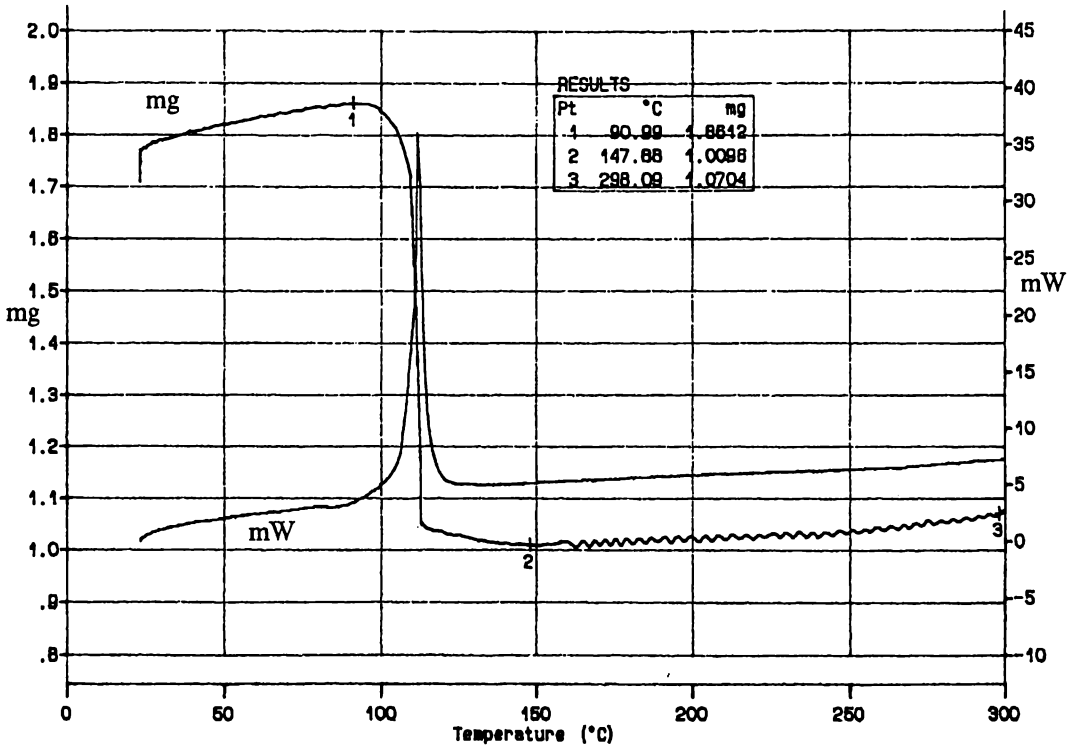

Figure 5·17 STA of (XyNC)$AuNO_3$

Sample weight = 1.757 mg

Weight loss between points one and two ~**49%** of the total weight

- Calculated weight loss of XyNC and nitrate from (XyNC)$AuNO_3$ ~**49%**

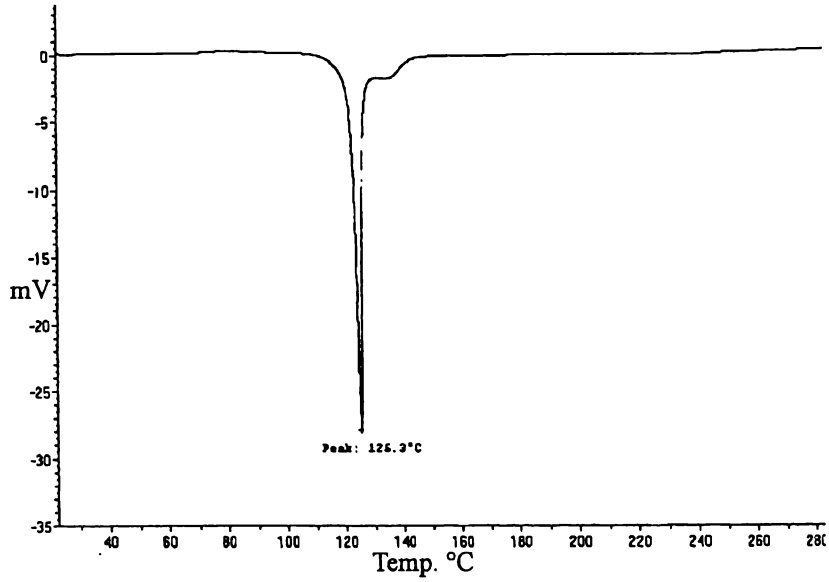

Figure 5·18 DSC of (XyNC)$AuNO_3$ *M.p. 122 °C (Decomp.)

The results of STA and DSC of the LAuX complexes are summarised in Table 5·1, with the temperatures associated with decomposition and the apparent loss of ligands L and X being listed. The approximated data provides a guide to the thermostability of the crystalline complexes and therefore insight to the potential of these complexes as gold catalyst precursors. It is apparent that the (RNC)$AuNO_3$ complexes decompose under moderate temperatures.

Table 5·1 Temperatures of thermolysis processes

	‡Decomp.	Loss of L	Loss of X
$(Ph_3P)AuCl$	245	>250	>250
$(Ph_3P)AuMe$	170	150-275	150
$(Bu^tNC)AuCl$	165	165	300-500
§$(Bu^tNC)AuCl$	165	165	250-300
(EtNC)AuCl	200	>200	>200
(XyNC)AuCl	250	>250	>250
$(Bu^tNC)AuNO_3$	120	120	120
$(EtNC)AuNO_3$	110	120	120
$(XyNC)AuNO_3$	120	120	120

All values are °C (± 5)

‡Based on DSC

All STA were run in air except § was run in 5% H_2/95% N_2

5·2·3 The support oxide

The gold complexes were mixed with $Fe(OH)_3$,‡ FeO(OH), Fe_2O_3 or YSZ.§ Emphasis was placed on preparing Fe_2O_3 supported gold materials, allowing comparison to be made with the Fe_2O_3/gold catalysts prepared by coprecipitation and gold-sputtering. The use of white yttria-stabilised zirconia (YSZ) allowed colour changes to be monitored during the catalyst preparations.

‡ $Fe(OH)_3$ was only used with $(Bu^tNC)AuNO_3$.

§ YSZ was supplied by the University of Waikato Technology Department.

Preparation of $Fe(OH)_3$, FeO(OH) and Fe_2O_3

$Fe(OH)_3$ was prepared using a similar technique to the preparation of coprecipitate A (refer to 5.1), by mixing aqueous solutions of Na_2CO_3 and iron(III). Hydrated iron(III) oxide, represented by the formula FeO(OH), was prepared by drying $Fe(OH)_3$ under vacuum for 10 hours. Fe_2O_3 was prepared by heating FeO(OH) at 400 °C for 4 hours.[249] The specific surface area of the prepared Fe_2O_3 was measured by 7-point BET analysis and found to be 73 $m^2\ g^{-1}$. The particle size distribution was measured for the Fe_2O_3 powder and is depicted in Figure 5·19. The average particle size was 24 μm.

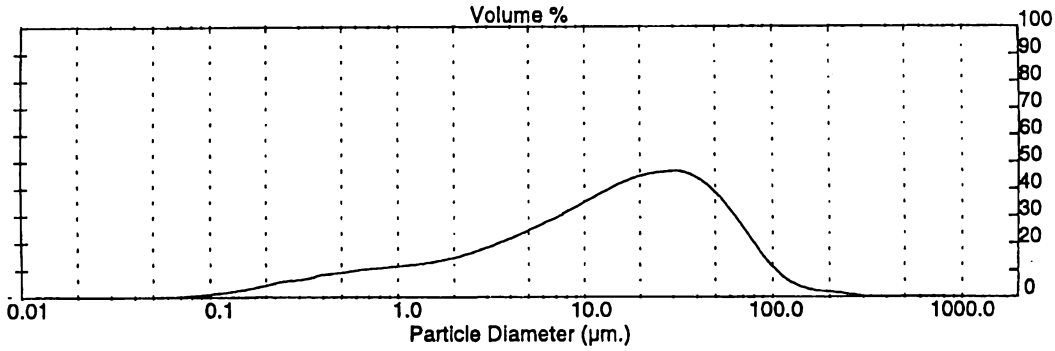

Figure 5·19 Size distribution of Fe_2O_3 particles

DSC of the hydroxides and oxides of iron has been described in detail.[250] The weight loss in STA of the prepared FeO(OH) was attributed to the loss of H_2O during Fe_2O_3 formation (Figure 5·20).

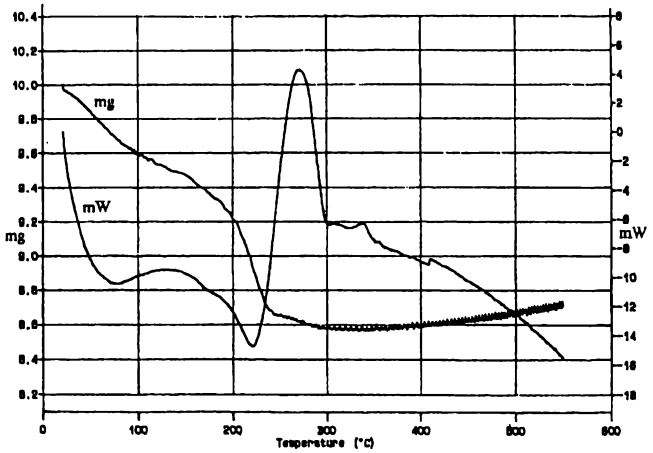

Figure 5·20 STA of FeO(OH)

---

[249] Q. Li and Y. Wei, *Mater. Res. Bull.*, 1998, **33**, 779; and refs. therein.

[250] R. C. MacKenzie and G. Berggren, in *Differential Thermal Analysis*, ed. R. C. MacKenkie, Academic Press, London, 1970, p 272-279.

5·3 CATALYST PREPARATIONS

This section describes the preparation of supported gold materials from gold complex precursors. The sub-section 5·3·1 focuses on the complexes $(Ph_3P)AuCl$, $(Ph_3P)AuMe$ and $(Bu^tNC)AuCl$. The use of $(Bu^tNC)AuNO_3$ is described in sub-section 5·3·2.

All of the prepared materials had the following in common:

(i) They were 3% w/w gold.

- The subsequent loss of water during calcination was taken into account when depositing gold complexes onto FeO(OH) (the H_2O content of which was ~15% w/w) and as-precipitated $Fe(OH)_3$ (the H_2O content of which was ~90% w/w).

(ii) They are given the nomenclature; [complex/solvent/support/temperature].

- Two calcining procedures were used; either 400 °C for two hours or 300 °C for two hours.

- $[(Ph_3P)AuCl/CH_2Cl_2/Fe_2O_3/300]$ for example, represents a material prepared by mixing Fe_2O_3 in a CH_2Cl_2 solution of $(Ph_3P)AuCl$, followed by drying under vacuum and heating at 300 °C for two hours.

5·3·1 $(Ph_3P)AuCl$, $(Bu^tNC)AuCl$ and $(Ph_3P)AuMe$

CH_2Cl_2 or MeCOMe solutions of $(Ph_3P)AuCl$, $(Bu^tNC)AuCl$ or $(Ph_3P)AuMe$ were mixed with Fe_2O_3, FeO(OH) or YSZ. After removal of the solvents, a significant quantity of crystalline gold complex was generally observed on the support and on the glassware. This indicated that adsorption of these complexes onto the support surfaces was not particularly efficient. The % w/w of gold on these materials, subsequent to calcination, was therefore less than 3%.

The complexes appeared to be stable in the metal oxide slurries, as evidenced by the recrystallisation when the solvents were removed. However, it was apparent that some decomposition was occurring.

The surfaces of Fe_2O_3 and FeO(OH) appeared to act as decomposition catalysts for (Bu^tNC)AuCl in that the odour of Bu^tNC was present *before* the removal of the solvent. Furthermore, YSZ turned purple when mixed with solutions of (Bu^tNC)AuCl, (Ph_3P)AuCl or (Ph_3P)AuMe. The purple colour on the YSZ, attributable to tiny gold particles, persisted throughout the calcining steps.

In comparison, CH_2Cl_2 and MeCOMe solutions of (Ph_3P)AuCl or (Bu^tNC)AuCl (in the absence of YSZ) exhibited prolonged stability. CH_2Cl_2 and MeCOMe solutions of (Ph_3P)AuMe exhibited a faint purple colour after stirring for ten hours under ambient conditions.

Figure 5·21 depicts four glass tubes each packed with a different material. The purple material (1) is [(Ph_3P)AuMe/CH_2Cl_2/YSZ/300]. The white material (2) is pure YSZ. The black (3) and brown (4) materials are Fe_2O_3 materials prepared by calcination at 400 °C and 300 °C respectively.

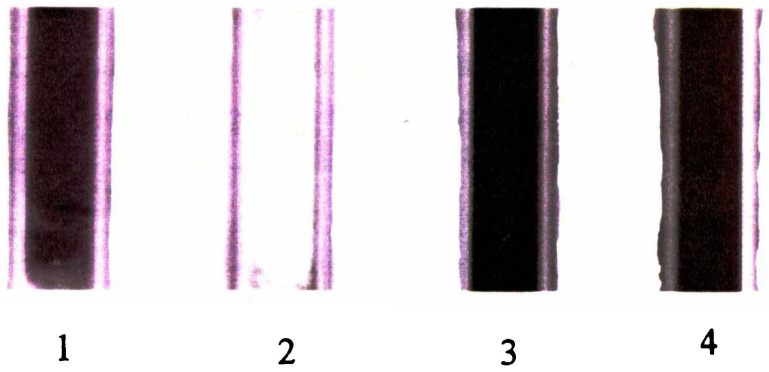

Figure 5·21 Colours of catalyst materials

5·3·2 (Bu^tNC)$AuNO_3$

Parallel research was published during the course of this project, which described the preparation of active CO oxidation catalysts by mixing as-precipitated $Fe(OH)_3$ with MeOH solutions of (Ph_3P)$AuNO_3$.[242]

It was envisaged that if $[(Bu^tNC)Au]^+NO_3^-$ could be prepared, it would have potential as a precursor to active supported gold materials. It became evident that isonitrile ligands provide a stability sufficient to allow crystalline $(RNC)AuNO_3$ (R = Bu^t, Et or Xy) materials to be obtained. Full characterisation of these complexes is provided in Chapter Three, in which it was noted that solutions of $(RNC)AuNO_3$ are particularly unstable.

MeCOMe, MeOH or CH_2Cl_2 solutions of $(Bu^tNC)AuNO_3$ were mixed with Fe_2O_3 or as-precipitated $Fe(OH)_3$. The wet $Fe(OH)_3$ material did not form a thin slurry with CH_2Cl_2 solutions of $(Bu^tNC)AuNO_3$; this particular mixture precipitated visible metallic gold on the glassware. $(Bu^tNC)AuNO_3$ always decomposed on contact with the supports, as evidenced by the odour of Bu^tNC before removal of the solvents. No crystalline material was observed when removing the solvents, indicating that $(Bu^tNC)AuNO_3$ (or a decomposed fragment) was efficiently adsorbed onto the Fe_2O_3 or as-precipitated $Fe(OH)_3$ surfaces.

5·4 SURFACE CHARACTERISATION

This section describes the surface characteristics of the materials prepared by coprecipitation, gold-sputtering and the deposition of gold complexes. Emphasis was placed on the identification of supported gold particles by SEM. The resolution of the SEM was ~5 nm.

5·4·1 Coprecipitate and gold-sputtered materials

SEM was not able to resolve gold particles on the surfaces of the calcined coprecipitate materials (refer to 5·1). However, as displayed in Figure 5·22, EDAX analysis was able to detect gold on the surface of these materials. XPS analysis confirmed the presence of gold. It was proposed that the heated coprecipitate materials consist of metallic gold particles (of a diameter less than 5 nm) supported on Fe_2O_3.

Similarly, SEM was not able to resolve any gold particles on the materials prepared by gold-sputtering, but gold was detected by both EDAX and XPS.

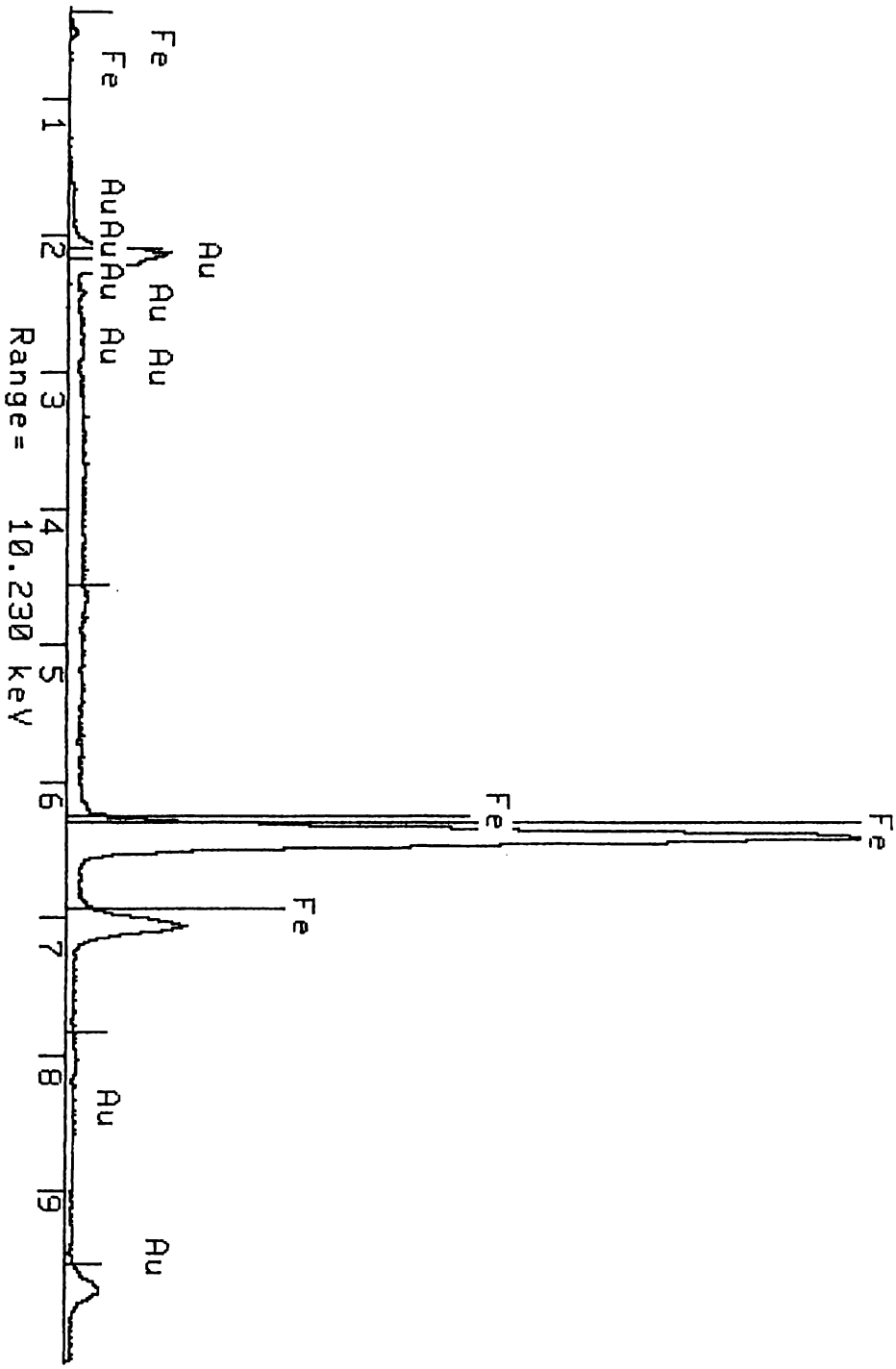

Figure 5·22 EDAX of calcined coprecipitate A

5·4·2 $(Ph_3P)AuCl$, $(Bu^tNC)AuCl$ and $(Ph_3P)AuMe$ precursor materials

Uncalcined materials

Evidence for the presence of highly dispersed microcrystalline $(Bu^tNC)AuCl$ was observed upon the surface of the uncalcined $[(Bu^tNC)AuCl/CH_2Cl_2/Fe_2O_3/-]$ material (Figure 5·23). Even though $(Bu^tNC)AuCl$, $(Ph_3P)AuCl$ and $(Ph_3P)AuCl$ formed visible crystalline material when removing the solvents, this was the only microcrystalline material observed using SEM.

Calcined materials

SEM of the calcined materials generally revealed metallic gold particles (~5-200 nm) dispersed over the surfaces of aggregated oxide particles. Figures 5·24-5·32 display selected micrographs in which the gold particles are identified as bright entities upon the dark oxide surfaces. The gold particle sizes (estimated) are noted for each micrograph.

The micrographs of $[(Ph_3P)AuCl/CH_2Cl_2/FeO(OH)/300]$ (Figure 5·24), $[(Bu^tNC)AuCl/CH_2Cl_2/Fe_2O_3/300]$ (Figures 5·25 and 5·26), and $[(Bu^tNC)AuCl/MeCOMe/FeO(OH)/300]$ (Figures 5·27) exhibit a relatively high dispersion of metallic gold particles. The average diameter of the gold particles in Figure 5·24 appears to be ~10-30 nm, which is similar to the gold particles upon the surface of a catalyst prepared by alloy oxidation (see Figure 4·5).

The gold particles on the surface of $[(Ph_3P)AuCl/MeCOMe/FeO(OH)/400]$ (Figure 5·28) were also well dispersed. A micrograph of $[(Bu^tNC)AuCl/CH_2Cl_2/Fe_2O_3/400]$ is depicted in Figure 5·29 and exhibits gold particles of relatively large size.

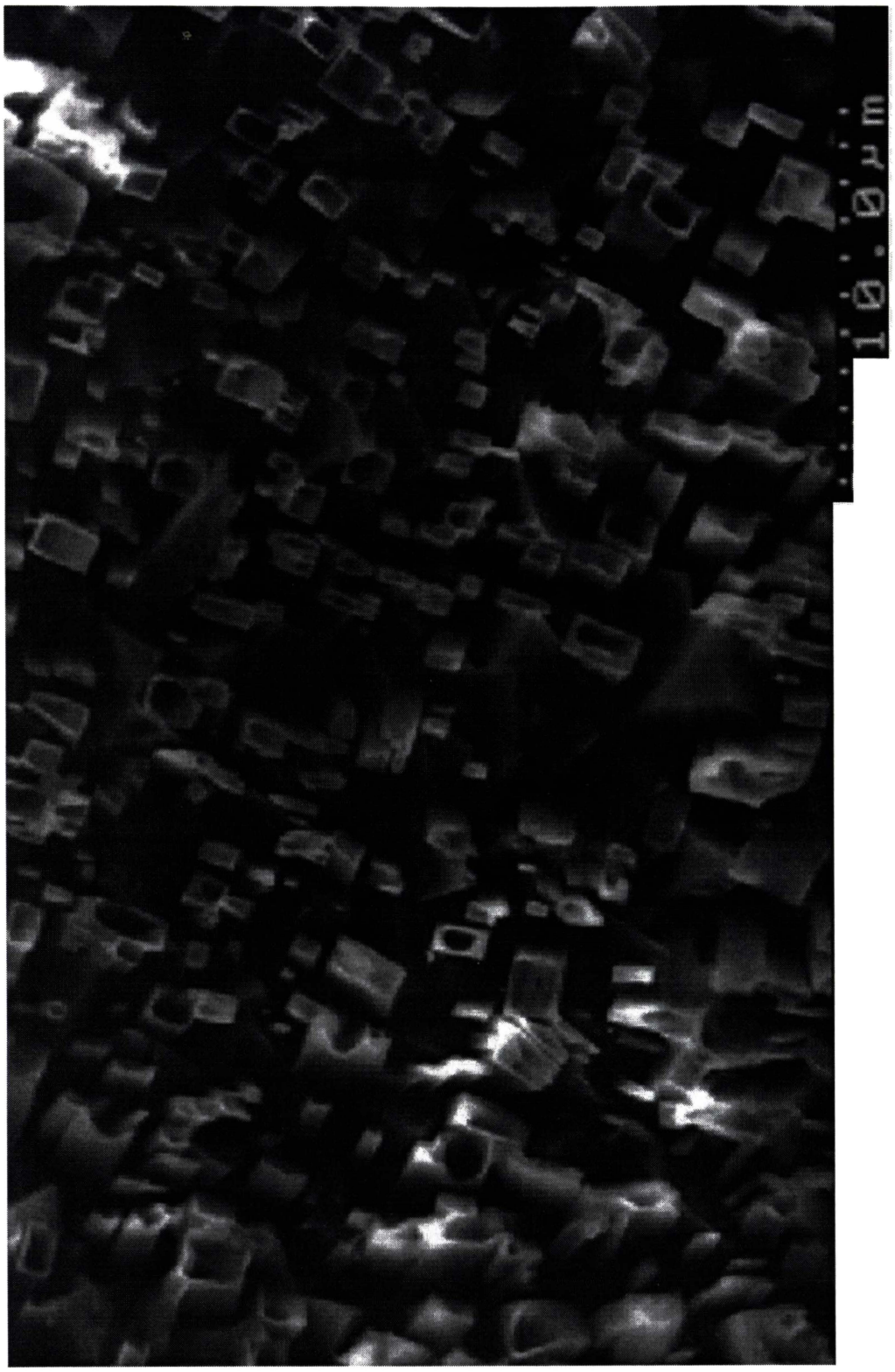

Figure 5·23 SEM of [(Bu^tNC)AuCl/CH_2Cl_2/Fe_2O_3/-]

Crystal size range 0·5 - 3 µm

The use of $(Ph_3P)AuMe$ as a precursor was unusual in that interspersed metallic gold polygons were present on the calcined materials. Crystalline gold polygons have been observed on surfaces previously[251] and controlled synthesis of microscopic metallic crystals has been developed.[252] The polygons were numerous on the $[(Ph_3P)AuMe/CH_2Cl_2/Fe_2O_3/300]$ material (Figure 5·30). The micrograph depicted in Figure 5·31 exhibits a trigon (1), diamond (2), pentagon (3) and hexagon (4) of metallic gold. In contrast, the purple material $[(Ph_3P)AuMe/CH_2Cl_2/YSZ/300]$ did not exhibit polygons (Figure 5·32).

General observations from SEM of the prepared materials were:

(i) There was little evidence for the presence of highly dispersed microcrystalline material on the uncalcined materials. There was only one exception, that of the material $[(Bu^tNC)AuCl/CH_2Cl_2/Fe_2O_3/-]$.

(ii) It appeared that calcination at 400 °C resulted in larger gold particles compared with calcination at 300 °C. The higher temperature presumably promoted coalescence and migration of the gold particles on the oxide surface. The process of coalescence can be visualised in Figures 5·26 and 5·27, in which gold particles are shown joining to form one.

(iii) There was indication that the use of FeO(OH) resulted in smaller gold particles compared with the use of Fe_2O_3.

(iv) In terms of the surface morphology of the calcined materials, there was no obvious difference between the use of the CH_2Cl_2 or MeCOMe.

5·4·3 $(Bu^tNC)AuNO_3$ precursor materials

SEM of the uncalcined and calcined materials exhibited featureless support surfaces. EDAX was able to detect the presence of gold on the surface of the calcined materials, the particles of which were evidently too small (less than 5 nm) to be resolved by SEM. High resolution TEM (see Figure 4·3) was not available to the author during the course of this project. The use of TEM, XRD and XPS as probes of gold particle size are suggested for future research in New Zealand of supported gold catalysts.

---

251 Ref. 129, p.255.

252 D. G. Duff, A. C. Curtis, P. P. Edwards, D. A. Jefferson, B. F. G. Johnson and D. E. Logan, *J. Chem. Soc., Chem. Commun.*, 1264, 1987.

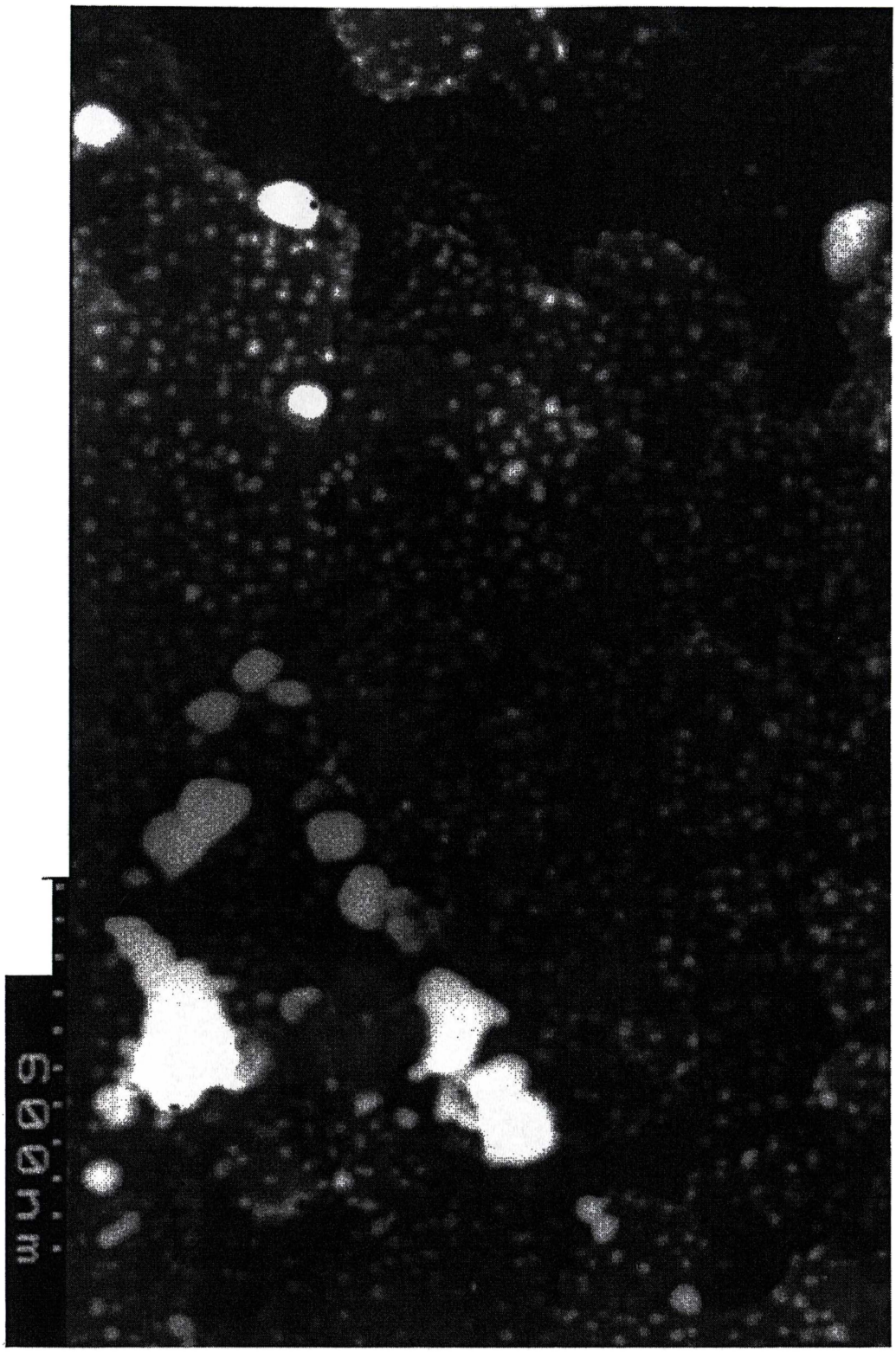

Figure 5·24 SEM of [$(Ph_3P)AuCl/CH_2Cl_2/FeO(OH)/300$]

Gold particle size range 10 - 30 nm

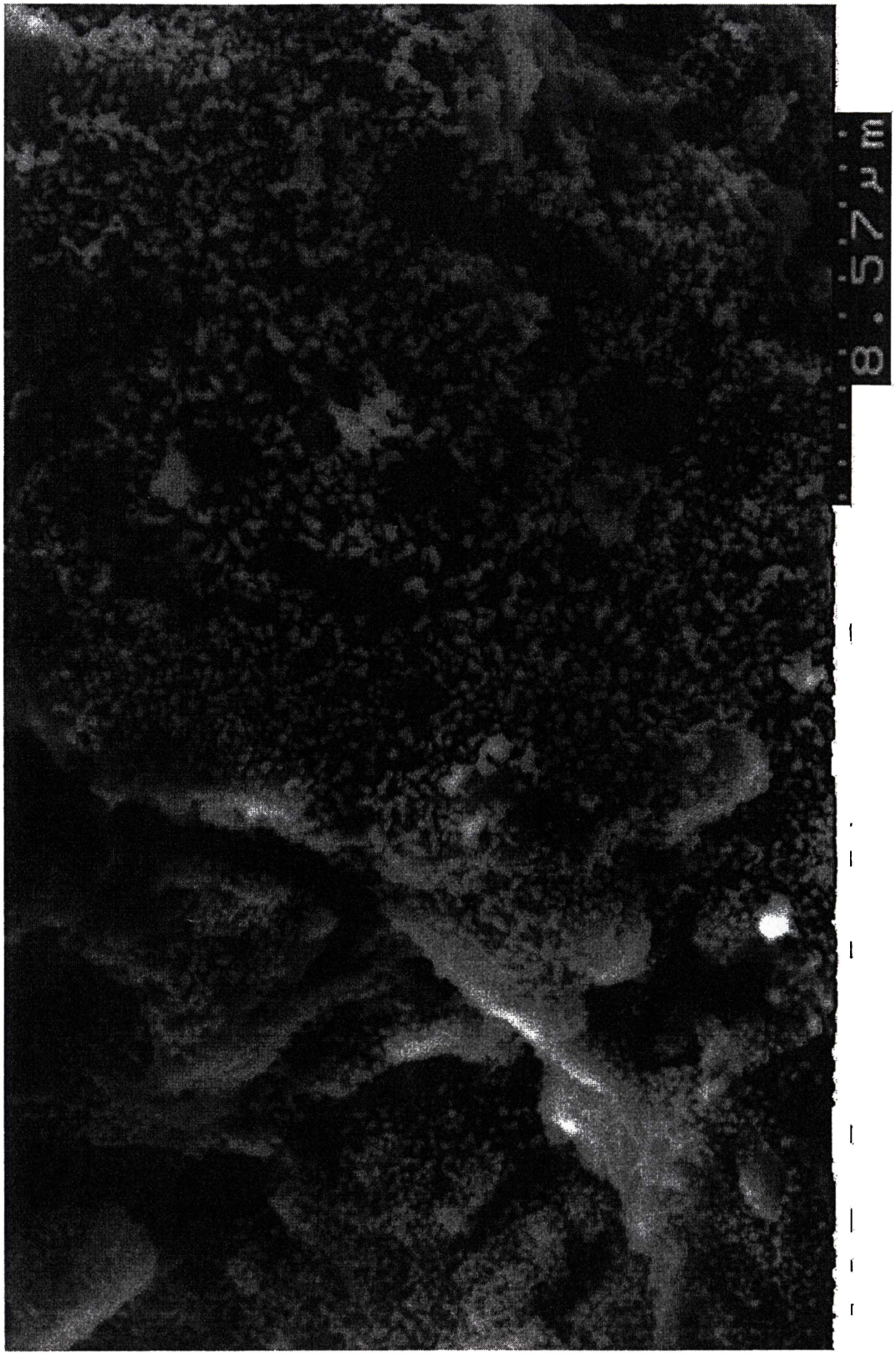

Figure 5·25 SEM of [(Bu^{t}NC)AuCl/CH_2Cl_2/Fe_2O_3/300]

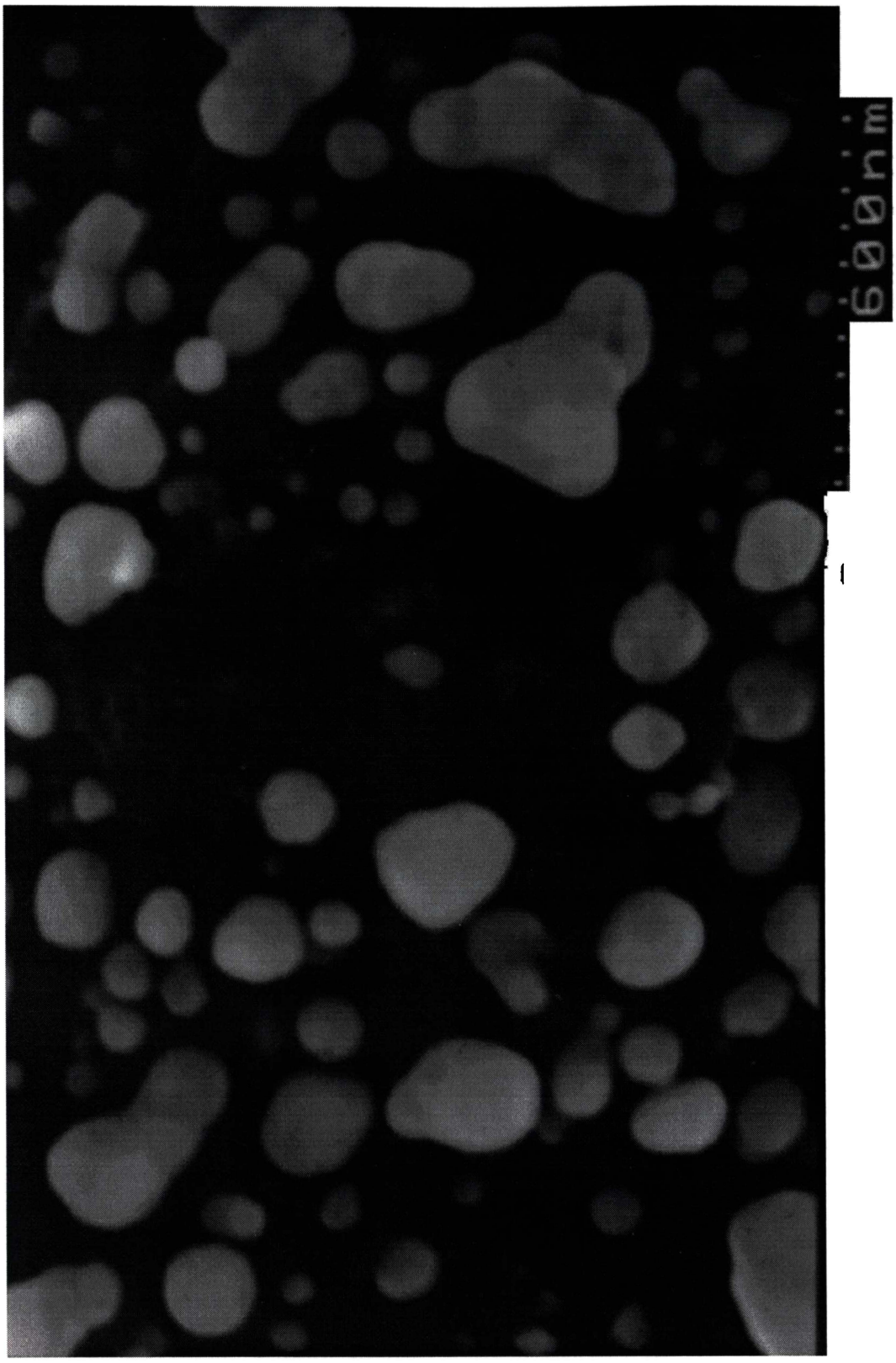

Figure 5·26 SEM of [(Bu^tNC)AuCl/CH_2Cl_2/Fe_2O_3/300]

Gold particle size range 60 - 300 nm

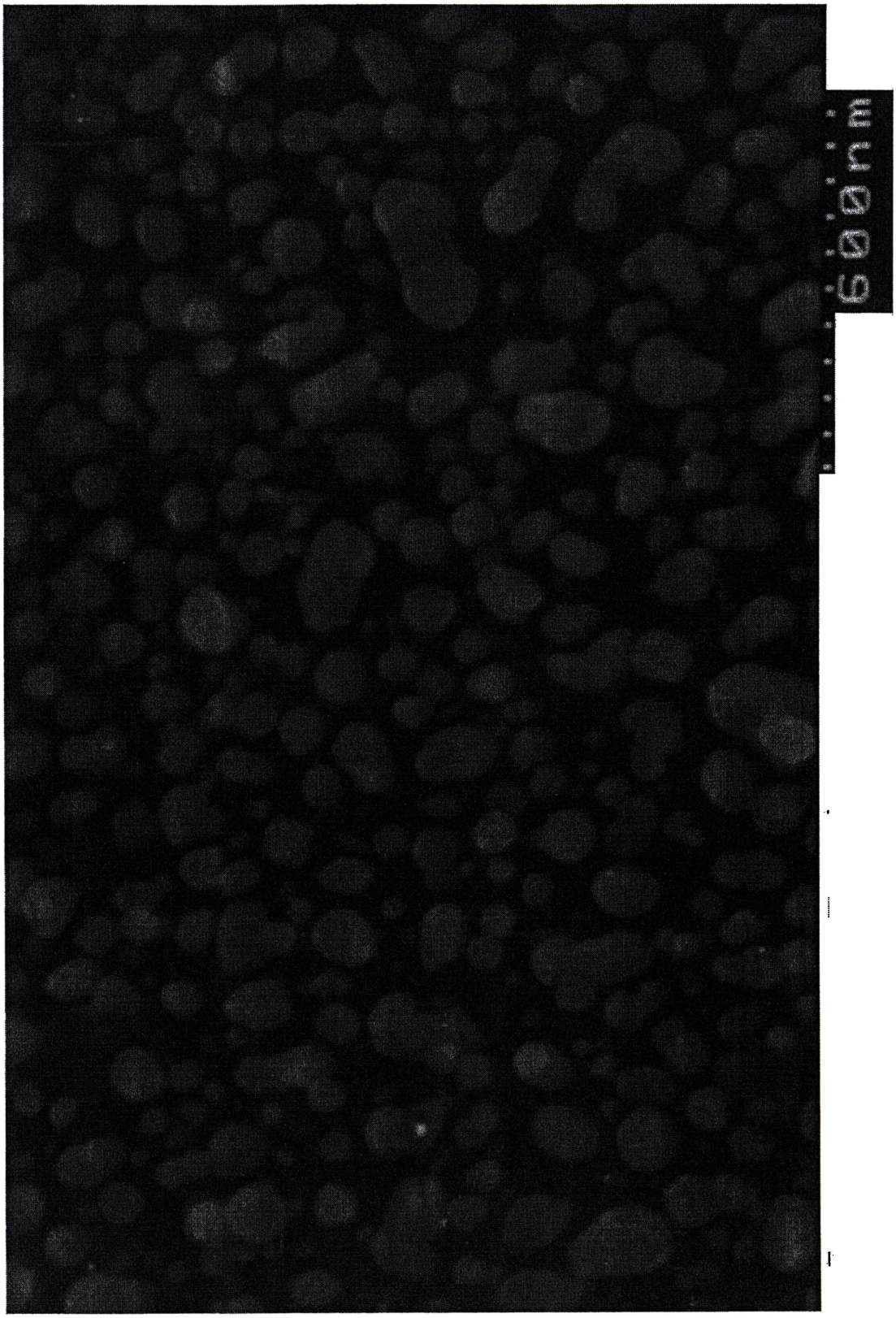

Figure 5·27 SEM of [(Bu^{t}NC)AuCl/MeCOMe/FeO(OH)/300]

Gold particle size range 30 - 150 nm

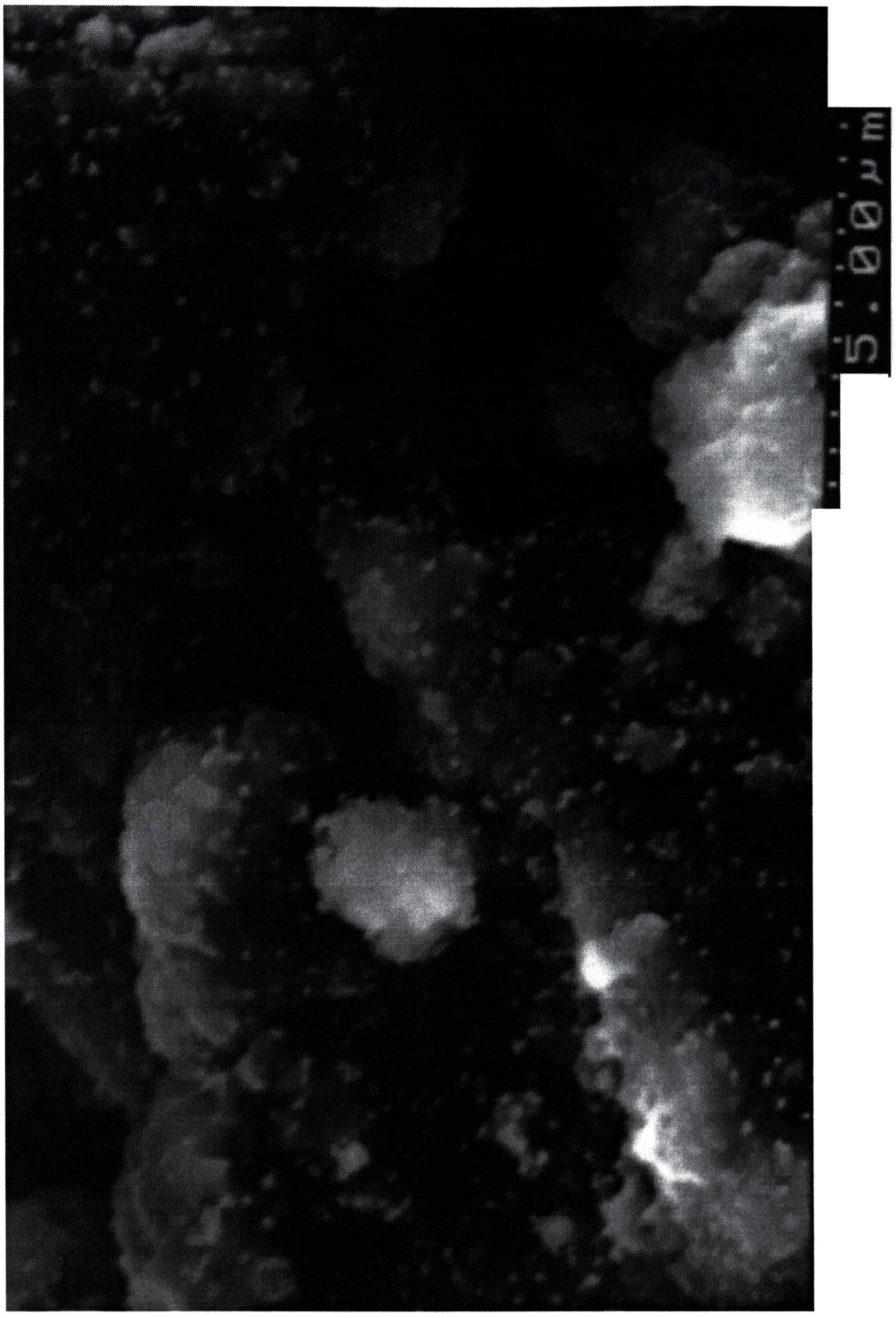

Figure 5·28 SEM of [(Ph_3P)AuCl/CH_2Cl_2/FeO(OH)/400]

Gold particle size range 200 - 300 nm

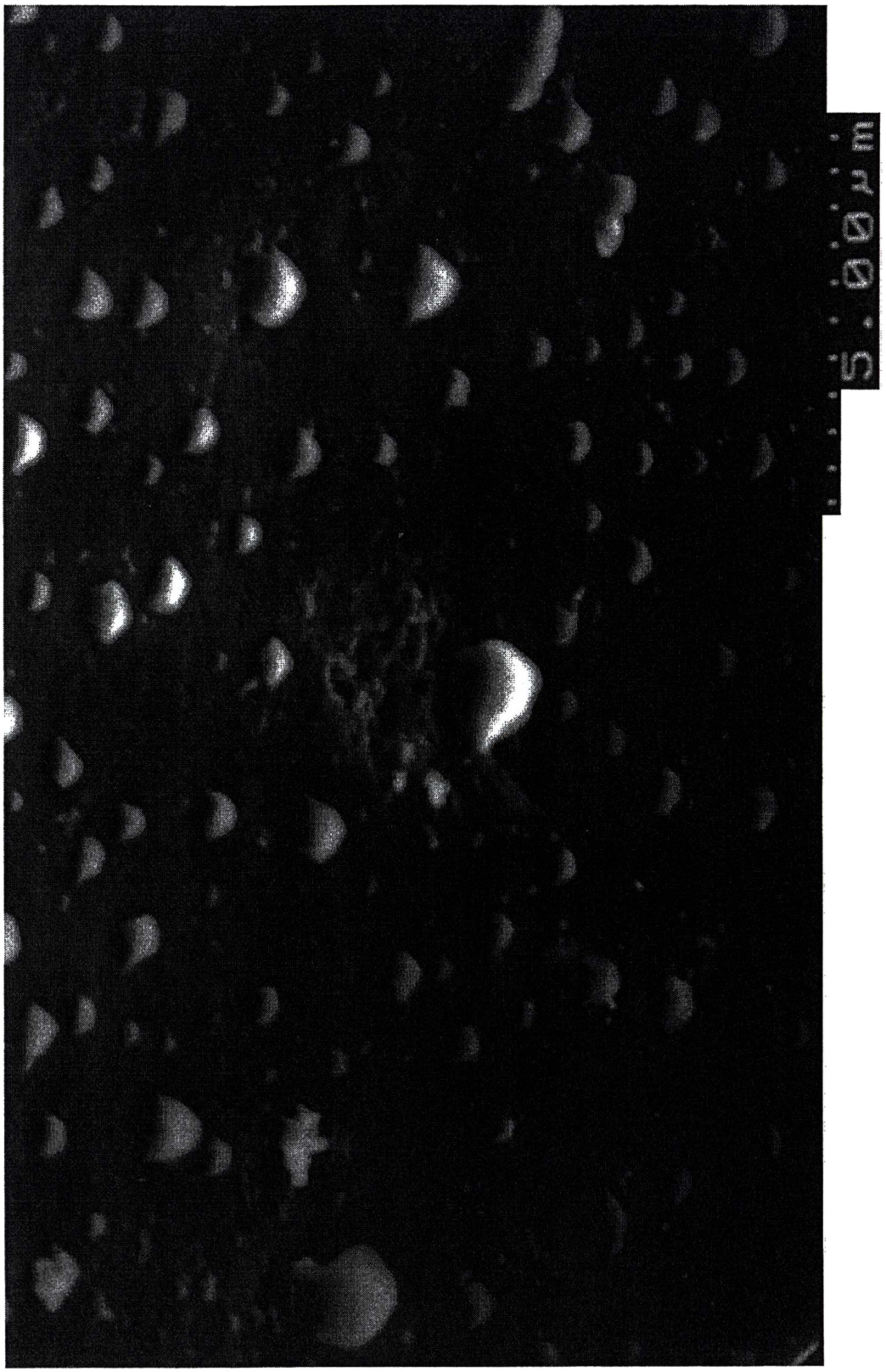

Figure 5·29 SEM of [(Bu^{t}NC)AuCl/CH_2Cl_2/Fe_2O_3/400]

Gold particle size range 0·5 - 2 µm

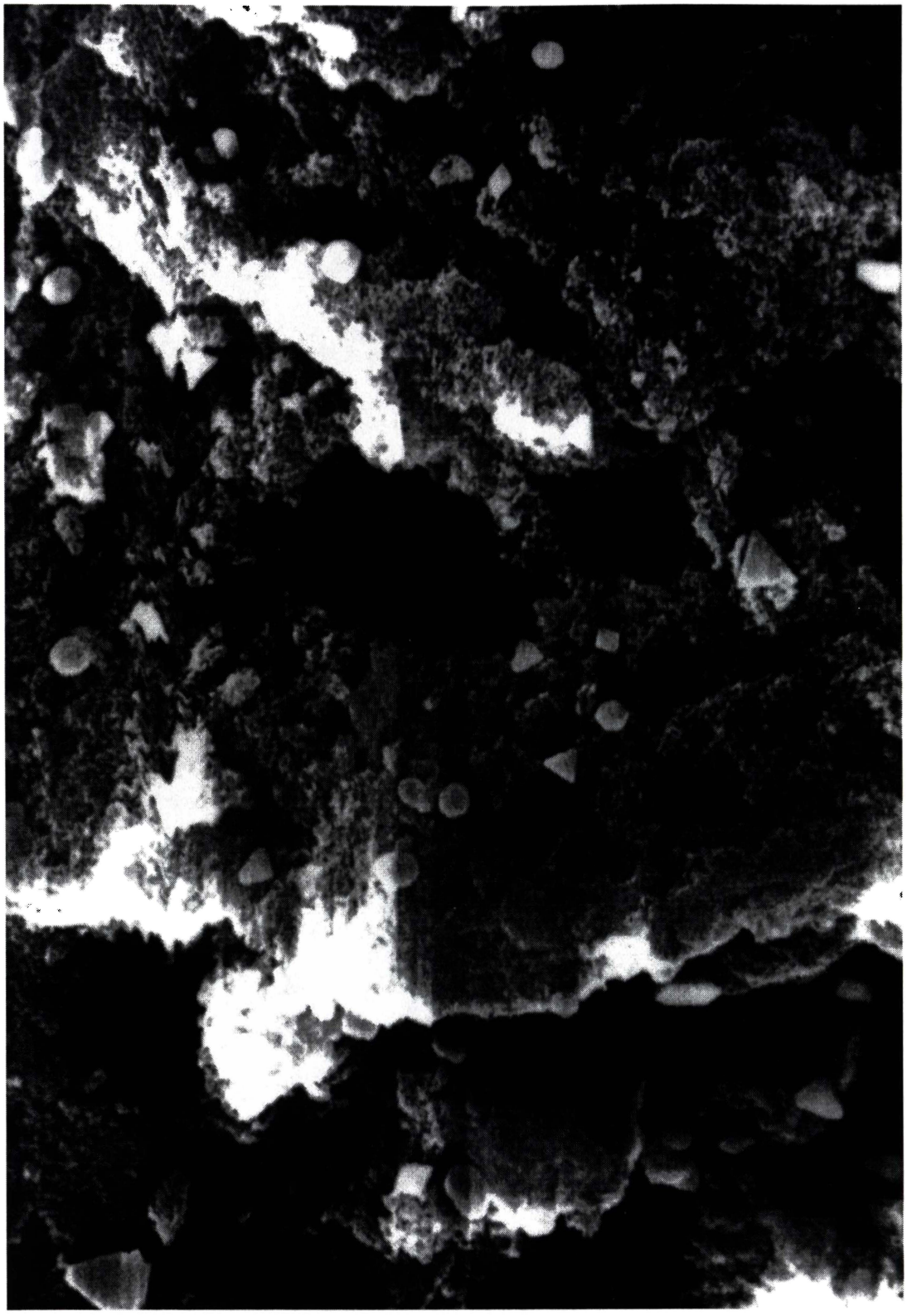

Figure 5·30 SEM of [$(Ph_3P)AuMe/CH_2Cl_2/Fe_2O_3/300$]

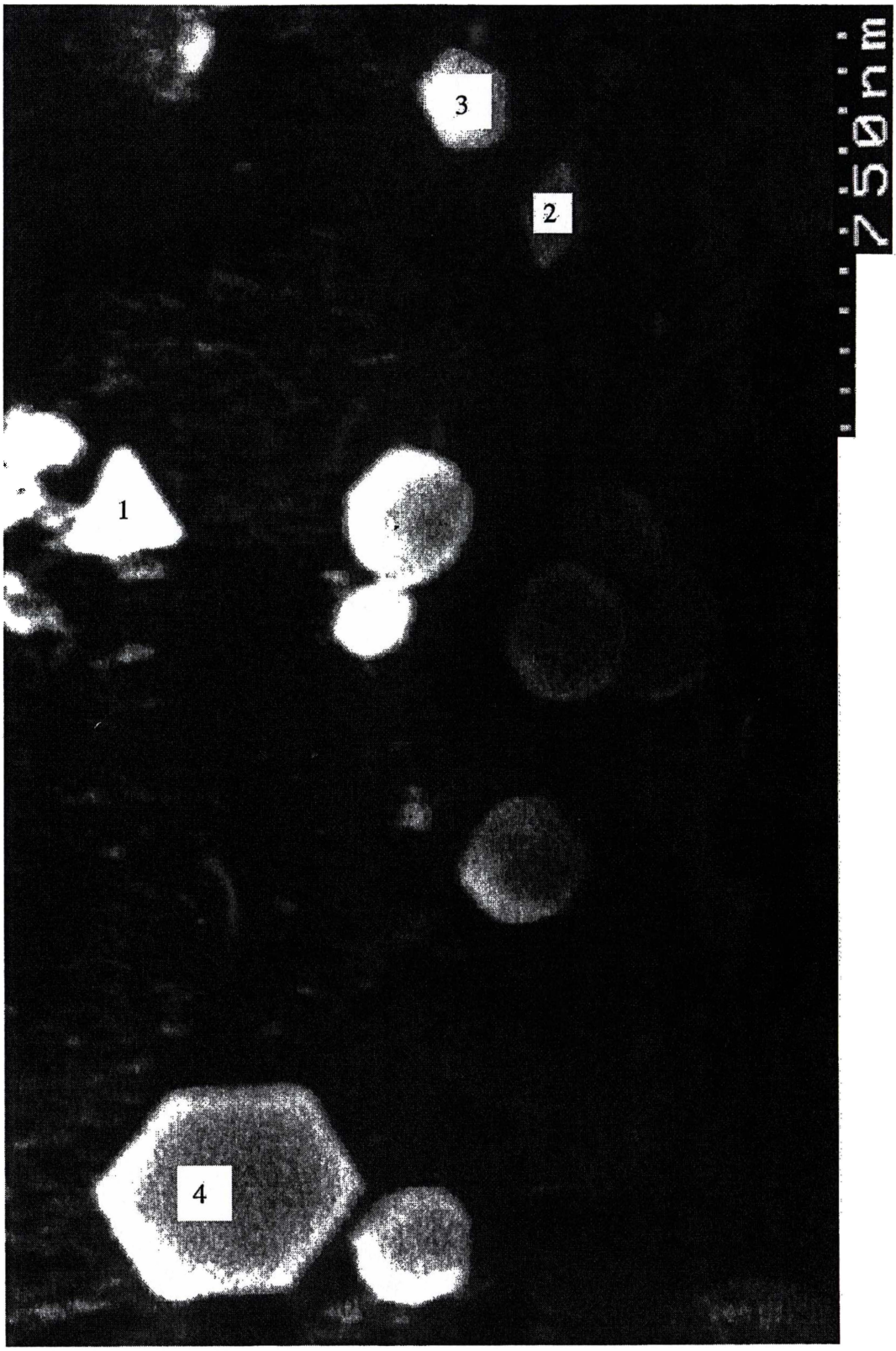

Figure 5·31 Regular polygons on [$(Ph_3P)AuMe/CH_2Cl_2/Fe_2O_3/300$]

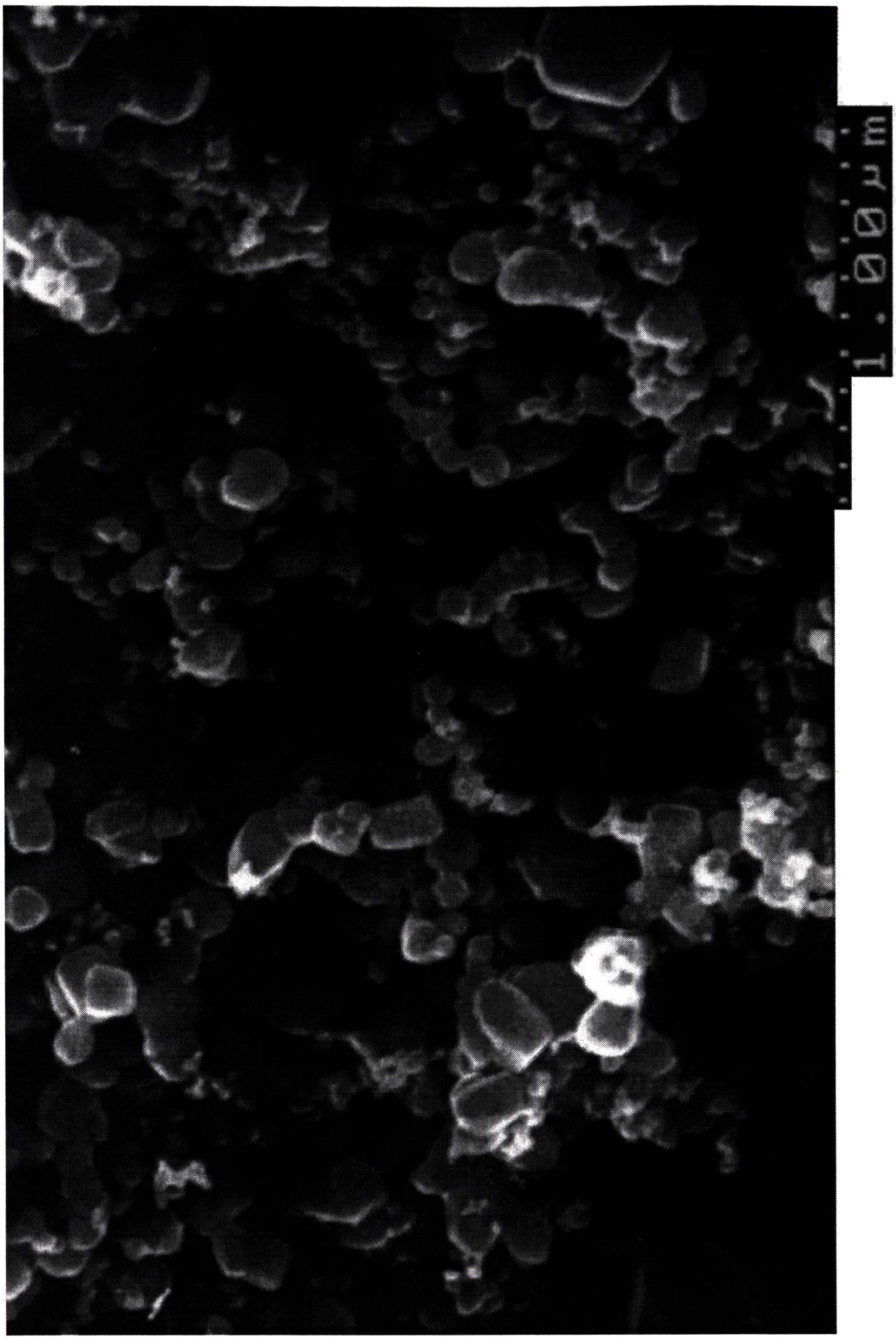

Figure 5·32 SEM of [$(Ph_3P)AuMe/CH_2Cl_2/YSZ/300$]

Gold particle size range 100 - 300 nm

5·5 CATALYTIC CO OXIDATION TESTING

5·5·1 Catalyst testing procedure

The prepared supported gold materials were tested for catalytic CO oxidation.‡ The testing strategy was to pass a gas mixture of CO-in-air through a catalyst bed contained within a glass tube. The tubes had an internal diameter of ~2·5 mm. The outflow was monitored with a CO detector. A diagrammatic representation of the testing apparatus is displayed in Figure 5·33. Features of the testing apparatus are as follows:

(i) A three-way tap was positioned to allow the gas flow to be switched between a by-pass and the catalyst bed.

(ii) Two flow meters were positioned; one at the start of the apparatus (a mass-flow controller) and one prior to the CO detector. Monitoring both meters ensured that a consistent flow was maintained.

(iii) H_2O vapour was able to be introduced to the gas flow by positioning a H_2O impinger before the sample.

(iv) CO was detected by a SnO_2-based fuel cell. This produced a voltage (mV) output proportional to the quantity of oxidisable gaseous species passing through it.

(v) Controlled heating of the catalyst bed was made possible with a programmable temperature controller (PTC) linked to a heating mantle beside the catalyst bed.

‡ Testing was carried out by the author at Industrial Research Limited (IRL), Wellington.

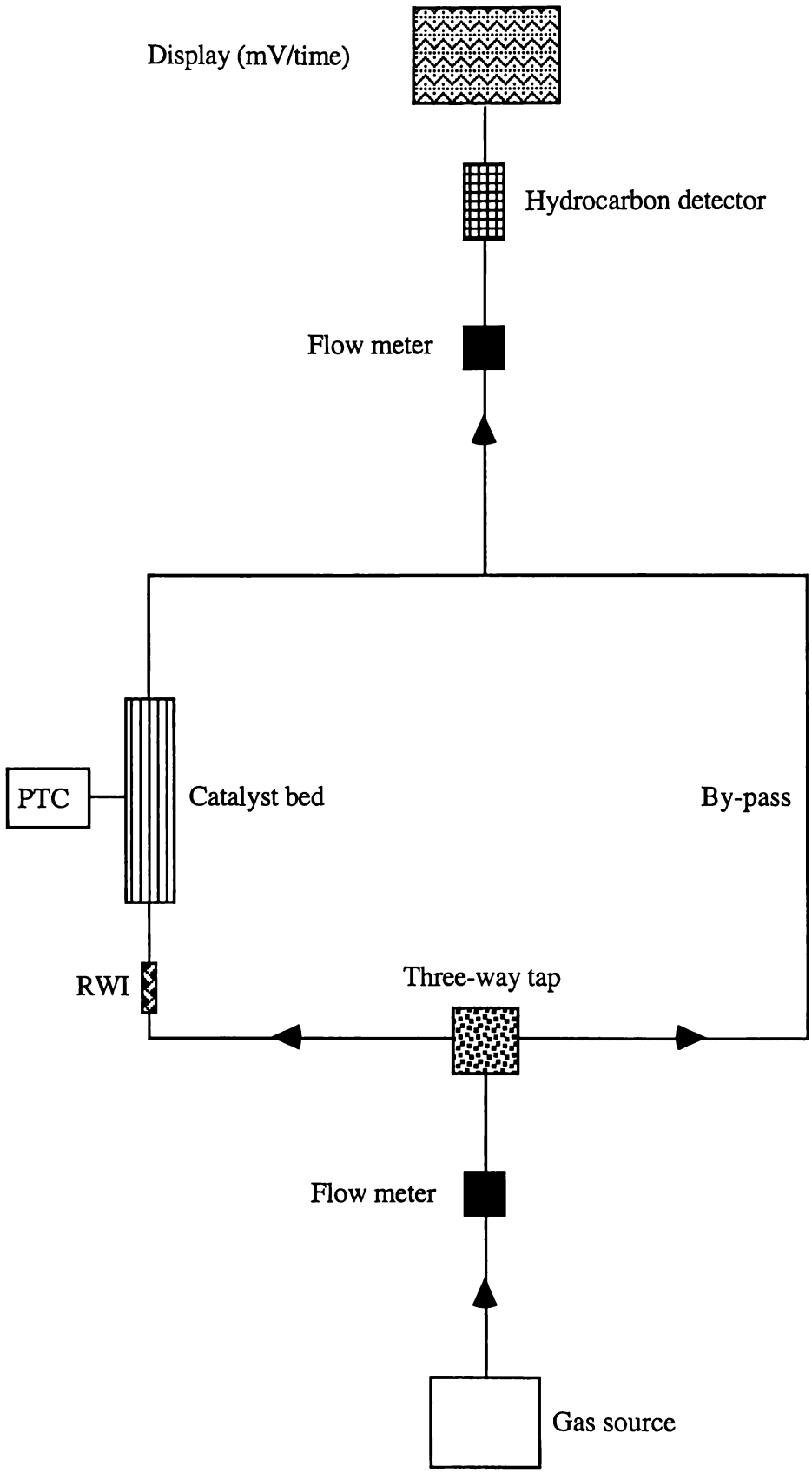

Figure 5·33 Testing apparatus

PTC - Programmed temperature controller

RWI - Removable water impinger

Catalysis testing of the prepared supported gold materials was generally carried out at ambient (13-19 °C) temperature. All supported gold materials described as *active for CO oxidation* refers to activity under these conditions, unless noted otherwise. When catalysts are described as having no activity, this indicates that the testing resulted in a trace comparable to that observed for pure Fe_2O_3 (see Figure 5·35).

Assessing the potential for catalytic oxidation of CO was based on the following three procedures:

(i) Pure air was passed through the catalyst bed at a known flow rate, creating a baseline detector response. This is represented by X on all of the testing traces.

(ii) A gas mixture of known CO% in air was passed through the by-pass, creating an upper level detector response which represents no CO removal (Y).

(iii) The CO-in-air gas mixture was passed through a known mass of catalyst. The observed detector response indicated the effectiveness of the catalyst to remove CO by oxidation to CO_2 (Z).

The testing strategy was developed to incorporate all three procedures (X, Y and Z) on a single trace of detector response (mV) versus total time (minutes). The catalysts were screened for CO oxidation capacity by passing ~1% CO-in-air through the catalyst materials (~10 mg) at 120 cm^3 $hour^{-1}$ (space velocity ~12000 cm^3 $hour^{-1}$ g^{-1}).

5·5·2 Testing a single-component catalyst

A preliminary catalytic test for CO oxidation was carried out on the commercially available catalyst "Platinum Kontakt".§ This material consists of platinum nano-particles dispersed over a Al_2O_3 support. The material was not active for CO oxidation at ambient temperature, but functioned effectively at temperatures greater than ~150 °C (Figure 5·34). The observed activity was characteristic of a single-component CO oxidation catalyst (refer to 4·3·1).

It was surmised that the platinum particles were covered with CO at ambient temperature, not permitting oxygen on the surface. CO was oxidised only when the temperature was raised above 150 °C (A in Figure 5·34). Under these conditions significant CO desorption rates permitted dissociative oxygen adsorption and hence favourable CO and oxygen surface contact and reaction.

§ Supplied by the German company Leuna.

When the temperature was reduced from ~300 °C, activity appeared to be lost at ~100 °C (B). To explain this relatively low temperature of deactivation, it was proposed that when reducing the temperature, a period of time (in which no further oxygen adsorption occurred) was required for the CO to replace the oxide on the platinum surface.

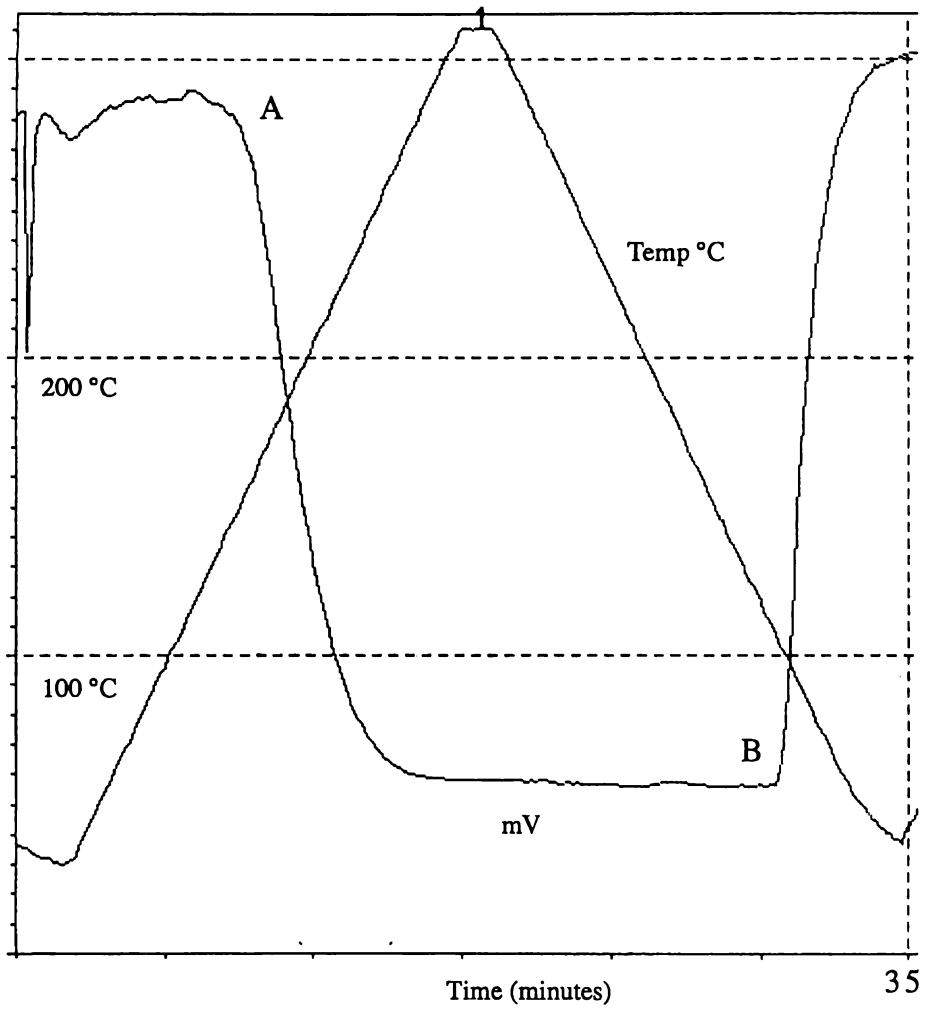

Figure 5·34 Testing of Platinum Kontakt

Baselines were not recorded on this preliminary testing trace

5·5·3 Fe_2O_3

A sample of pure Fe_2O_3 was tested and the resulting trace is depicted in Figure 5·35. The detector signal (mV) at Z is similar to that of Y, which indicates that the Fe_2O_3 had a negligible capacity to oxidise CO at room temperature. During active catalysis the signal at Z would be expected to be similar to X. Figure 5·35 provides details at various stages of the trace, which are applicable to traces displayed in later figures.

5·5·4 Coprecipitation materials

The calcined coprecipitate materials (refer to sub-section 5·1·1) were found to be active for CO oxidation. A test for the CO oxidation efficiency of coprecipitation A is displayed in Figure 5·36.

Both coprecipitate materials were found to display prolonged activity. Figure 5·37 displays an extended test of CO oxidation of coprecipitate B, in which the catalytic activity did not diminish significantly for three days.

5·5·5 Gold-sputtered materials

Of the three Fe_2O_3 samples treated by gold-sputtering, one exhibited activity for CO oxidation (Figure 5·38). The remaining two samples had no activity under the same testing conditions. This was difficult to explain as each of the three samples were prepared under similar conditions.

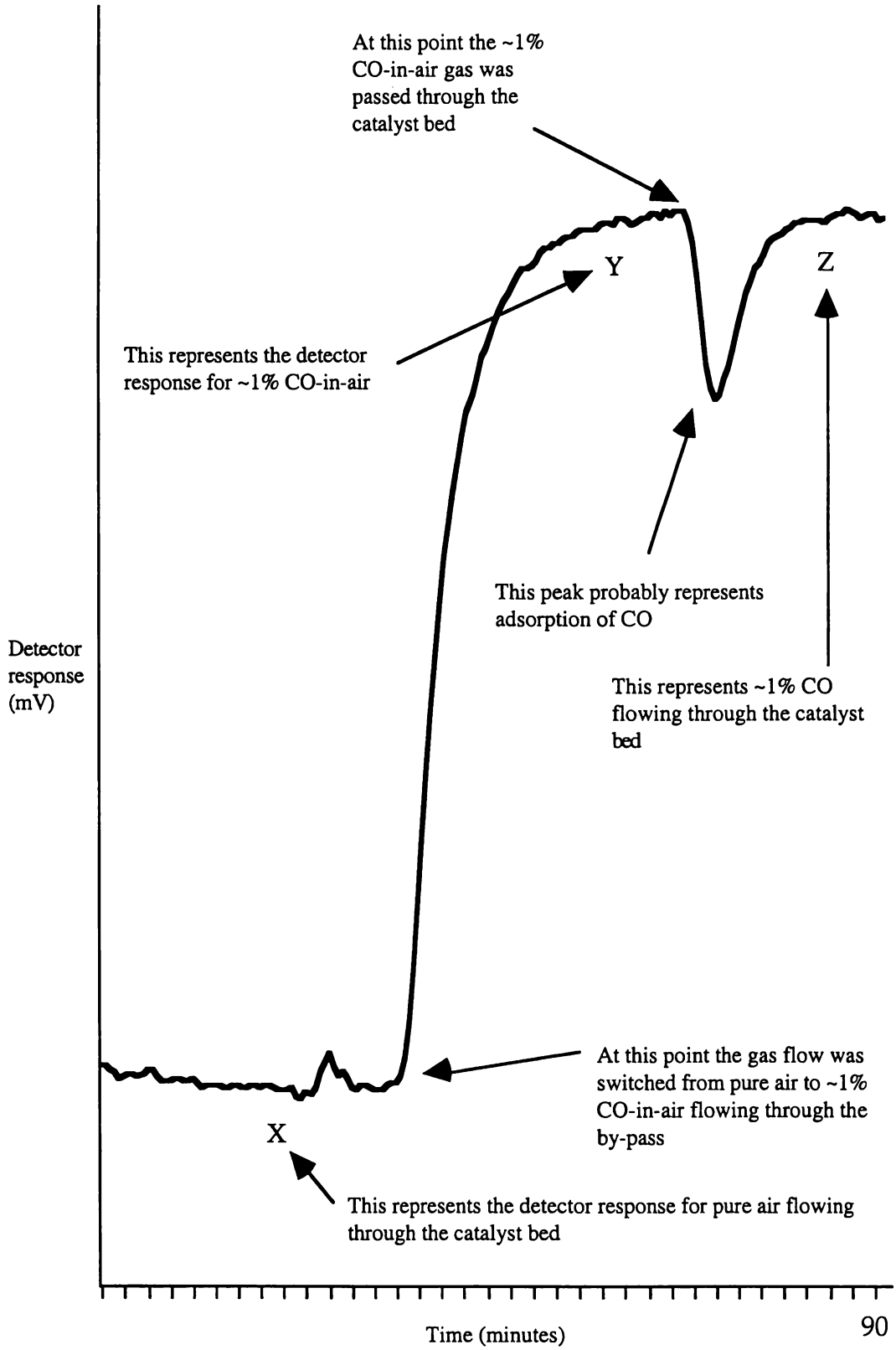

Figure 5·35 Testing of pure Fe_2O_3

Figure 5·36 Testing of coprecipitate A

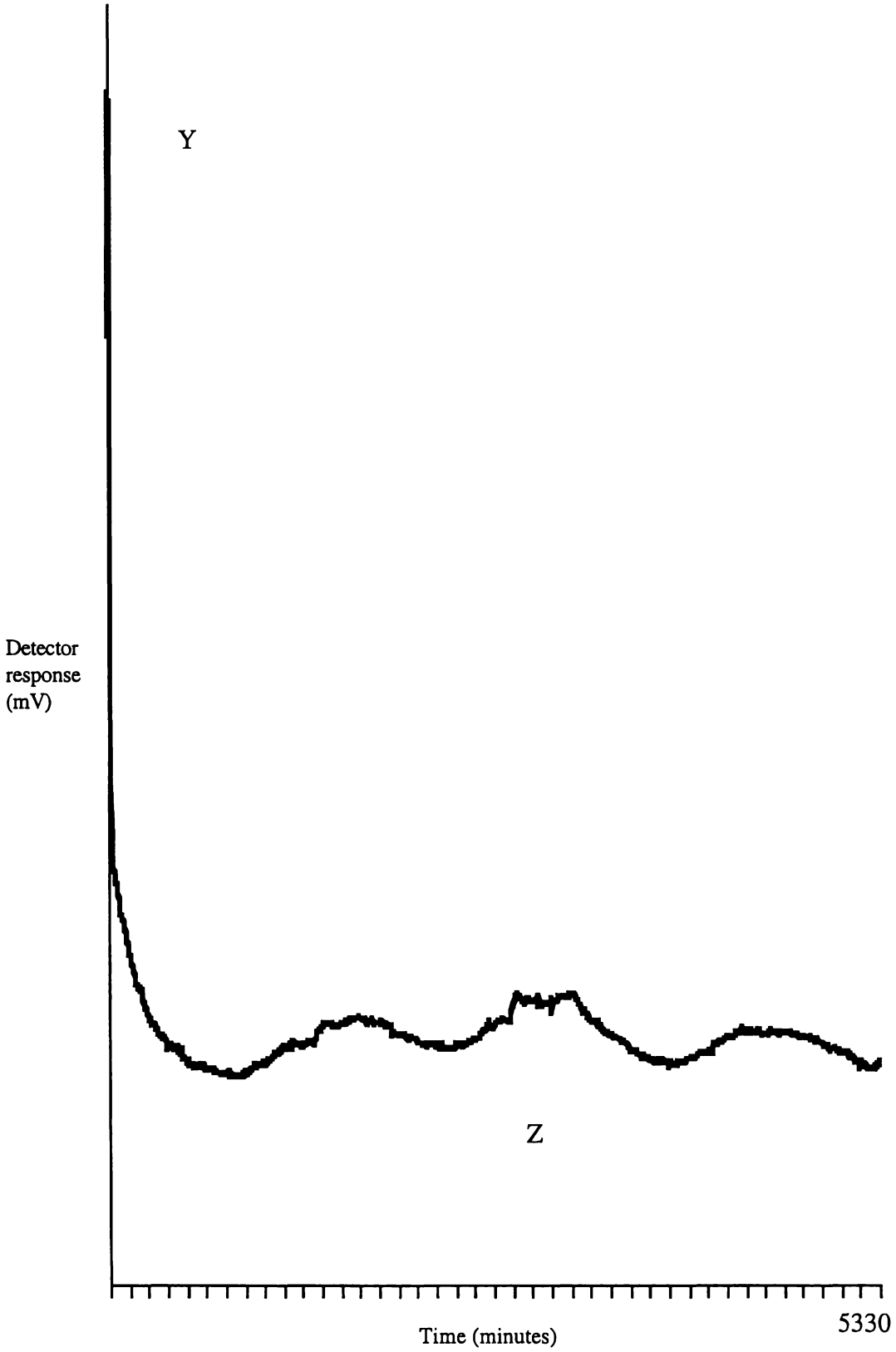

Figure 5·37 Prolonged testing of coprecipitate B

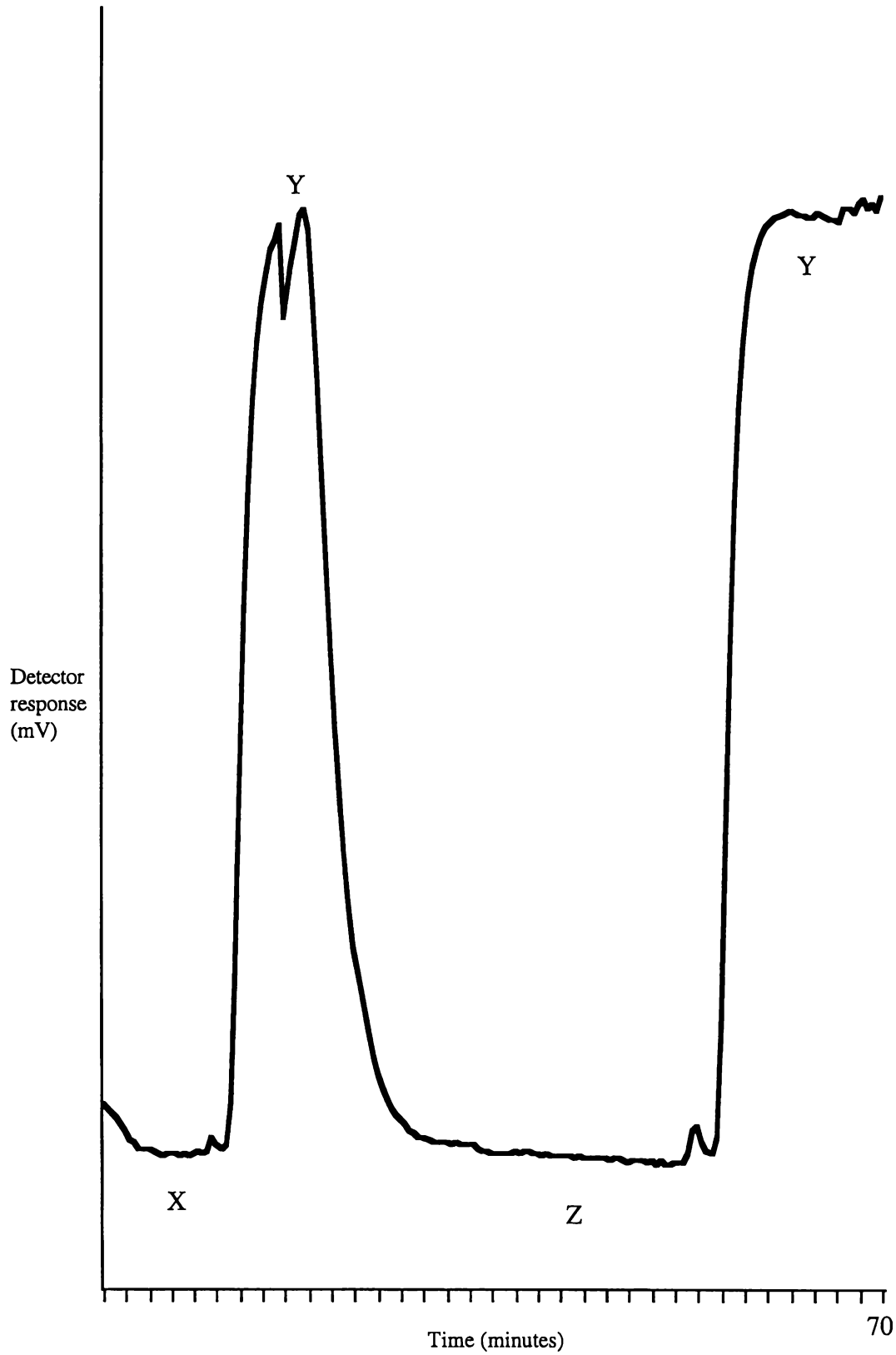

Figure 5·38 Active CO oxidation over gold-sputtered Fe_2O_3

5·5·6 $(Ph_3P)AuCl$, $(Bu^tNC)AuCl$ and $(Ph_3P)AuMe$ precursor materials

None of the samples prepared by using $(Ph_3P)AuCl$, $(Ph_3P)AuMe$ or $(Bu^tNC)AuCl$ (Figure 5·39) as precursors displayed activity for CO oxidation. Iwasawa and co-workers used $(Ph_3P)AuCl$ as a catalyst precursor;[242] they also found that this precursor resulted in inactive catalysts.

The lack of activity when using $(Ph_3P)AuCl$ or $(Bu^tNC)AuCl$ may have been a result of chloride being present on the surface of the gold particles. A sample of [$(Bu^tNC)AuCl$/MeCOMe/FeO(OH)/300] was heated again at 300 °C for one hour in a gas flow of 2% H_2/98% N_2. The intention of this was to remove any chloride that was present on the catalyst. STA of $(Bu^tNC)AuCl$ under reducing conditions (see Figure 5·13) indicated that this pre-treatment would be suitable for this purpose. However, it did not improve the activity of this material for CO oxidation.

It was assumed that no chloride remained after this reducing pre-treatment. The lack of activity was attributed to the size of the gold particles being too large or the gold-support interface lacking a particular feature present in, for example, the coprecipitation catalysts. The reducing pre-treatment may have had a detrimental effect on the oxidising support. It has been noted previously that oxidising pre-treatments of supported gold oxidation catalysts result in superior activity.[16]

5·5·7 $(Bu^tNC)AuNO_3$ precursor materials

A material prepared by using $Fe(OH)_3$ and a CH_2Cl_2 solution of $(Bu^tNC)AuNO_3$ exhibited no activity for CO oxidation (Figure 5·40). A material prepared by using Fe_2O_3 and a MeCOMe solution of $(Bu^tNC)AuNO_3$ also exhibited no activity for CO oxidation (Figure 5·41).

The materials prepared by using $Fe(OH)_3$ and MeCOMe or MeOH solutions of $(Bu^tNC)AuNO_3$ exhibited activity for CO oxidation (Figures 5·42 and 5·43 respectively). Consistent with previous results,[232] it was shown that the activity was not affected by moisture. For comparative purpose, [$(Bu^tNC)AuCl$/MeCOMe/$Fe(OH)_3$/300] was prepared and found to have no activity for CO oxidation (Figure 5·44). These results were consistent with those of Iwasawa and co-workers.[242]

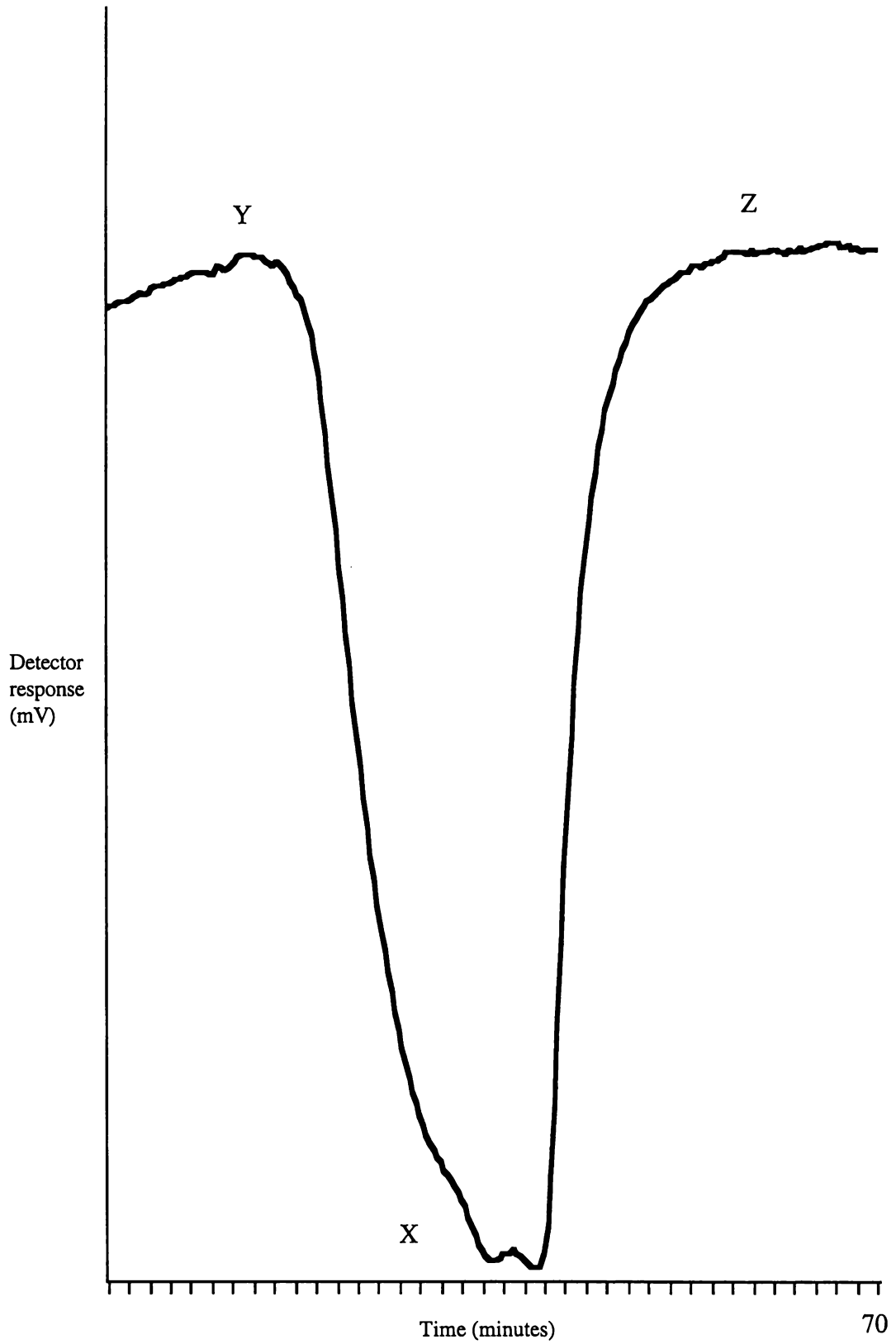

Figure 5·39 Testing of [(Bu^{t}NC)AuCl/MeCOMe/FeO(OH)/300]

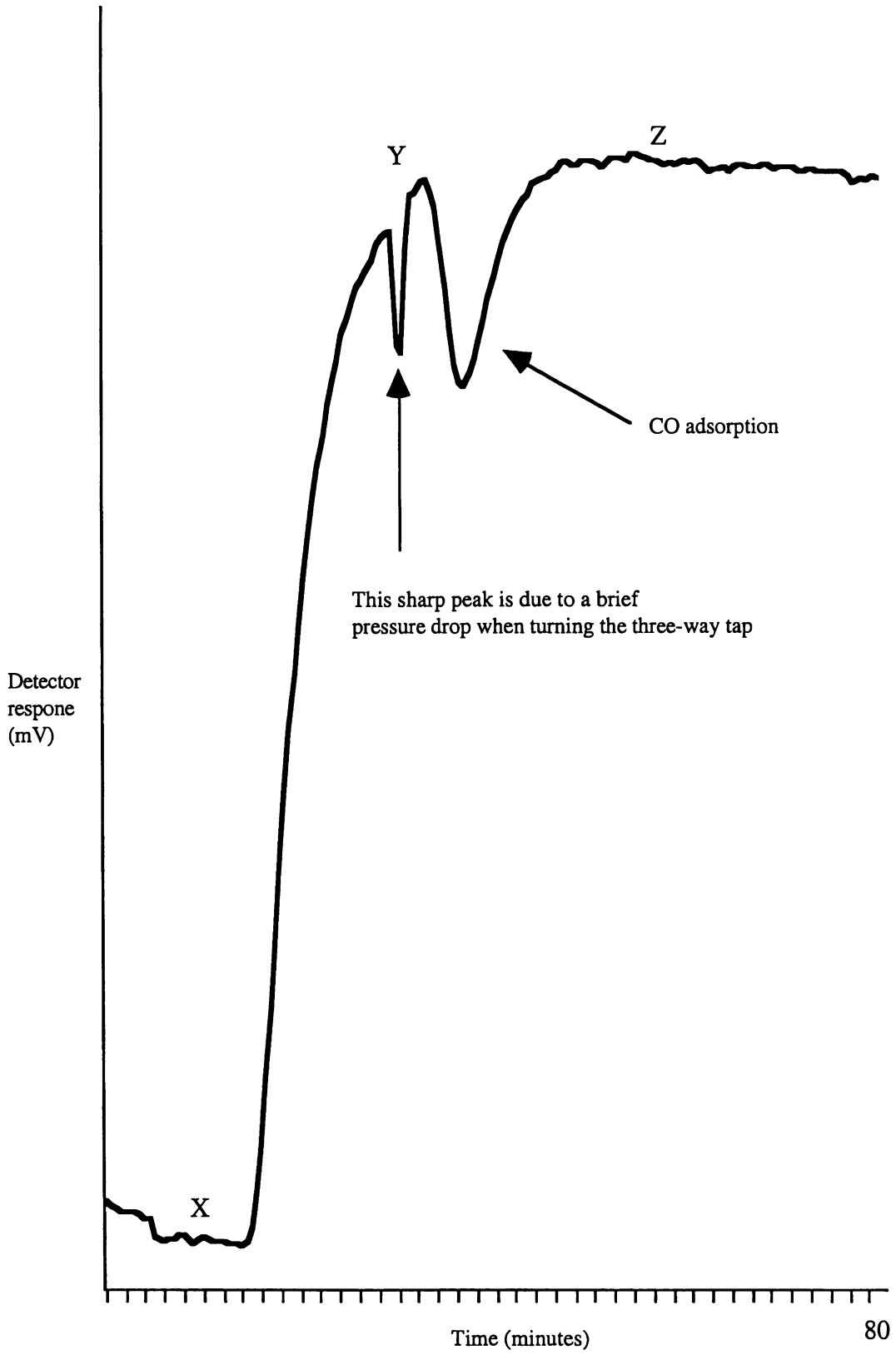

Figure 5·40 Testing of [(Bu^{t}NC)AuNO$_3$/CH$_2$Cl$_2$/Fe(OH)$_3$/300]

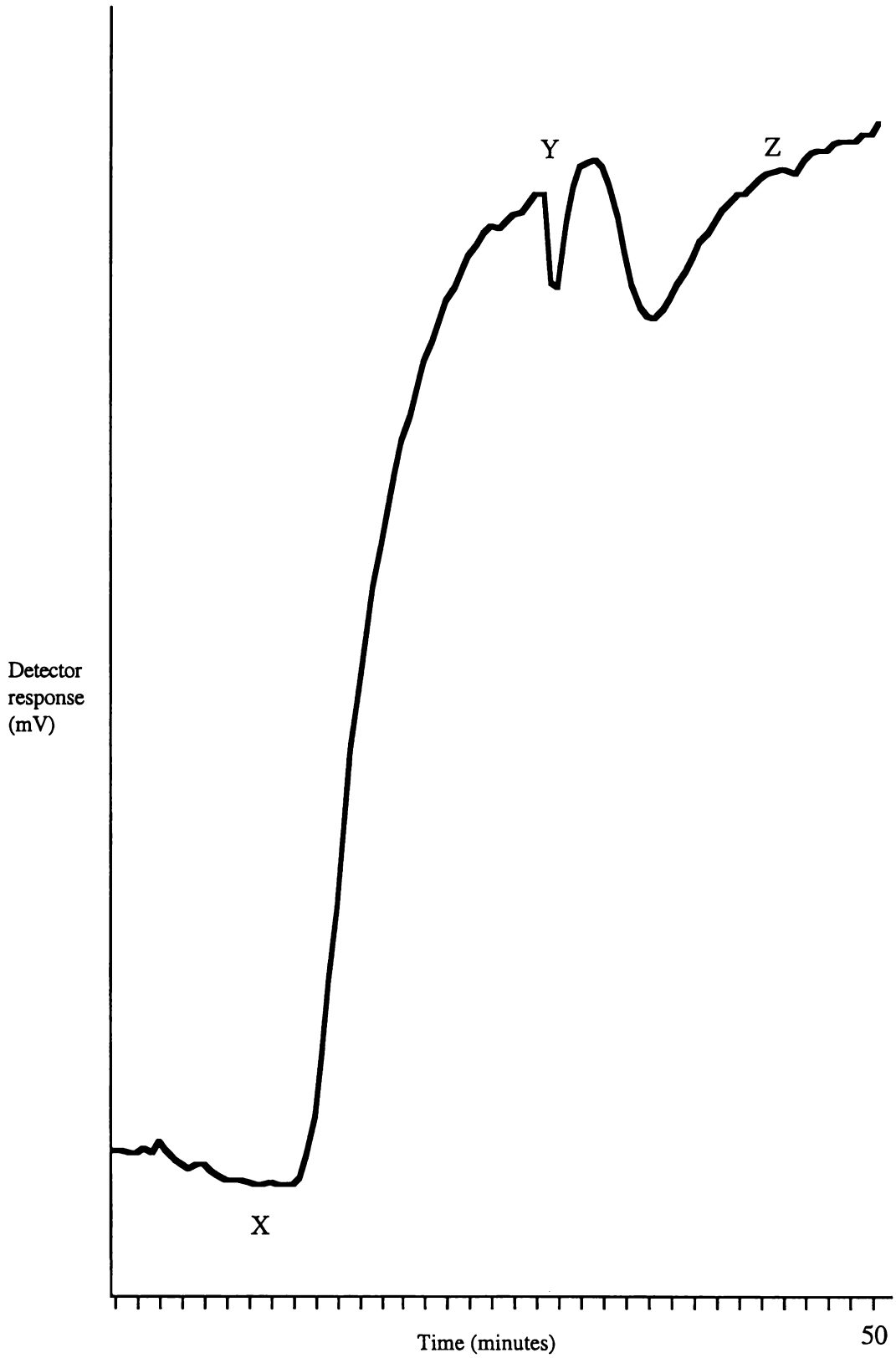

Figure 5·41 Testing of [(Bu^{t}NC)AuNO$_3$/MeCOMe/Fe$_2$O$_3$/300]

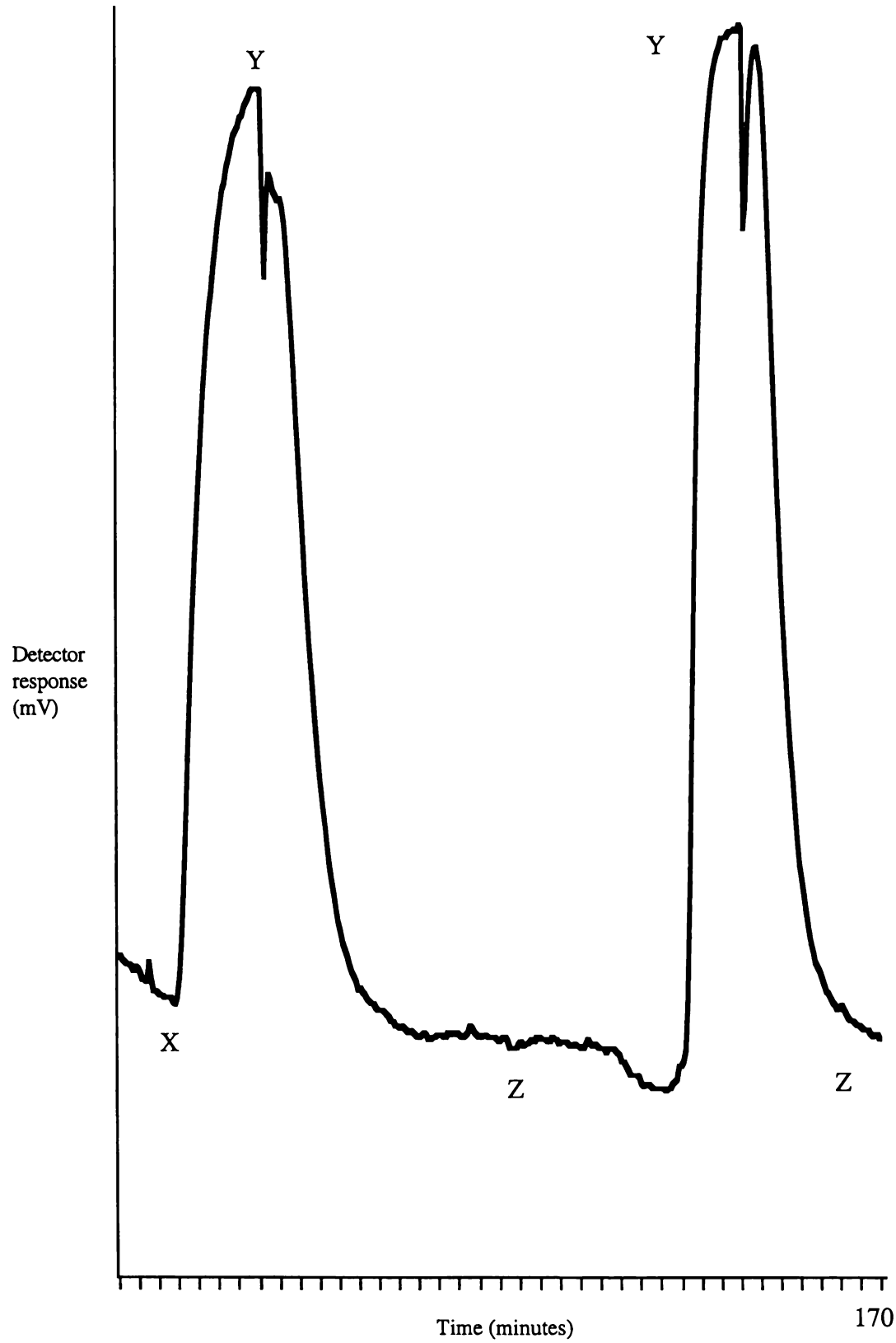

Figure 5·42 [(Bu^{t}NC)AuNO$_3$/MeCOMe/Fe(OH)$_3$/300]

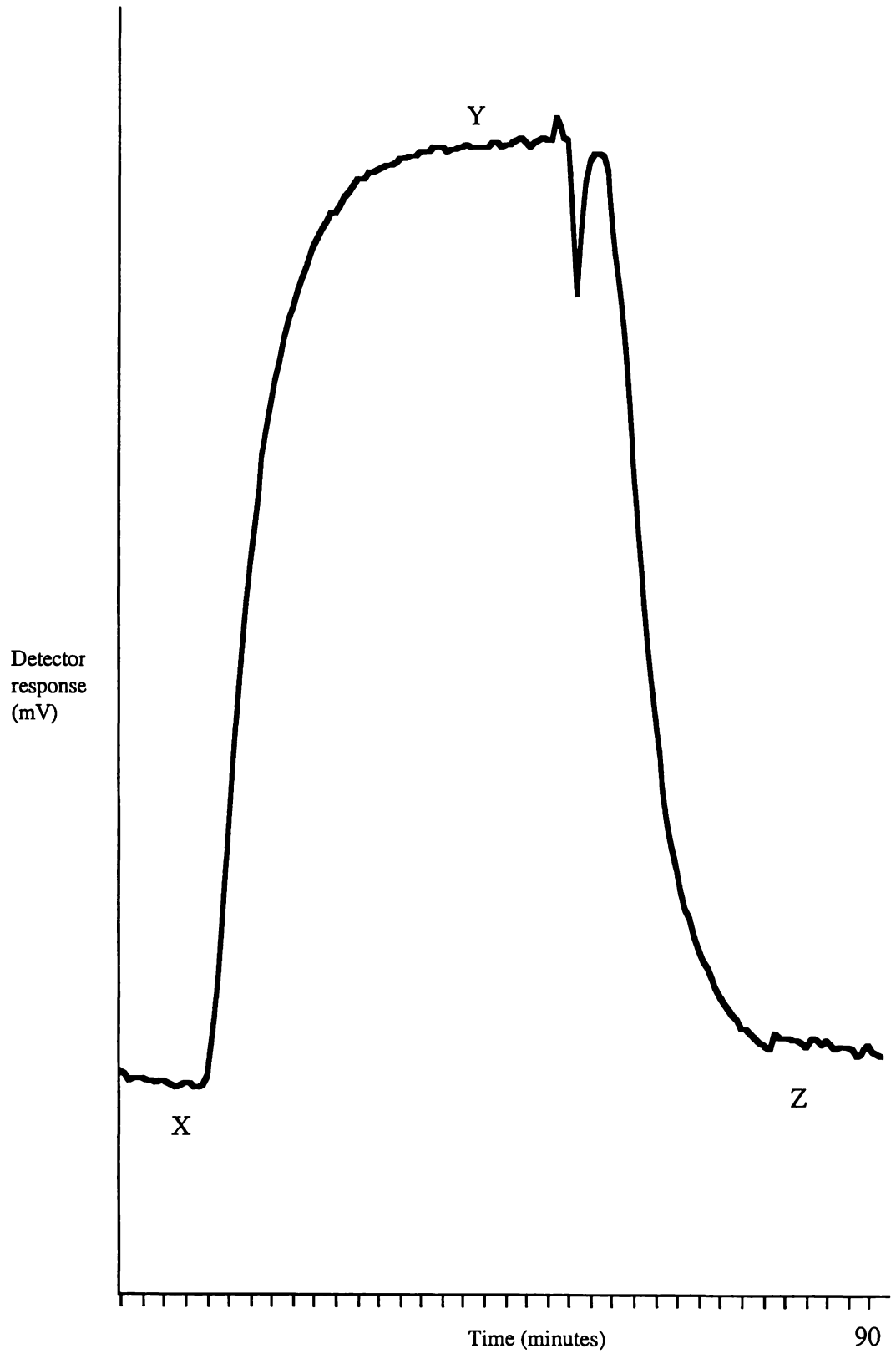

Figure 5·43 [(Bu^{t}NC)AuNO$_3$/MeOH/Fe(OH)$_3$/300]

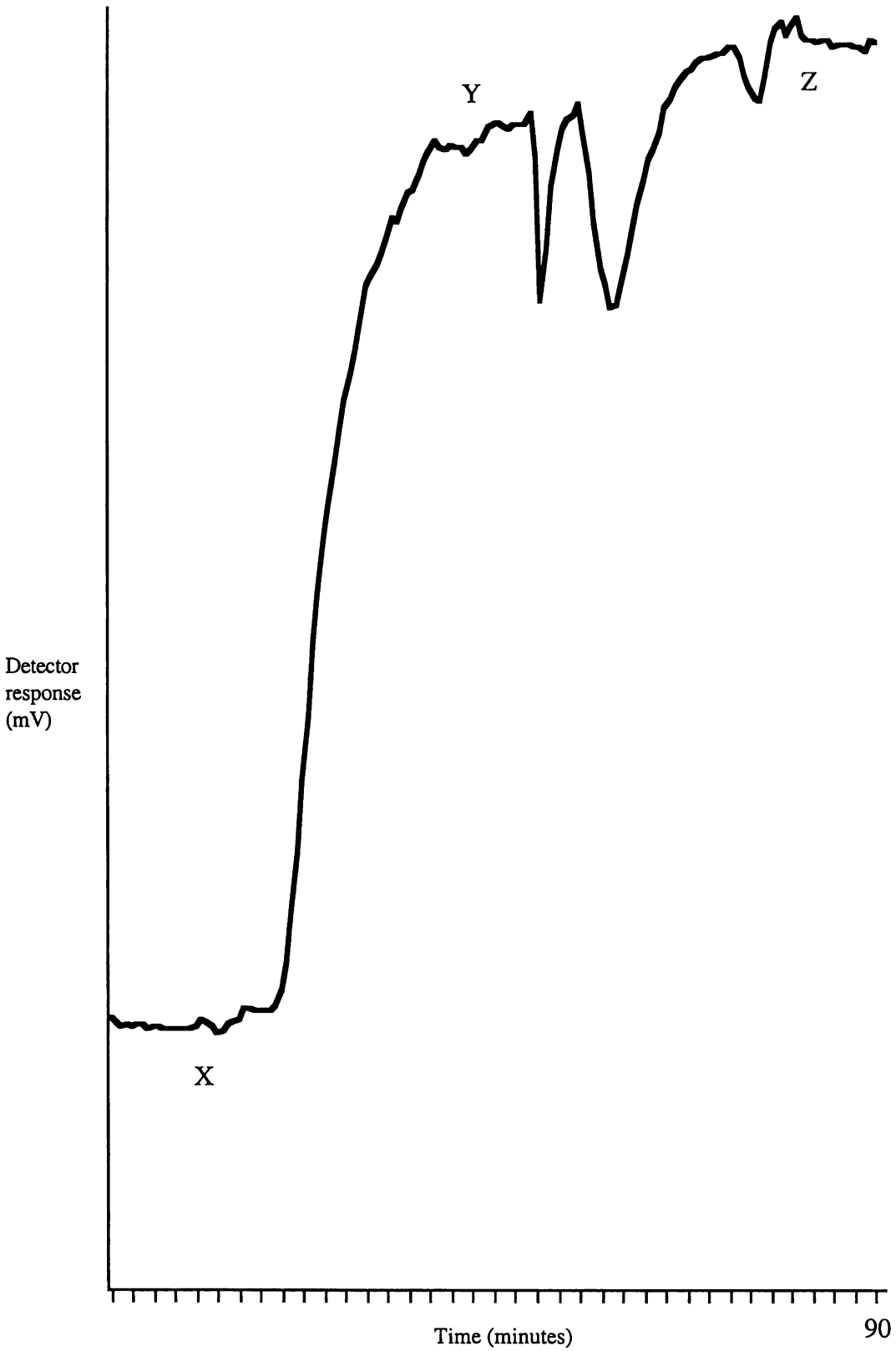

Figure 5·44 [(Bu^{t}NC)AuCl/MeCOMe/Fe(OH)$_3$/300]

5·6 QUANTITATIVE ANALYSIS

This section describes an initial quantifying study of the SnO_2-fuel cell CO detector response. This was carried out to ascertain the potential of the testing apparatus (see Figure 5·33) for kinetic study of the CO oxidation reaction.

5·6·1 Detector calibration

A SnO_2-fuel cell CO detector was selected for calibration. The calibration was achieved by passing a CO-in-air gas mixture through the by-pass at different flow rates. The gas mixture used was (on a mol/mol basis) 5·1% ± 0·1 CO and 20·6% ± 0·2 oxygen with a balance of nitrogen.§

Two separate calibrations were carried out. The flow meter that was positioned before the detector was different for each. During the first calibration, the flow rate was measured directly and a mV vs time trace was produced (Figure 5·45). The second calibration was carried out three months later with a calibrated-scale flow meter. On this occasion numerical mV data was obtained directly from the detector (Table 5·2), rather than displayed as a trace of detector response vs time.

Table 5·2 Detector response for the second calibration

Scale reading	Actual flow ($cm^3\ hr^{-1}$)	Detector response (mV)
10	60	7.1
20	96	7.8
30	144	8.9
40	192	9.8
50	246	11.0
60	312	12.1

§ This was prepared by BOC Gases Limited, Wellington.

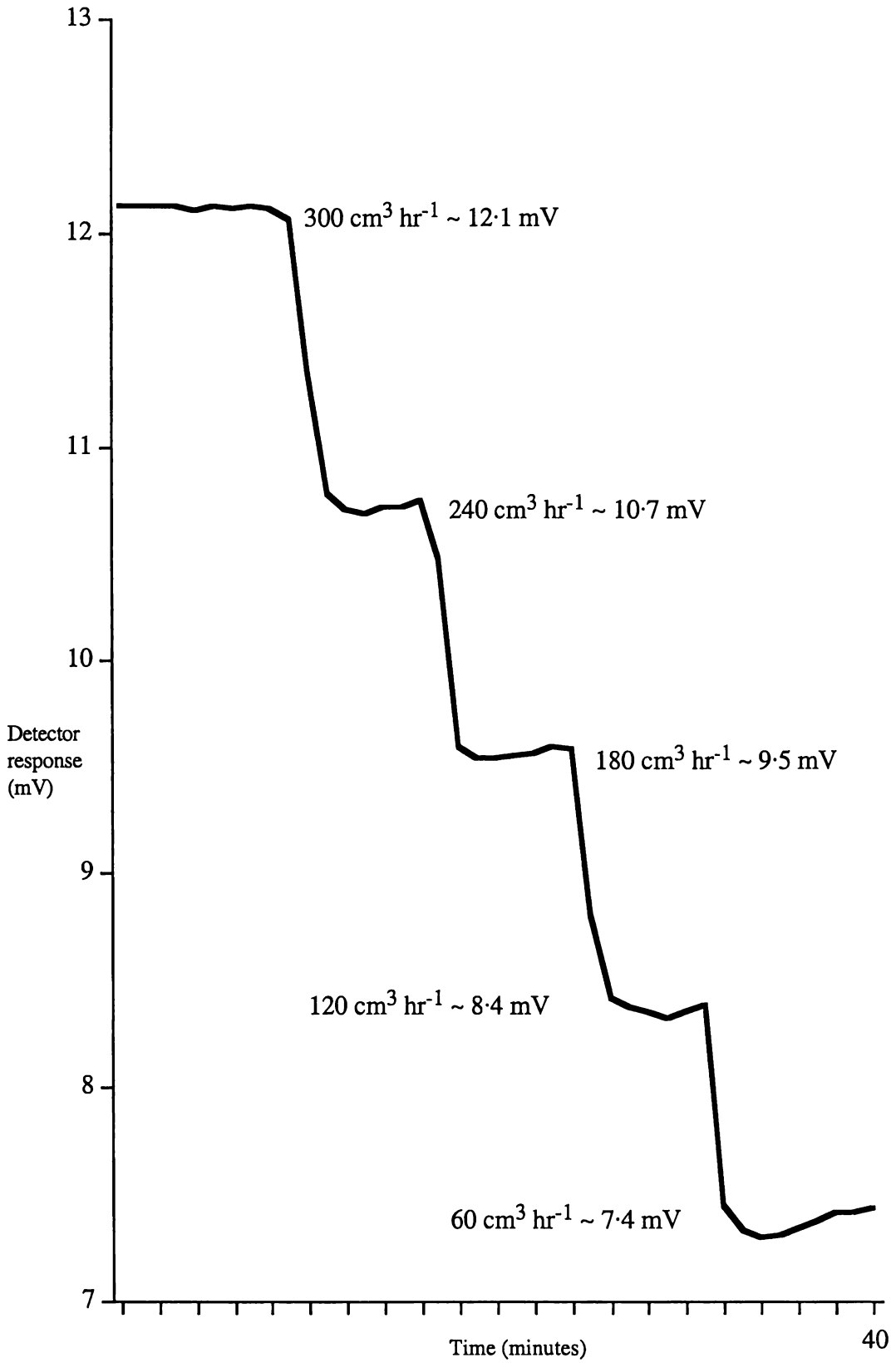

Figure 5·45 Detector response for the first calibration

The graphs of detector response (mV) vs flow rate ($cm^3\ hr^{-1}$) for both the first (1) and second (2) calibrations are displayed in Figure 5·46. The calibrations are superimposed indicating that the response of the detector was reproducible. Furthermore, the detector response was linear over the tested range.

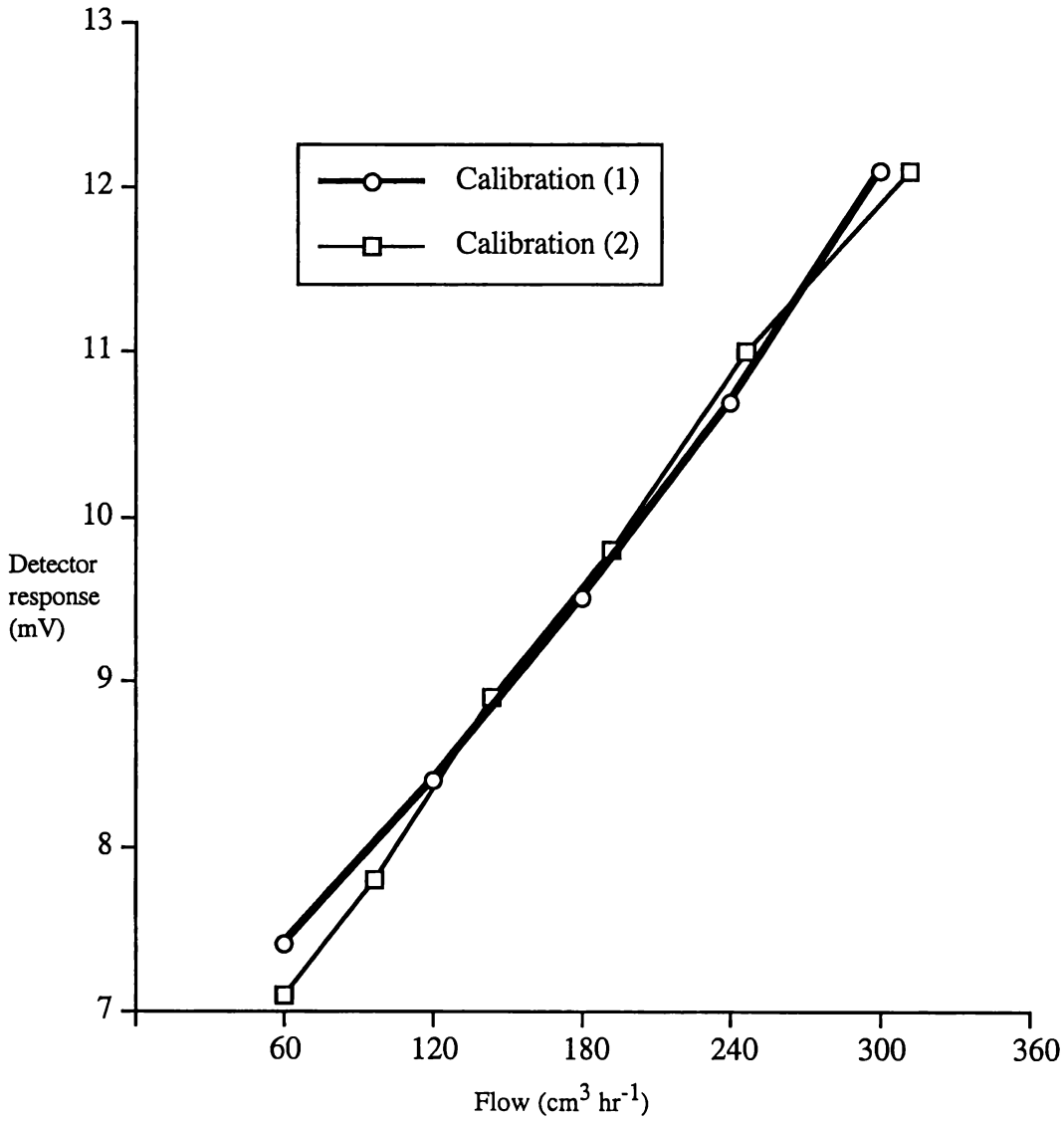

Figure 5·46 Detector response as a function of flow rate

5·6·2 [(Bu^{t}NC)AuNO$_3$/MeCOMe/Fe(OH)$_3$/300]

At the various flow rates used in the second calibration, the ~5% CO-in-air gas mixture was passed through two different weights of the catalyst [(Bu^{t}NC)AuNO$_3$ /MeCOMe/Fe(OH)$_3$/300]. The resulting detector responses are listed in Table 5·3 and are graphically depicted in Figure 5·47.

Table 5·3 Detector responses (mV) for separate weights of catalyst

Flow (cm^3 hr^{-1})	21 mg	6 mg
60	5·0	5.9
96	5·4	6.8
144	5·9	7.6
192	6.3	8.4
246	6.9	9.1
312	8.0	9.9

The detector responses for 6 mg of catalyst are in between those of calibration (2) and those obtained for 21 mg of catalyst (Figure 5·47). This was predictable and provides further evidence for the reliability of the detector response. A curious feature of the linear plots is that they slightly diverge over the tested range. Presumably, they would converge at a sufficiently high flow.

Overall, the results of the detector calibration were encouraging in that the response of the detector appeared to be proportional to the quantity of CO. Future kinetic study of CO oxidation catalysis, using this apparatus, will require further calibrations. These should include the baseline responses for air (in the absence of CO) and the responses for various CO-in-air mixtures at the flow rates of interest.

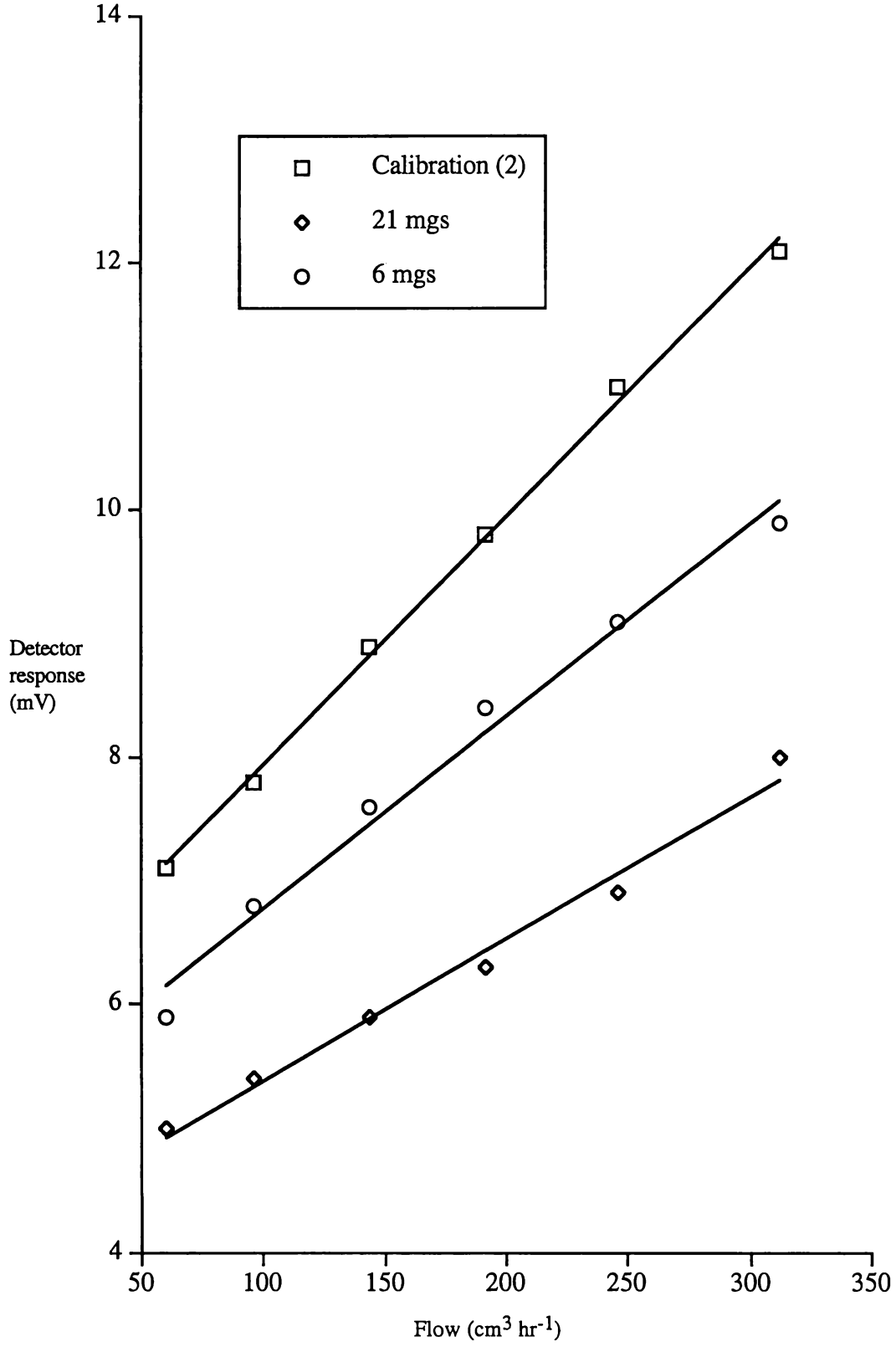

Figure 5·47 Detector responses for separate weights of catalyst

5·7 SYNTHESIS OF GOLD COMPLEX PRECURSORS

The preparation of (Bu^tNC)AuCl and (Bu^tNC)$AuNO_3$ complexes is described in section 3·1. Sub-sections 5·7·3 and 5·7·4 describe the attempted synthesis of gold complexes that were intended to be used as catalyst precursors.

5·7·1 $(Ph_3P)AuCl$

$$HAuCl_4 + 2Ph_3P \rightarrow (Ph_3P)AuCl + Ph_3PO + 3HCl$$

Ph_3P (2·31 g, 8·8 mmol) was dissolved in EtOH (50 cm^3). To this stirred solution was added dropwise $HAuCl_4.3H_2O$ (1·72 g, 4·4 mmol) in EtOH (10 cm^3).[253] The resulting white precipitate was stirred as a slurry for 15 minutes before being collected on a fritted glass filter and washed with two 5 cm^3 portions of EtOH. The solid was dried under vacuum affording microcrystalline (Ph_3P)AuCl (1·79 g, 83%).

5·7·2 $(Ph_3P)AuMe$

$$MeMgI + Ph_3PAuCl \rightarrow (Ph_3P)AuMe + IMgCl$$

MeMgI was prepared in 15 cm^3 of ether from magnesium (1·0 g, 43 mmol) and MeI (2·5 cm^3, 40 mmol). To this was added dropwise a suspension of (Ph_3P)AuCl (3·00 g, 6·06 mmol) in ether (25 cm^3) under argon at 0 °C. The reaction mixture was refluxed for an hour and then added to 100 cm^3 of ice-cooled 0·5% H_2SO_4. Ether was added (20 cm^3) and the mixture was filtered. The solid residue was extracted three times with 20 cm^3 portions of C_6H_6. The ether layer and the C_6H_6 extracts were combined and washed with H_2O. The organic layer was dried with Mg_2SO_4, filtered into a 250 cm^3 flask and evaporated under vacuum to ~50 cm^3. 150 cm^3 of petroleum spirits (30-40 °C) was added and the sealed flask was chilled at -25 °C for 8 hours. This provided thin needles of crystalline (Ph_3P)AuMe (2·11 g, 73%). M.p. 169 °C (lit.[254] 173 °C).

---

[253] M. I. Bruce, B. K. Nicholson and O. B. Shawkataly, *Inorg. Synth.*, 1989, **26**, 324.
[254] B. J. Gregory and C. K. Ingold, *J. Chem. Soc. B*, 1969, 276.

5·7·3 (Bu^{t}NC)Au(acac)

An attempt was made to synthesis the compound (Bu^{t}NC)Au(acac) because it had potential as a catalyst precursor. It became apparent that (Bu^{t}NC)Au(acac) was prone to decomposition. This sub-section focuses on an attempt to identify the complex in solution by low-temperature NMR.

Preparation of Tl(acac)

Tl_2CO_3 (5 g, 0·01 mol) was mixed with acetylacetone (20 cm^3) in C_6H_6 (40 cm^3). The mixture was refluxed for 12 hours. When the solution cooled, crystals formed which were collected on a fritted glass filter. Recrystallisation from boiling EtOH providing colourless Tl(acac) (4·8 g, 80%) M.p. 162 °C (lit.[255] 161 °C).

Preparation and NMR of (Bu^{t}NC)Au(acac)

The synthesis of (Bu^{t}NC)Au(acac) was adapted from the preparation of (Ph_3P)Au(acac).[256]

$$\textbf{(Bu}^t\textbf{NC)AuCl + Tl(acac)} \rightarrow \textbf{(Bu}^t\textbf{NC)Au(acac) + TlCl (s)}$$

An argon-flushed Schlenk flask containing Tl(acac) (116 mg, 0·4 mmol) in dry $CDCl_3$ (15 cm^3) was fitted with a self-pressurising dropping funnel and a magnetic stirring bar. The flask was covered with tin foil to exclude light and chilled to -45 °C; these conditions were maintained throughout the reaction. Added dropwise was (Bu^{t}NC)AuCl (120 mg, 0·4 mmol) dissolved in dry $CDCl_3$ (5 cm^3). After addition was complete the mixture was stirred for 3 hours. The volume was then reduced under vacuum to ~5 cm^3.

An appropriate volume of the reaction solution was filtered under vacuum into a NMR tube,§ the temperature of which was held at -196 °C. The NMR tube was sealed and allowed to warm to -30 °C at which temperature NMR analysis was carried out. After the analysis the NMR tube was left overnight under ambient conditions. This resulted in a coherent film of metallic gold forming on the interior.

---

[255] E. C. Taylor, G. H. Hawks and A. McKillop, *J. Am. Chem. Soc.*, 1968, **90**, 2421.
[256] D. Gibson, B. F. G. Johnson. and J. Lewis, *J. Chem. Soc. A*, 1970, **3**, 367.
§ A Quik-Fit™ socket had been attached to the NMR tube.

Spin-spin coupling to ^{14}N and the ^{13}C chemical shift for $Bu^tN\underline{C}$ were not resolved but observed ^1H and ^{13}C chemical shifts (Table 5·4) could be assigned[103] to the proposed structure (Figure 5·48) of (Bu^tNC)Au(acac).

Table 5·4 NMR Data for (Bu^tNC)Au(acac)

	^{13}C (δ)		^1H (δ)
C(1)	29·7	C(1)**H**$_3$	1·55
C(6)	31·6	C(6)**H**$_3$	2·28
C(2)	58·9	C(4)**H**	4·35
C(4)	69·5		
C(3)	-		
C(5)	204·6		

Figure 5·48 provides the numbering scheme

The spectra were collected at -30 °C

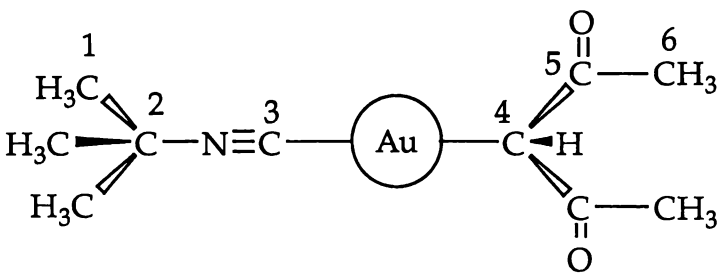

Figure 5·48 Proposed structure of (Bu^tNC)Au(acac)

The NMR results of (Bu^tNC)Au-acac encouraged several attempts to obtain a crystalline product. These were hindered by excessive decomposition. Tl(acac) was also reacted with (XyNC)AuCl but this resulted in immediate decomposition even at -45 °C. It was also noted during the synthesis of the (RNC)$AuNO_3$ (R = Bu^t, Et or Xy) complexes that the aromatic Xy homologue was less stable (Chapter Three).

A concurrent attempt to isolate crystalline (Bu^tNC)Au(acac) was reported recently.[110] In this case a decomposition-prone oil was produced from which crystals could not be obtained.

5·7·4 $(Me_2AuOH)_4$

The gold(III) complex $(Me_2AuOH)_4$ was identified as having excellent potential as a catalyst precursor. The structure of this complex is illustrated in Figure 5·49 and features a tetrameric ring with bridging hydroxide groups.[257] As a catalyst precursor, $(Me_2AuOH)_4$ would have affinity for an oxide surface and thermolysis would presumably release ethane and H_2O. It was reported to be synthesised in high yield from $(Me_2AuI)_2$.[258]

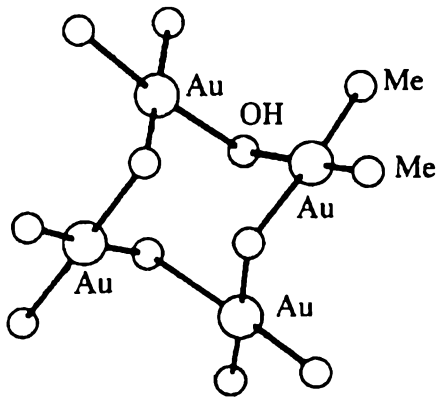

Figure 5·49 Structure of $(Me_2AuOH)_4$

Unfortunately, the appraisal of $(Me_2AuOH)_4$ as a catalyst precursor was not possible because of difficulties in preparing $(Me_2AuX)_2$ (X = Cl or I). The original preparation of $(Me_2AuI)_2$ involved a low-yielding reaction of (pyridine)$AuCl_3$ and MeMgI.[259] This reaction was attempted twice with no success.

An 'improved' synthesis of $(Me_2AuCl)_2$ was recently reported.[260] The homogeneous reaction of $SnMe_4$ with $[AuCl_4]^-$ (in MeOH at -50 °C) was quoted as giving reproducible yields of 40-45%, with by-products of metallic gold and Me_3SnCl.

$SnMe_4$ was prepared by the addition of MeMgI to $SnCl_4$ in di-butyl ether.[261] ^1H NMR confirmed the purity of the $SnMe_4$ product which was distilled directly from the di-butyl ether at 77-78 °C. Four attempts were made to react $SnMe_4$ with $[AuCl_4]^-$ as described.[260] In each case, only metallic gold and Me_3SnCl were isolated.

---

257 G. E. Glass, J. H. Konnert, M. G. Miles, D. Britton and R. S. Tobias, *J. Am. Chem. Soc.*, 1968, **90**, 1131.
258 M. G. Miles, G. E. Glass and R. S. Tobias, *J. Am. Chem. Soc.*, 1966, **88**, 5738.
259 F. H. Brain and C. S. Gibson, *J. Chem. Soc.*, 1939, 762.
260 M. Paul and H. Schmidbaur, *Z. Naturforsch.*, 1994, **49b**, 647.
261 W. F. Edgell and C. H. Ward, *J. Am. Chem. Soc.*, 1954, **76**, 1169.

CHAPTER SIX

CONCLUSIONS

6·1 AURIOPHILIC LAuX COMPLEXES

The crystal packing arrangements of linear LAuX (L = neutral ligand; X = mono-anionic ligand) complexes often exhibit close Au--Au contacts. This phenomenon has been termed auriophilicity.[8] The Au--Au contacts are indicative of energetically attractive interactions. The overall auriophilic energy (kJ mol^{-1}) is dependent on both the Au--Au contact distances and the number of interactions each gold(I) centre makes.

The Au--Au interactions are influenced by the steric and electronic properties of the coordinated ligands. The steric influence is prominent because the extent of the molecular aggregation is related to the size of the ligands. Large ligands may quench the attractions completely by physically precluding their formation, for example the molecular packing of $(Ph_3P)AuCl$ exhibits no Au--Au interactions. In contrast, the crystal structure of (MeNC)AuCN exhibits a gold sheet, in which each gold(I) centre is auriophilic six-coordinate. When the crystal structures of gold(I) molecules with ligands of moderate size are characterised, dimeric, oligomeric or polymeric chain aggregations are observed. As the extent of aggregation increases, the Au--Au distances also increase. This can be attributed to either:

(i) steric congestion of the ligands or,

(ii) intermolecular auriophilic bonding inherently weakening when dispersed over multiple gold(I) centres.

It is yet to be established how the coordinated ligands electronically influence Au--Au interactions. The polarisability of the ligands will influence the electron density on the gold(I) centres, conceivably altering their propensity to form attractive interactions. Thus, ligands may electronically 'tune' the gold(I) centres to possess a particular 'attractiveness' to other gold(I) centres. The ability of the inherent attraction to act is then controlled by the steric bulk of the ligands.

Pyykkö has provided theoretical evidence for the electronic effect of the coordinated anion on the Au--Au interaction.[59] These calculations were based primarily on hypothetical crossed dimers. The results indicated that the strength of the Au--Au attraction increases with polarisability, therefore soft anions (such as iodide) should promote shorter Au--Au interactions.

The best experimental evidence for the electronic influence of the anion is procured from series of LAuX complexes, in which L remains constant. These are particularly useful if isostructural packing arrangements are characterised. The differences in the Au--Au distances can then be attributed with more certainty to the different electronic properties of the various anions.

Complications can arise when attempting to quantify the electronic influence of the anion, even if isostructural LAuX aggregations are compared. This is because Au--Au interactions do not completely control the molecular packing, indeed the Au--Au contacts may be influenced by subtle ligand interactions. As an example, there is potential for interaction between the anion and the adjacent neutral ligand in anti-parallel aggregations of linear LAuX complexes. These additional interactions could be attractive (for example, hydrogen bonding) but repulsions are also possible.

The structures of a series of $(Me_2PhP)AuX$ dimers (X = Cl, Br or I) are described in Chapter Two. The observed Au--Au contact distances provided supportive evidence for the theory of Pyykkö. However, comparing the Au--Au distances in two (1,3,5-triaza-7-phosphaadamantane)AuX (X = Cl or Br) dimers was less conclusive and the series of $(Me_3P)AuX$ (X = Cl, Br or CN) appeared to contradict the theory.

Comparative series of (RNC)AuX supramolecular structures (X = Cl, Br or I) are also described. Polymeric structures were typically characterised for the chloride and bromide examples. The large iodide ion appeared to be unfavoured in polymeric structures, which is proposed to be a result of repulsive contact between the isonitrile C≡N bond and the iodide ligand.

6·2 (RNC)AuX COMPLEXES

The chemistry of gold is characterised by the stability of the metallic form. However, a large number of coordination complexes have been routinely prepared and isolated. The (RNC)AuCl complexes prepared in this project are typical examples, incorporating two ligands with a relatively strong affinity for gold(I).

The gold(I) cation is a soft ion and substitution reactions of gold(I) complexes are characterised by the replacement of a ligand with one of greater polarisability. The opposite can only be achieved by using a driving force. This is exemplified by the syntheses of (RNC)$AuNO_3$ complexes, which involves the precipitation of AgCl from a homogeneous reaction of (RNC)AuCl and $AgNO_3$. The (RNC)$AuNO_3$ complexes were characterised unequivocally in this project by elemental analysis, IR, NMR and X-ray crystallography.

Complexes containing ligands for which gold has little affinity are generally prone to decomposition back to the metallic state. This was illustrated by the (RNC)$AuNO_3$ complexes, which belong to the rare set of compounds containing a weak oxygen-gold(I) bond. They are the first gold(I) complexes to be characterised exhibiting both a gold-oxygen and gold-carbon bond.

It can be envisaged that novel molecular packing structures will be observed when complexes are prepared with new combinations of L and X ligands. The nitrate anion is asymmetric (when coordinated as an η^1-mono-dentate ligand) and non-polarisable. It is therefore dissimilar from the majority of anions characterised in LAuX complexes, such as the halides or CN. The molecular packing of a set of (RNC)AuX (R = Bu^t, Et or Xy; X = Cl or NO_3) complexes is described in Chapter Three. The supramolecular architecture was based on Au--Au interactions although graphitic π-π interactions were also apparent when R = Xy. The five auriophilic structures characterised in this project are depicted in Figure 6·1. Each of the characterised auriophilic motifs was rationalised in terms of ligand influences.

A crystal of $[(XyNC)_2Au]NO_3$ was selected from one recrystallisation of (XyNC)$AuNO_3$ and characterised. The structure is based on *infinite* π-π stacking. This is common for aromatic hydrocarbons, but appears to have little precedent in organometallic chemistry.

The complexes (EtNC)AuCl [Figure 6·1 (1)] and (Bu^tNC)$AuNO_3$ (2) both crystallised as zig-zag chains. The Au--Au contact distances observed in the polymeric (Bu^tNC)$AuNO_3$ chain were relatively short. The concertinaed chain structure of (EtNC)$AuNO_3$ (3) exhibited more extensive Au--Au interactions, with each gold centre auriophilic three-coordinate. The (EtNC)$AuNO_3$ structure forms appropriate comparison with both the (EtNC)AuCl and (Bu^tNC)$AuNO_3$ structures, based on the influence of the anion and isonitrile ligand respectively. The crystal structure of (XyNC)AuCl (4) exhibited a short-chain tetrameric aggregate. Monomers of (XyNC)$AuNO_3$ (5) formed a compressed chain structure with each gold centre potentially auriophilic four-coordinate.

These results show that the asymmetric, non-polarisable nitrate anion enhances the auriophilic interaction for (RNC)AuX (X = Cl or NO_3) species. Whether this should be attributed to the nitrate anion promoting the inherent Au--Au attraction (which is contrary to Pyykkö's theoretical calculations), or to lesser repulsion between adjacent ligands, cannot be unequivocally stated from these examples.

Some understanding of the factors involved in the formation of these auriophilic structures is provided by the following observations and conclusions (the details of which are in Chapter Three):

(i) (Bu^tNC)AuX (X = Cl, Br, CN or NO_3) complexes all crystallise as isostructural zig-zag chains. For X = NO_3, the anti-parallel Au--Au interactions were significantly shorter and the Au-Au-Au chain angle was relatively wide.

- The short Au--Au distance when X = NO_3 could be due to the nitrate anion being positioned so that steric congestion with the adjacent isonitrile is minimised. This was also apparent for the structures of (RNC)$AuNO_3$ (R = Et or Xy).

- Alternately, an electronic enhancement of the Au--Au interaction may occur when nitrate is coordinated.

- The theory of electronic enhancement is supported by the fact that anti-parallel Au--Au interactions for (RNC)AuX (X = Cl or Br) have been observed with distances less than those observed in the chain structures of (Bu^tNC)AuX (X = Cl or Br). Hence, the relatively long distances in (Bu^tNC)AuX (X = Cl or Br) do not appear to be restricted by adjacent ligand repulsions.

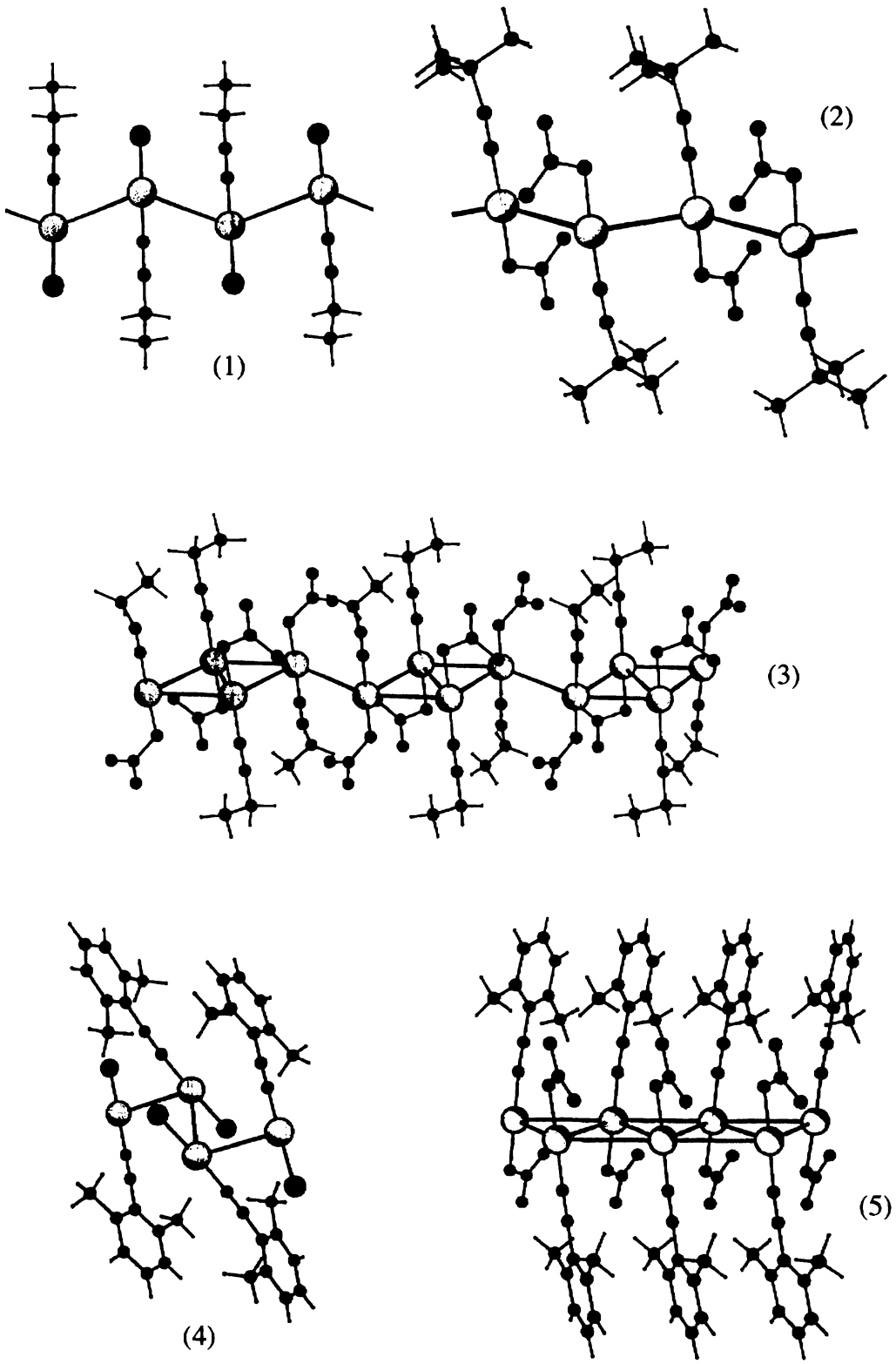

Figure 6·1 Auriophilic (RNC)AuX structures

- The wide chain angle in the crystal structure of (Bu^tNC)$AuNO_3$ may be due to interchain packing effects. It is unlikely to influence possible interactions between the anions and the adjacent isonitrile triple bonds.

(ii) The (EtNC)$AuNO_3$ structure exhibits extensive short Au--Au interactions, in comparison with the zig-zag chains of (Bu^tNC)$AuNO_3$ and (EtNC)AuCl.

- The difference between the crystal structure of (EtNC)$AuNO_3$ and that of (Bu^tNC)$AuNO_3$ is attributed to the smaller isonitrile permitting more Au--Au contacts.

- The comparison of (EtNC)$AuNO_3$ and (EtNC)AuCl indicates that the nitrate enhances the Au--Au interaction electronically. However, the crystal structure of (EtNC)$AuNO_3$ may not have been attainable for (EtNC)AuCl due to repulsion between the chloride anion and the adjacent C≡N bond.

(iii) The polymeric molecular packing of (XyNC)$AuNO_3$ exhibits extensive Au--Au contacts and infinite π-π stacking of Xy rings. The (XyNC)AuCl tetramers appear to be fragments from a broken polymeric chain, with the terminal molecules of the tetramers forming crossed-ligand Au--Au interactions.

- As for the (Bu^tNC)AuX and (EtNC)AuX comparative analogues, the nitrate enhances the Au--Au attraction, which appears best explained by an electronic effect. Again, this cannot be stated with certainty, as the observed structures may be a result of the subtle steric differences between the anions.

- The crossed-ligand interaction in the (XyNC)AuCl tetramer is not particularly short and is not restricted by adjacent ligand repulsion. This supports the nitrate effect being one of electronic enhancement.

- The positioning of the tetramers appears to be the result of both Xy--Xy graphitic and Au--Xy interactions between adjacent tetramers.

6·3 FUTURE DEVELOPMENT OF GOLD(I) CRYSTALLOGRAPHY

The key to understanding the phenomenon of auriophilicity is the ability to make rational comparisons between auriophilic structures with different ligands. Two appropriate examples are the zig-zag chain series of (Bu^tNC)AuX (X = Cl, Br, CN or NO_3) complexes and the helical chain series of (Me_3P)AuX (X = Cl, Br or CN). Both series would be enhanced by the structural characterisation of (Me_3P)$AuNO_3$ and (Bu^tNC)AuI.

To calculate the energy of Au--Au interactions, one must account for the auriophilic coordination number, the type of ligands present and the Au--Au distances. It could be predicted that more auriophilic energy is produced in polymers (where each gold centre is linked to two or more gold centres), compared with dimers which produce a single gold interaction. However, a single short interaction may be stronger (in terms of kJ mol^{-1}) than the Au--Au contacts in polymeric aggregations.

As the understanding of auriophilicity increases, the future challenge will be the prediction and design of auriophilic architecture. Given that the inherent Au--Au attraction is present, gold(I) monomers can be predicted to crystallise in such a fashion as to maximise Au--Au contacts in all directions. This is influenced by the size and electronic properties of the ligands. Other possible interactions between ligands, for example π-π stacking and hydrogen bonding, would also need to be accounted for in any successful crystal engineering procedure for LAuX complexes.

Some suggested synthetic and structural targets for the future are:

(i) (MeNC)$AuNO_3$

- (MeNC)AuCl crystallises as a zig-zag chain. In contrast, (MeNC)AuCN has been characterised as a sheet of gold(I) centres.

(ii) (OC)$AuNO_3$

- (OC)AuCl crystallises as a sheet. If (OC)$AuNO_3$ could be synthesised, the η^1-mono-dentate nitrate anion may incorporate into a sheet structure.

(iii) (EtNC)AuCN

- Based on the sheet structure of (MeNC)AuCN molecular packing and the interchain packing of (EtNC)AuCl, (EtNC)AuCN could potentially form a sheet.

(iv) A crossed ligand dimer of $LAuNO_3$

- If the nitrate influence is an electronic effect, a crossed dimer would have a particularly short intermolecular Au--Au contact. Using a relatively large neutral ligand may quench the inherent auriophilic attraction sufficiently to allow only one crossed ligand interaction to form. L would need to have a steric influence intermediate of that of Bu^tNC and Ph_3P. $(Bu^tNC)AuNO_3$ crystallises as a zig-zag chain. The $(Ph_3P)AuNO_3$ complex exhibits no Au--Au contacts in the solid-state.

(v) A hetero-nuclear intermolecular contact

- By carefully selecting the complexes there would be some potential to observe this unprecedented metallophilic interaction. As an example, $(Ph_3P)AuCl$ (which does not form Au--Au contacts) and a small HgX_2 complex may form an attractive intermolecular Au(I)--Hg(II) contact in the solid-state.

6·4 HETEROGENEOUS CO OXIDATION

Solid surfaces have potential as catalytic materials. Using CO oxidation as the classic example, it is unlikely that oxygen and CO will collide and react in the homogeneous gas phase. However, if CO and oxygen are chemisorbed and held adjacent to one another on a surface, the thermodynamically favoured CO oxidation reaction is likely to proceed. The oxidation of CO on surfaces is important, as it provides an excellent model for the study of processes that occur during surface chemisorption and catalysis.

One of the major problems associated with heterogeneous catalysis is the potential for surface poisoning. The poisoning may result from chemisorbed species that are not involved in the actual reaction. Alternately, one of the reactants in a bi-molecular surface reaction may cover the surface, which is termed reactant inhibition. A uniform catalyst surface, which presents only one type of chemisorption site, is prone to reaction inhibition during bi-molecular reactions because each of the reacting species has a different affinity for the surface.

CO oxidation on metal surfaces is unfavoured under ambient conditions. On platinum for example, the surface is prone to CO reactant inhibition. The reaction can be initiated by heat, which promotes CO desorption, hence allowing oxygen adsorption. In theory, there is more potential for CO oxidation on specific metallic surface defects and bimetallic materials because CO and oxygen contact is promoted.

Low temperature CO oxidation has been observed on dry metal oxide materials where CO coordinates weakly to surface cations and reacts with adjacent oxide ions. However, the activity of oxide catalysts is inhibited by traces of moisture. Recently, it has become apparent that CO can be effectively oxidised under ambient conditions over two-component catalysts, in which both reactants, CO and oxygen, are provided by different sources. The development of two-component catalysts for CO oxidation was primarily due to M. Haruta and co-workers,[16] who initially prepared active supported gold catalysts by heating coprecipitate materials.

Haruta's proposed mechanism indicated that the potential for reactant inhibition was eliminated on this form of catalyst. It is postulated that the reaction takes place at the gold/support interface, the mechanism involving weakly coordinated CO migrating across the tiny supported gold particles (Figure 6·2). Metallic gold has little affinity for oxygen or H_2O. The CO molecules come into contact with the oxidising support and are converted to carbon dioxide. The introduction of gaseous oxygen to the oxide support is not inhibited by the presence of CO. Similar results have been observed over calcined gold alloy materials.

It is apparent from these recent findings that metallic gold has potential as a catalytic material. The activity is dependent on the gold being highly dispersed and in intimate contact with an oxidising transition metal support. These structural features provide guidance to the development of novel preparative methods.

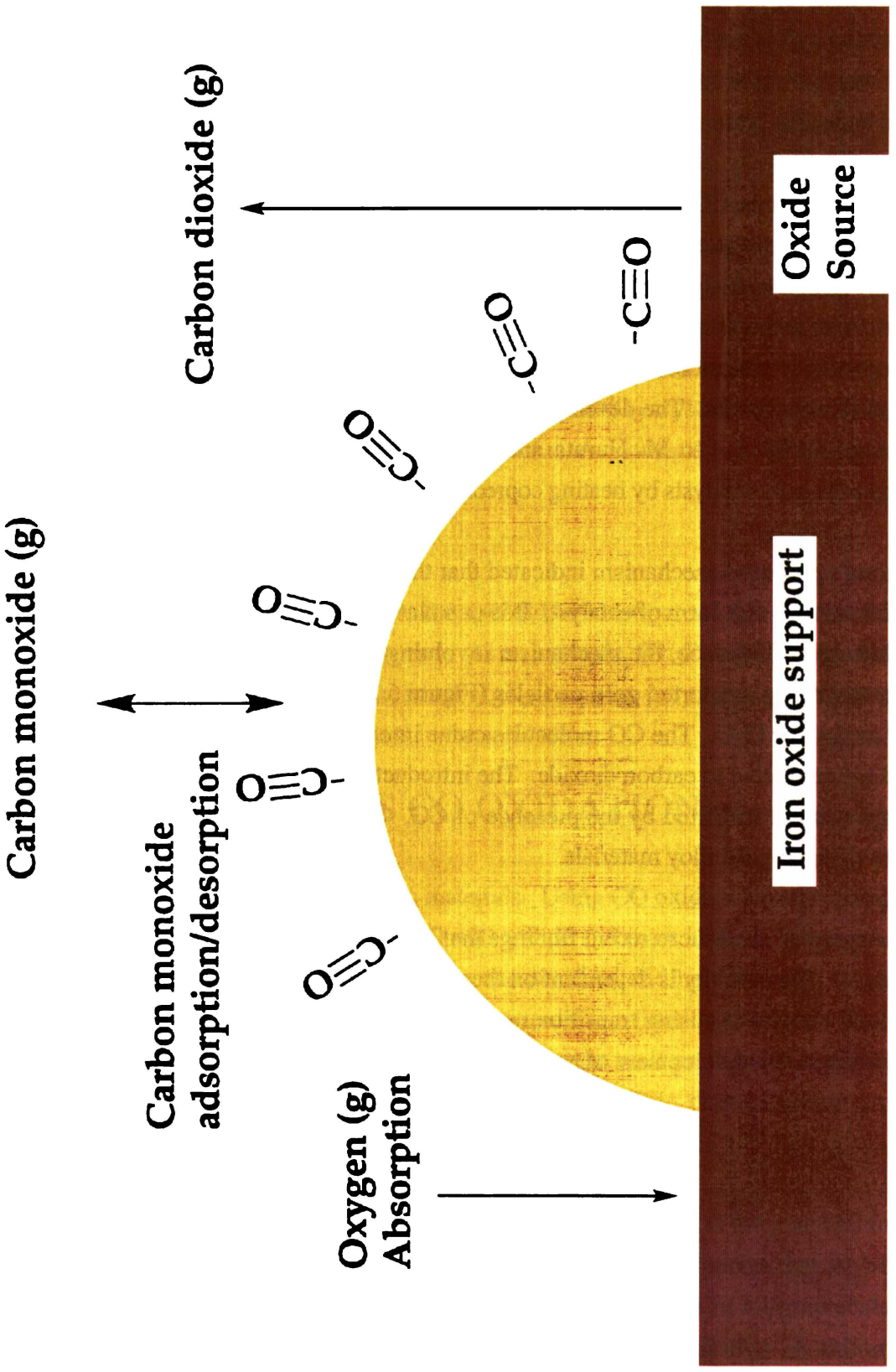

Figure 6·2 CO oxidation under ambient conditions

A greater understanding of two-component catalysts should allow improvement of other heterogeneous catalytic reactions in the future. It could be possible to design a two-component catalyst for reaction between two chemical species. Two different catalytic sites would be required on a catalyst surface, each with binding properties tailored for one of the reactants. Once both are chemisorbed with specific geometry, fast rates of reaction will be likely.

6·5 GOLD COMPLEX PRECURSORS

Supported gold catalysts were prepared in this project (see Chapter Five) by adsorbing gold(I) complexes onto $Fe(OH)_3$, $FeO(OH)$, Fe_2O_3, and yttria-stabilised ZrO_2 (YSZ). This was achieved by forming a slurry of the support in a solution of the gold(I) complex. After removing the solvent the material was calcined.

When the solvent was removed from the mixtures containing $(Ph_3P)AuCl$, $(Ph_3P)AuMe$ or $(Bu^tNC)AuCl$, crystals were observed. This indicated that these relatively stable complexes were not efficiently adsorbed on the oxide surfaces. However, the oxide surfaces appeared to act as decomposition catalysts for the complexes. When the stable solution of $(Ph_3P)AuCl$, for example, was added to white YSZ, the oxide turned purple. This indicated that tiny particles of metallic gold had formed.

The materials prepared by using $(Ph_3P)AuCl$, $(Ph_3P)AuMe$ or $(Bu^tNC)AuCl$ as precursors were tested for catalytic CO oxidation under ambient conditions. They exhibited no activity, even though SEM of the calcined materials revealed metallic gold particles dispersed over the oxide surfaces. The lack of catalytic activity was attributed to the size of the gold particles being too large.

During synthesis of the novel $(RNC)AuNO_3$ complexes (Chapter Three) it was noted that their solutions were particularly prone to decomposition. Solutions of $(Bu^tNC)AuNO_3$ were mixed with $Fe(OH)_3$ and no crystalline material was observed when the solvent was removed. This showed that $(Bu^tNC)AuNO_3$ (or a decomposed fragment) was efficiently adsorbed on the support surface. The calcined materials, which are proposed to consist of finely dispersed metallic particles supported on Fe_2O_3, exhibited efficient activity for CO oxidation under ambient conditions. SEM was not able to resolve gold particles on the support surface but gold was detected by EDAX.

Supported gold catalysts were also produced by coprecipitation (which is an established technique) and gold-sputtering. The coprecipitates produced active catalysts but the results of catalytic testing of gold-sputtered Fe_2O_3 were inconsistent. The results of using $(Bu^tNC)AuNO_3$ as a catalyst precursor represents the preliminary development of a convenient and reproducible method for preparing active CO oxidation catalysts.

Appendices

Appendix One
Experimental and Instrumentation

A1·1 Experimental

(i) For synthesis of gold complexes;

CH_2Cl_2 (drum grade) was dried and purified by distillation from calcium hydride under nitrogen. Di-ethyl ether (analytical grade) was dried by distillation from sodium/benzophenone under nitrogen. Petroleum spirits (30-40 °C), MeOH and C_6H_6 were all analytical grade. A chlorobenzene slush bath (-45 °C) was used during the synthesis of the $(RNC)AuNO_3$ complexes. A *meta*-xylene slush bath (-49 °C) was used during the attempted synthesis of $(Me_2AuCl)_2$. All glassware was cleaned and oven dried before use.

(ii) For catalyst preparations;

Drum grade CH_2Cl_2, MeOH and acetone were used. H_2O was distilled and deionised.

A1·2 X-ray crystallography

Unit cell dimensions and intensity data were obtained from Auckland University on a Siemens SMART CCD diffractometer. This operated at 203 K, with mono-chromatic Mo-Kα radiation, λ 0·71073 Å. The data collection nominally covered over a hemisphere of reciprocal space, by a combination of three sets of exposures; each set had a different ϕ angle for the crystal and each exposure covered 0·3° in ω. The crystal to detector distance was 5·0 cm. The data sets were corrected empirically for adsorption and other effects using SADABS.[262] The SHELX-97 programs were used for all calculations.[263]

---

[262] R. H. Blessing, *Acta Cryst.*, 1995, **A51**, 33.
[263] G. M. Sheldrick, *SHELX-97, Programs for X-ray crystallography*, University of Göttingen, 1997.

The structural determinations for (RNC)AuNO$_3$ (R = Bu^t, Et or Xy) and (RNC)AuCl (R = Et or Xy) were solved by automatic interpretation of Patterson maps and developed normally. In the final cycles of least-squares refinement based on F^2 against all data, all non-hydrogen atoms were treated anisotropically and hydrogen atoms were included in their calculated positions.

Structural Refinement Definitions

a;b;c - The dimensions of the unit cell (Å). For a monoclinic cell $a \neq b \neq c$

β - For a monoclinic cell $\alpha = \gamma = 90° \neq \beta$

V - The volume of the unit cell (Å^3)

Z - The number of molecules in the unit cell

D$_c$ - The calculated crystal density

μ - Absorption coefficient

T$_{max, min}$ - The maximum and minimum transmission factors

F(000) - The number of electrons in the unit cell

Crystal size - The dimensions of the crystal from which data was collected

θ-range - The Bragg angle (°) range

Total data - The total number of reflections collected

Unique data - Independent reflections collected

R$_{int}$ = $\Sigma / F_o^2 - F_o^2$ (mean)$/ / \Sigma [F_o^2]$

R$_1$ = $\Sigma // F_o / - / F_c / / / \Sigma [F_o]$

wR$_2$ = $\{\Sigma [w(F_o^2 - F_c^2)^2] / \Sigma [w(F_o^2)^2]\}^{1/2}$

GoF - Goodness-of-fit based on F^2; = $\{\Sigma [w(F_o^2 - F_c^2)^2] / (n-p)\}^{1/2}$

Final Δe - Largest diff. peak and hole (e.Å^{-3})

A1·3 NMR spectroscopy

^{1}H and ^{13}C NMR spectra of (RNC)AuX (R = Bu^t, Et or Xy; X = NO$_3$ or Cl) were recorded on a Bruker DRX400 spectrometer from CDCl$_3$ solutions, at 400·13 and 100·61 MHz for ^{1}H and ^{13}C respectively. ^{1}H and ^{13}C NMR spectra of (RNC)Au(acac) were recorded on a Bruker AC300 spectrometer from a CDCl$_3$ solution at -30 °C, at 300·13 and 75·47 MHz for ^{1}H and ^{13}C respectively. All chemical shifts were referenced externally to tetramethylsilane (SiMe$_4$) at 0·0 ppm.

A1·4 IR spectroscopy

IR spectra were recorded from KBr disks on a Perkin Elmer Model 1600 FTIR.

A1·5 Melting points

Melting points were observed on a Reichart Thermovar apparatus and are uncorrected.

A1·6 DSC

This was carried out on a Perkin Elmer Model DSC6. The sample and reference were heated at a rate of 15 °C min^{-1}. Positive peaks in the traces represent endothermic processes.

A1·7 STA

This was carried out on a Rheometrics STA 1500 at Industrial Research Limited, Wellington. The heating rate was 10 °C min^{-1}. Positive peaks in the heat flow traces represent exothermic processes.

A1·8 SEM and EDAX

Scanning Electron micrographs were obtained at the Waikato Microscope Unit on a Hitachi S4000 SEM. This was operated at 15-20 kV. An Hitachi EDAX instrument was coupled to the SEM.

A1·9 Gold-sputtering

Gold-sputtering catalyst preparations were carried out at the Waikato Microscope Unit using a Hitachi E-1030 Ion Sputter.

A1·10 XPS

XPS analyses on selected catalyst samples were carried out by Dr. T. Fujimoto at the National Institute of Materials and Chemical Research, Ibaraki, Japan.

A1·11 Surface area analysis

The surface area of the Fe_2O_3 was determined on a Quantachrome Corporation NOVA-1000 BET Surface Area Analyser

A1·12 Particle size analysis

The particle size distribution of the Fe_2O_3 was determined on a Malvern Instruments Laser Mastersizer.

A1·13 ESMS

Spectra of (RNC)AuX complexes were obtained on a VG Platform II machine from MeCN solutions. The spectra were of little diagnostic use, always exhibiting the $[(RNC)_2Au]^+$ ion as the major peak.

Appendix Two
$(Bu^tNC)AuNO_3$ Crystallography Tables

Table A2·1

Atomic coordinates and equivalent isotropic displacement parameters

	x	y	z	U(eq)
Au(1)	0·2348(1)	0·4746(1)	0·4606(1)	0·033(1)
O(1)	0·2218(14)	0·6142(7)	0·3846(9)	0·045(2)
O(2)	0·3024(14)	0·7035(7)	0·2330(8)	0·045(2)
O(3)	0·383(2)	0·5487(7)	0·2448(10)	0·064(3)
N(1)	0·3034(14)	0·6206(7)	0·2807(8)	0·032(2)
N(2)	0·2257(14)	0·2683(7)	0·5775(8)	0·031(2)
C(1)	0·2335(15)	0·3460(9)	0·5368(10)	0·033(2)
C(2)	0·1864(17)	0·1706(8)	0·6267(11)	0·035(2)
C(3)	-0·0368(16)	0·1390(9)	0·5522(10)	0·035(2)
C(4)	0·1907(19)	0·1814(10)	0·7724(10)	0·041(3)
C(5)	0·3660(19)	0·1027(9)	0·6003(13)	0·045(3)

U(eq) is defined as one third of the trace of the orthogonalized Uij tensor

Table A2·2

Bond lengths [Å]

Au(1)-C(1)	1·922(12)	O(3)-N(1)	1·193(13)
Au(1)-O(1)	2·053(9)	N(2)-C(1)	1·14(2)
Au(1)-Au(1)'	3·2963(8)	N(2)-C(2)	1·46(2)
Au(1)-Au(1)"	3·3232(8)	C(2)-C(3)	1·515(14)
O(1)-N(1)	1·312(11)	C(2)-C(5)	1·52(2)
O(2)-N(1)	1·232(12)	C(2)-C(4)	1·55(2)

Symmetry transformations used to generate equivalent atoms: Au' -x,-y+1,-z+1
Au" -x+1,-y+1,-z+1

Table A2·3

Angles [deg]

C(1)-Au(1)-O(1)	176·6(4)	O(2)-N(1)-O(1)	115·9(9)
C(1)-Au(1)-Au(1)'	90·0(3)	C(1)-N(2)-C(2)	172·9(10)
O(1)-Au(1)-Au(1)'	86·7(2)	N(2)-C(1)-Au(1)	176·9(9)
C(1)-Au(1)-Au(1)"	100·1(3)	N(2)-C(2)-C(3)	106·0(9)
O(1)-Au(1)-Au(1)"	82·1(3)	N(2)-C(2)-C(5)	107·2(9)
Au'(1)-Au(1)-Au"(1)	142·29(3)	C(3)-C(2)-C(5)	111·7(10)
N(1)-O(1)-Au(1)	113·6(7)	N(2)-C(2)-C(4)	107·5(9)
O(3)-N(1)-O(2)	125·5(9)	C(3)-C(2)-C(4)	111·6(9)
O(3)-N(1)-O(1)	118·5(10)	C(5)-C(2)-C(4)	112·5(10)

Symmetry transformations used to generate equivalent atoms: Au' -x,-y+1,-z+1
Au" -x+1,-y+1,-z+1

Table A2·4

Anisotropic displacement parameters ($Å^2$)

	U11	U22	U33	U23	U13	U12
Au(1)	0·0359(3)	0·0265(3)	0·0372(3)	0·0046(2)	0·0075(2)	-0·001(1)
O(1)	0·059(5)	0·030(4)	0·051(5)	0·009(4)	0·025(4)	0·007(4)
O(2)	0·053(5)	0·036(5)	0·046(5)	0·011(4)	0·013(4)	0·000(4)
O(3)	0·118(9)	0·034(5)	0·046(5)	0·003(4)	0·033(6)	0·020(6)
N(1)	0·038(4)	0·032(5)	0·026(4)	0·007(4)	0·006(3)	0·003(4)
N(2)	0·032(4)	0·031(5)	0·031(4)	0·004(4)	0·005(3)	-0·003(4)
C(1)	0·024(4)	0·032(7)	0·040(6)	0·004(4)	0·000(4)	0·002(4)
C(2)	0·034(5)	0·025(6)	0·043(6)	0·000(5)	0·004(4)	-0·001(4)
C(3)	0·039(5)	0·028(6)	0·034(5)	0·000(4)	0·000(4)	-0·008(4)
C(4)	0·045(6)	0·043(7)	0·032(6)	0·003(5)	0·005(4)	-0·004(5)
C(5)	0·042(6)	0·031(7)	0·060(7)	0·007(6)	0·009(5)	0·009(5)

The anisotropic displacement factor exponent takes the form:
$-2\pi^2$ [h^2 a^{*2} U11 +···+ 2 h k a* b* U12]

Table A2·5

Hydrogen coordinates and isotropic displacement parameters

	x	y	z	U(eq)
H(3A)	-0·1465	0·1844	0·5700	0·052
H(3B)	-0·0685	0·0730	0·5784	0·052
H(3C)	-0·0383	0·1394	0·4606	0·052
H(4A)	0·0733	0·2247	0·7842	0·061
H(4B)	0·3297	0·2092	0·8155	0·061
H(4C)	0·1720	0·1172	0·8087	0·061
H(5A)	0·5063	0·1251	0·6491	0·067
H(5B)	0·3667	0·1037	0·5090	0·067
H(5C)	0·3392	0·0360	0·6262	0·067

Appendix Three
(EtNC)AuCl Crystallography Tables

Table A3·1

Atomic coordinates and equivalent isotropic displacement parameters

	x	y	z	U(eq)
Au(1)	0·3749(1)	0·2500	0·4339(1)	0·032(1)
Cl(1)	0·6095(11)	0·2500	0·2437(5)	0·040(1)
C(1)	0·166(4)	0·2500	0·588(2)	0·036(4)
N(1)	0·045(3)	0·2500	0·6893(16)	0·040(4)
C(2)	-0·105(4)	0·2500	0·8085(18)	0·038(4)
C(3)	0·122(4)	0·2500	0·933(2)	0·044(4)

U(eq) is defined as one third of the trace of the orthogonalized Uij tensor

Table A3·2

Bond lengths [Å]

Au(1)-C(1)	1·90(2)	N(1)-C(2)	1·43(2)
Au(1)-Cl(1)	2·277(5)	C(2)-C(3)	1·52(3)
C(1)-N(1)	1·20(2)	Au(1)'-Au(1)"	3·5536(6)

Table A3·3

Angles [deg]

C(1)-Au(1)-Cl(1)	177·9(6)	C(1)-N(1)-C(2)	178·9(18)
N(1)-C(1)-Au(1)	177·1(18)	N(1)-C(2)-C(3)	111·0(14)
Au(1)'-Au(1)-Au(1)"	124·90(1)	Au(1)-Au(1)'-Cl(1)	99·22(6)
Au(1)-Au(1)'-C(1)	81·8(3)		

Table A3·4

Anisotropic displacement parameters ($Å^2$)

	U11	U22	U33	U23	U13	U12
Au(1)	0·0381(5)	0·0228(4)	0·0345(5)	0·000	0·0015(3)	0·000
Cl(1)	0·050(2)	0·029(2)	0·042(2)	0·000	0·011(1)	0·000
C(1)	0·043(9)	0·016(8)	0·051(11)	0·000	0·008(8)	0·000
N(1)	0·032(7)	0·046(9)	0·040(8)	0·000	-0·011(6)	0·000
C(2)	0·033(8)	0·035(9)	0·048(11)	0·000	0·018(7)	0·000
C(3)	0·044(9)	0·033(9)	0·056(12)	0·000	0·008(8)	0·000

The anisotropic displacement factor exponent takes the form:

$-2\pi^2$ [h^2 a^{*2} U11 +···+ 2 h k a* b* U12]

Table A3·5

Hydrogen coordinates and isotropic displacement parameters

	x	y	z	U(eq)
H(2A)	-0·2335	0·1242	0·8093	0·045
H(2B)	-0·2335	0·3758	0·8093	0·045
H(3A)	0·0156	0·2500	1·0118	0·066
H(3B)	0·2476	0·3757	0·9326	0·066
H(3C)	0·2476	0·1243	0·9326	0·066

Appendix Four
(EtNC)AuNO$_3$ Crystallography Tables

Table A4·1

Atomic coordinates and equivalent isotropic displacement parameters

	x	y	z	U(eq)
Au(1)	0·4364(1)	0·3296(1)	0·4625(1)	0·042(1)
N(11)	0·3895(14)	0·0985(15)	0·5669(6)	0·047(3)
N(12)	0·3382(14)	0·4977(15)	0·3284(6)	0·045(3)
O(11)	0·5043(12)	0·2065(14)	0·5491(5)	0·052(3)
O(12)	0·2588(17)	0·0859(18)	0·5288(7)	0·085(4)
O(13)	0·4230(14)	0·0207(14)	0·6180(6)	0·064(3)
C(11)	0·3788(16)	0·4379(16)	0·3781(6)	0·041(3)
C(12)	0·289(2)	0·5753(19)	0·2639(7)	0·052(3)
C(13)	0·408(2)	0·7082(19)	0·2473(9)	0·060(4)
Au(2)	0·8240(1)	0·4118(1)	0·4687(1)	0·049(1)
N(21)	0·8600(16)	0·573(2)	0·3457(8)	0·066(4)
N(22)	0·898(2)	0·149(2)	0·5778(11)	0·110(8)
O(21)	0·7674(13)	0·5820(14)	0·3939(7)	0·070(3)
O(22)	0·8435(19)	0·687(2)	0·3054(8)	0·104(5)
O(23)	0·9547(18)	0·459(2)	0·3452(8)	0·101(5)
C(21)	0·8707(18)	0·245(2)	0·5384(9)	0·064(5)
C(22)	0·957(3)	-0·049(4)	0·6155(14)	0·123(11)
C(23)	0·860(2)	0·000(5)	0·6561(12)	0·131(12)

U(eq) is defined as one third of the trace of the orthogonalized Uij tensor

Table A4·2

Bond lengths [Å]

Au(1)-C(11)	1·924(12)	Au(2)-C(21)	1·94(2)
Au(1)-O(11)	2·028(9)	Au(2)-O(21)	2·038(12)
Au(1)-Au(2)	3·1932(7)	Au(2)-Au(2)"	3·2865(11)
Au(1)-Au(1)'	3·1941(10)	Au(2)-Au(1)'	3·3575(7)
Au(1)-Au(2)'	3·3574(7)	N(21)-O(23)	1·18(2)
N(11)-O(13)	1·21(2)	N(21)-O(22)	1·21(2)
N(11)-O(12)	1·24(2)	N(21)-O(21)	1·31(2)
N(11)-O(11)	1·34(2)	N(22)-C(21)	1·11(2)
N(12)-C(11)	1·13(2)	N(22)-C(22)	1·78(4)
N(12)-C(12)	1·46(2)	C(22)-C(23)	1·27(3)
C(12)-C(13)	1·49(2)		

Symmetry transformations used to generate equivalent atoms: Au' -x+1,-y+1,-z+1
Au" -x+2,-y+1,-z+1

Table A4·3

Angles [deg]

C(11)-Au(1)-O(11)	177·0(5)	C(21)-Au(2)-O(21)	177·8(5)
C(11)-Au(1)-Au(2)	94·4(4)	C(21)-Au(2)-Au(1)	89·7(4)
O(11)-Au(1)-Au(2)	84·3(3)	O(21)-Au(2)-Au(1)	88·4(3)
C(11)-Au(1)-Au(1)'	94·9(4)	C(21)-Au(2)-Au(2)"	85·4(4)
O(11)-Au(1)-Au(1)'	87·0(3)	O(21)-Au(2)-Au(2)"	96·8(3)
Au(2)-Au(1)-Au(1)'	63·42(2)	Au(1)-Au(2)-Au(2)"	154·61(3)
C(11)-Au(1)-Au(2)'	90·5(4)	C(21)-Au(2)-Au(1)'	100·5(6)
O(11)-Au(1)-Au(2)'	92·5(3)	O(21)-Au(2)-Au(1)'	79·5(3)
Au(2)-Au(1)-Au(2)'	121·70(2)	Au(1)-Au(2)-Au(1)'	58·30(2)
Au(1)'-Au(1)-Au(2)'	58·28(2)	Au(2)"-Au(2)-Au(1)'	98·13(2)
O(13)-N(11)-O(12)	125·8(12)	O(23)-N(21)-O(22)	125(2)
O(13)-N(11)-O(11)	117·6(11)	O(23)-N(21)-O(21)	119(2)
O(12)-N(11)-O(11)	116·6(11)	O(22)-N(21)-O(21)	116(2)
C(11)-N(12)-C(12)	178·9(14)	C(21)-N(22)-C(22)	159(3)
N(11)-O(11)-Au(1)	114·5(7)	N(21)-O(21)-Au(2)	115·4(9)
N(12)-C(11)-Au(1)	176·9(12)	N(22)-C(21)-Au(2)	179(2)
N(12)-C(12)-C(13)	112·7(12)	C(23)-C(22)-N(22)	82(3)

Symmetry transformations used to generate equivalent atoms: Au' -x+1,-y+1,-z+1
Au" -x+2,-y+1,-z+1

Table A4·4

Anisotropic displacement parameters ($Å^2$)

	U11	U22	U33	U23	U13	U12
Au(1)	0·0436(4)	0·0430(4)	0·0384(4)	0·0002(2)	0·0034(2)	-0·004(1)
N(11)	0·051(7)	0·055(7)	0·034(6)	0·008(5)	0·003(5)	-0·005(5)
N(12)	0·049(6)	0·049(6)	0·034(6)	0·000(6)	-0·001(5)	-0·001(5)
O(11)	0·042(5)	0·067(6)	0·046(6)	0·025(5)	-0·003(4)	-0·013(5)
O(12)	0·077(9)	0·092(10)	0·077(9)	0·024(7)	-0·023(7)	-0·037(7)
O(13)	0·072(7)	0·067(7)	0·054(7)	0·026(6)	0·011(5)	0·005(6)
C(11)	0·049(7)	0·043(7)	0·030(7)	0·011(6)	0·002(5)	-0·010(6)
C(12)	0·064(9)	0·053(8)	0·038(8)	0·002(7)	0·007(6)	-0·006(7)
C(13)	0·073(10)	0·046(8)	0·062(10)	0·010(7)	0·011(8)	-0·007(7)
Au(2)	0·0401(4)	0·0430(4)	0·0658(5)	0·0008(3)	0·0087(3)	0·0004(2)
N(21)	0·044(8)	0·076(9)	0·077(10)	0·018(8)	0·007(7)	0·001(7)
N(22)	0·098(13)	0·099(12)	0·112(15)	0·071(12)	-0·065(12	-0·050(11
O(21)	0·047(6)	0·060(6)	0·108(10)	0·027(6)	0·023(6)	0·015(5)
O(22)	0·093(11)	0·138(15)	0·080(10)	0·028(10)	0·011(8)	-0·015(10
O(23)	0·076(9)	0·142(14)	0·090(11)	0·019(10)	0·035(8)	0·033(10)
C(21)	0·039(8)	0·068(10)	0·082(13)	0·005(10)	-0·013(7)	-0·019(8)
C(22)	0·055(12)	0·18(3)	0·13(2)	-0·11(2)	0·004(12)	-0·004(14
C(23)	0·047(11)	0·25(4)	0·092(17)	-0·09(2)	-0·005(10	-0·004(16

The anisotropic displacement factor exponent takes the form:
$-2\pi^2$ [h^2 a^{*2} U11 +···+ 2 h k a* b* U12]

Table A4·5

Hydrogen coordinates and isotropic displacement parameters

	x	y	z	U(eq)
H(12A)	0·1787	0·6261	0·2635	0·062
H(12B)	0·2817	0·4867	0·2298	0·062
H(13A)	0·4211	0·7928	0·2823	0·090
H(13B)	0·3651	0·7622	0·2059	0·090
H(13C)	0·5147	0·6565	0·2431	0·090
H(22A)	0·9195	-0·1495	0·5894	0·148
H(22B)	1·0745	-0·0574	0·6338	0·148
H(23A)	0·8100	-0·0977	0·6748	0·196
H(23B)	0·7733	0·0712	0·6333	0·196
H(23C)	0·9223	0·0652	0·6913	0·196

Appendix Five
(XyNC)AuCl Crystallography Tables

Table A5·1

Atomic coordinates and equivalent isotropic displacement parameters

	x	y	z	U(eq)
Au(1)	0·8614(1)	0·0271(1)	0·5711(1)	0·047(1)
Au(2)	1·0134(1)	0·0656(1)	0·8499(1)	0·059(1)
Cl(1)	0·8616(2)	-0·1028(1)	0·5597(2)	0·066(1)
Cl(2)	0·8598(2)	0·1372(2)	0·9180(2)	0·073(1)
N(1)	0·8453(6)	0·2047(5)	0·5768(6)	0·047(2)
C(1)	0·8531(7)	0·1385(6)	0·5754(6)	0·049(2)
C(11)	0·8295(7)	0·2838(5)	0·5767(7)	0·045(2)
C(12)	0·7216(8)	0·3127(5)	0·6199(7)	0·050(2)
C(13)	0·7069(9)	0·3932(6)	0·6202(8)	0·062(2)
C(14)	0·8036(12)	0·4407(6)	0·5785(10)	0·076(3)
C(15)	0·9046(11)	0·4086(6)	0·5377(8)	0·064(3)
C(16)	0·9219(8)	0·3305(5)	0·5361(7)	0·051(2)
C(17)	0·6283(9)	0·2610(6)	0·6661(9)	0·070(3)
C(18)	1·0380(8)	0·2953(6)	0·4924(9)	0·067(3)
N(2)	0·7735(7)	0·0272(5)	0·2417(6)	0·060(2)
C(2)	1·1483(9)	0·0059(7)	0·7929(9)	0·065(3)
C(21)	0·6746(8)	0·0684(6)	0·2839(7)	0·058(2)
C(22)	0·6858(8)	0·1489(7)	0·2896(7)	0·060(3)
C(23)	0·5880(9)	0·1901(7)	0·3323(8)	0·071(3)
C(24)	0·4846(9)	0·1503(9)	0·3679(8)	0·075(3)
C(25)	0·4774(9)	0·0739(9)	0·3602(8)	0·078(4)
C(26)	0·5707(9)	0·0272(7)	0·3192(8)	0·067(3)
C(27)	0·8003(9)	0·1892(7)	0·2540(9)	0·074(3)
C(28)	0·5655(11)	-0·0583(7)	0·3100(10)	0·087(4)

U(eq) is defined as one third of the trace of the orthogonalized Uij tensor

Table A5·2

Bond lengths [Å]

Au(1)-C(1)	1·931(10)	C(14)-C(15)	1·34(2)
Au(1)-Cl(1)	2·251(2)	C(15)-C(16)	1·365(13)
Au(1)-Au(2)	3·3554(5)	C(16)-C(18)	1·517(12)
Au(1)-Au(1)'	3·6545(6)	N(2)-C(2)	1·121(12)
Au(2)-Au(2)"	4·0712(8)	N(2)-C(21)	1·404(12)
Au(2)-C(2)	1·945(11)	C(2)-N(2)	1·121(12)
Au(2)-Cl(2)	2·263(2)	C(21)-C(22)	1·400(14)
N(1)-C(1)	1·149(11)	C(21)-C(26)	1·416(13)
N(1)-C(11)	1·380(11)	C(22)-C(23)	1·397(12)
C(11)-C(16)	1·395(11)	C(22)-C(27)	1·503(13)
C(11)-C(12)	1·396(11)	C(23)-C(24)	1·40(2)
C(12)-C(13)	1·403(13)	C(24)-C(25)	1·33(2)
C(12)-C(17)	1·480(12)	C(25)-C(26)	1·40(2)
C(13)-C(14)	1·44(2)	C(26)-C(28)	1·48(2)

Table A5·3

Angles [deg]

Au(1)-Au(1)'-Au(2)'	97·60(1)	C(14)-C(15)-C(16)	122·0(10)
Au(1)-Au(2)-Au(2)"	124·32(1)	C(15)-C(16)-C(11)	117·9(8)
C(1)-Au(1)-Cl(1)	177·1(2)	C(15)-C(16)-C(18)	121·3(9)
C(1)-Au(1)-Au(2)	78·3(2)	C(11)-C(16)-C(18)	120·8(8)
Cl(1)-Au(1)-Au(2)	104·25(7)	C(2)-N(2)-C(21)	179·4(9)
C(2)-Au(2)-Cl(2)	178·6(3)	N(2)-C(2)-Au(2)	178·4(10)
C(2)-Au(2)-Au(1)	83·1(3)	N(2)-C(21)-C(22)	117·2(8)
Cl(2)-Au(2)-Au(1)	97·84(7)	N(2)-C(21)-C(26)	119·1(10)
C(1)-N(1)-C(11)	177·1(8)	C(22)-C(21)-C(26)	123·7(9)
N(1)-C(1)-Au(1)	178·4(7)	C(23)-C(22)-C(21)	117·4(9)
N(1)-C(11)-C(16)	119·0(7)	C(23)-C(22)-C(27)	121·4(10)
N(1)-C(11)-C(12)	117·5(7)	C(21)-C(22)-C(27)	121·1(9)
C(16)-C(11)-C(12)	123·6(8)	C(22)-C(23)-C(24)	119·7(11)
C(11)-C(12)-C(13)	117·0(8)	C(25)-C(24)-C(23)	120·9(10)
C(11)-C(12)-C(17)	121·7(8)	C(24)-C(25)-C(26)	123·9(10)
C(13)-C(12)-C(17)	121·3(9)	C(25)-C(26)-C(21)	114·4(11)
C(12)-C(13)-C(14)	118·8(9)	C(25)-C(26)-C(28)	125·1(10)
C(15)-C(14)-C(13)	120·8(9)	C(21)-C(26)-C(28)	120·4(10)

Table A5·4

Anisotropic displacement parameters ($Å^2$)

	U11	U22	U33	U23	U13	U12
Au(1)	0·0436(2)	0·0500(2)	0·0493(2)	0·0072(1)	0·0145(1)	0·0022(1)
Au(2)	0·0471(2)	0·0751(3)	0·0568(2)	-0·0083(2	0·0108(2)	0·0026(2)
Cl(1)	0·0629(14	0·0506(1)	0·0910(2)	0·0088(2)	0·0332(2)	0·0098(2)
Cl(2)	0·0632(15	0·0814(2)	0·0796(1)	0·0082(1)	0·0244(1)	0·0124(1)
N(1)	0·046(4)	0·054(5)	0·043(4)	0·001(3)	0·011(3)	-0·001(3)
C(1)	0·048(5)	0·068(6)	0·032(4)	0·007(4)	0·014(3)	0·006(4)
C(11)	0·045(4)	0·048(5)	0·042(4)	-0·002(3)	0·009(3)	0·002(4)
C(12)	0·050(5)	0·063(6)	0·035(4)	-0·001(4)	0·006(3)	-0·005(4)
C(13)	0·065(6)	0·070(7)	0·049(5)	-0·007(4)	-0·001(4)	0·019(5)
C(14)	0·100(9)	0·047(6)	0·071(7)	-0·001(5)	-0·016(6)	0·007(6)
C(15)	0·082(7)	0·054(6)	0·056(5)	-0·002(4)	0·011(5)	-0·018(5
C(16)	0·052(5)	0·056(5)	0·046(4)	-0·005(4)	0·013(4)	-0·008(4)
C(17)	0·052(5)	0·099(8)	0·064(6)	0·003(5)	0·024(5)	-0·001(5)
C(18)	0·050(5)	0·084(7)	0·073(6)	-0·022(5)	0·024(5)	-0·020(5)
N(2)	0·038(4)	0·098(7)	0·044(4)	-0·015(4)	0·007(3)	-0·005(4)
C(2)	0·040(5)	0·098(8)	0·056(5)	-0·011(5)	0·005(4)	-0·007(5)
C(21)	0·049(5)	0·088(8)	0·036(4)	-0·006(4)	0·001(4)	0·006(5)
C(22)	0·040(5)	0·101(8)	0·041(4)	-0·007(5)	0·006(4)	0·007(5)
C(23)	0·064(6)	0·104(9)	0·045(5)	-0·009(5)	0·013(4)	0·012(6)
C(24)	0·047(5)	0·130(11)	0·048(5)	-0·013(6)	0·011(4)	0·019(6)
C(25)	0·045(5)	0·149(12)	0·043(5)	-0·015(6)	0·018(4)	-0·017(7)
C(26)	0·050(5)	0·111(9)	0·042(5)	0·004(5)	0·009(4)	-0·014(6)
C(27)	0·058(6)	0·101(9)	0·065(6)	-0·019(6)	0·016(5)	-0·015(6)
C(28)	0·091(9)	0·117(11)	0·057(6)	0·002(6)	0·018(6)	-0·025(7)

The anisotropic displacement factor exponent takes the form:

$-2\pi^2$ [h^2 a^{*2} U11 +···+ 2 h k a* b* U12]

Table A5·5

Hydrogen coordinates and isotropic displacement parameters

	x	y	z	U(eq)
H(13)	0·6354	0·4158	0·6471	0·075
H(14)	0·7958	0·4948	0·5799	0·091
H(15)	0·9652	0·4409	0·5094	0·077
H(17A)	0·6697	0·2317	0·7348	0·105
H(17B)	0·5936	0·2258	0·6020	0·105
H(17C)	0·5604	0·2916	0·6917	0·105
H(18A)	1·0974	0·3359	0·4794	0·101
H(18B)	1·0129	0·2680	0·4165	0·101
H(18C)	1·0779	0·2595	0·5531	0·101
H(23)	0·5916	0·2443	0·3371	0·085
H(24)	0·4195	0·1781	0·3977	0·089
H(25)	0·4055	0·0496	0·3835	0·094
H(27A)	0·7929	0·2443	0·2667	0·111
H(27B)	0·8060	0·1792	0·1689	0·111
H(27C)	0·8759	0·1700	0·3036	0·111
H(28A)	0·6211	-0·0808	0·3774	0·131

H(28B)	0·5928	-0·0744	0·2338	0·131
H(28C)	0·4794	-0·0757	0·3125	0·131

Appendix Six
(XyNC)$AuNO_3$ Crystallography Tables

Table A6·1

Atomic coordinates and equivalent isotropic displacement parameters

	x	y	z	U(eq)
Au(1)	0·8305(1)	0·0595(2)	0·2984(1)	0·034(1)
O(1)	0·8833(7)	0·124(3)	0·2058(6)	0·039(3)
O(2)	0·9956(8)	-0·160(4)	0·2772(6)	0·052(3)
O(3)	1·0101(8)	0·063(3)	0·1715(7)	0·045(3)
N(1)	0·9681(9)	0·000(3)	0·2196(8)	0·034(3)
N(2)	0·7763(8)	-0·035(3)	0·4493(8)	0·031(3)
C(1)	0·7915(10)	0·013(4)	0·3907(9)	0·031(3)
C(2)	0·7614(9)	-0·093(4)	0·5215(7)	0·025(3)
C(3)	0·6768(9)	-0·003(3)	0·5313(9)	0·025(3)
C(4)	0·6610(10)	-0·076(4)	0·6020(9)	0·030(3)
C(5)	0·7272(9)	-0·234(4)	0·6578(7)	0·034(3)
C(6)	0·8096(10)	-0·319(4)	0·6459(8)	0·030(3)
C(7)	0·8301(9)	-0·251(3)	0·5761(8)	0·028(3)
C(8)	0·6053(10)	0·159(4)	0·4702(8)	0·033(3)
C(9)	0·9216(9)	-0·336(4)	0·5613(8)	0·035(3)

U(eq) is defined as one third of the trace of the orthogonalized Uij tensor

Table A6·2

Bond lengths [Å]

Au(1)-C(1)	1·905(16)	N(2)-C(2)	1·393(19)
Au(1)-O(1)	2·033(10)	C(2)-C(3)	1·37(2)
Au(1)-Au(1)'	3·2456(8)	C(2)-C(7)	1·386(19)
Au(1)-Au(1)"	3·2457(8)	C(3)-C(4)	1·38(2)
Au(1)'-Au(1)"	3·7802(2)	C(3)-C(8)	1·482(18)
O(1)-N(1)	1·330(16)	C(4)-C(5)	1·37(2)
O(2)-N(1)	1·190(16)	C(5)-C(6)	1·35(2)
O(3)-N(1)	1·216(16)	C(6)-C(7)	1·39(2)
N(2)-C(1)	1·15(2)	C(7)-C(9)	1·504(19)

Symmetry transformations used to generate equivalent atoms: Au' -x+3/2,y+1/2, -z+1/2; Au" -x+3/2,y-1/2,-z+1/2·

Table A6·3

Angles [deg]

C(1)-Au(1)-O(1)	174·8(5)	C(3)-C(2)-C(7)	116·3(14)
C(1)-Au(1)-Au(1)'	100·2(4)	C(3)-C(2)-N(2)	116·4(13)
O(1)-Au(1)-Au(1)'	82·9(3)	C(7)-C(2)-N(2)	118·3(13)
C(1)-Au(1)-Au(1)"	94·0(5)	C(2)-C(3)-C(4)	116·1(13)
O(1)-Au(1)-Au(1)"	90·9(3)	C(2)-C(3)-C(8)	122·8(14)
Au(1)'-Au(1)-Au(1)"	71·23(2)	C(4)-C(3)-C(8)	121·1(14)
N(1)-O(1)-Au(1)	110·7(8)	C(5)-C(4)-C(3)	120·6(13)
O(2)-N(1)-O(3)	126·4(13)	C(6)-C(5)-C(4)	121·6(13)
O(2)-N(1)-O(1)	117·5(13)	C(5)-C(6)-C(7)	120·8(13)
O(3)-N(1)-O(1)	116·1(12)	C(2)-C(7)-C(6)	115·8(13)
C(1)-N(2)-C(2)	177·8(15)	C(2)-C(7)-C(9)	121·9(13)
N(2)-C(1)-Au(1)	172·7(13)	C(6)-C(7)-C(9)	122·3(13)

Symmetry transformations used to generate equivalent atoms: Au' -x+3/2,y+1/2, -z+1/2; Au" -x+3/2,y-1/2,-z+1/2·

Table A6·4

Anisotropic displacement parameters (Å^2)

	U11	U22	U33	U23	U13	U12
Au(1)	0·0267(4)	0·0606(5)	0·0153(4)	0·0024(2)	0·0030(2)	0·0008(2)
O(1)	0·027(6)	0·067(8)	0·023(5)	0·010(5)	0·005(4)	0·012(5)
O(2)	0·043(7)	0·084(9)	0·022(6)	0·015(6)	-0·004(5)	0·015(6)
O(3)	0·039(6)	0·070(8)	0·028(6)	0·001(5)	0·014(5)	-0·002(5)
N(1)	0·030(7)	0·045(8)	0·025(7)	0·005(5)	0·001(6)	0·001(5)
N(2)	0·025(6)	0·033(7)	0·034(8)	-0·006(5)	0·005(6)	-0·003(5)
C(1)	0·023(7)	0·046(10)	0·024(8)	0·003(6)	0·006(6)	0·005(6)
C(2)	0·027(7)	0·034(8)	0·012(6)	0·003(6)	-0·001(5)	-0·004(6)
C(3)	0·021(7)	0·021(7)	0·026(8)	-0·002(5)	-0·008(6)	-0·002(5)
C(4)	0·020(7)	0·042(8)	0·029(8)	-0·003(7)	0·007(6)	0·000(6)
C(5)	0·037(8)	0·051(10)	0·012(6)	-0·005(6)	0·000(6)	-0·004(7)
C(6)	0·038(8)	0·032(7)	0·016(7)	-0·002(6)	0·000(6)	-0·002(6)
C(7)	0·023(7)	0·023(8)	0·033(8)	-0·003(6)	-0·004(6)	-0·003(5)
C(8)	0·028(7)	0·044(9)	0·020(7)	0·003(6)	-0·009(6)	0·003(7)
C(9)	0·027(7)	0·047(9)	0·027(8)	0·000(7)	0·001(6)	-0·001(7)

The anisotropic displacement factor exponent takes the form:

$-2\pi^2$ [h^2 a*^{2} U11 +···+ 2 h k a* b* U12]

Table A6·5

Hydrogen coordinates and isotropic displacement parameters

	x	y	z	U(eq)
H(4)	0·6045	-0·0181	0·6121	0·036
H(5)	0·7148	-0·2832	0·7053	0·041
H(6)	0·8535	-0·4261	0·6851	0·036
H(8A)	0·6320	0·3451	0·4456	0·050
H(8B)	0·5580	0·2586	0·4921	0·050
H(8C)	0·5790	-0·0199	0·4330	0·050
H(9A)	0·9585	-0·1235	0·5670	0·052
H(9B)	0·9134	-0·4265	0·5099	0·052
H(9C)	0·9518	-0·5133	0·5974	0·052

Appendix Seven
$[(XyNC)_2Au]NO_3$ Crystallography Tables

Table A7·1

Atomic coordinates and equivalent isotropic displacement parameters

	x	y	z	U(eq)
Au(1)	0·0000	0·0000	0·0000	0·070(1)
N(1)	0·1507(3)	0·0000	0·0055(9)	0·046(1)
C(1)	0·0957(5)	0·0000	0·0039(13)	0·057(2)
C(2)	0·2184(4)	0·0000	0·0062(9)	0·041(2)
C(3)	0·2305(4)	0·0000	-0·1503(9)	0·041(2)
C(4)	0·2983(4)	0·0000	-0·1441(9)	0·044(2)
C(5)	0·3500(4)	0·0000	0·0099(11)	0·047(2)
C(6)	0·3352(4)	0·0000	0·1615(10)	0·045(2)
C(7)	0·2685(4)	0·0000	0·1631(9)	0·041(2)
C(8)	0·1742(5)	0·0000	-0·3139(10)	0·055(2)
C(9)	0·2509(5)	0·0000	0·3255(10)	0·056(2)
N(11)	0·4384(12)	0·0000	0·687(3)	0·15(3)
O(11)	0·4077(5)	0·175(2)	0·6478(19)	0·064(3)
O(12)	0·5016(8)	0·0000	0·694(5)	0·23(2)
Cl(1)	0·0250(5)	0·0000	0·3728(9)	0·112(3)
C(91)	0·0000	0·174(7)	0·5000	0·081(13)
C(92)	0·4328(16)	0·075(4)	0·628(3)	0·079(9)

U(eq) is defined as one third of the trace of the orthogonalized Uij tensor

Table A7·2

Bond lengths [Å]

Au(1)-C(1)	1·973(9)	C(5)-C(6)	1·389(12)
Au(1)-C(1)'	1·973(9)	C(6)-C(7)	1·388(11)
N(1)-C(1)	1·136(11)	C(7)-C(9)	1·506(10)
N(1)-C(2)	1·401(10)	N(11)-O(12)	1·29(3)
C(2)-C(7)	1·398(11)	N(11)-O(11)	1·33(2)
C(2)-C(3)	1·403(11)	N(11)-O(11)"	1·33(2)
C(3)-C(4)	1·389(11)	Cl(1)-C(91)	1·76(3)
C(3)-C(8)	1·498(11)	C(91)-Cl(1)	1·76(3)
C(4)-C(5)	1·397(12)	C(92)-C(92)"	1·01(5)

Table A7·3

Angles [deg]

C(1)-Au(1)-C(1)'	180·0	C(6)-C(5)-C(4)	121·0(7)
C(1)-N(1)-C(2)	179·6(9)	C(7)-C(6)-C(5)	120·6(7)
N(1)-C(1)-Au(1)	179·7(9)	C(6)-C(7)-C(2)	116·5(7)
C(7)-C(2)-N(1)	117·2(7)	C(6)-C(7)-C(9)	121·8(7)
C(7)-C(2)-C(3)	125·2(7)	C(2)-C(7)-C(9)	121·7(7)
N(1)-C(2)-C(3)	117·5(7)	O(12)-N(11)-O(11)	114·3(12)
C(4)-C(3)-C(2)	115·7(7)	O(12)-N(11)-O(11)"	114·3(12)
C(4)-C(3)-C(8)	121·9(7)	O(11)-N(11)-O(11)"	125(2)
C(2)-C(3)-C(8)	122·4(7)	Cl(1)-C(91)-Cl(1)	97(2)
C(3)-C(4)-C(5)	121·0(7)		

Table A7·4

Anisotropic displacement parameters (Å^2)

	U11	U22	U33	U23	U13	U12
Au(1)	0·0293(3)	0·0692(4)	0·1237(5)	0·000	0·0427(3)	0·000
N(1)	0·026(3)	0·055(4)	0·065(4)	0·000	0·023(3)	0·000
C(1)	0·034(5)	0·059(5)	0·085(6)	0·000	0·028(4)	0·000
C(2)	0·032(4)	0·044(3)	0·050(4)	0·000	0·019(3)	0·000
C(3)	0·030(4)	0·047(4)	0·050(4)	0·000	0·016(3)	0·000
C(4)	0·037(4)	0·052(4)	0·051(4)	0·000	0·025(3)	0·000
C(5)	0·023(3)	0·051(4)	0·073(5)	0·000	0·022(3)	0·000
C(6)	0·029(4)	0·052(4)	0·052(4)	0·000	0·008(3)	0·000
C(7)	0·035(4)	0·047(4)	0·044(4)	0·000	0·016(3)	0·000
C(8)	0·048(5)	0·064(5)	0·049(4)	0·000	0·010(3)	0·000
C(9)	0·066(6)	0·061(5)	0·051(4)	0·000	0·031(4)	0·000
N(11)	0·016(8)	0·42(8)	0·000(10)	0·000	-0·008(8)	0·000
O(11)	0·022(5)	0·112(9)	0·062(5)	0·019(7)	0·018(4)	-0·001(5)
O(12)	0·001(7)	0·40(7)	0·25(4)	0·000	-0·006(12	0·000
Cl(1)	0·099(6)	0·149(7)	0·080(4)	0·000	0·016(4)	0·000
C(91)	0·07(3)	0·06(2)	0·14(4)	0·000	0·08(3)	0·000
C(92)	0·088(17)	0·14(2)	0·020(9)	-0·025(8)	0·030(11)	-0·046(2)